RP TU Rheinland-Pfälzische Technische Universität Kaiserslautern Landau

Dynamic modulation of endocytic protein sorting for counteracting stress conditions

vom Fachbereich Biologie

der Rheinland-Pfälzischen Technischen Universität Kaiserslautern-Landau

zur Verleihung des akademischen Grades Doctor rerum naturalium genehmigte

Dissertation

von

Fiorella Mazzone, M.Sc.

Mündliche Prüfung: 27.11.2025

Dekan:	Prof. Dr. Stephan Kins
Promotionskommissionsvorsitzender:	Prof. Dr. Jan Pielage
Berichterstattende:	Prof. Dr. Tanja Maritzen
	Prof. Dr. Zuzana Storchová

D 386

Acknowledgements

First, to **Gabi** – thank you for your wisdom, guidance, and for never letting me forget that stress can be productive (at least when it's a research topic). Your help during the Stressistance project was invaluable.

To my **family**, who have always been proud of me no matter what I do, even when my explanations about "what I actually work on" left them with more questions than answers. Your pride has been my fuel, and I carry you in my heart even though none of you will ever read this dissertation due to not speaking English (or understanding a word of biology!).

To **Julian**, who not only believed in me but literally followed me to this part of the country so I could chase my PhD dream. Thank you for the countless times you listened to my rants, celebrated the little victories, and made sure I didn't get lost in my own experiments. I appreciate you for being ready to save me, through a ride if I got stuck somewhere thanks to Deutsche Bahn, or volunteering to help me with coding skills...or Excel!

To **Antonia**, my friend, logic-checker, and occasional emergency life coach – thank you for trusting my judgement, even when I didn't. You reminded me to trust myself and always brought strength (and perspective) when I needed it most.

To **Alex, Jasmeet, Fabian, Marlen,** and all my amazing **labmates** – thank you for making the lab a place I looked forward to coming to, even on the longest days.

And then, there is you, **Tanja.** I want to thank you so much for taking a chance on me from the very start, for seeing potential where I only saw uncertainty, and for giving me the space to grow without micromanagement. Your office (and your mind) was always open, whether for long scientific discussions (that would many times include pen, paper and drawings), or for me to casually smile and say "Do you have time for a dumb question?." You never made me feel anything but welcome. And thank you for letting humour have a place in science: your laughter often turned my day around.

Finally, to everyone who has been part of my journey in big or small ways – thank you. I couldn't have done this without you, and I wouldn't have wanted to.

Summary

The plasma membrane with its embedded proteins plays a vital role in maintaining cellular homeostasis by regulating nutrient uptake, signalling, and osmotic balance. A potential key mechanism for remodelling the surface proteome in response to environmental stressors is clathrin-mediated endocytosis (CME), which governs the internalization of transmembrane proteins. Despite its importance, the contribution of endocytosis to cellular stress adaptation remains poorly understood. Here, we investigate how acute stress conditions, specifically oxidative, hyperosmotic, and heat stress, modulate surface protein dynamics and endocytic flux in mammalian cells.

Using surface biotinylation combined with high-resolution microscopy, Western blotting, and mass spectrometry, we profiled global and protein-specific endocytic alterations under stress. Our analysis revealed that all stressors impair endocytosis to some extent. Focusing on hyperosmotic stress, we found that it causes the surface accumulation of key proteins, including the cation-independent mannose-6-phosphate receptor (CI-M6PR), the transferrin receptor (TrfR), and the intracellular Na^+/H^+ exchanger NHE7. Notably, we could show that CI-M6PR endocytosis was indeed decreased upon osmotic stress and that its surface enrichment was recapitulated by pharmacological CME inhibition. Additionally, our data suggest that lysosomal exocytosis contributes to CI-M6PR surface accumulation under hyperosmotic conditions, as shown by inhibitor and agonist experiments.

Functional assays revealed that CI-M6PR contributes to cellular resilience under osmotic stress. Silencing CI-M6PR exacerbated stress-induced defects in proliferation and increased rates of apoptosis and necrosis. Given its dual role in lysosomal hydrolase trafficking and IGF2 signalling, we explored the physiological implications of CI-M6PR redistribution Interestingly, CI-M6PR depletion led to compensatory changes involving the cation-dependent M6PR (CD-M6PR), which was also enriched at the surface under stress. Further experiments involving knockdown of both M6PRs, coupled with the analysis of lysosomal enzyme activity and morphology, suggested the involvement of additional compensatory pathways. In addition, our experiments did not provide evidence for an IGF2 signalling-based role of the CI-M6PR surface accumulation. Therefore, further experiments are needed to resolve how CI-M6PR might contribute to cellular resilience under osmotic stress.

In summary, our findings support a model in which stress-induced modulations of endocytic protein sorting, particularly of CI-M6PR, play a key role in promoting cell survival and proliferation. This study underscores the role of endocytic remodelling as a dynamic, selective, and stress-responsive process with broad implications for membrane trafficking and cellular homeostasis under adverse conditions.

Zusammenfassung

Die Plasmamembran mit ihren eingebetteten Proteinen spielt eine entscheidende Rolle bei der Aufrechterhaltung der zellulären Homöostase, indem sie die Nährstoffaufnahme, die Signalübertragung und das osmotische Gleichgewicht reguliert. Ein potenzieller Schlüsselmechanismus für die Umgestaltung des Oberflächenproteoms als Reaktion auf Stressbedingungen ist die Clathrin-vermittelte Endozytose (CME), die die Internalisierung von Transmembranproteinen steuert. Trotz ihrer Bedeutung ist der Beitrag der Endozytose zur zellulären Anpassung an Stress noch weitgehend unverstanden. Hier untersuchen wir, wie akute Stressbedingungen, insbesondere oxidativer, hyperosmotischer und Hitzestress, die Proteindynamik von Oberflächenproteinen und den endozytotischen Fluss in Säugetierzellen modulieren.

Mithilfe von Oberflächenbiotinylierung in Kombination mit hochauflösender Mikroskopie, Western Blotting und Massenspektrometrie haben wir globale und proteinspezifische endozytotische Veränderungen unter Stressbedingungen untersucht. Unsere Analyse ergab, dass alle Stressoren die Endozytose in gewissem Maße beeinträchtigen. Mit Fokus auf hyperosmotischen Stress haben wir festgestellt, dass dieser die Anreicherung wichtiger Proteine an der Oberfläche verursacht, darunter der kationenunabhängige Mannose-6-Phosphat-Rezeptor (CI-M6PR), der Transferrin-Rezeptor (TrfR) und der intrazelluläre Na^+/H^+-Austauscher NHE7. Zudem konnten wir zeigen, dass die Endozytose von CI-M6PR bei osmotischem Stress verringert ist und dass die Oberflächenanreicherung von CI-M6PR durch pharmakologische CME-Inhibition rekapituliert werden kann. Darüber hinaus deuten unsere Daten darauf hin, dass die Exozytose von Lysosomen unter hyperosmotischen Bedingungen zur Oberflächenanreicherung von CI-M6PR beiträgt, wie Inhibitor- und Agonist-Experimente demonstriert haben.

Unsere funktionellen Assays zeigten, dass CI-M6PR die Widerstandsfähigkeit der Zellen bei osmotischem Stress erhöht. Der Knockdown von CI-M6PR verstärkte stressbedingte Proliferationsdefekte und erhöhte die Apoptose- und Nekrose-Raten. Angesichts seiner doppelten Rolle beim Transport von lysosomalen Hydrolasen und der IGF2-Signalübertragung haben wir die physiologischen Auswirkungen der CI-M6PR-Umverteilung untersucht. Interessanterweise führte der Knockdown von CI-M6PR zu kompensatorischen Veränderungen, an denen der kationenabhängige M6PR beteiligt war, der unter Stress ebenfalls an der Oberfläche angereichert war. Weitere Experimente, bei denen beide M6PRs ausgeschaltet und lysosomale Enzymaktivität und Morphologie analysiert wurden, deuteten auf die Beteiligung zusätzlicher kompensatorischer Signalwege hin. Letztlich lieferten unsere Experimente auch keine Hinweise auf einen Effekt der CI-M6PR-Oberflächenakkumulation auf IGF2-abhängige Prozesse. Daher sind weitere Experimente erforderlich, um zu klären, wie genau CI-M6PR zur Widerstandsfähigkeit osmotisch gestresster Zellen beiträgt.

Zusammenfassend stützen unsere Ergebnisse ein Modell, in dem die stressinduzierte Modulation der Endozytose, insbesondere der Internalisierung von CI-M6PR, eine Schlüsselrolle für das Überleben und die Proliferationsfähigkeit von Säugetierzellen spielt. Diese Studie unterstreicht die Rolle der Endozytose als dynamischer, selektiver und durch Stress-regulierten Prozess mit weitreichenden Auswirkungen auf den Membrantransport und die zelluläre Homöostase unter widrigen Bedingungen.

Table of contents

1. Introduction

1.1 At the cellular frontier: the wonder of the plasma membrane

The plasma membrane is a dynamic and selectively permeable boundary that defines the limits of the cell and mediates its interactions with the external environment. Composed of a complex mosaic of lipids, proteins, and carbohydrates, the plasma membrane not only serves as a physical barrier but also functions as an essential platform for communication, transport, and structural organization. It regulates the exchange of ions, nutrients, and signalling molecules, thereby maintaining cellular homeostasis and coordinating responses to extracellular stimuli. Additionally, the membrane hosts a wide array of integral and peripheral proteins involved in receptor signalling, cell adhesion, immune recognition, and endocytosis. Through these roles, the plasma membrane is a central player in numerous physiological processes and is critical for both individual cell function and the integrated behaviour of tissues and organs.

The advent of electron microscopy revealed the intricate architecture of cellular membranes, underscoring their essential role in compartmentalizing cellular processes. Membranes regulate biochemical reactions either by concentrating proteins on their surfaces therefore enhancing protein interactions, or by creating diffusion barriers between compartments, which lead to a reduction of undesired interactions. Dynamic membrane remodelling through fission and fusion events governs many extranuclear cellular functions (Doherty & McMahon, 2009).

The plasma membrane serves as the primary interface between the cell and its environment, making its composition tightly regulated. Some impressive characteristics that describe the mammalian plasma membrane are:

- As it is the selective barrier that defines the cell, it integrates tens of thousands of lipids with thousands of integral proteins into a dynamic, non-equilibrated mosaic (van Meer & de Kroon, 2011; Harayama & Riezman, 2018) (Fig. 1.1).
- Its composition is tuned to reconcile: 1) mechanical robustness, 2) rapid traffic of cargo, and 3) ultrafast signal initiation/termination (Ingólfsson et al., 2014; Fujimoto & Parmryd, 2017).
- Small (5–10 %) shifts in cholesterol, phosphatidylserine externalization, or transporter surface density can trigger apoptosis, alter drug uptake, or reshape immune recognition (Harayama & Riezman, 2018; Lorent et al., 2020; Symons et al., 2021).

1.1.1 Lipid composition

The plasma membrane presents a leaflet asymmetry as a defining factor, with the outer leaflet being more tightly packed and less diffusive, containing more saturated acyl chains, phosphatidylcholine (30-40% mol), sphingomyelin (5-15% mol), many glycosphingolipids (3–8% mol) and cholesterol (Ingólfsson et al., 2014).

In contrast, the inner leaflet contains more polyunsaturated acyl chains conferring greater fluidity, harbouring phosphatidylethanolamine (15–25% mol), phosphatidylserine (5–10% mol) and phosphatidylinositol and derivatives (2–8% mol) (Ingólfsson et al., 2014).

Submicron domains (rafts, nanodomains) of a transient nature, characterized by being cholesterol and sphingolipid-enriched regions, organize proteins and function as signalling platforms (Ingólfsson et al., 2014; Fujimoto & Parmryd, 2017; T. Zhang et al., 2025)

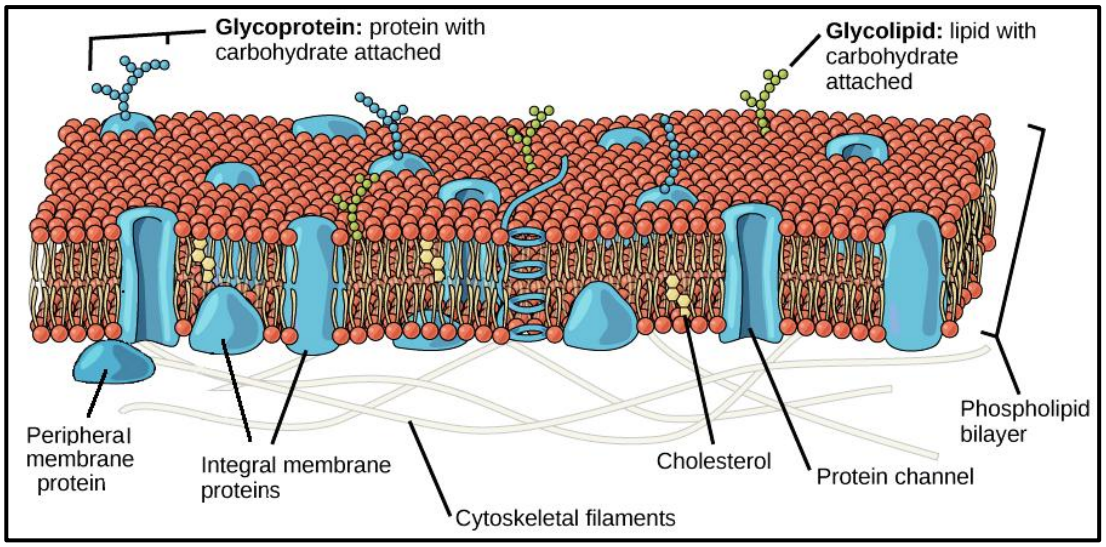

Fig. 1.1: **General representative scheme of a mammalian plasma membrane**, with its asymmetric phospholipid bilayer, cholesterol embedded, and some typical transmembrane and associated membrane proteins. Image modified from OpenStax Biology.

1.1.2 Integral membrane proteins

The plasma membrane owes much of its functions to the network of proteins it harbours. To date, there have been over 5000 human transmembrane proteins predicted (Bausch-Fluck et al., 2018). Indeed it is the *surfaceome* (the complete set of proteins present on the cell surface) which acts as the primary interface between the cell and its surrounding microenvironment. Despite its pivotal role in orchestrating cellular responses to external cues, the composition, regulation, and functional dynamics of the surfaceome remain incompletely understood. One major challenge lies in the difficulty of determining which proteins are genuinely localized at the plasma membrane and how they interact in a temporally and spatially regulated manner to enable context-specific signalling functions.

Cell surface proteins are of immense biomedical relevance. Their accessibility and functional diversity make them attractive candidates for therapeutic intervention. This is underscored by the fact that approximately 66% of all approved human drugs target a cell surface protein, according to the DrugBank database (Bausch-Fluck et al., 2018; Z. Hu et al., 2021). Moreover, it is estimated that 10–20% of all genes in the human genome encode cell surface proteins (Rose et al., 2021), highlighting the magnitude and complexity of this proteome compartment. However, despite this significance, only a limited number of all predicted human transmembrane proteins have been experimentally confirmed to localize to the plasma membrane. As such, a comprehensive mapping and functional characterization of the surfaceome remains a key frontier in both basic and translational research.

Broadly speaking, the different integral membrane proteins can be divided into a number of functional categories (Fig. 1.2), some of which follow here:

A) **Transporters and channels** which facilitate the movement of ions, small molecules, or macromolecules across the plasma membrane (V. H. L. Lee, 2000; Sáez et al., 2003; Bezanilla, 2008). Examples include:

- Glucose transporter (GLUT1): facilitates glucose uptake into the cell (Macheda et al., 2005).
- Na^+/K^+ ATPase: maintains electrochemical gradients across the plasma membrane (Aperia et al., 2016).
- Aquaporin-1 (AQP1): it is a water channel for the membrane (Takata et al., 2004).
- Voltage-gated K^+ channel (Kv1.2): modulates the resting and action potential of the membrane (Bezanilla, 2008).
- NHE7: mediates the electroneutral exchange of Na^+ and H^+ ions along their concentration gradients and play a vital role in various physiological functions, including the regulation of intracellular pH, maintenance of cell volume, and the overall balance of electrolytes, acid-base status, and fluid volume homeostasis (Orlowski & Grinstein, 2004) and the adaptation to osmotic stress (López-Hernández, Haucke, et al., 2020) as will be discussed later.

B) **Receptors** which mediate signal transduction by binding ligands and triggering intracellular pathways. Examples include:

- Epidermal Growth Factor Receptor (EGFR): receptor tyrosine kinase that mediates a variety of functions, including proliferation and autophagy (H. Li et al., 2017).
- G Protein-Coupled Receptors (GPCRs): facilitate most of our physiological responses to hormones, neurotransmitters and environmental stimuli (Rosenbaum et al., 2009).

C) **Nutrient receptors** which mediate the uptake of diverse nutrients via endocytosis. Examples include:

- Transferrin Receptor (TrfR): promotes iron uptake into the cells (Aisen, 2004).
- Low-Density Lipoprotein Receptor (LDLR): promotes cholesterol uptake into the cells (Goldstein & Brown, 2009).

D) **Cell Adhesion Molecules (CAMs)** which mediate cell-cell or cell-matrix adhesion and are critical for tissue integrity and signalling. Examples include:

- Cadherins such as E-cadherin: homophilic cell-cell adhesion, with roles in epithelial cell behaviour, tissue formation, and suppression of cancer (van Roy & Berx, 2008).
- Integrins such as $\alpha5\beta1$: mediate the attachment of cells to the extracellular matrix and take part in cell-cell interactions; thereby playing important roles during developmental and pathological processes (Pang et al., 2023).

E) **Enzymes** which catalyse the synthesis, degradation, or modification of a substrate. Examples include:

- Matrix metalloproteases: degrade the components of the extracellular matrix, important for embryogenesis, tissue remodelling, wound healing, and angiogenesis (Sekhon, 2010).

F) **Scaffolds** which anchor cytoskeletal elements or organize signalling complexes. Examples include:

- Caveolins: implicated in numerous signalling pathways, control of protein subcellular localization, and organization of the plasma membrane into functionally distinct domains, amongst others (Parton & del Pozo, 2013).

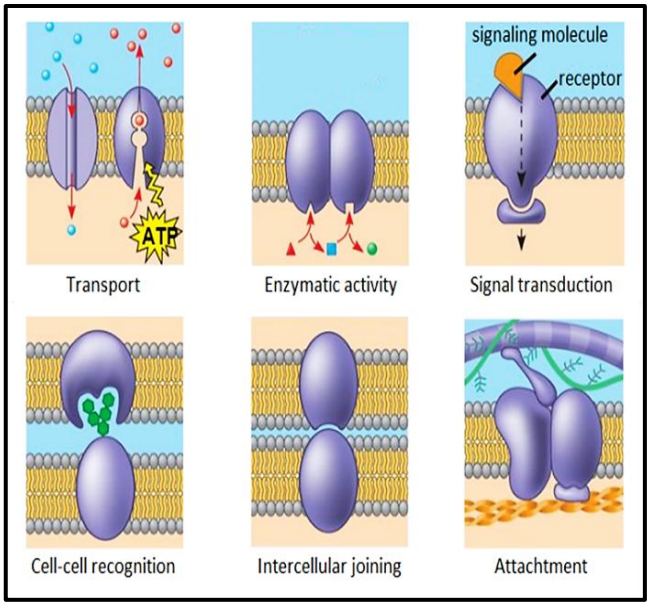

Fig. 1.2: **Different functional categories of integral plasma membrane proteins.**
Adapted from Campbell et al, 9th edition.

1.2 Navigating cellular stress: Remodelling cell surface proteome in response to environmental challenges.

Optimal cell function and survival depend on the cellular ability to adjust to changes in external physical or chemical conditions. These adaptive systems are commonly referred to as "cellular stress responses" and are critical because macromolecules and cellular processes perform best within narrow biochemical parameters, such as specific temperatures, solute concentrations, or ionic strengths. When these conditions shift away from the ideal range, molecular functions become impaired, leading to cellular stress (Ho, 2006).

When cells encounter a cellular stress that challenges their homeostatic equilibrium, a central aspect of their adaptive response may involve the dynamic remodelling of the cell surface proteome (Fig. 1.3).

This strategy allows the cell to swiftly adjust its interface with the extracellular environment, modulating, for instance, ion uptake, signalling, adhesion, and immune recognition according to the nature of the insult. For example, under conditions of nutrient deprivation, cells may increase the surface expression of specific nutrient transporters such as GLUT1 to enhance glucose uptake, or amino acid transporters to boost metabolic influx (López-Hernández, Haucke, et al., 2020).

In the context of oxidative stress, certain scavenger receptors like CD36 or LOX-1 may be upregulated to assist in the clearance of oxidized lipids or damaged molecules (Lara-Guzmán et al., 2018).

During hypoxia, the surface expression of integrins and adhesion molecules such as ICAM-1 is altered, facilitating interactions with immune cells or promoting angiogenic responses (Liang et al., 2019).

Hyperosmotic stress, for example, has been shown to induce a redistribution of the ion transporters NHE7 to the plasma membrane, where it allows entry of $Na^{2+,}$ thereby triggering a downstream protective autophagic pathway (López-Hernández, Puchkov, et al., 2020).

Collectively, these stress-specific changes in surface protein composition are not merely passive consequences of stress but represent active, regulated processes aimed at preserving cellular viability and function.

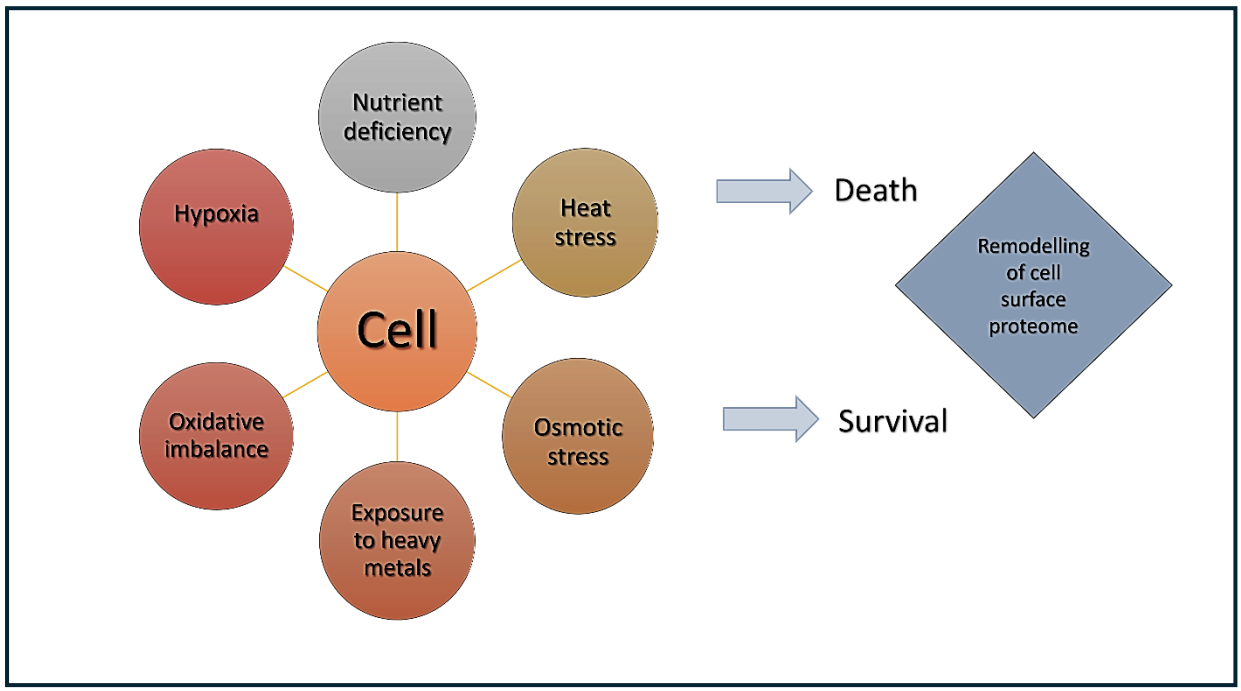

Fig. 1.3: **Remodelling cell surface proteome in response to environmental challenges.**
Cells face many environmental stress types to which they need to adapt in order to maintain homeostasis and survive. One of the main ways by which they can adapt to these stressors is to dynamically remodel the protein contents of their plasma membrane in response to each stressor type. This could sometimes make all the difference between death and survival.

1.3 Endocytosis and exocytosis: Pathways to dynamically modulate plasma membrane composition.

There are two main pathways that allow the cells to dynamically alter the contents of lipids and membrane proteins according to the cells needs: endocytosis and exocytosis.

Endocytosis is the process by which cells internalize portions of the plasma membrane along with embedded proteins, lipids, and enclosed extracellular fluid (Doherty & McMahon, 2009). It is functionally opposed to exocytosis, where intracellular membranes fuse with the plasma membrane to release contents outside the cell and/or deliver proteins or lipids to the membrane (Jahn & Südhof, 1999). These two processes are crucial for controlling cell-environment interactions, such as modulating receptor availability and thus cellular sensitivity to ligands.

Beyond receptor downregulation, endocytosis is increasingly recognized as a regulator of diverse processes, including mitosis, antigen presentation, migration, cell reshaping, and intracellular signalling (Lundmark et al., 2008; Burgdorf & Kurts, 2008; Snijder et al., 2009; Kaur et al., 2014; Boucrot et al., 2015; Holst et al., 2017; Hinze & Boucrot, 2018). For example, endocytosis of transmembrane receptors, which removes them from the surface, makes them unable to interact with extracellular cues and regulates the sensitivity of cells to their specific ligands. On the other hand, endocytosis has a key role in the positive regulation of many intracellular signalling cascades (Hoeller et al., 2005).

While clathrin-mediated endocytosis (CME) accounts for a significant portion of internalization events, many cargoes are internalized via clathrin-independent pathways (Kirkham & Parton, 2005; McMahon & Boucrot, 2011) (Fig. 1.4). Among these, caveolae-mediated endocytosis is well-characterized. Caveolae, which are flask-shaped plasma membrane invaginations (~60–80 nm), are rich in caveolin-1 and abundant in certain cell types like smooth muscle cells, adipocytes, and endothelial cells (Parton & Simons, 2007). They can cluster into multicaveolar grape-like structures connected to the plasma membrane and have been implicated in endocytosis, often observable in live-cell imaging (Rothberg et al., 1992; Parton & Simons, 2007).

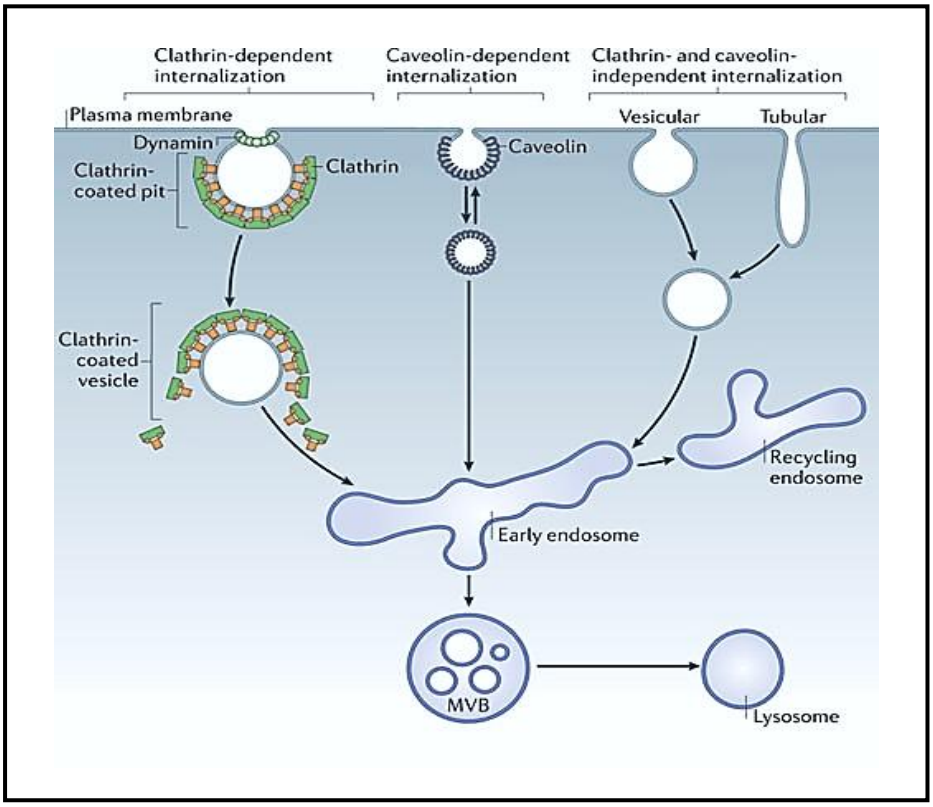

Fig. 1.4: Multiple endocytosis pathways.
Cells internalize extracellular material through multiple endocytic routes, including clathrin-mediated and caveolin-mediated pathways, but also pathways that are independent of both clathrin and caveolin. Once internalized, cargo is delivered to endosomes, where it undergoes sorting either for recycling to the plasma membrane or for degradation via downstream compartments such as multivesicular bodies (MVBs) and lysosomes. Among the endocytic pathways, clathrin-mediated endocytosis is the best-characterized mechanism for directing cargo to endosomes. In contrast, the specific cargo profile of caveolae remains poorly defined. The clathrin- and caveolin-independent pathways are less understood, and ongoing molecular studies are needed to clarify their distinct mechanisms, which may involve both vesicular and tubular transport structures. Adapted from (McMahon & Boucrot, 2011).

However, the uptake of many cargoes remains unaffected by inhibition of both CME and caveolae-mediated pathways (Sandvig et al., 2018). These cargoes are often internalized through cholesterol-dependent, clathrin- and caveolin-independent endocytic routes, suggesting the existence of distinct lipid-dependent mechanisms. These pathways facilitate the uptake of various molecules, including extracellular fluid, SV40 virus, cholera toxin B subunit, glycosphingolipids, GPI-anchored proteins, and multiple receptors such as those for IL-2, growth hormone, AMF, and endothelin (Damm et al., 2005; Kirkham & Parton, 2005). Despite this, few molecular regulators of these pathways have been identified.

As it was found that approximately 95% of all endocytic flux is conducted by CME (Bitsikas et al., 2014), I will focus on this pathway.

1.3.1 Clathrin-mediated endocytosis

CME is the primary and most extensively characterized mechanism for the selective internalization of transmembrane proteins, often referred to as "cargo," along with their bound ligands. These cargos include, for example, nutrient receptors, adhesion molecules, signalling receptors, and various transporters responsible for the uptake of amino acids, glucose, and ions. By mediating their uptake, CME regulates the surface density and thus overall activity of these proteins, thereby exerting critical control over intercellular communication, signal transduction, adhesion dynamics, and cellular homeostasis.

CME stands out as the best-understood endocytic pathway, largely due to the accessibility of its key component clathrin to electron microscopy which allowed already early on a visualization of the assembling clathrin lattices which are critical for membrane bending in CME (J. Heuser, 1980). Since then, the intricate network of protein-protein interactions within the CME machinery has been systematically analyzed and experimentally manipulated, underscoring its significance in both fundamental cell biology and human disease.

Mechanistically, CME starts with the formation of clathrin-coated pits (CCPs) at the plasma membrane. These pits arise through the recruitment of clathrin triskelia, each composed of three heavy chains (CHCs) paired with associated light chains (CLCs). CCP formation is initiated and stabilized by the proteins of the pioneer module including the adaptor protein complex 2 (AP-2), a heterotetrameric complex composed of α, β2, μ2, and σ2 subunits, which serves as a central platform for cargo recognition and coat assembly (Mettlen et al., 2018). CME unfolds in the following distinct stages (E. M. Schmid & McMahon, 2007; McMahon & Boucrot, 2011; Robinson, 2015) (Fig. 1.5):

1. **Initiation**, where adaptor recruitment and cargo selection occur.
2. **Stabilization**, ensuring the nascent pit is maintained at the membrane.
3. **Growth and maturation**, during which curvature increases, and endocytic accessory proteins (EAPs) facilitate coat growth.
4. **Membrane fission**, mediated by the large GTPase dynamin, which oligomerizes into helical structures around the pit neck, catalysing scission to release the vesicle.
5. **Uncoating**, where the components are liberated and become available for another round of clathrin-coated vesicle formation.

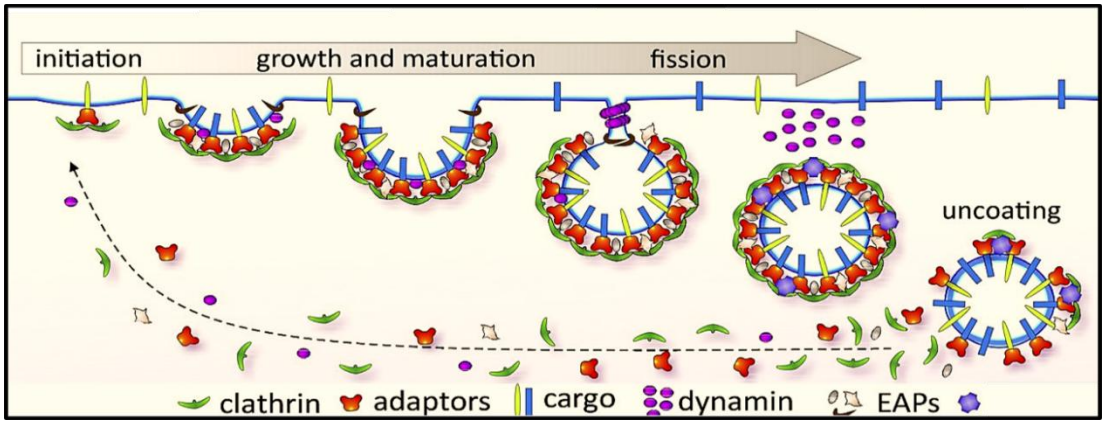

Fig. 1.5: **CME unfolds in highly regulated stages to allow cargo internalization into the cell.** The process begins with adaptor proteins that recognize specific sorting signals in the cytosolic tails of surface receptors (cargo), initiating the recruitment of clathrin to form nascent clathrin-coated pits (CCPs). As these pits grow and mature, various endocytic accessory proteins (EAPs) facilitate further cargo concentration and membrane bending. The GTPase dynamin is recruited early to developing CCPs, where it plays a regulatory role in pit maturation. As the neck of the invaginating pit is sufficiently narrowed by EAPs, dynamin assembles into helical collar-like structures around it, driving membrane scission and vesicle release. Finally, clathrin and associated proteins are removed in an uncoating step, allowing the vesicle to proceed through intracellular trafficking pathways. Adapted from S. L. Schmid, (2017).

Key EAPs and their effect on CCPs

		Function	Effect on CCP
Major coat proteins	CHC	Coat	KD ↓ initiation
	CLCa	Coat	KD ↓ initiation
	CLCb	Coat	KD ↓ initiation
	AP2	Adaptor	KD ↓ initiation
	Dyn1	GTPase	KO no effect; A: ↑ initiation and maturation
	Dyn2	GTPase	KD ↓ initiation
Easy arriving, pioneer proteins	FCHo1/2	Scaffold	KD ↓ initiation
	Eps15	Scaffold	KD ↓ maturation
	Intersectin	Scaffold	KD ↓ stabilization and maturation
	NECAP	Adaptor	KD ↓ maturation
	CALM	Adaptor	KD ↓ maturation
	Epsin	Adaptor	KD ↓ maturation
CCP maturation and fission	Amphiphysin	Curvature	ND
	Endophilin	Curvature	KD ↑ abortive
	N-WASP	Actin	ND
	Cortactin	Actin	ND
	Myosin 1E	Actin	ND
	Hip1R	Actin	ND
	SNX9	Scaffold	KD ↓ maturation
	Synaptojanin	Lipids	KD ↑ maturation
	PI3KC2α	Lipids	KD ↓ maturation
	PIP5K	Lipid	KD ↓ maturation OX ↑ initiation and maturation
Uncoating	GAK	Kinase	KD ↑ abortive
	Hsc70	ATPase	ND
	OCRL	Lipids	M: ↑ CCVs ↑ U-shaped CCPs

Table 1: The effect of key EAPs and their effect on CCPs summarized.

Abbreviations: A, activation; AP2, adaptor protein-2; CALM, clathrin assembly lymphoid myeloid leukemia; CCP, clathrin-coated pit; CHC, clathrin heavy chain; CLC, clathrin light chain; Dyn, dynamin; EAPs, endocytic accessory proteins; Eps15, EGF-receptor phosphorylation substrate; FCHo1/2, Fer/Cip4 homology domain-only proteins 1/2; GAK, cyclin G associated kinase; Hip1R, Huntingtin interacting protein-1 related; Hsc70, heat shock protein 70 kD; KD, knockdown; KO, knockout; M, mutation; ND, not determined; NECAP, adaptin-ear-binding coat-associated protein; N-WASP, neural Wiskott-Aldrich syndrome protein; OCRL, oculocerebrorenal Lowe syndrome protein; OX, overexpression; PI3KC2α, phosphatidylinositol 3-kinase C2α; PIP, phosphatidylinositol phosphate; SNX9, sorting nexin 9. table adapted from Mettlen et al., (2018)

Following internalization, clathrin-coated vesicles (CCVs) rapidly shed their coat proteins, allowing the vesicles to fuse homotypically or with early endosomes for cargo sorting. Beyond clathrin and AP2, CME depends on a suite of EAPs that perform diverse roles: scaffold formation, membrane bending, cargo clustering, and regulation of pit dynamics (Mettlen et al., 2018) (Table 1).
Altogether, CME exemplifies a highly coordinated molecular process fundamental to cellular regulation, whose dysregulation is implicated in various pathologies, including neurodegenerative diseases, cancer, and metabolic disorders (McMahon & Boucrot, 2011; Jaye et al., 2024).

1.3.1.1 Consequences of defective CME

To contextualize the central importance of CME in maintaining human health and cellular homeostasis, it is essential to highlight its broad functional scope and the spectrum of pathological consequences arising from its dysfunction. CME is a highly conserved and tightly regulated pathway that plays pivotal roles in several physiological processes. These include but are not limited to the following: the modulation and downregulation of key surface receptors, such as receptor tyrosine kinases, G protein-coupled receptors, and the low-density lipoprotein receptor, which are crucial for maintaining balanced signal transduction and lipid homeostasis. CME also contributes to synaptic vesicle recycling, thereby ensuring sustained neurotransmission and proper neuronal communication (L.-G. Wu et al., 2014; Jaye et al., 2024). In addition, it facilitates cellular nutrient acquisition (e.g. through the internalization of iron-bound transferrin and lipoproteins), supports immune system function via antigen presentation and immune receptor trafficking, and is the main pathway allowing the dynamic regulation of plasma membrane composition.

Given this fundamental involvement across diverse cellular systems, it is unsurprising that defects in CME machinery have been linked to a wide range of human diseases. Aberrant endocytic regulation of cell surface receptors has been implicated in tumorigenesis, where persistent or misregulated receptor signalling contributes to uncontrolled cell proliferation and cancer progression (Seimiya et al., 2008; Elkin et al., 2015; Schmid, 2017; Xiao et al., 2018; Imbastari et al., 2021; Xie et al., 2023). Disruption of CME-dependent lipoprotein uptake, particularly due to defects in the adaptor protein ARH, underlies conditions such as autosomal recessive hypercholesterolemia and other sterol metabolism disorders (Garuti et al., 2005; Cui et al., 2020; Anderson et al., 2021). In the nervous system, impaired synaptic vesicle recycling compromises neurotransmission, contributing to neurological conditions including epilepsy (Dhindsa et al., 2015; Azarnia Tehran et al., 2019; Helbig et al., 2019), while CME-associated defects in neuronal trafficking have also been implicated in neurodegenerative disorders such as Alzheimer's disease (Maninger et al., 2024). Furthermore, mutations affecting CME components such as dynamin 2 *(DNM2)* have been identified in several neuromuscular and neurodevelopmental syndromes, such as centronuclear myopathy (CNM), characterized by progressive muscle weakness, and Charcot-Marie-Tooth disease (CMT), a demyelinating peripheral neuropathy (Böhm et al., 2012; Sidiropoulos et al., 2012; González-Jamett et al., 2013; Abath Neto et al., 2015; Moulay et al., 2020; Gómez-Oca et al., 2021). Together, these findings underscore CME as a critical cellular mechanism whose perturbation is intricately associated with a diverse array of pathological outcomes.

1.3.1.2 Dynamic regulation of endocytosis as a central hub for cellular sensing and signalling

CME is a highly regulated and dynamic process, with each stage modulated by cargo recognition, phosphatidylinositol lipids, protein kinases, and a network of EAPs when the cells need to adapt to a certain status. For instance, membrane recycling is transiently halted during mitosis, when cells adopt a rounded morphology, and then overshoots normal activity upon completion of mitosis as cells spread again (Boucrot & Kirchhausen, 2007).

Live-cell imaging has revealed that CME does not always progress in a uniform, deterministic manner; indeed, up to 50% of nascent CCPs fail to mature into cargo-loaded CCVs and are instead aborted. Such regulation often occurs at the earliest steps of the pathway, enabling cells to rapidly adapt to changing physiological and environmental conditions.

The complexity of the endocytic membrane system reflects its central role in both cellular logistics and signal regulation. This plasticity allows endocytosis to oscillate, stabilize, or reconfigure through feedback loops and built-in adaptive principles, enabling the endocytic system to respond to diverse and fluctuating cues (Kholodenko, 2006).

One way by which cells can respond to these internal and external environmental cues is by having a diverse array of membrane-associated sensors that continuously detect fluctuations in nutrient and energy status, ion concentrations, membrane tension, and other key parameters. These sensors, such as integrins, ion channels, receptor tyrosine kinases, Toll-like receptors, pH sensors, etc., depend on dynamic trafficking between membrane compartments to maintain their sensing capacity (Chang et al., 2006; Cota et al., 2006; M. R. Morgan et al., 2007). Therefore, endocytosis plays a pivotal role in this process by defining the spatial and temporal context in which incoming signals are transduced, processed, and integrated into cellular responses (Kholodenko, 2006).

A central regulatory mechanism linking endocytosis and signalling is protein phosphorylation. This post-translational modification enables protein kinases to influence every stage of the endocytic pathway, thereby integrating signalling cues with membrane trafficking. Phosphorylation regulates adaptor recruitment to the membrane, clathrin coat assembly and disassembly, curvature generation and stabilization, vesicle fission, actin polymerization, vesicle transport along microtubules, docking at target membranes, and membrane fusion. Several kinases serve as key hubs in this regulatory network, each targeting multiple components of the endocytic machinery (Liberali et al., 2008) (Fig.1.6).

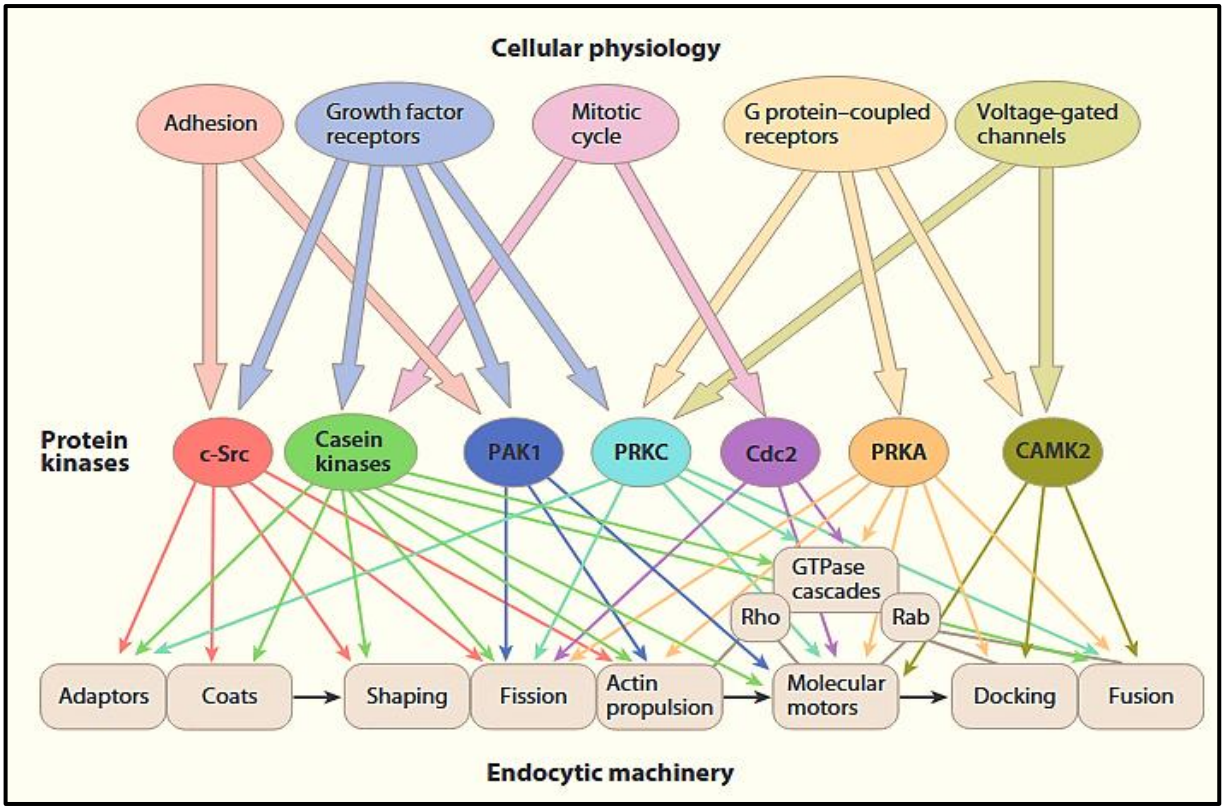

Fig. 1.6: **Schematic overview depicting a simplified hierarchy of regulatory control over the endocytic machinery by key physiological inputs.**
Cellular signals, mainly from GPCRs, calcium channels, growth factor receptors, adhesion sensors, and cell-cycle checkpoints, converge on seven principal protein kinase hubs. The tyrosine kinase c-Src predominantly regulates vesicle formation, while casein kinases and protein kinase C (PRKC) influence all stages of the endocytic trafficking cycle. p21-activated kinase 1 (PAK1) and cell division cycle 2 (CDC2) govern membrane fission, cytoskeleton-mediated transport, and GTPase signalling cascades. Protein kinase A (PRKA) and calcium/calmodulin-dependent kinase 2 (CAMK2) modulate vesicle fission, cytoskeletal transport, and membrane fusion. Adapted from Liberali et al., (2008).

Among these, the non-receptor tyrosine kinase c-Src is particularly well studied (Ishizawar & Parsons, 2004; Sandilands & Frame, 2008; Reinecke & Caplan, 2014). Anchored at the plasma membrane and potentially associated with intracellular organelles, SRC phosphorylates proteins involved in the early stages of endocytic trafficking, including vesicle formation, fission, and actin-driven propulsion. Acting downstream of growth factor receptors and integrins, SRC functions as a general “on” switch for endocytic trafficking, effectively coupling extracellular stimuli to rapid membrane remodelling events (Liberali et al., 2008).

Collectively, these examples illustrate only a subset of the pathways through which CME and endocytic trafficking are finely tuned in response to physiological and environmental cues. They highlight the intricate and extremely sensitive nature of this hierarchical regulatory network, underscoring its capacity to integrate multiple inputs to precisely modulate membrane trafficking dynamics.

1.3.2 Exocytosis

Regulated exocytosis is a fundamental cellular process by which secretory vesicles deliver their cargo to the extracellular space in response to specific stimuli. This highly orchestrated mechanism involves the directed transport of vesicles to specialized plasma membrane domains, known as "active zones", where they undergo fusion with the membrane (Campos-Toimil et al., 2002; Pickett & Edwardson, 2006). Vesicle fusion serves multiple essential functions: it incorporates integral membrane proteins, such as ion channels and transporters, into the plasma membrane; it contributes lipid components to the membrane structure; and it releases intra-vesicular contents, including enzymes, signalling molecules and neurotransmitters, into the extracellular milieu (Izquierdo et al., 2002; Ren et al., 2016).

Historically, exocytosis was viewed as a unidirectional process culminating in the complete merger of the vesicle with the plasma membrane, referred to as "full fusion" (Fig. 1.6a). In this model, the fusion pore dilates fully, allowing the total release of vesicle contents, with the vesicle membrane subsequently integrated into the plasma membrane and later retrieved via endocytosis. Support for this model has come from various experimental approaches, including electron microscopy, amperometry, fluorescence imaging, and patch-clamp recordings, all of which have provided compelling evidence for full vesicle collapse during secretion which has been described, for example, in neurons and endocrine cells (Q. Zhang et al., 2007; Ren et al., 2016).

However, accumulating evidence over recent decades has revealed an alternative mode of exocytosis known as "kiss-and-run"(Wightman & Haynes, 2004; Q. Zhang et al., 2007) (Fig. 1.6b). In this mechanism, vesicles transiently fuse with the plasma membrane, forming a narrow fusion pore (typically 2–4 nm in diameter) that permits partial cargo release. The fusion pore then reseals, allowing the vesicle to disengage and maintain its structural integrity. This transient fusion behaviour has been observed across multiple systems through patch-clamp techniques, capacitance measurements, and high-resolution imaging modalities such as fluorescence and atomic force microscopy, and has sometimes been detected in secretory cells, including nerve terminals.

The regulation of fusion pore dynamics is increasingly recognized as a critical determinant of the mode and efficiency of exocytosis. Beyond the classical SNARE-mediated fusion machinery, additional factors such as dynamin, the GTPase already mentioned for its role in endocytosis, have been implicated in controlling pore formation and stabilization. Pharmacological inhibition of dynamin activity has been shown to modulate exocytosis in a dose-dependent manner, suggesting a direct role in secretion (Trouillon & Ewing, 2013). Furthermore, the actin cytoskeleton, in concert with dynamin and other mechanochemical proteins, appears to influence the opening, maintenance, and closure of the fusion pore, highlighting a complex interplay between membrane remodelling factors (Trouillon & Ewing, 2014).

Taken together, these findings challenge the traditional view of exocytosis as a binary, all-or-none event. Instead, they support a model in which multiple fusion modalities coexist within cells, governed by finely tuned regulatory mechanisms. Understanding the molecular control of these distinct exocytic pathways is essential for elucidating their physiological relevance in neurotransmission, hormone release, and other secretory processes.

1.3.3 Lysosomal exocytosis

Recent advances in cell biology have shed light on lysosomal exocytosis as a key mechanism, now recognized as central to membrane dynamics and cellular adaptation.

Lysosomes are a dynamic population of acidic organelles that play a central role in intracellular digestion and macromolecular recycling. Enclosed by a single lipid bilayer, lysosomes harbor two main categories of proteins that underpin their degradative and recycling function: soluble enzymes within the lumen to degrade various substances and integral membrane proteins embedded in the lysosomal membrane (Saftig & Haas, 2016) to export the breakdown products from the lysosome. The luminal enzymes include a diverse array of more than 60 acid hydrolases, such as proteases, lipases, sulfatases, phosphatases, nucleases, and glycosidases, which together enable the breakdown of proteins, lipids, nucleic acids, and carbohydrates (H. Xu & Ren, 2015; Ballabio & Bonifacino, 2020).

In mammalian cells, lysosomes are abundant and widely distributed, with individual cells containing anywhere from 50 to over 1,000 lysosomes, depending on cell type and physiological state (Ballabio & Bonifacino, 2020). Rather than forming a uniform population, lysosomes exhibit considerable heterogeneity in size, morphology, enzymatic content, and subcellular positioning (Ebner et al., 2025). This structural and functional diversity reflects the plasticity of lysosomes and allows them to adapt to varying cellular demands, including responses to nutrient availability, stress, and signalling cues.

Traditionally viewed as terminal degradative compartments, lysosomes have been reported to contribute to a wide range of intracellular and extracellular processes. Beyond their well-established roles in hydrolytic degradation and recycling of cellular components, recent evidence highlights their capacity for regulated exocytosis, wherein lysosomes fuse with the plasma membrane, donating integral proteins and lipids to the plasma membrane and releasing their contents into the extracellular space. This process, termed “lysosomal exocytosis”, is now recognized as a ubiquitous and finely tuned mechanism across virtually all cell types (Brozzi et al., 2013; Buratta et al., 2020; Trojani et al., 2024; H. Xu & Ren, 2015).

1.3.3.1 Mechanism and functions of lysosomal exocytosis

Lysosomal exocytosis plays a central role in maintaining cellular homeostasis, particularly through its involvement in plasma membrane repair (PMR). Upon membrane injury, a local influx of Ca^{2+} activates lysosomes to migrate toward the damaged site and fuse with the plasma membrane. This rapid response is mediated by key molecular regulators, including synaptotagmin VII, a Ca^{2+}-sensitive lysosomal membrane protein, and the SNARE complex, which drives vesicle fusion via VAMP7, syntaxin-4, and SNAP23 (Rao et al., 2004). The process not only restores membrane integrity but also releases luminal enzymes such as acid sphingomyelinase (ASM) and cathepsins, which contribute to membrane remodelling and endocytosis to support full repair.

Mechanistically, the lysosomal exocytosis can be divided into four stages, which are simplified as follows (Trojani et al., 2024) (Fig 1.7):

1. Direct transport of lysosomes from perinuclear zones (specifically the microtubule organizing centre) to the cell periphery, involving the coordinated activity of microtubule-dependent motors such as Kinesins and Myosins.
2. Docking of lysosomes to the plasma membrane, requiring a prominent cytoplasmatic Ca^{2+} rise and interactions between several lysosomal and plasma membrane proteins. A rapid, localized influx of Ca^{2+} at sites of plasma membrane injury has been shown to trigger a conformational change in Synaptotagmin VII (SYT VII), a widely expressed lysosomal membrane protein that functions as a Ca^{2+} sensor.
3. Fusion of lysosomes with the plasma membrane induced by a Ca^{2+} release which is amplified by lysosomal ion channels such as TRPML1, which is transcriptionally regulated by TFEB in response to cellular stress (Miyano et al., 2025). A conformational change in SYT VII promotes its interaction with the proteins VAMP7, SYNTAXIN-4, and SNAP23.
4. Exocytosis of lysosomes leading to the extracellular release of lysosomal luminal content.

Lysosome-Associated Membrane Protein 1 (LAMP1) is a well-characterized transmembrane protein predominantly localized to lysosomal membranes. Beyond its role in maintaining lysosomal integrity, LAMP1 has been implicated in the anterograde trafficking of lysosomes, a process that involves its interaction with Myosins (Reddy et al., 2001; Trojani et al., 2024). This interaction facilitates the movement of lysosomes toward the cell periphery, enabling their docking and fusion with the plasma membrane. As a result of this fusion, lysosomal contents are secreted extracellularly, and LAMP1 becomes transiently exposed at the cell surface, a feature that is frequently utilized as a surface marker for detecting lysosomal exocytosis (Laulagnier et al., 2011; Andrews, 2017).

Beyond membrane repair, lysosomal exocytosis contributes to diverse biological processes including bone resorption by osteoclasts, melanosome secretion, neurite outgrowth, immune defense, and antigen presentation (Brozzi et al., 2013; Anding & Baehrecke, 2017; Galluzzi et al., 2018; Oyarzún et al., 2019; de Araujo et al., 2020). It also underpins several non-classical secretion pathways. Organelles traditionally destined to deliver cargo for lysosomal degradation, such as endosomes and autophagosomes, can be rerouted to the plasma membrane to release their contents, enabling processes such as exosome secretion and secretory autophagy (Maxfield & McGraw, 2004; Braulke & Bonifacino, 2009) These alternative pathways are not merely disposal mechanisms but are increasingly appreciated as means of intercellular communication, modulating immune surveillance and extracellular signalling (Idone, Tam, Goss, et al., 2008; Medina et al., 2011; Ballabio & Bonifacino, 2020). With regards to stress, recent reports indicated that low levels or oxidative stress stimulated lysosomal exocytosis, but inhibited it at high levels, as well as the triggering of lysosomal exocytosis upon irradiation of cells with UVA (Appelqvist et al., 2013; Ravi et al., 2016).

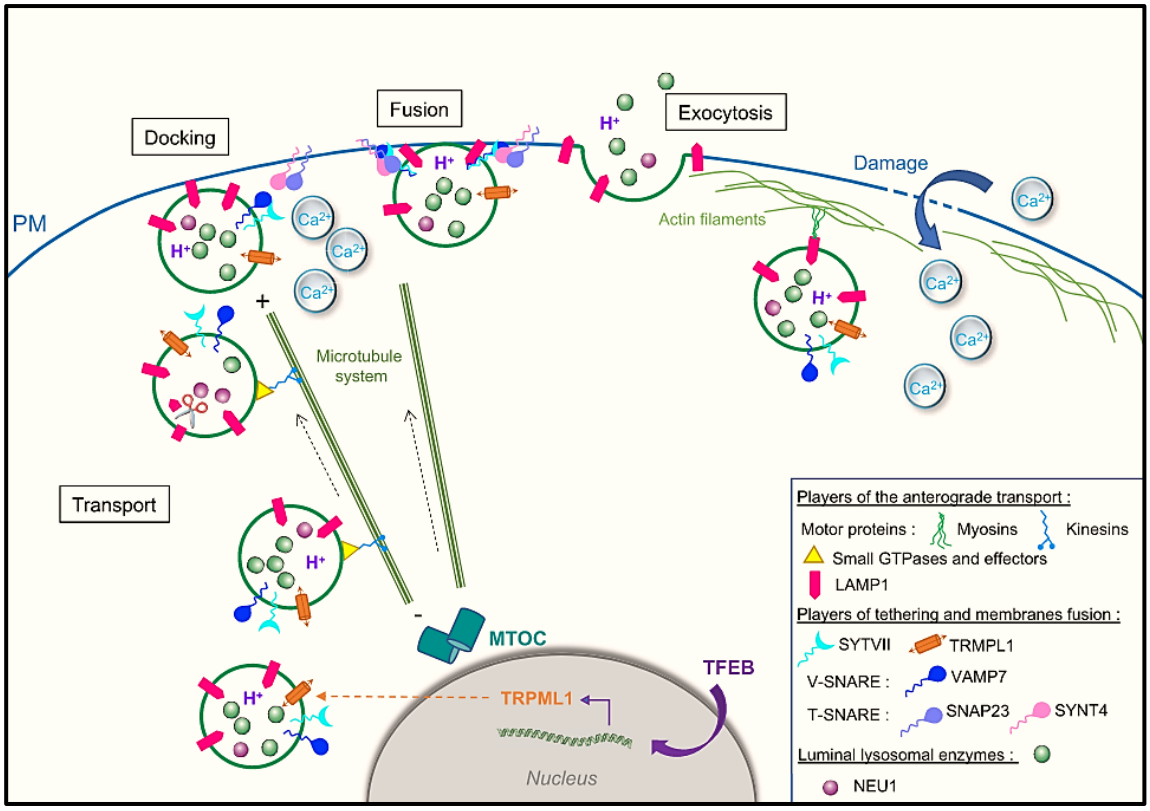

Fig.1.7: Simplified schematic representation of molecular steps leading to lysosomal exocytosis. Lysosomal exocytosis involves several key steps. First, lysosomes move from the centre of the cell toward the plasma membrane using the microtubule network. Then, LAMP1 helps them dock and fuse with the plasma membrane. A rise in Ca^{2+} levels trigger a conformational change in SYT VII, allowing it to interact with SNARE proteins (VAMP7, SNAP23, Syntaxin4) that drive the fusion of lysosomes with the plasma membrane. This leads to the release of lysosomal contents outside the cell and the appearance of LAMP1 on the cell surface. The process can be limited by NEU1, an enzyme that removes sugars from LAMP1 and thereby prevents efficient docking. Adapted from Trojani et al., (2024).

Altogether, lysosomal exocytosis exemplifies a key intersection between degradation and secretion, contributing to both cellular protection and functional plasticity in response to environmental cues.

1.4 Modulation of clathrin-mediated endocytic flux by stress conditions.

Previous studies have reported that environmental stressors have the capacity to modulate bulk endocytic pathways, including CME, macropinocytosis, and caveolar endocytosis, although to-date there are very few studies that focus on bulk endocytic effects upon stress conditions (López-Hernández, et al., 2020). Adjusting bulk endocytic flux of surface proteins would serve to non-selectively upregulate or downregulate the dynamic internalization of various cargos in response to an environmental stressor. For example, increased bulk endocytosis could boost nutrient intake to improve the cell's resilience, while less bulk endocytosis might help the cell to preserve energy that can be used for other more important processes.

Among the different modes of endocytosis, CME has been the most studied, also because CME has been attributed to be responsible for more than 95% of all endocytic bulk uptake (Bitsikas et al., 2014).

Acute hyperosmotic and oxidative stress have both been shown to rapidly inhibit CME in human cells. In particular, hyperosmotic stress has been extensively studied and is associated with a marked reduction in the uptake of canonical CME cargos such as transferrin and LDL. This impairment has been further corroborated by altered clathrin-coated pit dynamics, including reduced pit formation and impaired vesicle scission, suggesting a broad suppression of CME progression under osmotic imbalance (Hansen, 1993; X. Wu et al., 2001; S. Wang et al., 2011; López-Hernández, Haucke, et al., 2020).

Similarly, although less comprehensively characterized, acute oxidative stress has also been reported to interfere with CME function (Thibaut-Vercruyssen et al., 1992; Malorni et al., 1993; Cheng & Vieira, 2006; Parry et al., 2008; Volpert et al., 2017; López-Hernández, Haucke, et al., 2020). Some studies documented that relatively short exposures to oxidative stress either decreased cargo internalization, provoked potential alterations in the activity or recruitment of key endocytic regulators like HSC70, caused dynamin impairment following reactive oxygen species exposure, or found that ceramide-triggered oxidative imbalance inhibited CME.

In contrast, despite the relevance of heat as a physiological and pathological stressor, there is a notable lack of direct studies addressing how acute thermal stress affects CME in human cells (López-Hernández, Haucke, et al., 2020). This gap highlights the need for further investigation to determine whether heat stress elicits similar disruptions in endocytic trafficking as observed with other stress modalities.

1.5 Stress-induced modulation of the uptake of specific cargo proteins upon osmotic or oxidative insults

Most of the studies focus on an individual cargo and how its internalization is affected by a specific stressor. Here are some examples of specific changes in individual membrane protein surface levels upon osmotic and oxidative stress and their proposed function:

- **GLUT4:** Physiologically, hyperosmolarity is often caused by elevated blood glucose levels, a state called hyperglycemia, which influences endocytosis. Similar to insulin, an acute stimulus consisting of 10 min hyperosmotic stress was seen to reduce AP-2-mediated endocytosis of the glucose transporter GLUT4 in muscle cells, leading to its accumulation at the cell surface, thereby promoting glucose uptake from the blood (D. Li et al., 2001).
- **AQP2:** In kidney epithelial cells, 10-30 min of hyperosmotic conditions were shown to reduce the internalization of aquaporin-2 (AQP2), resulting in increased surface expression of the channel (Hasler et al., 2008). This adaptation supports transcellular water movement, which may help the cell withstand hypertonic stress.
- **NHE7:** Under normal conditions, the Na^+/H^+ exchanger NHE7 is primarily localized to intracellular compartments such as endosomes and the trans-Golgi network. However, upon hyperosmotic shock, it accumulates at the plasma membrane. This redistribution is also observed when CME is inhibited, suggesting that NHE7 is normally subject to constitutive internalization. Importantly, the surface localization of NHE7 under hypertonic stress supports cell survival. By modulating ion homeostasis, NHE7 triggers the activation of the transcription factors TFEB and TFE3, which in turn enhance the

biogenesis of autophagosomes and lysosomes, strengthening the cell's degradative and recycling capacity during stress. This adaptive response helps to clear aggregated proteins that accumulate under osmotic challenge and promotes cellular resilience (López-Hernández, Puchkov, et al., 2020) (Fig. 1.8). The precise mechanisms by which hypertonic stress suppresses CME of NHE7 remain to be elucidated.

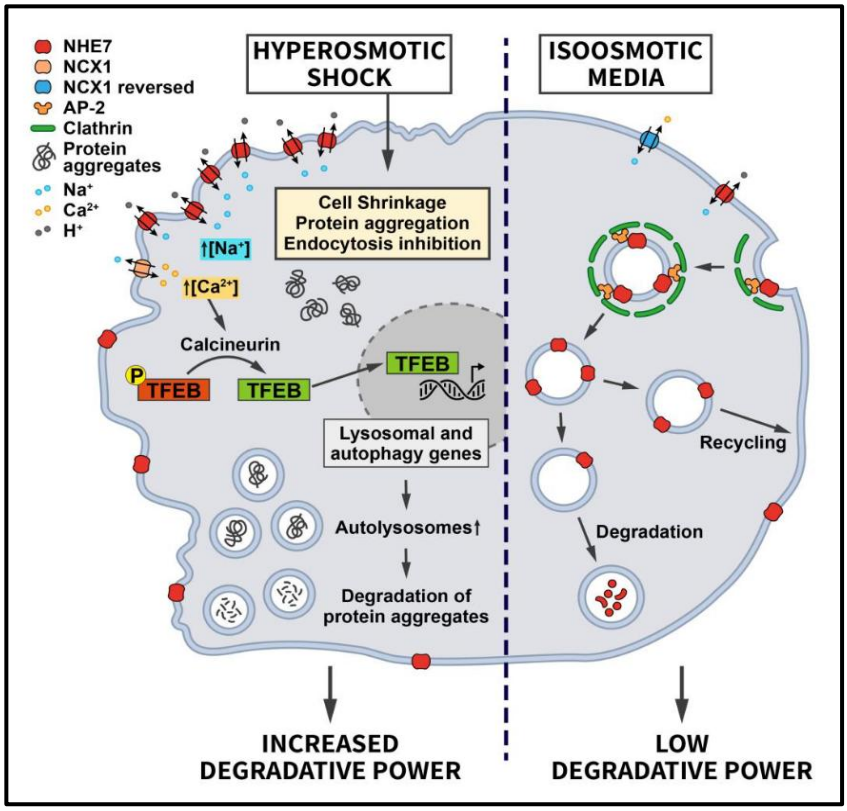

Fig.1.8: Osmotic stress regulates NHE7 endocytosis and downstream adaptive signalling. Under iso-osmotic conditions, NHE7 is continuously internalized via CME, limiting its surface activity. Hyperosmotic stress inhibits NHE7 endocytosis, increasing its presence at the plasma membrane. This enhances Na^+ influx, triggering Ca^{2+} entry via NCX1, activation of calcineurin, and dephosphorylation of TFEB. Activated TFEB promotes lysosomal and autophagy gene expression, enhancing cellular clearance mechanisms to combat stress-induced protein aggregation (López-Hernández, Haucke, et al., 2020).

- **Mrp2 and Bsep**: In hepatocytes, ROS promote the internalization of apical membrane transporters such as the multidrug resistance-associated protein 2 (Mrp2) and the bile salt export pump (Bsep) (B. Ji et al., 2004; Sekine et al., 2008; Basiglio et al., 2014), both critical for bile secretion. This enhanced endocytosis is thought to result from ROS-induced disruption of the actin cytoskeleton, likely mediated by altered Ca^{2+} homeostasis and activation of protein kinase C (PKC). Notably, the application of exogenous bilirubin—a known antioxidant—can reverse these effects, stabilizing the actin network and restoring surface levels of Mrp2 and Bsep (Basiglio et al., 2014), thereby protecting against hepatobiliary dysfunction under oxidative stress.
- **EGFR and lectin receptor:** Elevated ROS were shown to inhibit EGFR and lectin receptor endocytosis in fibroblasts, likely by preventing their ubiquitination (De Wit et al., 2001).

1.6 From stress sensing to survival: The cellular response to environmental challenges.

Since cells are constantly exposed to a wide range of environmental stressors that threaten their homeostasis and survival, they need to counteract these potentially harmful conditions. The importance of these adaptive responses is highlighted by the fact that proteins involved in cellular stress responses represent the most highly conserved amongst all organisms (Kültz, 2003).

Among the most common environmental stressors are nutrient deprivation, changes in oxygen or CO_2 saturation (e.g. hypoxia and hypercapnia, respectively), osmotic imbalance, oxidative stress, heat stress, and exposure to toxins or heavy metals.

For instance, nutrient scarcity, such as glucose or amino acid limitation, triggers cellular energy-sensing pathways like AMPK and mTOR, promoting catabolic processes including autophagy to maintain energy production (Ebner et al., 2023). Hypoxia, a condition of low oxygen availability often encountered in tumours or ischemic tissues, activates hypoxia-inducible factors (HIFs) that drive transcriptional programs to enhance anaerobic metabolism and angiogenesis (Ratcliffe, 2013). Toxic insults, including heavy metals such as cadmium or mercury, or xenobiotics, can interfere with protein function, redox balance, or DNA integrity, therefore cells mount detoxification responses, such as metallothionein expression or activation of the unfolded protein response (UPR), to mitigate these threats (Koyama et al., 2024).

Having evolved such sophisticated molecular mechanisms that enable stress detection, signal transduction, and activation of protective responses, these adaptive programs aim to restore homeostasis or, if damage is irreparable, initiate programmed cell death to prevent further harm to the organism.

In the following passages, I will explore in more detail the stress conditions that will be the focus of this project: osmotic stress, heat stress and. oxidative stress.

1.6.1 Cellular mechanisms underlying hyperosmotic stress response.

Under normal physiological conditions, mammalian cells are protected from substantial fluctuations in environmental osmolality due to systemic homeostatic regulation. For instance, in humans the normal plasma osmolality of 290 mOsm/kg H_2O is typically maintained within a narrow range (±2-3%) by renal control of fluid and electrolyte balance (R. J. Ellis, 2001; Ho, 2006; Neuhofer, 2010). However, certain tissues are naturally exposed to highly hyperosmotic environments, reaching up to 1500 mOsm/kg H_2O in the renal medulla during antidiuresis, creating a unique challenge for cellular homeostasis (Go et al., 2004; Neuhofer, 2010) (Fig. 1.9 A).

Water, beyond acting as a solvent, functions as a crucial reactant influencing a broad spectrum of biochemical reactions. Its intracellular concentration is finely tuned, and any deviation can significantly disrupt molecular interactions, enzymatic activities, and protein structure through changes in hydration. Experimental approaches using inert osmolytes to manipulate water activity have confirmed the sensitivity of various biochemical processes, such as ion channel gating, DNA and protein binding, and enzyme function, to subtle shifts in water availability (Rand, 2004). Consequently, cells must preserve intracellular water content within strict limits to maintain proper biochemical function and structural organization.

Osmosis, or the passive diffusion of water across semi-permeable membranes like the plasma membrane, is driven by solute concentration gradients. This process is facilitated by aquaporin channels and is particularly influenced by membrane-impermeable solutes, or osmolytes, which create osmotic gradients that draw water out of the cell under hypertonic conditions (King et al., 2004). The resulting water efflux causes cell shrinkage, increased macromolecular crowding, elevated intracellular ionic strength, and disruption of subcellular architecture). If uncompensated, these changes impair cellular processes and can culminate in apoptotic cell death. amongst others (Ho, 2006; Neuhofer, 2010; López-Hernández, Haucke, et al., 2020) (Table 2). The brain is particularly sensitive to shifts in osmotic balance, with hyperosmotic stress linked to various neurological disorders. In glial cells, it serves as a strong trigger for protein aggregation and has been implicated as a contributing factor in osmotic demyelination syndrome (López-Hernández, Haucke, et al., 2020).

Table 2. Pleiotropic effects of hypertonic stress on cell function. Adapted from Ho, (2006)

Effect	References
DNA damage	Kultz and Chakravarty (2001); Dmitrieva et al. (2004)
Inhibition of DNA repair	Dmitrieva et al. (2004)
Induction of p53	Dmitrieva et al. (2001a,b)
Cell cycle arrest	Michea et al. (2000); Alexander et al. (2001); Belli et al. (2001); Dmitrieva et al., (2001b); Escote et al. (2004)
Disruption of mitochondrial function	Desai et al. (2002); Copp et al. (2004)
Dissociation of protein from chromatin	Proft and Struhl (2004)
Alteration in cytoskeletal architecture	Di Ciano et al. (2002)
Induction of secondary oxidative stress	Zhang et al. (2004)
Inhibition of growth factor-dependent signaling	Copp et al. (2004)
Inhibition of mTor pathway	Copp et al. (2004); Fumarola et al. (2004)
Inhibition of protein translation; polysome disaggregation	Morley and Naegele (2002); Naegele and Morley (2004)
Apoptosis	Dmitrieva et al. (2001b); Copp et al. (2004)

To counteract osmotic imbalance, cells initiate a two-phase response: an immediate and a delayed adaptation (Ho, 2006; Neuhofer, 2010) (Fig. 1.9 B):

1) The **immediate response** comprises intracellular signalling and occurs within seconds of hyperosmotic exposure. It involves the uptake of inorganic ions such as Na^+, K^+, and Cl^- through pre-existing ion transporters, including the $Na^+/K^+/2Cl^-$ cotransporter, Na^+/H^+ exchanger, and Cl^-/HCO_3^- exchanger. This regulatory volume increase restores cell volume but results in elevated intracellular ionic strength, which is incompatible with long-term cellular function. Consequences include an increase in macromolecular crowding and alterations in subcellular architecture.

2) The **delayed adaptive response** is mediated through the transcription of genes involved in the synthesis and uptake of small uncharged organic osmolytes that can accumulate intracellularly in the range of >500 mmol/l without perturbing biochemical processes. These include sorbitol, myoinositol, and betaine, taurine, alanine. This adaptive osmolyte accumulation maintains osmotic balance while avoiding the detrimental effects of ionic overload.

A central regulator of the mammalian delayed adaptive response is the transcription factor **NFAT5** (nuclear factor of activated T-cells 5), originally designated tonicity enhancer binding protein or TonEBP (Miyakawa et al., 1999). The increased intracellular ionic strength produced by the immediate response is directly sensed by its N-terminal transactivation domain (Ferraris et al., 2002; Neuhofer et al., 2002). It has been reported that the activity of the latter directly correlates with extracellular osmolality (Ferraris et al., 2002).

NFAT5 activates the expression of genes harbouring tonicity-responsive enhancer elements (TonE) in their promoters. These genes encode enzymes and transporters that facilitate osmolyte accumulation, as well as protective proteins like HSP70, which support protein folding under hypertonic conditions. NFAT5 activity is modulated by several mechanisms: sensing of intracellular ionic strength by its N-terminal domain, phosphorylation by kinases such as p38, Fyn, ATM, and PKA, and nuclear translocation, and homodimer formation, all of which contribute to its transcriptional activation under hypertonic stress (Ho, 2006; Neuhofer, 2010) (Fig. 1.9 B).

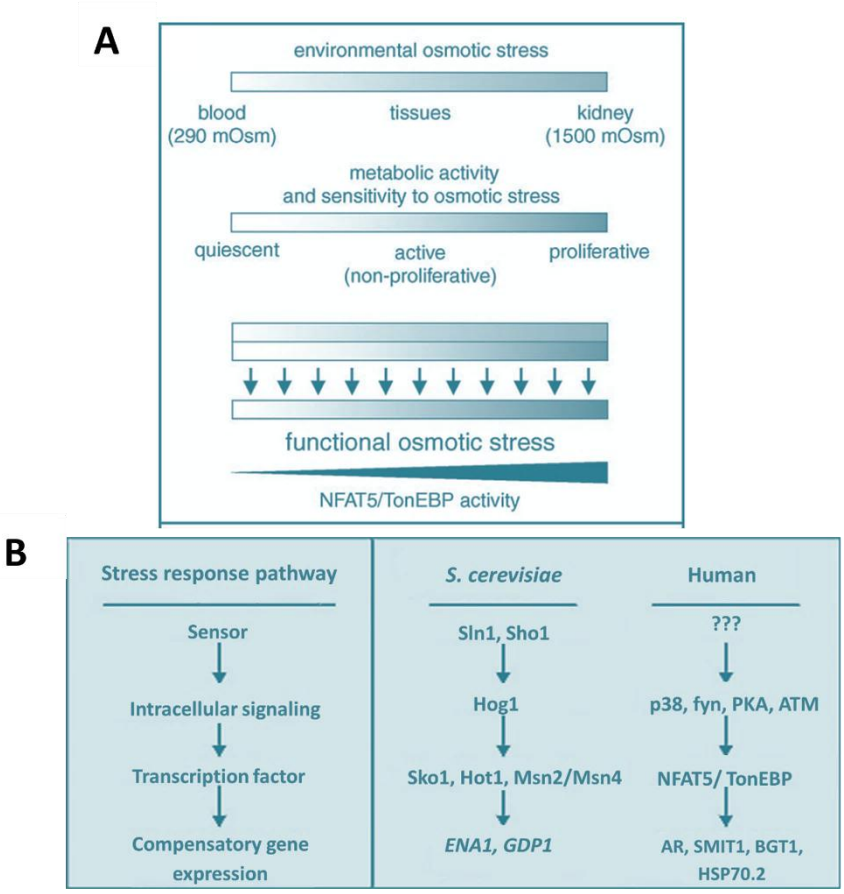

Fig 1.9: Cellular hyperosmotic stress and the adaptive response.
A) Functional osmotic stress in tissues arises from a combination of extracellular osmolality and intrinsic cellular metabolic activity. In humans, extracellular osmolality varies from ~290 mOsm in the blood to over 1,500 mOsm in the renal medulla under antidiuretic conditions. Some non-renal tissues like spleen or liver

can also reach higher osmolality values (~350 mOsm). Cells with higher metabolic activity, such as activated lymphocytes, are more vulnerable to disruptions in water balance, particularly in hyperosmotic environments, as their demand for biochemical stability is greater. Thus, both extracellular and intracellular factors determine the level of osmotic stress experienced by a cell. B) The osmotic stress response is a conserved adaptive program initiated upon detection of changes in extracellular conditions. While yeast rely primarily on the Hog1 MAP kinase pathway, mammalian cells employ a broader network of kinases, including p38, Fyn, PKA, and ATM, to regulate gene expression via the transcription factor NFAT5. These signalling cascades enable cells to adjust osmolyte composition, maintain volume, and protect macromolecular function. Despite advances, the precise osmotic sensing mechanisms in mammalian cells remain to be fully elucidated. Adapted from Ho, (2006)

As we know, cellular metabolic activity ranges widely, going from low levels in quiescent cells like naïve lymphocytes, to moderate levels in metabolically active but non-proliferative cells such as hepatocytes or renal tubular epithelial cells, to very high levels in rapidly dividing cells like activated lymphocytes. Accordingly, the extent to which a cell experiences functional osmotic stress and relies on osmoadaptive responses and therefore expresses NFAT5/TonEBP likely depends not only on fluctuations in extracellular osmolality but also on its intrinsic metabolic state (Fig. 1.9 A). Both factors influence intracellular water balance. For example, a cell with low or moderate metabolic activity located in a hyperosmotic environment (e.g. those found in the renal medulla) is especially susceptible to perturbations in water homeostasis (Ho, 2006).

While the upstream sensors of osmotic changes in mammalian cells remain incompletely defined (Fig. 1.9 B), the involvement of NFAT5 in systemic pathologies such as salt-sensitive hypertension underscores its physiological relevance. For instance, chronic high salt intake leads to hypertonic sodium storage in skin interstitial tissues, where it is detected by macrophages. These immune cells then activate NFAT5-driven pathways, contributing to inflammatory and hypertensive responses, thereby linking local osmotic stress to systemic cardiovascular dysfunction (Lifton et al., 2001).

Together, these findings underscore the importance of tightly regulated water and osmolyte homeostasis for cellular viability. The ability of cells to detect and respond to osmotic stress, particularly through rapid ion transport and NFAT5-mediated osmolyte management, constitutes a fundamental adaptive strategy for preserving biochemical integrity in the face of fluctuating extracellular conditions.

Beyond disrupting the plasma membrane, osmotic stress alters intracellular ionic strength and macromolecular crowding. Increasing evidence points to a role for **biomolecular condensates**: membraneless, phase-separated compartments whose physical state depends on environmental conditions and can rapidly undergo phases transitions (e.g., from liquid to solid) to reach more energetically desirable states (Banani et al., 2017).

Recent work by (Watanabe et al., 2021) identified apoptosis signal-regulating kinase 3 (ASK3) as a biomolecular condensate-forming protein that is phosphorylated under hypoosmotic stress but dephosphorylated and inactivated during hyperosmotic stress via liquid-liquid phase separation (LLPS). ASK3 droplet liquidity is maintained by poly(ADP-ribose) (PAR), which is essential for this inactivation. These advances demonstrate that cells recognize osmotic stress through LLPS of ASK3 with the help of PAR.

On the other hand, NHE7, for example, represents a novel type of component of the osmotic stress response, operating through mechanisms that are independent of transcriptional regulation. Rather

than being driven by changes in gene expression, its regulation under hyperosmotic conditions reflects rapid post-translational events and trafficking dynamics (López-Hernández, Puchkov, et al., 2020). This positions NHE7 as a potentially fast-acting mediator of cellular adaptation, capable of modulating ion homeostasis and downstream signalling within minutes. Beyond this example, however, relatively little is understood about how cells exploit changes in endocytic trafficking as part of their broader osmotic stress response, representing an important but underexplored area of research.

1.6.2 The heat shock response and proteostasis in cellular stress adaptation

The heat shock response (HSR) is an ancient and highly conserved molecular response that plays a critical role in protecting essential biosynthetic functions, including DNA repair, protein folding, and clearance of damaged proteins, from acute insults such as elevated temperatures, oxidative stress, and heavy metal exposure, as well as chronic challenges like the accumulation of aggregation-prone proteins seen in aging and protein misfolding diseases (Åkerfelt et al., 2010; Kim et al., 2011; Mahat et al., 2016).

The HSR is a central component of the broader proteostasis network (PN), a dynamic system that monitors the functional state of the proteome by regulating protein folding, trafficking, and degradation. The PN comprises molecular chaperones and protein clearance systems such as the ubiquitin-proteasome and autophagy pathways (Morimoto, 2011). Together with compartment-specific unfolded protein responses (UPRs), it senses imbalances in protein homeostasis and coordinates adaptive responses to restore proteome stability (Ron & Walter, 2007; Koyama et al., 2024). Stressors or mutations that disrupt protein folding pose a significant challenge to this system. Over time, especially during aging, the cumulative burden of damaged or misfolded proteins may overwhelm the PN, contributing to proteostatic collapse and the pathogenesis of neurodegenerative, metabolic, and malignant diseases.

Activation of the HSR serves as a frontline defense against such proteotoxic stress. This response rapidly induces the expression of heat shock proteins (HSPs), which function as molecular chaperones to stabilize folding intermediates, refold misfolded proteins, and prevent aggregation (Kim et al., 2011). The transcriptional regulation of HSPs is governed by a conserved family of heat shock transcription factors (HSFs), primarily HSF-1, functionally conserved from yeast to humans.

Upon sensing temperature stress (Hentze et al., 2016), monomeric HSF-1 undergoes trimerization and translocates to the nucleus, where it binds to heat shock elements (HSEs) in the promoters of target genes, driving transcriptional upregulation of chaperones in proportion to the intensity and duration of the stress signal (Åkerfelt et al., 2010) (Fig. 1.10).

HSF-1 is maintained in an inactive state through transient interactions with chaperones such as Hsp70, Hsp90, and Hsp40 (Åkerfelt et al., 2010; Hentze et al., 2016). Under stress, these chaperones are titrated away by the appearance of unfolded proteins, releasing HSF-1 to activate the HSR. As part of a negative feedback loop, the increased expression of Hsp70 and Hsp90 eventually reins in HSF-1 activity to avoid excessive chaperone production. In addition to transcriptional control, the HSR is fine-tuned at the post-transcriptional and translational levels, including regulation of mRNA stability and selective translation of heat shock transcripts (Morimoto, 2011).

Importantly, the efficiency of the HSR is modulated by the cell's metabolic and nutritional state. For example, intracellular NAD^+ levels, which are linked to energy availability, can influence HSR activity, implying that it can protect organisms from obesity by regulating their energy expenditure (Ma et al., 2015). Despite its potency in protecting against acute proteotoxic stress, the HSR often becomes attenuated in chronic stress states or with aging, raising the question of why this otherwise robust system fails to confer protection in diseases marked by persistent protein misfolding and aggregation (Morimoto, 2011).

All in all, the HSR is critical for survival of all organisms. However, its scope, extent, and its molecular mechanism of regulation are still poorly understood, and more research is needed to elucidate its mysteries. Recent reports have found a link between heat shock proteins and a modulation of CME (Vega et al., 2010), which constitutes a new paradigm for the crosstalk between HSR and endocytic mechanisms.

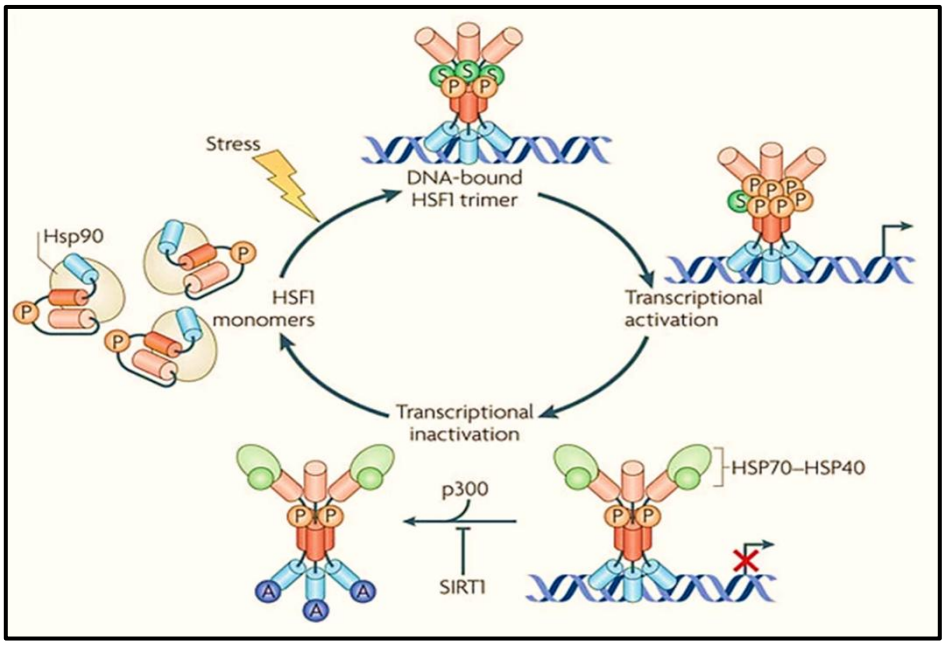

Fig. 1.10: The HSF1 activation and attenuation cycle.
In the resting state, HSF1 is a monomer and already phosphorylated under non-stress conditions, while interacting with HSP90. Upon stress, HSF1 dissociates from HSP90 and allows HSF1 to trimerize and bind to the heat shock elements (HSEs) in HSP genes. Several PTMs, such as phosphorylation and sumoylation, assist in regulating HSF1 transactivation capacity. HSF1 acquires transcriptional activity, which is abrogated during the attenuation phase. Attenuation involves negative feedback from HSPs, which represses the transactivation of DNA-bound HSF1, and inhibition of DNA binding. SIRT1 mediates the attenuation phase by preventing HSF1 acetylation. Adapted from Åkerfelt et al., (2010)

1.6.3 Oxidative stress: principles and cellular implications

Oxidation-reduction (redox) homeostasis, like pH control, is essential for sustaining life. Redox reactions are deeply integrated into nearly all vital cellular processes, including energy production and metabolic regulation. Importantly, cells do not maintain a single uniform redox state; instead, distinct cellular and extracellular compartments exhibit diverse redox conditions, each finely tuned to their specific functional and physiological contexts (Sies et al., 2017).

The definition of "oxidative stress" derives from a situation when the balance between oxidants and antioxidants is disrupted in favour of oxidants, leading to the impairment of redox signalling

or direct damage to vital biomolecules such as DNA, proteins, and lipids. This concept is foundational to understanding how cells respond to environmental and metabolic stress and how such responses can lead to either adaptive outcomes or pathological consequences (Burton & Jauniaux, 2011; Sies et al., 2017).

At the core of oxidative stress is the generation of reactive oxygen species (ROS), which include superoxide anion (O_2^-), hydrogen peroxide (H_2O_2), hydroxyl radicals (•OH), and organic peroxides. These molecules are primarily by-products of normal cellular respiration, particularly within the mitochondrial electron transport chain, where incomplete reduction of oxygen leads to electron leakage, notably from complexes I and III (Cadenas & Davies, 2000). Additionally, the endoplasmic reticulum (ER) contributes significantly to ROS production during oxidative protein folding, particularly in cells with high secretory activity or under ER stress conditions (B. P. Tu & Weissman, 2004).

While ROS are often seen as harmful, at low to moderate concentration they serve crucial physiological functions. The biological impact of ROS thus depends on their concentration, duration of exposure, and the cellular context, illustrating that oxidative stress is not a binary condition but rather a spectrum that ranges from physiological signalling to harmful stress (Burton & Jauniaux, 2011).

Beyond ROS, several other classes of reactive molecules play key roles in redox biology and contribute to oxidative stress (though to a lesser extent than ROS). These include: 1) reactive nitrogen species (RNS), such as nitric oxide, nitrogen dioxide (both free radicals), peroxynitrite, and nitrite/nitrate, 2) reactive sulfur species (RSS) encompassing various sulfur-containing molecules, including modified forms of cysteine and methionine, as well as small thiol compounds like glutathione, trypanothione, and mycothiol, 3) reactive carbonyl species (RCS) consisting mainly of metabolically derived aldehydes and excited-state (triplet) carbonyls, 4) reactive selenium species (RSeS) including low-molecular-weight selenium compounds, along with selenium-containing amino acids such as selenocysteine and selenomethionine found in proteins (Sies et al., 2017).

The concept of "redox tone" extends beyond a simple oxidant-antioxidant dichotomy. Just as each cellular compartment has an optimal pH, it also maintains specific redox environments. These include peroxide tone, carbonyl tone, and sulfide tone, which reflect the finely tuned balances of ROS, reactive carbonyl species, and thiols, respectively. For instance, the ratio of reduced to oxidized glutathione (GSH/GSSG) or the redox potential of this couple can directly influence processes like platelet activation and protein glutathionylation (Jones, 2008; Sies et al., 2017).

Consequently, in order to maintain redox homeostasis cells are equipped with elaborate antioxidant defense systems. These are broadly classified into enzymatic and non-enzymatic components:

- The **enzymatic defenses** include superoxide dismutase (SOD), which converts superoxide to hydrogen peroxide; catalase, which decomposes hydrogen peroxide into water and oxygen; and glutathione peroxidase (GPx), a selenium-dependent enzyme that uses reduced glutathione (GSH) to detoxify peroxides. Glutathione itself is a major cellular redox buffer synthesized in the cytosol and recycled via glutathione reductase using NADPH as an electron donor. Thioredoxin (Trx) and its reductase counterpart (TrxR) further participate in detoxifying peroxides and maintaining disulfide bond integrity.

- **Non-enzymatic antioxidants** include small molecules like ascorbate (vitamin C), tocopherol (vitamin E), and thiol compounds, which synergize with enzymatic systems to scavenge free radicals.

1.6.3.1 Oxidative stress sensing modules

A key regulatory axis in oxidative stress sensing and response is the **Keap1–Nrf2–ARE pathway**. Under normal conditions, the transcription factor Nrf2 (nuclear factor erythroid 2-related factor 2) is bound to its cytoplasmic inhibitor Keap1, which targets it for ubiquitination and proteasomal degradation (W. Tu et al., 2019; S et al., 2021) (Fig. 1.11).

However, upon oxidative or electrophilic stress, specific cysteine residues on Keap1 are modified, disrupting its interaction with Nrf2. Stabilized Nrf2 accumulates, translocates into the nucleus, dimerizes with small Maf proteins, and binds to antioxidant response elements (ARE) in the promoters of target genes (W. Tu et al., 2019; S et al., 2021; Thiruvengadam et al., 2021). This triggers the expression of a wide array of antioxidative and cytoprotective genes, including those coding for heme oxygenase-1, NAD(P)H quinone dehydrogenase 1, GSH synthesis enzymes, SOD, catalase, and phase II detoxifying enzymes (Liu et al., 2017; Loboda et al., 2016).

The Nrf2 pathway is further modulated by autophagy-related proteins such as p62, which can sequester Keap1 and enhance Nrf2 activity, creating a feedback loop that links oxidative stress to protein quality control mechanisms. Kinases such as protein kinase C (PKC), MAPKs (ERK, JNK, p38), and PERK can also phosphorylate Nrf2, influencing its stability and transcriptional activity (Thiruvengadam et al., 2021). Beyond oxidative stress responses, Nrf2 is involved in regulating inflammation, autophagy, and metabolic adaptation, with its expression subject to epigenetic regulation via DNA methylation, histone modifications, and microRNAs (Guo et al., 2015).

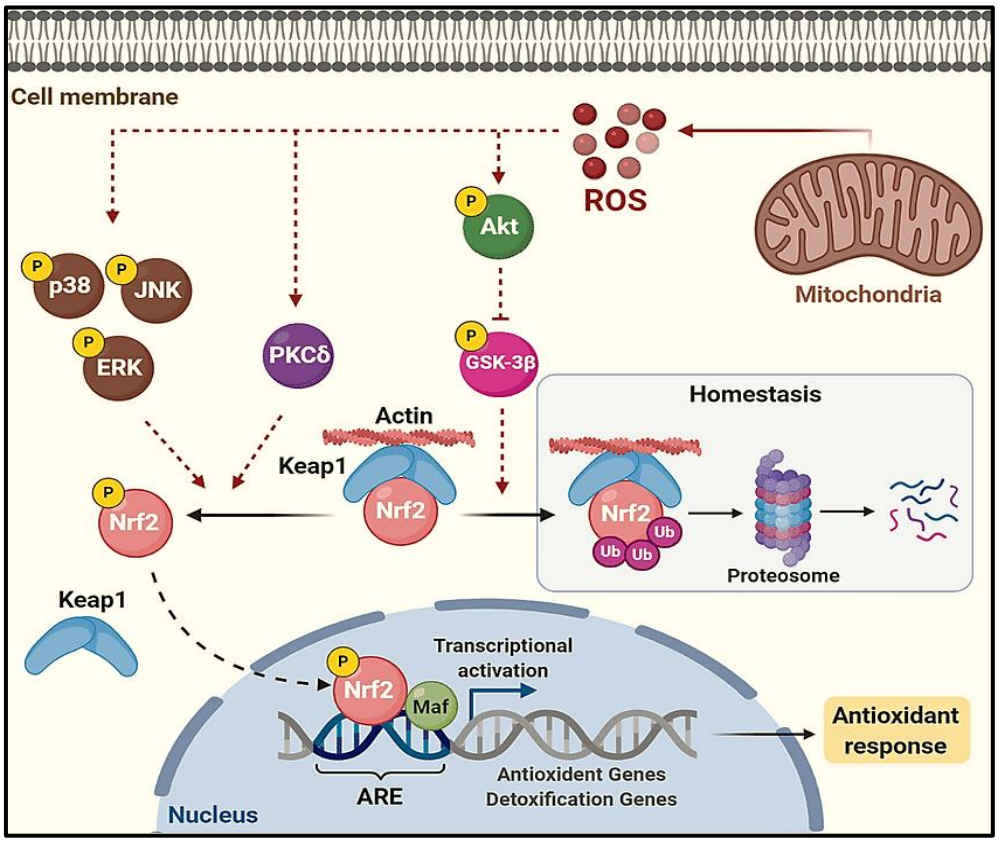

Fig. 1.11: Nrf2/Keap1/ARE mechanism in oxidative stress.
Under normal conditions, Nrf2 is bound by Keap1 in the cytoplasm, leading to its continuous degradation via the proteasome. However, during oxidative stress, high levels of ROS activate several pathways, including Akt/PI3K, PKCδ, and MAPKs such as p38, JNK, and ERK. These pathways promote the release of Nrf2 from the Keap1 complex, allowing it to accumulate and move into the nucleus. Once there, Nrf2 binds to ARE in the DNA, initiating the expression of antioxidant genes and enhancing the cellular antioxidant defense mechanisms. Adapted from Rahman et al., (2021).

Another major redox-sensitive transcription factor is **NF-κB** (nuclear factor kappa-light-chain-enhancer of activated B cells), which plays a central role in inflammation and immune responses (Burton & Jauniaux, 2011; Sies et al., 2017).

In resting cells, NF-κB is held inactive in the cytoplasm by its inhibitor IκB. Oxidative stress leads to the phosphorylation and degradation of IκB, allowing NF-κB to translocate into the nucleus and activate pro-inflammatory genes. ROS can both stimulate and inhibit NF-κB activity, depending on their subcellular localization and intensity. For example, nuclear ROS levels can modulate the activity of nuclear thioredoxin (Trx1), which enhances NF-κB DNA binding, while excess H_2O_2 may impair NF-κB function (Hirota et al., 1999; Halvey et al., 2007).

It is important to keep in mind that oxidative stress rarely acts in isolation but intersects with other forms of cellular stress. Mitochondrial and ER stress are often interconnected via calcium signalling and energy homeostasis. For example, the unfolded protein response of the ER is activated under conditions that challenge protein folding capacity. It attempts to restore homeostasis by halting global protein synthesis, enhancing chaperone expression, expanding ER membrane structures, and promoting degradation of misfolded proteins. If these efforts fail, prolonged ER stress can lead to apoptosis through pathways involving C/EBP homologous protein and caspase activation.

In summary, oxidative stress is a dynamic and multifaceted condition that influences virtually all aspects of cellular physiology. While moderate ROS levels are essential for normal signalling, excess or mismanaged ROS can lead to significant cellular damage. The balance between ROS generation and detoxification, mediated by key players like the Nrf2/Keap1/ARE and NF-κB pathways, determines whether cells adapt to stress or succumb to injury. Understanding these mechanisms provides a framework for exploring oxidative stress-related diseases and for developing therapeutic strategies that target redox homeostasis.

From what we have read about the three stress conditions, we can conclude that in all of them the research on the sensing and effector mechanisms to modulate them are based on cytoplasmic/ translational regulation of proteins, whereas currently we have little knowledge of players upstream of the cascade, such as plasma membrane first responders. There is clearly a gap that exists in this regard that would be most interesting to close.

1.7 Aims

The preceding sections have highlighted the remarkable complexity and functional diversity of the cell surface proteome, which plays a central role in mediating the cell's interactions with its environment and maintaining internal homeostasis. Over 5,000 human transmembrane proteins are predicted to localize to the plasma membrane (Bausch-Fluck et al., 2018) , where they form a highly specialized and dynamic interface with the extracellular milieu. The biomedical relevance of this interface is underscored by the observation that more than 66% of all approved drugs listed in the DrugBank database target plasma membrane proteins (Z. Hu et al., 2021).

Despite this striking significance, the functional roles of only a fraction of the predicted surfaceome have been elucidated. Among the primary mechanisms modulating the composition of the surface proteome is CME, which is essential for basic cellular functions and becomes particularly crucial when cells are exposed to physiological stress. Under such conditions, cells activate diverse stress response pathways that can determine survival or death, and CME likely contributes as an early and adaptable regulatory mechanism in this context.

Yet, surprisingly little is known about how stress conditions impact the plasma membrane proteome or the regulatory mechanisms driving stress-induced endocytic remodelling. Current limitations in the field include: (1) a scarcity of identified stress-responsive signalling cascades linked to endocytosis (with few exceptions, such as the p38 pathway); (2) a lack of studies evaluating bulk endocytic activity under stress; and (3) a predominant focus on single cargo proteins rather than the broader surface proteome.

Building upon the pioneering work of López-Hernández et al. (2020), who demonstrated a stress-responsive endocytic adaptation involving NHE7 at the plasma membrane, this thesis aims to extend the understanding of how stress modulates endocytosis and surface protein composition. The specific objectives of this work are to:

1. **Uncover global changes in surface protein internalization** in response to defined physiological stressors using unbiased surface proteome labelling.
2. **Identify and validate specific surface proteins** whose endocytic trafficking is significantly altered upon stress exposure.
3. **Investigate the functional significance of these changes** by probing whether differential endocytosis of specific proteins contributes to cellular adaptation and survival under stress.
4. **Elucidate the underlying driver mechanisms** for such stress-dependent modulation of the selected proteins.

Through this integrative and systematic approach, this thesis seeks to advance our understanding of membrane proteome dynamics under stress and lay the groundwork for therapeutic strategies targeting stress-related cellular dysfunction.

2. Materials

2.1 Chemicals and reagents

Chemical / reagent	Manufacturer, catalog no.
1,4-dithiothreitol (DTT)	Carl Roth, 6908
Acetonitrile	Carl Roth, 8825
Acrylamide-bisacrylamide (37.5:1)	Carl Roth, 3029
Ammonium persulfate (APS)	Carl Roth, 9178
Ampicillin	Carl Roth, K029
D- Mannitol	Merck, M4125
D- Sucrose	Carl Roth, 4621
Dimethyl sulfoxide (DMSO)	Merck, D2650
Dulbecco's Modified Eagle Medium (DMEM), high glucose	Sigma-Aldrich, D5796
DMEM-F12	Sigma-Aldrich, D8437
Ethanol	VWR, 85651.360
Ethylenediamine tetraacetic acid (EDTA)	Carl Roth, 8043
Fetal bovine serum (FBS)	Thermo Fisher Scientific, 10270106
Formic acid	Carl Roth, 1EHK
Glycerol	Carl Roth, 7530
Glycine	Carl Roth, 3908
Goat serum	Thermo Fisher Scientific, 16210072
HEPES	Carl Roth, 6763
Human IGF-II R / IGF2R Antibody (neutralizing)	Biotechne, AF2447
ImmuMount	Fisher Scientific, 10662815
Intercept (TBS) blocking buffer	LI-COR Biosciences, 927-60001
Iodoacetamide	Merck, 804744
Kanamycin	Carl Roth, T832
KCl	Carl Roth, 6781
KH_2PO_4	Carl Roth, 3904
Lipofectamine 2000 transfection reagent	Thermo Fisher Scientific, 11668019
Lipofectamine RNAiMAX transfection reagent	Thermo Fisher Scientific, 13778075
Mammalian protease inhibitor cocktail	Merck, P8340
MESNa	Sigma, M1511
Methanol	VWR, 20846.361

$MgCl_2$	Carl Roth, 2189
$MgSO_4$	Carl Roth, 0261
ML-SI3 (TRPML 1/2 channel inhibitor)	MedChem Express, HY-139426
ML-SA1 (TRPML1/2 channel agonist)	MedChem Express, HY-108462
Molecular biology grade H2O	Carl Roth, T143
Na_2HPO_4	Carl Roth, 4984
NaCl	Carl Roth, 3957
Neutravidin Beads (Pierce)	Thermo Fisher Scientific, 29200
Opti-MEM	Thermo Fisher Scientific, 31985062
PageRuler prestained protein ladder	Thermo Fisher Scientific, 26616
Paraformaldehyde (PFA)	Carl Roth, 0335
Penicillin-streptomycin	Thermo Fisher Scientific, 15140122
Pierce BCA Protein assay kit	Thermo Fisher Scientific, 23225
Pierce™ Coomassie (Bradford) Protein-Assay-Kit	Thermo Fisher Scientific, 23200
Recombinant Human IGF-II	Thermo Fisher Scientific, 100-12
RIPA 10x lysis buffer	Merck, 20-188
Sodium deoxycholate	Thermo Fisher Scientific, 89904
Sodium dodecyl sulfate (SDS)	Carl Roth, CN30
Tetramethylethylenediamine (TEMED)	Carl Roth, 2367
Tris(hydroxymethyl)aminomethane (TRIS)	Carl Roth, 4855
Tris(2-carboxyethyl)-phosphine (TCEP)	Carl Roth, HN95
Triton X-100	Carl Roth, 3051
TrypLE™ Express Enzyme	Thermo Fisher Scientific, 12605010
Tween-20	Carl Roth, 9127
β-mercaptoethanol	Carl Roth, 4227

2.2 Buffers and media used for cell culture experiments

Buffer / medium	**Composition**
DAPI solution	1 mg/ml DAPI in PBS
DMEM	DMEM 10% (v/v) FBS 100 U/ml penicillin 100 µg/ml streptomycin
DMEM-F12	DMEM-F12 10% (v/v) FBS 100 U/ml penicillin 100 µg/ml streptomycin

DMEM (Starvation experiment)	DMEM without additions
Cryomedium (2×)	80% (v/v) FBS 20% (v/v) DMSO
Opti-MEM	Thermo Fisher Scientific
Goat serum dilution buffer (GSDB)	15% (v/v) goat serum 0.25% (v/v) Saponin (stock 1% solution) in PBS
HEPES-buffered saline (HBS, 2×)	50 mM HEPES pH 7.05 280 mM NaCl 10 mM KCl 1.5 mM Na2HPO4 12 mM D-(+)-glucose in H_2O
Dulbecco's Phosphate Salt Solution (DPBS)	Thermo Fisher Scientific
Phosphate-buffered saline (PBS)	137 mM NaCl 2.7 mM KCl 8.1 mM Na_2HPO_4 * 2 H_2O 1.4 mM KH_2PO_4 pH 7.4 in H_2O
Phosphate-buffered saline 2+ (PBS 2+)	137 mM NaCl 2.7 mM KCl 8.1 mM Na_2HPO_4 * 2 H_2O 1.4 mM KH_2PO_4 1 mM $CaCl_2$ * 2 H_2O 0.5 mM $CaCl_2$ * 6 H_2O pH 7.4 in H_2O
TE (0.1×)	1 mM TRIS pH 8.0 0.1 mM EDTA in H_2O

2.3 Buffers and solutions used for biochemical and molecular biology experiments

Solution	**Composition**
Antibody dilution buffer	50% (v/v) TBS-T 50% (v/v) Intercept (TBS) blocking buffer
Buffer A	3% (v/v) acetonitrile 0.1% (w/v) formic acid in H_2O
Buffer B	90% (v/v) acetonitrile 0.1% (w/v) formic acid in H_2O
Buffer A*	2 % acetonitrile 0.1 % trifluoracetic acid

Buffer A++	Mix A and A* 9:1
Glycine acid wash	0.1 M Glycine 0.02 M HCl pH 3.0
Lysis buffer	20 mM HEPES pH 7.4 100 mM KCl 2 mM $MgCl_2$ 1% (v/v) Triton X-100 1 mM PMSF 0.3% (v/v) mammalian protease inhibitor cocktail in H_2O
RIPA lysis buffer (commercial)	50 mM Tris-HCl, pH 7.4 150 mM NaCl 0.25% sodium deoxycholate 1% NP-40 (also called Igepal CA-630) 1 mM EDTA
MESNa buffer	50 mM Tris 100 mM NaCl 1 mM EDTA 0.2% BSA pH 8.6
Urea-containing wash buffer	2M urea 50 mM ammonium bicarbonate prepared fresh in ddH_20
Urea-containing buffer (MS sample processing)	6M urea 50 mM Tris HCl pH 7.5 5 mM DTT
SDS-PAGE running buffer	25 mM TRIS pH 8.3 192 mM glycine 0.1% (w/v) SDS in H_2O
SDS-PAGE sample buffer (6×)	375 mM TRIS pH 6.8 60% (v/v) glycerol 30% (v/v) β-mercaptoethanol 18% (w/v) SDS 0.3% (w/v) bromophenol blue in H_2O
Separating gel buffer (4×)	1.5 M TRIS pH 8.8 0.4% (w/v) SDS in H_2O
Stacking gel buffer (4×)	0.5 M TRIS pH 6.8 0.4% (w/v) SDS in H_2O
TRIS-buffered saline (TBS)	20 mM TRIS pH 7.6 140 mM NaCl in H_2O
TBS-T	0.1% (v/v) Tween-20 in TBS
Transfer buffer	25 mM TRIS pH 8.3 192 mM glycine 20% (v/v) methanol in H_2O
Glycerol stock solution (2×)	10 mM TRIS pH 8.0 50 mM MgSO4

	50% (v/v) glycerol in H2O
LB medium	1.0% (w/v) yeast extract 0.5% (w/v) NaCl 0.5% (w/v) tryptone

2.4 Cell lines

Mammalian cell lines name	Species, tissue	Source
HeLa	Human, cervical adenocarcinoma; adherent, epithelial	ATCC-CCL2
HFF (hTERT-HFF)	Human, foreskin fibroblasts	gift of Humphries lab
RPE-1 (hTERT-RPE-1)	Human, eye – retinal pigment epithelium	ATCC

2.5 Small interfering RNAs (siRNAs)

Small interfering RNAs (siRNAs) Target	Sequence (5'-3')	Manufacturer catalog number	Reference
CI-M6PR 1 [10 nM] used	CCUGCAAGAAAGACAUAUUA	Merck, custom synthesis	(Caixeiro et al., 2013)
CI-M6PR 2 [7 nM] used	CCUCUCCCAUGAAAGAGAAA GGAAA	Invitrogen, Stealth	(Takeda et al., 2019)
CI-M6PR 3 [9 nM] used	CUACCUGUAUGAGAUCCAA-	Ambion-Thermo Fisher s7217- Silencer Select IGF2R	(Takeda et al., 2019)
Control siRNA (siCtrl)	UGGUUUACAUGUCGACUAA, UGGUUUACAUGUUGUGUGA, UGGUUUACAUGUUUUCUGA, UGGUUUACAUGUUUUCCUA	Dharmacon, D-001810-10	
CD-M6PR 1 [10 nM] used	GGUUCCAUCUUACUUGUCA	Merck, custom synthesis	(Y. Hu et al., 2024)
CD-M6PR 2 [10 nM] used	GCUGUGGCAGUGAGAGAAU	Merck, custom synthesis	(Y. Hu et al., 2024)
CD-M6PR 3 [10 nM] used	GGCUGAAACCACUGUUUAA	Merck, custom synthesis	(Y. Hu et al., 2024)

2.6 Plasmids

Plasmids Name	Description	Source

CI-M6PR chimera 4.0 AAA (CIMPR SP and shorter luminal domain) in pEGFP.C1	CI-M6PR chimaera consisting of signal peptide - GFP – CI-M6PR transmembrane domain – CI-M6PR cytosolic tail, but lacking the luminal/extracellular part of CI-M6PR	gift of Pete Cullen's lab

2.7 Primary antibodies

Antigen (Human)	Host species	Dilution (WB)	Dilution (IF)	Manufacturer	Catalog number
ABCA1	Mouse	1:400	-	Santa Cruz	sc-58219
Aldolase A	Rabbit	1:5000	-	Proteintech	11217-1-AP
ATP7A	Mouse	1:300	1:200	Santa Cruz	sc-376467
Actin (beta)	Mouse	1:3000	-	Sigma	A5441
Alpha-Adaptin (AP-2 alpha)	Mouse	1:500	1:300	BD Transduction	610502
CI-M6PR	Rabbit	1:1000	1:400	Cell Signalling	14364S
CD-M6PR	Rabbit	-	1:200	Abcam	ab134153
CTR1	Mouse	-	1:400	Novus Biologicals	G8795
EEA1	Mouse	1:500	1:300	Santa Cruz	sc-137130
EGFR	Rabbit	1:1000	-	Cell Signalling	4267S
Gamma Adaptin (AP-1 gamma)	Mouse	1:2000	1:200	BD Transduction	610386
GAPDH	Mouse	1:4000	-	Sigma	G8795
GM-130	Mouse	-	1:200	BD transduction	610822
HSP70	Mouse	1:2000	-	Thermo Fisher	MA3006
Human Ephrin A5	Goat	1:500	1:100	R&D Systems	AF3743
IGF2R	Mouse	1:1000	1:300	Thermo Fisher	2G11
Integrin beta 5	Rabbit	1:1000	-	Cell Signalling	3629-T
LAMP1	Rabbit	1:1000	1:300	Cell Signalling	9091
SCARA3	Rabbit	1:1000	1:200	Novus Biologicals	NBP2-13286
SPPL2A	Rabbit	1:1000	1:200	Novus Biologicals	NBP2-93234
Transferrin Receptor	Rabbit	1:500	-	Sigma	HPA028598
TGN46	Rabbit	-	1:100	Abcam	ab546
VPS29	Rabbit	1:1000	-	Abcam	ab315334

2.8 Secondary antibodies

Antigen	Host species	Conjugated with	Application	Manufacturer	Catalog number

Mouse IgG	Goat	Alexa Fluor 488	IF	Thermo Fisher Scientific	A11029
Rabbit IgG	Goat	Alexa Fluor 488	IF	Thermo Fisher Scientific	A11036
Rabbit IgG	Goat	Alexa Fluor 647	IF	Thermo Fisher Scientific	A21244
Mouse IgG	Goat	IRDye 680RD	WB	LI-COR Biosciences	926-68070
Mouse IgG	Goat	IRDye 800CW	WB	LI-COR Biosciences	926-32210
Rabbit IgG	Goat	IRDye 680RD	WB	LI-COR Biosciences	926-68071
Rabbit IgG	Goat	IRDye 800CW	WB	LI-COR Biosciences	926-32211

2.9 Probes and dyes

Probe/ dye name	Target	Manufacturer	Catalog number
Streptavidin, Alexa Fluor 647	Biotinylated proteins	Thermo Fisher Scientific	S21374
Streptavidin, Alexa Fluor 488	Biotinylated proteins	Thermo Fisher Scientific	S11223
Transferrin, Alexa Fluor 647	Transferrin receptor	Invitrogen	T23366
DAPI	Nucleus	Carl Roth	6335.1
Hoechst	Nucleus	Thermo Fisher Scientific	62249
PROTEOSTAT Aggresome detection kit	Cytoplasm- protein aggregates	Enzo	ENZ-51035
CellROX green	Cytoplasm and nucleus	Thermo Fisher Scientific	C10444
IncuCyte Cas 3/7 green	Apoptotic cells	Sartorius	4440
SYTOX Green	Necrotic cell (nucleus)	Thermo Fisher Scientific	S7020
Acridine Orange	Lysosomes	Abcam	ab270772
Magic Red Assay kit	Cathepsin B/ lysosomes	Abcam	ab270772

2.10 Kits and consumables

Kits/consumable	Manufacturer
8-well µ-Slide (glass bottom)	Ibidi
Coverslips 18 mm	Carl Roth
Cell culture dishes (6 cm, 10 cm)	Sarstedt
Cell culture plates (12-well, 24well, 96-well)	Sarstedt
Cell scrapers	VWR

Cover slips	Thermo Fisher Scientific
Cryotubes	Sarstedt
Immobilon-FL Nitrocellulose membrane	Merck Millipore
Microscope slides	Epredia
QIAfilter Plasmid Midi Kit	Qiagen
QIAprep Spin Miniprep Kit	Qiagen
Parafilm	Bemis Company Inc.
Pierce Spin Columns- Snap Cap	Thermo Fisher Scientific
Pipette tips (10 µl, 200 µl, 1000 µl)	Sarstedt
Reaction tube (1.5 ml, 2 ml)	Sarstedt
Serological pipets (5 ml, 10 ml, 50 ml)	Corning
Syringes, 25 ml	Henke Sass, Wolf GmbH
Whatman paper	GE Healthcare

2.11 Technical equipment

Equipment	**Model, manufacturer**
Cell counting chamber	Neubauer, Paul Marienfeld
Cell culture incubator	CB170, Binder
Cell culture microscope	Axiocam 208 color, Carl Zeiss Microscopy GmbH
Centrifuge	Micro Star 17R, VWR Multifuge X1R, Thermo Fisher Scientific
Epifluorescence microscope	Eclipse Ti2-E, Nikon Laser: 405, 488, 561, 642 Perfect focus system, Nikon Objectives: 20× Plan Apo 0.75 NA Ph2 air objective, Nikon 40× Plan Apo 0.95 NA Ph2 air objective, Nikon 60× Apo TIRF 1.49 NA oil objective, Nikon
Heating block	PHMT-PSC24, Grant Bio
Laminar flow hood	Airstream Class II BSC, Esco
Liquid nitrogen tank	BSS-6000, VWR
Mass spectrometer	Orbitrap Q Exactive HF-X, Thermo Fisher Scientific equipped with Ion source: nano-electrospray

	LC system: Easy-nLC 1000, Thermo Fisher Scientific
Microliter pipettes	Transferpipette S, Brand
Osmometer	Osmomat 3000, Gonotec
Pasteur pipettes, 5 ml	Carl Roth GmbH + Co. KG
pH meter	FiveEasy, Mettler Toledo
Pipet boy	PipetBoy Acu 2, Integra Biosciences
Plate reader	Spectro Star
Precision scale	Entris II, Sartorius
SDS-PAGE and Western blot systems	Mini-PROTEAN Tetra, Bio-Rad
Shaker	SHRK07AL2, OHAUS Europe GmbH
Sonifier	Digital Sonifier 450, Branson Ultrasonics
Spectrophotometer	SpectroStar Nano, BGM Labtech
Spinning disk confocal microscope	Eclipse Ti2-E with CSU-W1 Sora, Nikon Spinning disk unit: CSU-X1, Yokogawa Electric Laser: 405, 488, 561, 640 Perfect focus system, Nikon Objectives: 40× Plan Apo 0.95 NA air objective, Nikon 60× Plan Apo 1.40 NA oil objective, Nikon 60× Plan Apo 1.20 NA water objective, Nikon
Vacuum pump	Vacusafe, Integra Biosciences
Vortex	Vortex-Genie 2, Scientific Industries
Water bath	Hydro, LAUDA
Western blot imaging system	Odyssey Fc, LI-COR Biosciences

2.12 Software and online tools

Software	Version
Affinity Designer	2.5.7.2948
Fiji/ImageJ	1.54f
GraphPad Prism	9.3.1 (Build 471)
Image Studio Lite	5.2
Microsoft Office	365
NIS Elements	5.30.06 (Build 1567)
Perseus	1.6.15.0
String database	www.string-db.org
SURFY *in silico* human surfaceome	www.wlab.ethz.ch/surfaceome

3. Methods

3.1 Cell lines

HeLa, RPE-1, and HFF-1 cells were used for this project (see cell line table information for further information).

3.2 Cell culture

Cells were cultured in petri dishes with cell culture medium and kept in incubators at 37 °C and 5 % CO^2; they were maintained at 70-90% confluence and passaged every 3-4 days. For passaging, cells were washed once with Dulbecco′s phosphate buffered saline (DPBS) to remove the medium, and treated with TrypLE for 5 min in the incubator for detachment. Fresh medium was added to stop the TrypLE, cells were centrifuged, and a portion of the pellet ranging from 1:5 to 1:10 was resuspended and transferred to a new dish containing fresh medium. HeLa and HFF-1 cells were cultured with Dulbecco′s modified eagle′s medium (DMEM) + 10 % (v/v) fetal bovine serum (FBS) + 1 % (v/v) Penicillin/Streptomycin (P/S) whereas RPE-1 cells were cultured in DMEM-F12 + 10 % (v/v) FBS + 1 % (v/v) P/S.

For long-term storage, cells were detached as described above, collected in medium, and pelleted by centrifugation at 280×g for 5 min. The supernatant was discarded, and cells were resuspended with DMEM or DMEM-F12. Afterwards, cell suspensions were mixed 1:1 with cryomedium and allocated to cryotubes. Cells were stored at -80°C overnight and the cryotubes were transferred to liquid nitrogen the following day.

3.2.1 Cell seeding

For immunofluorescence (IF) of fixed cells, 18 mm glass coverslips were placed in 12-well plates and for live cell imaging IBIDI 8-well glass-bottom chambers were used. Cells were then counted in a Neubauer chamber. The cell number seeded on each coverslip depended on the experiment to be done, but as a reference 20,000 cells were seeded on each IBIDI well in 200 µl medium and 45,000-50,000 cells per IF coverslip, in both cases the experiments were performed on the next day. To ensure equal distribution of cells, a p1000 pipette was used to resuspend the well medium 3-4 times over each surface. For western blot (WB) experiments, cells from confluent 10 cm dishes were treated and eventually lysed for sample preparation.

3.2.2 Cell treatments

3.2.2.1 Treatments to induce stress conditions

Heat stress is achieved by placing the cells in incubators at 42°C and 5 % CO^2 for 1 h.

To prepare the osmotic stress medium, first the osmolarity of the DMEM-F12 base medium was measured using an osmometer. Calculation of the amount of D-mannitol required to reach the desired osmolarity was reached using the following formulas:

$$\text{Osmolarity difference (mOsm/L)} = \text{Desired osmolarity} - \text{Measured osmolarity}$$

$$X\ \text{(g)} = 182.17\ \text{(g/mol)} \times \left(\frac{\text{Osmolarity difference}}{1000}\right) \times \left(\frac{\text{Volume of medium (mL)}}{1000}\right)$$

The calculated amount of D-mannitol was weighed and added directly to the medium, mixed thoroughly until fully dissolved, then the osmolarity of the medium was re-measured to confirm that the target value was achieved. Once confirmed, the adjusted medium was warmed to 37°C and applied to the cells for experimental treatment. Then the cells were placed in the incubator at 37°C and 5 % CO^2 for 1 h.

To prepare the oxidative stress-inducing medium, first a 0.5 M stock solution of tert-Butyl hydroperoxide (TBH) was prepared in distilled water. After mixing thoroughly by vortexing, the stock was aliquoted as needed, and stored at –20°C. For short-term use (e.g. 1 week), aliquots were kept at 4°C. Just before use, the stock aliquot solution was diluted in complete cell culture medium to a final concentration of 75 µM using the following formula:

$$C_1 \times V_1 = C_2 \times V_2$$

where C1 is the stock concentration (0.5 M), C2 is the desired final concentration (75 µM), and V2 is the final volume of medium required. The diluted medium was mixed thoroughly by vortexing, warmed to 37°C, and distributed to the cells. Then the cells were placed in the incubator at 37°C and 5 % CO^2 for 1 h.

Both prepared stress mediums were stored at 4°C for up to one week. After this period, a fresh batch was prepared.

3.2.2.2 Treatment of cells with endocytosis inhibitor (Pitstop)

Cells were seeded onto glass coverslips 24 h prior to treatment. Before starting the assay, cells were washed with DPBS and incubated in serum-free medium containing either 30 µM Pitstop 2 or vehicle control (DMSO), as Pitstop is inactive in the presence of serum. Cells were treated for at least 15 min in the respective medium. When applicable, transferrin uptake assays were conducted in the same medium containing the inhibitor or vehicle. Following treatment, cells were acid-washed, washed with PBS, and fixed with 4% PFA for 10 min at 4°C. After three PBS washes, cells were stained with DAPI, washed again, and mounted for imaging, with 60x magnification.

3.2.2.3 Treatment of cells with lysosomal exocytosis inhibitor and agonist

RPE-1 cells were cultured in 10 cm dishes until reaching 85-90% confluency. Cells were then subjected to one of four treatment conditions for 1 hour at 37°C: unstressed control, unstressed control with inhibitor or agonist, osmotic stress, and osmotic stress with inhibitor or agonist. The TRPML1 Ca^{2+} channel inhibitor ML-SI3 and agonist ML-SA1 had been purchased ready as DMSO stock solutions and were then diluted into complete culture medium to final concentrations of 10 µM and 50 µM, respectively, based on their reported IC_{50} values. Vehicle controls received an equivalent volume of DMSO. Following treatment, all samples were placed at 4°C and processed

for surface biotinylation. Protein levels were measured, and samples were prepared for analysis by western blotting.

3.2.2.4 Treatment of cells with human IGF-II receptor-specific antibody or human recombinant IGF-II

A double knockdown of CI-M6PR was performed in RPE-1 cells cultured in 12-well plates (see 3.3). On day 4 post-transfection, cells were counted and resuspended in complete growth medium, then evenly seeded into a new 12-well plate and incubated for 24 h. The following day, cell morphology and confluency were assessed by light microscopy, and cells were assigned to one of four treatment groups: (1) unstressed control with scrambled siRNA, (2) unstressed CI-M6PR knockdown (KD), (3) osmotic stress with scrambled siRNA, and (4) osmotic stress with CI-M6PR KD. Each group included duplicate wells, with one well receiving 0.1 µg/mL of human IGF-II receptor neutralizing antibody and the other receiving an equivalent concentration of mouse IgG as control. Following treatment, cells were allowed to proliferate for 24 h, after which they were trypsinized, resuspended in fresh medium, and manually counted using a Neubauer hemocytometer.

A parallel experiment was conducted to assess the effect of recombinant human IGF-II protein. In this case, cells were treated with 0.1 µg/mL of IGF-II or an equivalent concentration of BSA as a control. Treatments were prepared by diluting protein stocks in complete medium, mixing thoroughly, and distributing the solutions to the respective wells.

3.3 Transfection with siRNA

For knockdown experiments, 20,000 RPE-1 cells/well were seeded on a 12-well plate. The transfection was made using Lipofectamine RNAiMAX, diluting it 1:400 in Opti-MEM, after which 30 or 45 nM siRNA (concentration is siRNA-specific) are added to the mix, vortexed for 12-15 sec and incubated at room temperature for 15 min. This master transfection mix was then diluted with full DMEM-F12 in a 1:5 ratio, which gave a final siRNA concentration of 7-10 nM (see siRNA material table for specifics on concentration used for the different siRNAs). For all experiments, 2 rounds of knockdown were performed, one reverse transfection on the same morning as the seeding of the cells, with the following transfection generally done on the late afternoon of the following day. On the third day the wells were changed to fresh medium, on the fourth day in the morning the number of cells specified above were re-seeded either on glass coverslips or IBIDI chambers, and the final experiments were performed on the fifth day.

For WB lysates, 300,000 cells were seeded in 6 cm dishes, and the experiment was done four or five days after the first reverse transfection (depending on cells reaching the right confluence). The same procedure was used, only the reagents were scaled up for the larger surface of the 6 cm dish.

3.4 Plasmid transfection for overexpressing CI-M6PR in mammalian cells

3.4.1 Bacterial culture and plasmid preparation

Bacterial cultures were prepared prior to transfection to amplify plasmid DNA. A glycerol stock of *Escherichia coli* containing the CI-M6PR plasmid was inoculated into 2 mL of Luria-Bertani (LB)

broth supplemented with the appropriate antibiotic for plasmid selection. Cultures were incubated overnight at 37°C with shaking at 200 rpm. The following day, cultures were assessed for turbidity (indicative of sufficient bacterial growth) and harvested by centrifugation at 10,000 × *g* for 10 min at 4°C. The supernatant was discarded, and the bacterial pellet was either stored at −20°C or immediately used for plasmid extraction using a commercial mini-prep kit (Qiagen).

For the validation of NHE7, the same protocol was employed by Luwam Gebrezi, a student who did her Bachelor thesis, under my supervision.

3.4.2 Cell culture and transfection

One day prior to transfection, mammalian cells were seeded onto Matrigel-coated glass coverslips in 12-well plates at a density of 80,000 cells/well in 700 µL of complete growth medium. The target confluency at the time of transfection was 70–90%. The following day, cell confluency was confirmed using a standard optical microscope. Transfection complexes were prepared as follows: for each well of a 12-well plate, 4 µL of Lipofectamine 2000 were diluted in 100 µL of Opti-MEM and incubated for 5 min at room temperature. In parallel, 1.6 µg of CI-M6PR plasmid DNA were diluted in a separate 100 µL of Opti-MEM. The diluted Lipofectamine and DNA solutions were then combined, gently vortexed for approximately 12 sec, and incubated at room temperature for 20 min to allow complex formation.

The resulting transfection mix was added dropwise to each well, and the plate was gently rocked to ensure even distribution. Cells were returned to the incubator (37°C, 5% CO_2) and incubated for 5–6 h. After this period, the transfection medium was removed and replaced with fresh growth medium. Cells were maintained under standard culture conditions overnight. At least 24 h post-transfection, cells were processed for immunofluorescence (IF), and imaging by confocal microscopy at 60x magnification.

For the validation of NHE7, the same protocol was employed by Luwam Gebrezi, a student who did her Bachelor thesis, under my supervision.

3.5 Immunocytochemistry

The cells were washed once with phosphate buffered saline 2+ (see materials for composition of reagents and buffers), placed on ice and fixed with ice cold 4 % PFA for 10 min. Afterwards, the cells were washed 3x in PBS, blocked and permeabilized by incubating with goat serum dilution buffer (GSDB) for 30 min at RT. The primary antibodies used (see primary antibody table) were diluted with GSDB and distributed into droplets on parafilm in a humid chamber where the coverslips were transferred to (upside down) for 1 h incubation at RT. Then the coverslips were washed 3 times with PBS, followed by the transfer of the coverslips to the humidified chambers for a 30 min incubation with secondary antibodies (see secondary antibody table) also previously diluted in GSDB. After 3x washes with PBS, coverslips were incubated with 1 µg/ml DAPI solution in PBS and mounted with ImmuMount, allowing the slides to dry for at least 24 h before imaging. Images were taken at 60x magnification.

3.6 Cell lysis

Cells cultured and previously treated in 6- or 10-cm dishes were placed on ice and gently rinsed with cold PBS 2+. They were then harvested by scraping, transferred to 1.5 ml Eppendorf tubes, and centrifuged at 300×g for 3 min at 4°C. After discarding the supernatant, the resulting pellet was resuspended by tube inversion in lysis buffer, briefly vortexed for 10 sec, and incubated for 30 min at 4°C under rotation. Lysates were then cleared by centrifugation at 17,000×g for 10 min at 4°C. The supernatant containing the soluble protein fraction was transferred to a fresh tube, and protein concentrations were determined using the Bradford assay. Samples were then mixed with 2× Laemmli buffer and denatured at 92°C for 10 min. Lysates not used immediately were stored at −80°C.

3.7 Bradford assay for protein concentration measurements

To determine protein concentrations with the Bradford assay, 1 µl of each sample was added to 200 µl of Bradford reagent on a 96-well plate, mixed for 10 sec and incubated again for 5 min in the dark before performing a 595 nm absorbance reading with a spectrophotometer. The measurements were blank-corrected, and since each sample was measured in duplicates results were averaged. At last, the protein concentration was calculated using a previously determined linear equation based on a protein standard curve.

3.8 SDS polyacrylamide gel electrophoresis (SDS-PAGE)

Proteins were separated according to molecular weight using SDS-PAGE. Discontinuous polyacrylamide gels were prepared using the Mini-PROTEAN Tetra casting system. The separating gel was prepared first with the appropriate acrylamide concentration (mostly 9-12% was used), and polymerization was initiated by adding TEMED. The gel solution was poured between the glass plates and overlaid with isopropanol to ensure a smooth surface. After complete polymerization, the isopropanol was removed, and 3.8% stacking gel solution was poured on top and allowed to polymerize. Detailed compositions of the gel solutions are provided in the reference table below (table 15).

For electrophoresis, the gel was assembled into the Mini-PROTEAN Tetra chamber and submerged in SDS-PAGE running buffer. Samples and a Page Ruler pre-stained protein ladder were loaded into the wells. Electrophoresis was carried out at 85 V for 1 h and then at 120 V until protein separation was completed**.**

Table 15: Composition of separating and stacking gels used for SDS-PAGE gels

SDS-PAGE separating gel			**Stacking gel 3.8%**
	9%	**12%**	
30% acrylamide/ 0.8% bis acrylamide	4.5 ml	6 ml	0.625 ml
Separating gel buffer (4×)	3.75 ml	3.75 ml	-
Stacking gel buffer (4×)	-	-	1.25 ml
H_2O	6.5 ml	5 ml	3.25 ml
10% (w/v) APS	150 µl	150 µl	75 µl

TEMED*	15 µl	15 µl	7.5 µl

*: added directly before polymerization

3.9 Western blot

In order to assess protein expression levels, proteins separated by SDS-PAGE were transferred onto nitrocellulose membranes using Western blot. The gel and membrane were assembled in a transfer sandwich with Whatman paper and sponges, all pre-soaked in transfer buffer, and inserted into the western blot tank, previously filled with cold transfer buffer and placed on ice, where the protein transfer was completed at 110 V for 90 min.

Following transfer, membranes were briefly rinsed in TBS and then blocked for 1 h at room temperature using Intercept (TBS) blocking buffer on a shaker. Primary antibodies were diluted in antibody dilution buffer directly in falcon tubes and pre-cut membranes were transferred to the falcon tubes to be incubated overnight at 4°C on rotation. The next day, membranes were washed three times with TBS-T (3 min each) to remove unbound antibodies.

Secondary antibodies were then applied for 45 min at room temperature on a shaker, followed by another three washes with TBS-T (10 min each this time). Membranes were then imaged using the Odyssey Fc imaging system. Where applicable, band intensities were quantified using Image Studio Lite software and normalized to appropriate loading controls.

3.10 Microscopy-based analysis of biotinylated surface protein and transferrin bulk uptake

Cells were subjected to a 1 h stress treatment prior to surface labelling and endocytosis analysis. Endocytosis was temporarily halted by placing well plates on ice and washing cells with cold PBS containing Ca^{2+} and Mg^{2+} (PBS2+) (pH 7.8). Primary amines of extracellular parts of cell surface proteins were labelled with sulfo-NHS-SS biotin on ice for 30 min. Excess biotin was quenched with two 3 min incubations in cold glycine solution, followed by a PBS2+ wash. Endocytosis was re-initiated by incubating the cells at 37°C with pre-warmed full medium containing fluorescently labelled transferrin (25 µg/ml in 50 µl medium droplets on a humidified chamber) for 15 min. Afterward, endocytosis was immediately halted by cooling cells with cold PBS and washing them with ice-cold MESNa buffer. Residual surface biotin was removed by two 10 min incubations in MESNa solution, and transferrin remaining on the plasma membrane was removed with a 2-min acid wash at 4°C. Cells were then washed with PBS2+ and fixed in pre-cooled 4% paraformaldehyde in H_2O for 10 min. Following fixation, cells were blocked and permeabilized with blocking solution applied to the wells and left on a light shaker for 15 min, then incubated on a humidified chamber with 0.1 µg/ml of fluorescent Streptavidin in 50 µl droplets to detect internalized biotinylated proteins. DAPI solution was added to the wells (1 µg/ml DAPI in PBS) for nuclear staining, and cells were subsequently washed, mounted with ImmoMount, and stored in the dark at 4°C until imaging. Images were taken at 60x magnification.

3.11 Cell surface biotinylation and isolation of biotinylated proteins for Western blotting

Cells were seeded in 10 cm dishes at consistent densities using cell counting to ensure reproducibility across conditions, maintaining similar passage numbers and confluency by plating at the same time of day to reach a confluency of 90% at the time of the experiment. For stressed conditions, additional plates were prepared to compensate for reduced viability and to allow pooling of equal protein amounts during harvest. After applying stress or control treatments, cells were placed on ice to slow endocytosis and washed with cold PBS2+. Six ml of sulfo-NHS-SS biotin solution were added to each dish (except for the non-biotinylated controls), and cells were incubated at 4°C for 30 min to label surface proteins. Unbound biotin was quenched by adding cold glycine solution for 10 min, followed by a PBS2+ wash. Cells were then scraped into cold PBS (400 µl per 10 cm dish), and cell suspensions from replicate plates were combined if necessary. Cell suspensions were centrifuged, and pellets were resuspended in 300 µl lysis buffer, vortexed briefly, and incubated on a rotator at 4°C for 30 min. Lysates were vortexed again and centrifuged at 13,000 x g for 10 min. Pellets were discarded, and protein concentrations of the supernatants were determined using a Bradford assay at room temperature. Aliquots of the lysates were retained for Western blot analysis of total protein input. Neutravidin beads (80-100 µl suspension) were pre-washed 3x with RIPA buffer (without inhibitors) and incubated with lysates, adjusted to contain equal protein amounts (at least 550 µg) across experimental conditions. The incubation was done overnight at 4°C on rotation. After centrifugation, supernatants were collected for later analysis of the non-biotinylated fraction. Beads were washed sequentially for 5 min each time (6 1 ml washes for western blot samples and 18 times with 1 ml each for mass spectrometry samples) with RIPA buffer and 1 M NaCl (1:1 vol/vol), and 2 M urea in 50 mM ammonium bicarbonate, using snap-cap spin columns to minimize bead loss. For elution for subsequent Western blotting, 55 µl pre-heated 2× SDS-PAGE sample buffer with fresh DTT were added to the beads, incubated at 95°C, spun down, and the eluates were collected.

To assess bulk internalization of biotinylated surface proteins, the surface biotinylation protocol described above was modified in the following manner to include the addition of endocytosis and stripping steps: following biotin labelling at 4°C, cells were transferred to a pre-warmed 37°C heating block to allow endocytosis for 15 min. Cells were then rapidly washed with ice-cold MESNa buffer and subjected to two 10-min incubations with 100 mM MESNa in MESNa buffer at 4°C to remove remaining surface-bound biotin. Finally, cells were washed twice with PBS 2+ prior to lysis.

3.12 Antibody Feeding Assay

To assess internalization of membrane-bound proteins, an antibody feeding assay was performed as follows. Cells were subjected to stress treatments as indicated and then immediately placed on ice. After a single wash with ice-cold $PBS^{2+,}$ cells were incubated with the primary antibody (diluted in cell culture medium) for 30 min on ice to label surface antigens. Unbound primary antibody was removed by washing twice with PBS^{2+}. To initiate endocytosis, coverslips were transferred to a pre-warmed humidified chamber and incubated at 37°C for 15 min. Control samples underwent instead a 2-min acid wash using cold glycine buffer (pH ~3.0) to remove residual surface-bound antibody. Followed by two PBS^{2+}washes, cells were fixed with 4% PFA at 4°C for 10 min and permeabilized/

blocked with GSDB buffer for 15 min at room temperature. To visualize internalized primary antibody, cells were stained with Alexa Fluor 647-conjugated secondary antibody (diluted in GSDB buffer) for 30 min at room temperature. After three additional PBS washes, nuclei were counterstained with by adding 1 µg/ml DAPI in PBS to the cells for 10 min and washed again three times with PBS. Coverslips were mounted with ImmuMount and allowed to dry for at least 24 h before imaging. Images were taken at 60x magnification.

3.13 Sample preparation of biotinylated protein for mass spectrometry

Neutravidin bead-bound proteins were processed for mass spectrometry using a modified on-bead digestion protocol. Beads were incubated with 50 µl 6M urea-containing buffer and heated at 55°C to reduce disulfide bonds, followed by alkylation with 15 mM 2-chloroacetamide at room temperature in the dark with gentle shaking. A second 5mM DTT incubation was performed to quench excess alkylating agent. The sample was then diluted with 50 nM Tris-HCl buffer to reduce the urea concentration below 2 M. Trypsin (5 ng/ µl) was added directly to the beads, and digestion proceeded overnight at 37°C in a humidified chamber. Peptides were recovered by centrifugation by transferring the supernatant to new tubes, and a second elution step with 50 µl of 1.5 M of urea-containing buffer was performed to extract residual peptides. Both eluates were combined, and digestion was stopped by acidifying with approximately 25 µl of 1% trifluoroacetic acid (TFA) to pH < 2, and then verified using pH indicator paper. Samples were centrifuged at 13,000 x g for 10 min to pellet any insoluble material, and the supernatant was retained for desalting.

For desalting, C18 stage tips were assembled using triple-layer C18 material packed into standard 200 µl pipette tips. Tips were activated by loading and later centrifuging away 100 µl of methanol and equilibrated by adding and later centrifuging away 100 µl of 0.1% aqueous formic acid (buffer A). Acidified peptide samples were then loaded on the tips, and washed twice with buffer A as previously described, and finally loaded with 60 µl buffer B containing formic acid and acetonitrile. Elution was performed by centrifugation at 500 g using a dual-rack system to align collection tubes beneath the stage tips. Eluates were dried in a SpeedVac concentrator at room temperature and subsequently resuspended in 12 µl of buffer A. Samples were sonicated briefly, centrifuged to remove particulate materials, and either stored at –20°C or analyzed immediately. Approximately 2 µl of each sample were analyzed by LC-MS/MS using electrospray ionization on a Q-Exactive HF mass spectrometer.

For total proteome analysis, a slightly different protocol was used, as detailed further below.

3.13.1 Perseus analysis for differential proteomics of mass spectrometry readings

The “proteinGroups.txt” file from the mass spectrometry reading was provided by Dr. Markus Räschle after he analyzed the previous stage of the data using MaxQuant software. The file provided was loaded into Perseus software, taking all the LFQ intensities as the “expresión levels”. All the proteins that matched any of the following categorical annotations were deleted: 1) Only identified by site, 2) Reverse, 3) Contaminant, since those represent unreliable matches or possible contaminants matching the database. LFQ-intensities were converted into logarithms, then experiments were grouped into sample or control and proteins that were not detected in at least two

replicates (for n=4) or one replicate (for n=3) in at least one of the groups were deleted. After checking the histograms of intensity distribution and verifying the quality of the data, missing values were imputed by normal distribution with lowest values that were found in those histograms plots. A two-sided Student's T test was performed with a false discovery rate between 0.1 and 0.5% and results were read as volcano plots for candidate proteins.

3.12 Mass spectrometry for total proteome preparation from human cells

Cell pellets (~10^6 cells) were resuspended in 150 µL of lysis buffer (yielding ~1 µg/µL protein concentration) and lysed by heating at 99°C and 1000 x g for 10 min, followed by strong sonication to shear DNA—using a Branson Sonifier (1 min, 20% duty cycle, output 3). Lysates were clarified by centrifugation at 10,000 × g for 10 min, and supernatants were retained. Protein concentrations were determined using a BCA assay in a 96-well format by mixing 5 µL of sample or BSA standard with lysis buffer and water to 15 µL, followed by the addition of 200 µL of BCA working reagent (50:1 solution A:B), an incubation at 37°C for 30 min, and spectrophotometric analysis. For digestion, 25 µg of protein from each sample were adjusted to equal volume with lysis buffer, diluted 1:10 in digestion buffer, and incubated overnight at 37°C with LysC and trypsin (1:50 each; 1 µL of 0.5 µg/µL trypsin per sample). Digests were acidified with TFA to a final concentration of 1% (pH <2), centrifuged (3 min at 12,000 x g), and ~75% of the supernatant were loaded onto pre-equilibrated SDB-RPS stage tips (3-layer, 3M 2241). Stage tips were activated with 100 µL acetonitrile, equilibrated with 100 µL of 30% MeOH + 1% TFA, then 0.2% TFA, followed by peptide loading, washing (0.2% TFA), and elution with 60 µL of 80% acetonitrile + 5% ammonia. Eluates were dried by speed-vac (~40 min, RT), resuspended in 12 µL Buffer A++, sonicated for 5 min in a water bath, briefly centrifuged, and either stored at −20°C or analyzed via LC-MS/MS (2 µL injection).

The analysis of this experiment was conducted entirely by Dr. Markus Räschle due to time constraints.

Table 16: Samples analyzed by mass spectrometry in collaboration with Dr. Markus Räschle

Mass spectrometry project	Conditions tested	N° of replicates & experiments
P0199 Surface protein biotinylation	• Unstressed cells without Biotin • Unstressed cells with Biotin • Osmotically stressed cells with Biotin • Heat shocked cells (1h 42°C, no recovery) with Biotin	4 replicates per condition 2 independent experiments
P0207 Surface protein biotinylation	• Unstressed cells without Biotin • Unstressed cells with Biotin • Oxidatively stressed cells with Biotin • Heat shocked cells (1h 42°C, 4h at 37°C) with Biotin	3 replicates per condition 2 independent experiments

P0260 Lysates to obtain whole-cell proteome	• Unstressed cells • Oxidatively stressed cells • Osmotically stressed cells • Heat shocked cells (1h 42°C, no recovery) • Heat shocked cells (1h 42°C, 4h at 37°C)	4 replicates per condition 2 independent experiments

3.13 Aggresome detection assay

Protein aggregate formation was assessed using the Proteostat Aggresome Detection Kit. Cells were seeded directly onto 8-well glass-bottom chamber slides and cultured for 24-28 h before stress onset. Prior to staining, cells were checked under a light microscope to confirm healthy morphology and adequate confluency. Osmotic stress was applied to designated groups, while controls remained untreated. A positive control was added, with cells treated with 10 μM of MG-132 for 18 h, this a proteasome inhibitor which induces both the unfolded protein response and the heat shock response. Cells were fixed for 10 min with 4% paraformaldehyde in PBS at room temperature, followed by three PBS washes. Permeabilization was performed on ice for 30 min using a 0.3% Triton X-100/0.5% EDTA-based solution in the commercial assay buffer. Cells were then washed with PBS and incubated for 30 min at room temperature in the dark with a dual-staining reagent containing the Proteostat detection dye and Hoechst 33342. After a final PBS wash, cells were imaged using a confocal microscope with a 60× objective.

3.14 Cathepsin B activity assay

Cathepsin B activity was measured using the Magic Red Cathepsin B Assay Kit. For experiments involving siRNA-mediated gene silencing, cells were first transfected on glass coverslips in 12-well plates and cultured for five days. The day before the assay, transfected cells were re-seeded into 8-well glass-bottom chamber slides. Prior to staining, cells were examined under an optical microscope to confirm healthy morphology and appropriate confluency. Cells were then subjected to stress treatments, while control groups remained untreated. A staining solution was prepared by diluting stock Magic Red reagent 1:25 and 0.5% (v/v) Hoechst 33342 in culture medium. Cells were washed once with DPBS and incubated with the staining solution at 37°C in the dark for 30 min. After incubation, cells were washed twice with DPBS and incubated in Opti-MEM. Imaging was performed using a confocal microscope at 37°C with CO_2, using a 40× objective.

3.15 Transferrin uptake assay

Cells were seeded onto glass coverslips in 12-well plates one day prior to the experiment to allow proper adherence and spreading. On the day of the assay, cells were starved in serum-free medium for 1 h to enhance transferrin uptake. Alexa Fluor 488-labeled transferrin was dissolved 1:200 and distributed to in 50 µl droplets of serum-free medium, and cells were incubated with this solution for 20 min in a humidified chamber at either 37°C to allow endocytic uptake or at 4°C (control condition), depending on the condition. After incubation, coverslips were transferred back to well plates and washed twice with ice-cold PBS, followed by a 2-min glycine acid wash on ice to remove surface-bound transferrin. Cells were then washed twice more with cold PBS and fixed for 10 min with pre-cooled 4% paraformaldehyde in H_2O at room temperature. After fixation, cells were

washed with PBS, counterstained with DAPI for nuclear visualization, and washed again before being mounted on microscope slides using antifade mounting medium. Additional immunocytochemistry staining was performed as required. Images were taken at 60x magnification.

3.16 SYTOX cell death assay

RPE-1 cells were seeded onto glass-bottom IBIDI chambers at a density of 20,000 cells per well at least 24 h prior to the experiment. Cell morphology and confluency were assessed under a microscope to ensure healthy and extended appearance before initiating stress treatments. Specific wells were then exposed to stress conditions for 4, 6, or 8 h. Following treatment, the medium was replaced with fresh culture medium containing 100 nM SYTOX dye and Hoechst to stain dead and total nuclei, respectively. After 30 min incubation at 37°C, cells were imaged using a confocal microscope equipped with a temperature- and CO_2-controlled stage. Multiple fields (5 per well) were acquired (20x magnification) for analysis of cell death across conditions.

3.17 IncuCyte Cas 3/7 apoptosis assay

RPE-1 cells were seeded onto glass-bottom IBIDI chambers at a density of 20,000 cells per well at least 24 h prior to the experiment. Cell morphology and confluency were assessed under a microscope to ensure healthy and extended appearance before initiating stress treatments. Selected wells were then exposed to stress conditions for 4, 6, or 8 h. IncuCyte Cas 3/7 stock dye was diluted to a final concentration of 5µM in full cell culture medium, 0,5% v/v of Hoechst was added, the solution was thoroughly mixed and the medium in the IBIDI was replaced by this new mix. The cells were allowed to incubate at 37°C for 30 min before immediate imaging at 20x magnification.

3.18 CellROX green assay

CellROX green is a probe that allows the measurement of oxidative stress in live cells, by permeating the membrane showing strong fluorescence upon oxidation, with subsequent binding to the DNA.

After seeding 20,000 cells/ well on an IBIDI chamber, the next day the cells were treated with oxidative stress for 1 h at 37°C. CellROX stock solution in DMSO (2.5 mM) was dissolved to a final concentration of 5 µM in full cell culture medium 0,5% (v/v) of Hoechst was added, the medium was thoroughly mixed and distributed to the wells of the IBIDI chamber and incubated for 30 min at 37°C. Following that, the cells were washed 3 times with DPBS and imaged on the confocal microscope at 60x magnification. For the analysis, the fluorescence in the nuclear area was compared.

3.19 Acridine Orange assay

Acridine orange is a reagent that freely crosses the membrane and in live-cell assays settles inside organelles with low pH, showing us lysosomes (and melanosomes in this case).

RPE-1 cells underwent 2 rounds of knockdown before being subjected to the assay (see protocol above). As for the assay itself, first, acridine orange was diluted in cell culture medium necessary for all the wells to a final concentration of 0.1% v/v, the solution was vortexed and distributed to

the IBIDI wells to be incubated for 20 min at 37°C. After this time, nuclei were briefly labelled by adding Hoechst 33342, at approximately 0.5% v/v and cells were incubated for a further 10 min at 37°C. The cells were imaged immediately after or as fast as possible (without washing step), using the filter for red/orange (excitation at 550-590 nm; emission >610 nm), at 40x magnification on the confocal microscope.

3.20 Proliferation assay

Cells were counted, the total amount of cells needed for all conditions and wells was calculated and the total cell mix was prepared with fresh cell culture medium, thoroughly mixed and equally distributed onto a 12-well plate. After 24 h, the cells were checked for healthy morphology and spread under an optical microscope and the respective stress treatments/ control treatments were started; 24 h later, each well is treated with TrypLE for cell detachment (as detailed in 3.2), then cells were then collected in tubes containing fresh medium, mixed and counted on a Neubauer chamber.

If the proliferation assay was done on knockdown cells, then the knockdown procedure was performed 4 days before the protocol above, and the cells needed for the assay were then re-seeded from the KD experiment.

3.21 Image acquisition and analysis

Images were acquired as z-stacks (z=3, 0.5 µm per slide) on a Nikon spinning disk confocal microscope. A 20x, 40x, or 60x oil immersion objective was used. The setup was controlled by the image software NIS (Nikon). Microscopy images were imported and analyzed using FIJI.

Immunofluorescence images were analyzed using one of three approaches, depending on the specific requirements of the experiment and as indicated in the figure legends. In the first method, the fluorescence intensity of the channel of interest was quantified following the application of a Gaussian Blur filter (radius = 2 pixels) to reduce image noise. An automatic global thresholding algorithm, typically Otsu, Li, or Minimum (as indicated in the figure legends) was then applied to segment the channel, with the selected algorithm tailored to the staining intensity and experimental context. The total number of cells per image was determined by quantifying the nuclei (DAPI) channel, and fluorescence intensity was normalized and expressed on a per-cell basis.

For certain quantifications and colocalization analyses, the “ComDet” plugin in FIJI (ImageJ) was employed. This object-based colocalization tool enables analysis of multi-channel images by allowing independent adjustment of object size and intensity thresholds for each channel. ComDet provides a summary output including object counts, colocalization statistics, and references to specific regions of interest (ROIs), along with visual overlays of segmented objects for validation. An example workflow and output is provided in figure 3.1.

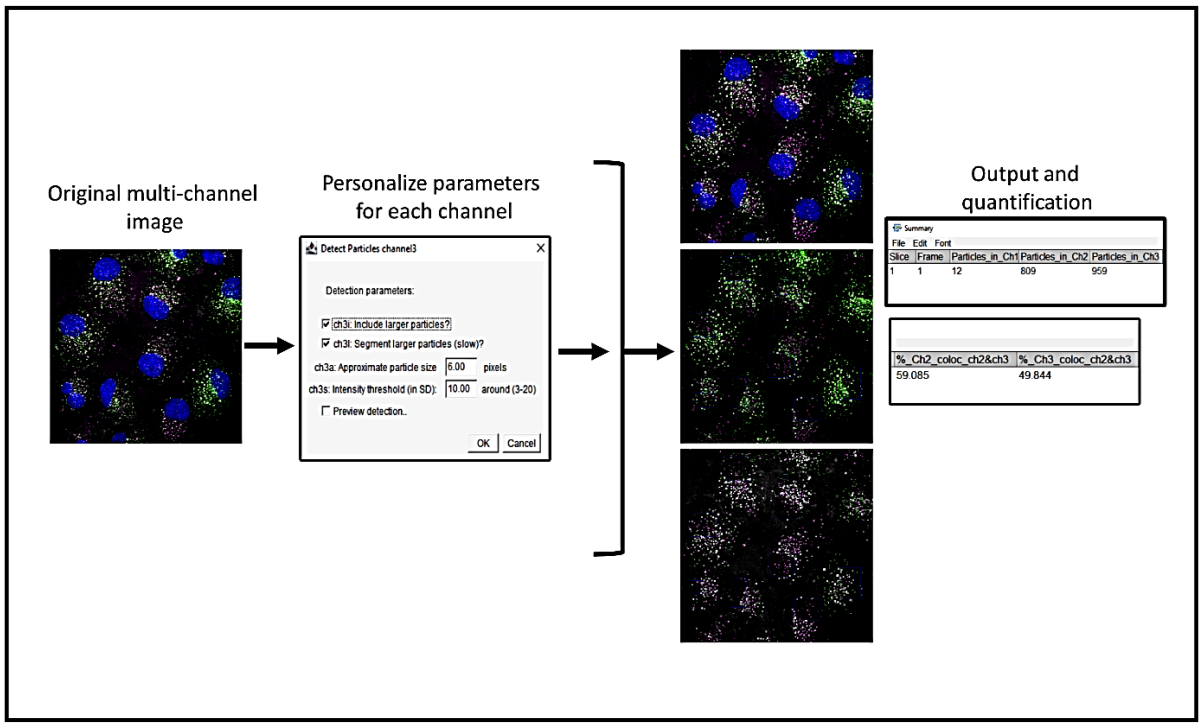

Fig.3.1: Schematics representing the workflow and results of the ComDet plugin (ImageJ).

For accurate analysis using Pearson’s correlation coefficient (PCC), fluorescence microscopy images must meet several key criteria. Signal intensities in both channels should exhibit a linear relationship and display sufficient dynamic range, avoiding saturation or excessive noise (Dunn et al., 2011) . Background fluorescence should be minimized or excluded through appropriate thresholding or region-of-interest (ROI) selection. Accurate image alignment is essential, as any channel misregistration can artificially distort the correlation (Dunn et al., 2011; Waters, 2009). In experiments where the images acquired in 16-bit format met the above criteria, the JACoP plugin in FIJI was utilized to compute colocalization metrics.

For each experimental condition, a minimum of three images per biological replicate was acquired and analyzed. The resulting values were averaged to yield a representative mean for each replicate set.

3.22 Statistical Analysis

All statistical analyses were conducted using GraphPad Prism software. Data are presented as mean ± standard error of the mean (SEM). Comparisons between two experimental groups with normally distributed data were evaluated using two-tailed Student's *t*-test. For analyses involving more than two groups, one-way analysis of variance (ANOVA) was employed, followed by either Tukey's or Dunnett's post hoc test, depending on the experimental design (as indicated in the figure legends). When assessing normalized datasets against a hypothetical value (e.g., 1 or 100%), a one-sample *t*-test was applied.

The number of independent biological replicates (*n*) used in each analysis is specified in the corresponding figure legends. Statistical significance is denoted in the figures as follows: ns, not significant; $p < 0.05$ (*), $p < 0.01$ (**), $p < 0.001$ (***), and $p < 0.0001$ (****).

4. Results

4.1 Biotinylation assay: methods optimization and testing of cell lines

Plasma membrane proteins, regardless of the cell or tissue of origin, are mostly under-represented mainly because of their low abundance (20-30% of the proteome) when compared to the whole cytosolic protein content (Shao & Hegde, 2011). This means that they require enrichment through subfractionation or isolation to not only to reduce the complexity of the sample but also to help overcome the low abundance as they only represent a small fraction of the cell (Griffin & Schnitzer, 2011), and therefore improve detection rates in following experiments.

For this project, we used an unbiased protein labelling approach to tag any transmembrane protein exposed to the extracellular surface and thus be able to track surfaceome changes upon different stress conditions. For this, we applied a chemically modified biotin reagent, Sulfo-NHS-SS-Biotin, that binds to primary amine groups which are found in lysine residues and at the N-terminus of proteins and thus are present in the majority of surface proteins (Rose et al., 2021). Since the reagent is unable to cross the plasma membrane, it can only react with surface-exposed proteins and will gain entry into the cell exclusively when internalization of labeled surface proteins is allowed. This provides a convenient experimental control, as labeling can be performed at 4°C (when endocytosis is minimal) and then the cells can be shifted to 37°C to permit endocytosis. Both the surface-labelled and internalized protein pool can be isolated with streptavidin or neutravidin beads and visualized by Western Blot. The selectivity of the biotinylation can be proven by probing for a membrane protein alongside a cytosolic protein, and comparing outcomes under different conditions: a control condition without biotin that should not lead to the isolation of any proteins, labelling at 4°C to capture only surface proteins, or internalization at 37°C followed by removal of remaining surface-localized biotin by cleavage of the disulfide bond within the functionalized biotin reagent to obtain only internalized proteins. The latter condition is particularly informative, as the amount and identity of proteins detected in each fraction can vary depending on the internalization time allowed and the trafficking kinetics of individual proteins in a specific cell type (Fig. 4.1 A).

With this in mind and given that some of the primary aims of our study were to find how bulk endocytic flux is affected by stressors and then identify specific proteins responsible for the stress coping mechanism, we first needed to establish and validate the efficiency of our surface biotinylation assay in a reliable cell model with proven endocytic capacity. For this purpose, HeLa cells were used to optimize the amounts and incubation times, as well as our reagents. Although HeLa cells are a well-established model, for cell biological research, as cancer cells they substantially differ from normal physiological cell types. Therefore, in the second stage, we extended the assay to test two non-cancerous cell lines: the human foreskin fibroblast cell line HFF-1 and the human retinal pigment epithelium cell line RPE-1. Another important consideration was ensuring a high proliferative capacity of the cells which we would use throughout the project, and as a result we employed telomerase-immortalized versions of these cell lines (see cell line table for further details).

After initial thought of the CME-modulated membrane proteins that we could detect reliably through Western blot, and some preliminary testing, we settled on using EGFR, since the antibody had a good level of sensitivity, was separated enough on nitrocellulose membranes not to interfere

with other probes and membrane cutting (at 180 kDa, so at the top of the gel) since we were aware that we would later use TrfR antibody, which stands at 90 kDa, and HSP70 which shows at 70 kDa. As reliable cytosolic proteins that could work as loading controls, during these first studies ß-actin was very reliable, with stable signal and suitable to our purposes, although afterwards we also adopted other cytosolic proteins such as GAPDH, AldoA, etc.

In the Western blot experiments we would see EGFR signal represented in terms of: 1) the *input* or fraction of total protein loaded to the beads (typically 5%) as a clear band due to having enough EGFR to detect in the total cell lysate, 2) the *intracelullar* fraction, being the amount of protein that was not isolated by the beads, 3) the eluate of the beads or *surface* fraction, which would show the levels of EGFR isolated by beads corresponding to the plasma membrane, or the *internalized* fraction, that would represent the portion of EGFR that was isolated by the beads after the internalization time at 37°C (Fig. 4.1 A).

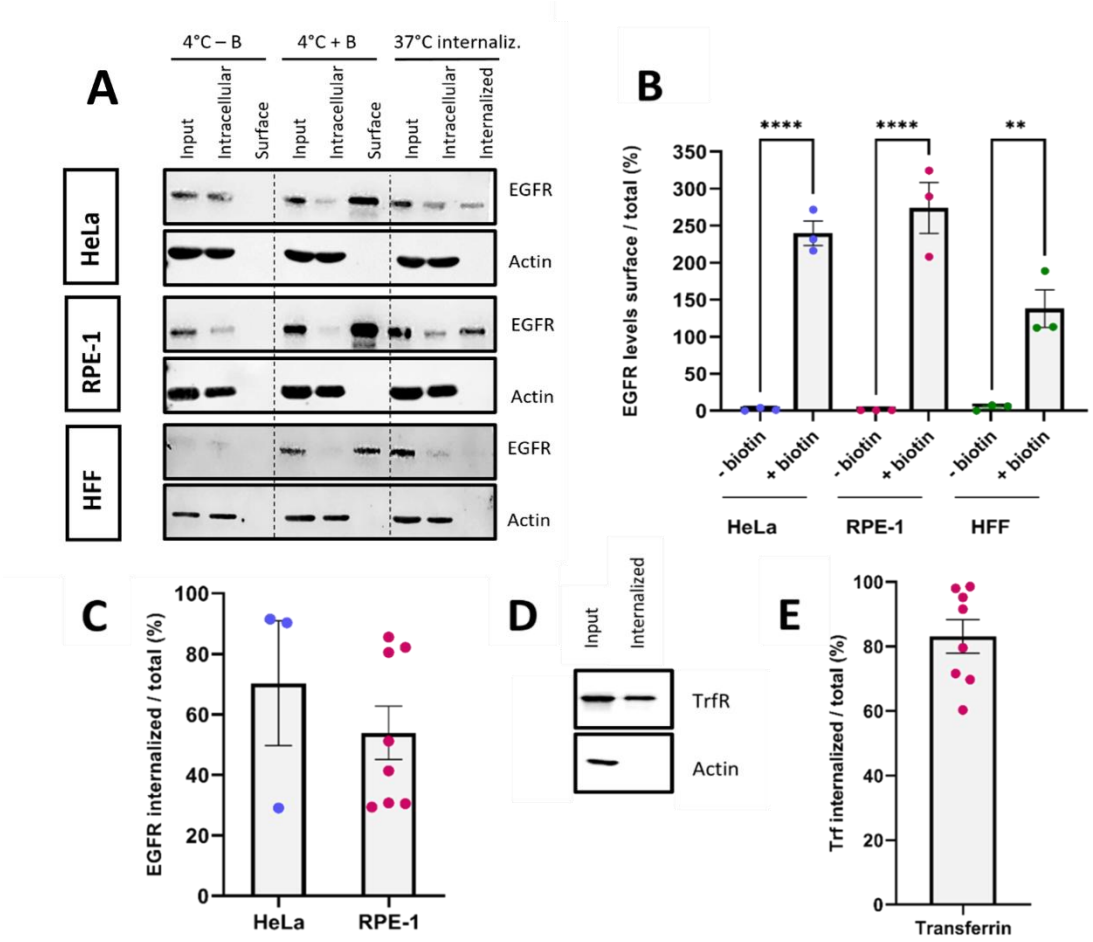

Figure 4.1: Biotinylation assay for labelling surface and internalized proteins.
A) Efficiency of surface biotinylation tested in HeLa, RPE-1 and HHF-1 cells. Representative western blots on all 3 cell lines, showing a no-biotin surface biotinylation control, a biotin surface biotinylation and a 37°C 15 min internalization. Inputs refer to the 5% of total protein loaded to the beads, intracellular fraction that was left after the beads pulldown and finally what is the surface/ internalized pulldown with streptavidin. B) Quantification of EGFR levels detected on the surface with regards to each cell line input. C) Quantification of EGFR that was internalized in 15 min with regards to their input on HeLa and RPE-1 cells. D) Representative blot showing RPE cells internalization of TrfR, as transferrin internalization is a signature cargo for clathrin mediated endocytosis. E) Quantification of internalized Trf versus the protein input. Data represent mean ± SEM; n= 3-9 independent experiments (indicated by puncta); Student's T-test (**p < 0.01, ****p < 0.0001).

By not adding biotin to our 4°C labelling control, and since there is nothing that would bind to the streptavidin beads, we would see a signal in both the *input* and the *intracellular* fractions but we should not see any signal of EGFR in the *surface* fraction. At the 4°C surface biotinylation with biotin, since biotin would bind more EGFR in relation to the total of proteins that also bind the streptavidin beads, we should see the *input* normally but a decreased *intracellular* fraction and in contrast, a richer EGFR band in the *surface* fraction. Finally, on our 37°C internalization condition, we should see the *input* as the normal total level lof protein, whereas a lower *intracellular* fraction (in this case it represents the rest of the total/intracellular protein excluding EGFR), and whichever level of EGFR that was internalized by the cells would be shown in the *internalized* fraction.

We tested the three different cell lines under various assay conditions until the results were reproducible and could not be attributed to technical artifacts.

The selectivity of the assay was confirmed by the quantification of EGFR levels that were normalized by the total protein (input), and this condition compared to the no-biotin control. HeLa cells had enriched EGFR levels of 200-250% the ones in the no-biotin control; RPE-1 had an enrichment of EGFR in an even higher range of 200-320%, whereas the HFF-1 had a worse enrichment of about 100-150% vs no-biotin control (Fig. 4.1 B).

When it came to the internalization performance HFF-1 produced very variable results, so these samples were excluded from quantification. After quantif1 internalized EGFR levels for both HeLa and RPE-1 we confirmed that both had rates of internalization ranging from 35-90% for HeLa, and from 35%- 85% for RPE-1 when normalized to their inputs (Fig. 4.1 C). Transferrin receptor internalization was also quantified for RPE-1 only, given that we were not considering HeLa cells, and that we had discarded HFF-1 previously. TrfR internalization showed less variability, ranging from 60-98% in 15 minutes (Fig. 4.1 D,E).

The times and rates are in line with literature reference for epithelial cells (non-RPE), pointing to a TrfR recycling $t^{1/2}$ of 5-12 min for the fast phase, and 15-30 min for the slow phase (Wiley et al., 1991; R. N. Ghosh & Maxfield, 1995; Sheff et al., 1999) and a EGFR recycling $t^{½}$ of 12-16 min for kinase-activated receptor or around 25 min for kinase-inactive or defective ones (Honegger et al., 1990; Wiley et al., 1991).

Finally, and in addition to evaluating endocytic capacity, we also considered factors such as ease of cell culture and protein yield. Here, HFF-1 cells were relatively easy to handle, but produced poor protein yield and therefore variable Western blot results (Fig 4.1 A and B), possibly due to the limited sensitivity of our available antibodies.

Since RPE-1 cells met all experimental requirements, including reliable endocytic activity, ease of handling and robust protein detection, they were chosen as our model for further experiments.

4.2 Establishment of stressors

One of the rationales behind the selection of the stressors used in this study and their specific dosage was that they needed to fall within a biologically relevant range; in other words, conditions that human cells might realistically encounter. Aiming to simulate pathological states, we intended to push cells beyond their baseline functional programming, but not so severely as to induce irreversible damage. The stress conditions, therefore, had to be strong enough to elicit a measurable cellular response in the long-term, but still under the physiological ceiling.

4.2.1 Heat stress

With these considerations, heat stress was identified as a suitable candidate. We selected a temperature of 42°C, which, while high, is comparable to febrile conditions observed in severe illness.

Since our focus was on the dynamic modulation of the cell surface proteome by CME, the stress conditions needed to strike a balance: they had to be sufficient to induce a cellular response, but not so prolonged as to engage confounding pathways such as protein translation. Therefore, we decided to test the effect of a 1 h heat shock which had previously been shown to be sufficient to induce the heat shock response (Vega et al., 2010; Zhou et al., 2015).

As an easy readout for the cellular response to elevated temperatures, we monitored HSP70 expression, a well-characterized molecular marker of heat shock (Vega et al., 2010).

We measured HSP70 levels following the 1-hour exposure to 42°C under two conditions: (1) immediate cell lysis post-treatment, and (2) a 4-hour recovery period at 37°C following the heat stress (Fig. 4.2 A, B). This was necessary since the heat-induced upregulation of HSP70 is based on its increased expression, and therefore, likely will only be visible with a delay. In line with this, we did not see a significant increase in HSP70 in any of the heat-shocked cell lines immediately after the stress treatment (Fig. 4.2 A, B). However, HSP70 levels increased in both non-cancerous cell lines, RPE-1 and HFF-1, and for RPE-1 cells we could show that this increase was reproducible and statistically significant (Fig. 4.2.1B). Only for the HeLa cells, we did not see an elevation of HSP70 levels after 4 h of recovery which might be linked to the fact that the HSP70 level in these cells was already very high at steady state in comparison to RPE-1 and HFF cells. This could argue for a deregulated heat shock response in these tumor cells, which was another argument against using HeLa cells for our project.

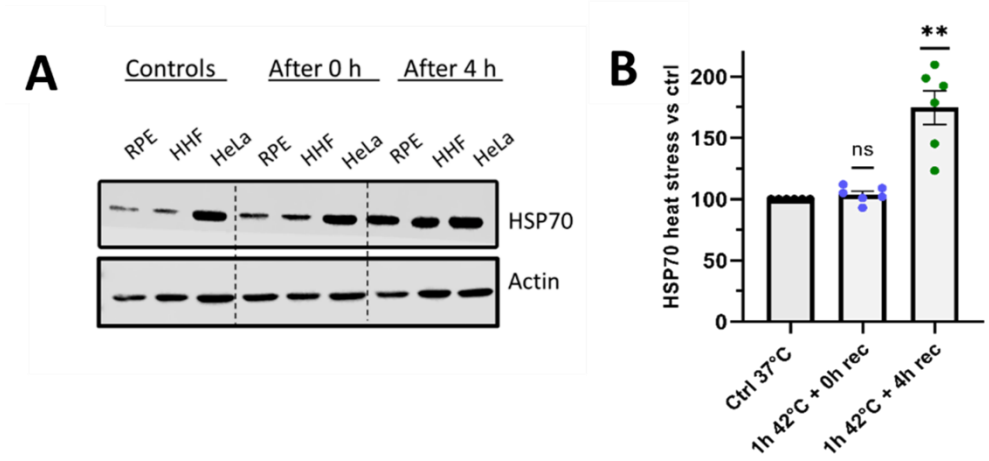

Figure 4.2: Validating the conditions for the induction of heat stress.
A) Representative western blot showing the levels of HSP70 after 1 hour at 42°C treatment on RPE-1, HHF, and HeLa cells. Actin was used as a loading control. B) Quantification of HSP70 levels in each condition for RPE-1 based on experiments as shown in (A). Data represent mean ± SEM; n = 5-6 independent experiments (indicated by puncta); one sample test (ns, not significant; **p < 0.01).

In conclusion, our findings supported the use of the 1-hour heat stress for RPE-1 cells as the preferred condition for further experiments, since this subsequently clearly leads to the expected induction of the heat shock response.

4.2.2 Osmotic stress

As López-Hernández, et al. (2020) reported, the transporter NHE7 accumulates at the plasma membrane of astrocytes upon hyperosmotic stress to promote an increase in cellular degradative capacity. Therefore, we considered it worthwhile to further investigate this stimulus in an independent cell line. Given that our model system consists of retinal pigment epithelial cells, and that evidence suggests that these cells are confronted with substantial osmotic fluctuations, e.g. in conditions of diabetic retinopathy (Willermain et al., 2014), osmotic stress represented a biologically relevant perturbation to explore in this cellular system. Additionally, hyperosmotic stress is known to promote the formation of intracellular protein aggregates, providing a measurable cellular response.

To find the right dosage of osmotic stress for RPE-1 cells, three medium osmolarities were tested: 600, 750 and 900 mOsm/kg adjusted using D-mannitol, being 600 mOsm/kg being the amount previously used for astrocytes (López-Hernández et al., 2020). To determine the extent of induced cellular stress, we quantified the number of protein aggregates per cell for each condition. Similarly to the heat stress induction, we decided for a 1 h exposure, but we also extended the treatment to 24 h to evaluate its long-term impact and reliably determine whether the different conditions were tolerable yet sufficient to induce a stress response (Fig. 4.2.2A). Our goal remained to identify a condition that was strong enough to produce a measurable response yet stayed still within the physiological range for RPE-1 cells. To quantify protein aggregation, we used the reagent Proteostat which intercalates into protein structures typical for misfolded and aggregated proteins and thereby becomes strongly fluorescent. As positive control for the assay we treated cells with a proteasomal inhibitor, MG-132, which is known to result in protein aggregation (Meyer-Helms et al., 2007) and indeed also strongly increased protein aggregation in our cell model (Fig. 4.3 A,B).

We found that the lowest osmolarity (600 mOsm/kg) had no measurable effect in RPE-1 cells, even after 24 h treatment, when compared to the negative control. In contrast, the intermediate osmolarity (750 mOsm/kg) produced a significant increase in protein aggregates after 24 h, relative to both the 1 h exposure and the negative control samples, while remaining non-lethal to the cells (Fig. 4.2.2B). The highest osmolarity (900 mOsm/kg) was nearly identical in effect to the intermediate osmolarity, even though the increase in protein aggregation remained non-significant, likely due to the lower number of experiments that were performed. However, at the highest osmolarity (900 mOsm/kg), there were significantly fewer viable cells after 24 h, and the cells exhibited pronounced shrinkage, effects that were not observed at 750 mOsm/kg (Fig. 4.2.2A). This prompted us to choose 750 mOsm/kg for our subsequent experiments.

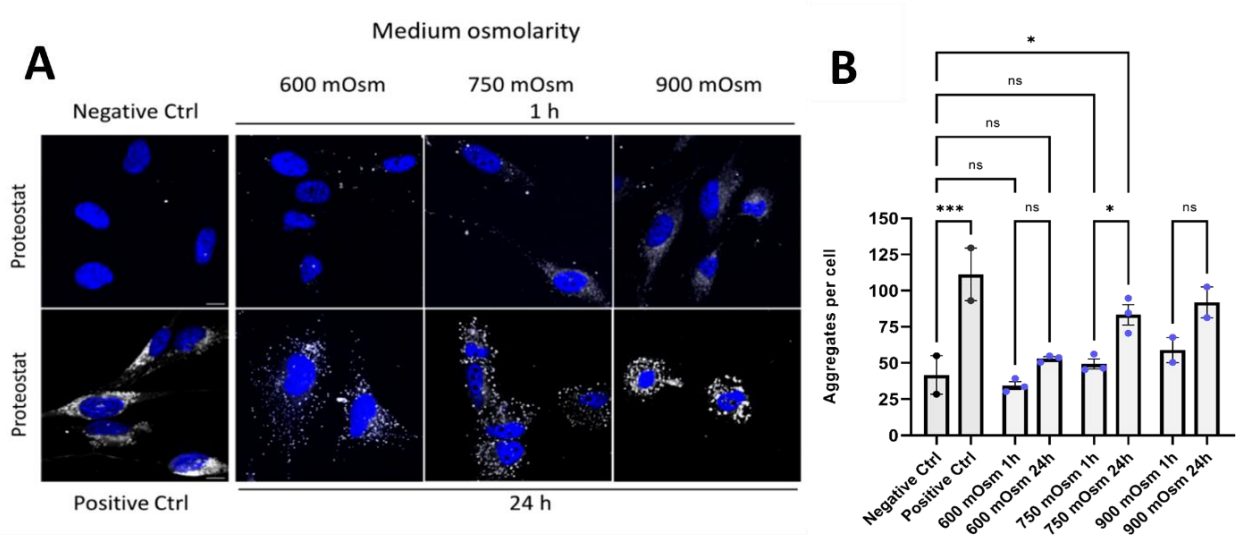

Figure 4.3: Validating the conditions for the induction of hyperosmotic stress.
A) Representative confocal images of RPE-1 cells after treatment with the three indicated osmolarities (adjusted by D-mannitol addition to the medium), for 1 h and 24 h. The images also show untreated cells as negative control and a positive control consisting of RPE-1 cells treated with10 µM of of the proteasome inhibitor MG-132 for 18 h. Protein aggregates were detected via the fluorescent probe Proteostat. Nuclei were visualized by DAPI. Scale bar = 10 µm. B) Quantification of the number of protein aggregates per condition. The results show no difference between cells exposed to 600 mOsm/kg and untreated cells, whereas a significant difference was found between untreated cells and cells exposed to 750 mOsm/kg for 24 h. The results for 900 mOsm/kg look similar but did not reach statistical significance. Data represent mean ± SEM; puncta indicate independent experiments (n = 2-3); One-way ANOVA with Tukey's post-test (ns, not significant, *p < 0.05, **p < 0.01, ***p < 0.001).

4.2.3 Oxidative stress

It has previously been shown that oxidative stress via the MAP kinase p38 can influence endocytic trafficking (Cavalli et al., 2001) even though no physiological relevance of this response has been demonstrated so far. Therefore, we decided that oxidative stress is a relevant stimulus for us to include in our panel of stressors.

After reviewing the current literature and evaluating commonly used reagents to induce oxidative stress, one compound emerged as particularly suitable: tert-butyl hydroperoxide (TBH). This reagent offers several advantages over more traditional oxidants such as H_2O_2 or Paraquat. Chemically, its moderate lipophilicity allows it to embed in membranes and generate tert-butoxyl and lipid-peroxyl radicals directly, so ROS production is less dependent on extracellular metal ions or cellular enzymes. The molecule is stable as a frozen stock and is degraded only slowly in low-serum media, giving highly reproducible dosing; by contrast, H_2O_2 is rapidly scavenged by serum catalase and drifts in potency during storage. The onset of stress with t-BHP can be tuned from min to days simply by adjusting concentration and exposure time, and investigators can keep serum in the medium without losing most of the oxidative hit (Glotin et al., 2006; Rabin et al., 2012). It is also optically silent, so it does not interfere with fluorescent ROS, lipid-peroxidation, or mitochondrial-potential probes, unlike autofluorescent drugs such as paraquat (S. Sun et al., 2014).

The literature reviewed did not show a clear consensus on the optimal concentration or exposure time for TBH, with reported concentrations ranging from 10 to 250 µM and treatment durations varying from 15 min to 72 h. With most of the studies falling into the category of "chronic"

treatment, yet sublethal to the cells (e.g. 10-50 µM for 12-72 h) as opposed to more "acute" treatment (e.g. 50-100 µM for 2-6 h) (Rabin et al., 2012; X. Xu et al., 2016), in order to have a measurable response in a shorter 1 h window, we needed to push the cells to a somewhat higher level. Based on this data, we selected a range of intermediate TBH concentrations (50–150 µM) for evaluation (Fig. 4.4 A).

To monitor oxidative stress, we employed CellROX Green, a fluorescent sensor that permeates the plasma membrane and emits a strong fluorescent signal upon oxidation, after which it intercalates into DNA. Accordingly, nuclear fluorescence intensity was measured as an indicator of oxidative stress at each concentration tested (Fig. 4.4 B). Already with a concentration of 50 µM there was a visible increase in CellROX signal even though this did not reach statistical significance with the analyzed number of samples due to high variation between experiments. With 75 µM there was still a tendency to higher CellROX levels, while higher TBH concentrations did not consistently lead to even further elevated CellROX signals.

Given these observations, we selected the intermediate concentration of 75 µM TBH as our working condition, as this dose showed clear nuclear fluorescence of the probe while remaining in the lower range of concentrations commonly reported in the literature, thereby minimizing potential cytotoxicity while ensuring a measurable oxidative response.

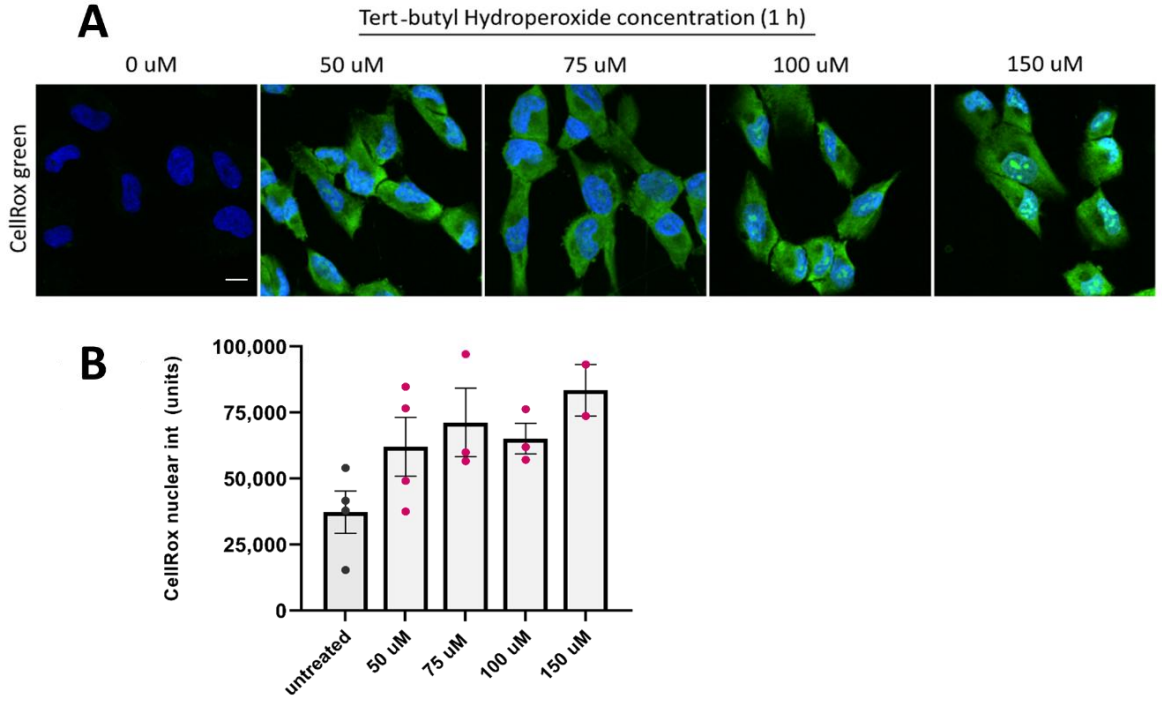

Figure 4.4: Validating the conditions for the induction of oxidative stress
A) Representative confocal images of RPE-1 cells treated with different concentrations of TBH for 1 h at 37°C. Oxidative stress was detected by the fluorescent reagent CellRox green. Nuclei were visualized by DAPI. Scale bar = 10 µm. B) Quantification of CellROX green fluorescence within the DAPI-outlined nuclei of the differently treated cells, showing a trend to increased fluorescence intensities in the treated cells, but no significant differences among the sets. Data represent mean ± SEM; puncta represent independent experiments (n = 2-4); One-way ANOVA with Tukey's post-test (not significant comparisons were not depicted).

4.3 Long-term effect of the chosen stress conditions

To determine the biological impact of the selected stressors in our RPE-1 cell model and to ascertain that they still had upon longer application only the intended mild effects, we assessed their impact on cell death and on proliferation rates as a sensitive readout for impairments of cellular fitness.

For measuring cell death rates, we employed a live-cell imaging approach based on two commercially available kits: SYTOX green to detect necrosis, and IncuCyte-Cas 3/7 green to detect apoptosis. Both reagents emit green nuclear fluorescence upon DNA-binding with some differences. While SYTOX cannot permeate the intact membranes of living cells, it can enter necrotic cells with compromised membranes which allows its binding to DNA causing a >500-fold increase in SYTOX fluorescence. Meanwhile IncuCyte Cas 3/7 is membrane-permeable and upon cleavage by active caspases during apoptosis (Fig. 4.5A, C) can bind DNA which likewise induces its fluorescence.

Cells were exposed to each stressor for 4 and 8 h, and 0.3% Triton X-100 was applied for 1 h as a positive control inducing cell death by membrane disruption (Fig. 4.5 E). The SYTOX green assay was performed by Sophie Meinhold, a bachelor student conducting her thesis under my supervision.

Quantification of SYTOX-positive nuclei revealed no significant increase in necrosis under heat or oxidative stress, whereas osmotic stress caused a modest but statistically significant increase, already apparent after 4 h of exposure (Fig. 4.5 B). Nevertheless, the overall levels of necrosis remained low, with 1–3% of cells affected.

When quantifying IncuCyte-positive cells as readout for apoptosis, it was again only the osmotic stress which caused already at 4 h of treatment a statistically significant increase in dead cells. However, at 8 h, in contrast to the results for necrosis, all stressors triggered increased apoptotic cell death compared to the untreated control (Fig. 4.5 D). As with necrosis, the percentages remained relatively small, in the range of 1.5–2% of the total cell population. Thus, the chosen stress conditions impact cell viability only marginally in line with the idea of the existence of cellular response programs that let cells successfully cope with moderate stress conditions.

To assess also whether the different stressors interfered with cell proliferation, RPE-1 cells were seeded and allowed to attach for 24 h prior to stress exposure. Cells were then treated for 24 h with the respective stressor, after which cells were washed, trypsinized and manually counted using a Neubauer chamber. This assay was carried out by Luwam Gebrezi, a bachelor student conducting her thesis under my supervision. After 24 h the number of untreated cells had roughly doubled in line with expectations indicating a normal proliferation rate of the untreated cells. In contrast, the numbers of the stressed cells, irrespective of the stressor, remained roughly at the level they had 1 day earlier (Fig. 4.5 F). These results suggest that, even if the rate of cell death remained low, the stress conditions strongly affected the proliferative capacity of the stressed cells.

In conclusion, we successfully set up conditions for three different physiological types of stress that clearly induced cellular responses, exerted very mild effects on cell viability across stressors, but already had a noticeable and comparable influence on cell fitness as judged based on proliferative capacity.

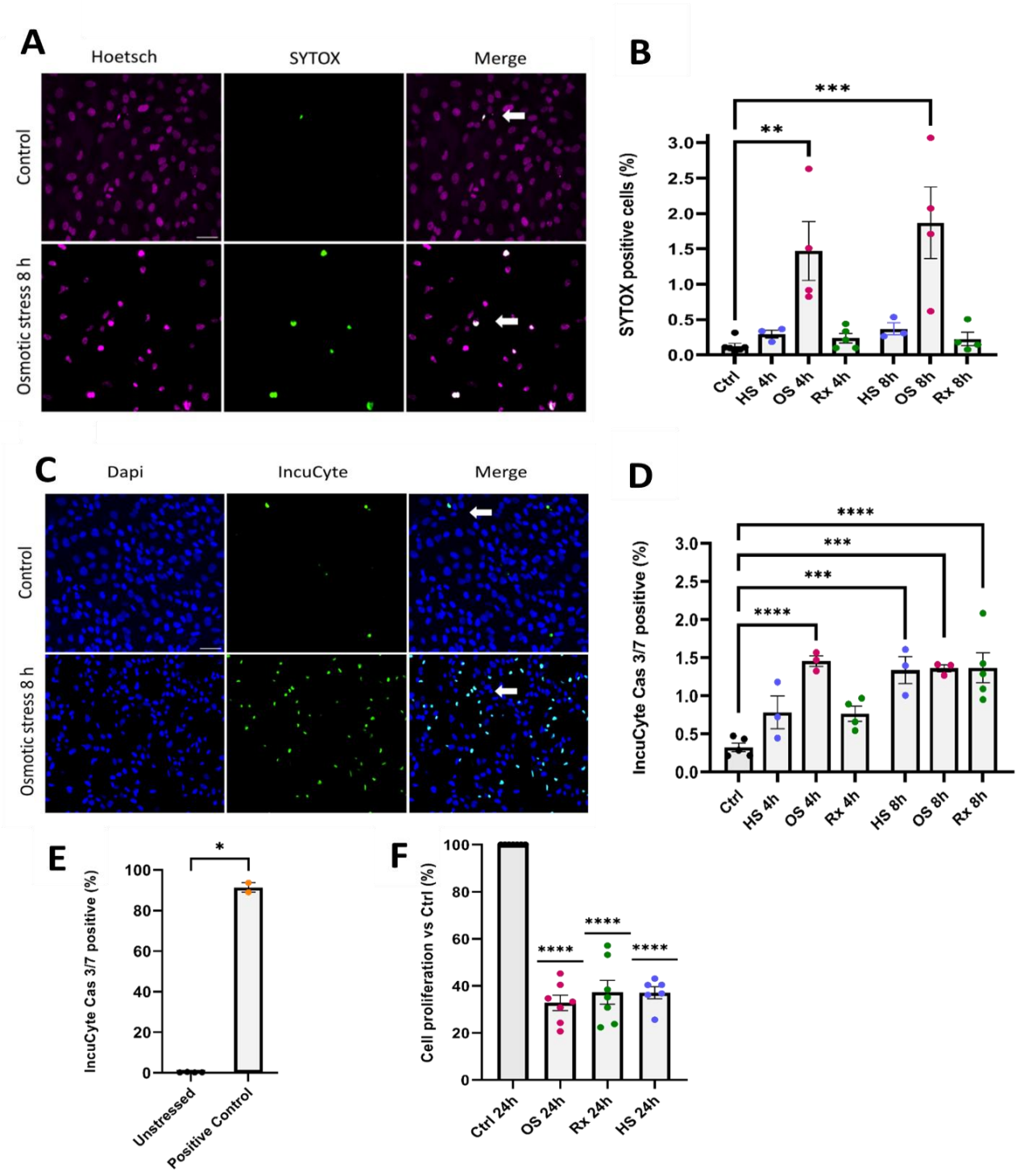

Figure 4.5: Exploring long-term effects of the chosen stress conditions on cell viability and proliferation.

A, B) RPE-1 cells were seeded within IBIDI chambers for live cell imaging and exposed to either heat stress (42°C), osmotic stress (750 mOsm /kg d-Mannitol) or oxidative stress (TBH 75 µM) for 4 or 8 h. A) Representative confocal images of unstressed RPE cells (control) and stressed cells treated with SYTOX green, exemplarily shown for osmotic stress. Nuclei were stained with Hoechst dye (magenta). B) Quantification of the percentage of SYTOX-positive nuclei per image for all indicated conditions based on images like in (A). C) Representative confocal images of unstressed RPE cells (control) and stressed cells treated with IncuCyte Cas 3/7 green, exemplarily shown for osmotic stress. Nuclei were stained with Hoechst dye (blue). D) Quantification of the percentage of IncuCyte-positive nuclei per image for all indicated conditions based on images like in (C). E) Quantification of IncuCyte-positive nuclei comparing unstressed cells with a positive control where cells were treated with 0,3% TritonX-100 for 1 h. F) 24 h after seeding

RPE-1 cells on 12-well plates exposed to either heat stress (42°C), osmotic stress (750 mOsm/kg d-Mannitol) or oxidative stress (TBH 75 μM) for 24 h before cell counting in a Neubauer chamber. B, D-F) Data represent mean ± SEM; n = 3-7 independent experiments (indicated by puncta); One-way ANOVA with Dunnett's post-test. (*p < 0.05, **p < 0.01, ***p < 0.001, ****p < 0.0001, not significant comparisons were not depicted). A,C) Scale bars = 10 μm.

4.4 Bulk endocytic uptake

Once the baseline parameters of the model, techniques, and effects of each stressor were established, the next objective was to assess the broader impact of these stress conditions on the endocytosis of surface proteins, with a particular focus on clathrin-mediated endocytosis.

It is known that environmental stress can influence how cells internalize surface proteins through bulk endocytic pathways like clathrin-mediated endocytosis (CME), macropinocytosis, and caveolar endocytosis. Although this area is not yet well-studied, changes in bulk endocytosis under stress could help cells adapt. For example, by increasing nutrient uptake or conserving energy. CME is the most investigated pathway and is believed to account for over 95% of bulk endocytic uptake (Bitsikas et al., 2014). Studies have shown that certain stressors, such as hyperosmotic and oxidative stress, can reduce CME efficiency in human cells (Malorni et al., 1993; X. Wu et al., 2001; Cheng & Vieira, 2006; Parry et al., 2008; S. Wang et al., 2011), while less is known about the effects of acute heat stress (López-Hernández, Haucke, et al., 2020). These insights led us to investigate whether our selected stress conditions alter the bulk internalization of surface proteins.

Following 1 h treatments with each stressor, surface-exposed transmembrane proteins were labelled with biotin at 4°C, a temperature that prevents endocytosis, and then shifted to 37°C to allow internalization for 15 min. To isolate only the internalized proteins, the residual surface biotin was chemically cleaved, and only the internalized pool of proteins was visualized and quantified through immunofluorescence, where they were detected using fluorescently-tagged streptavidin (Fig. 4.6 A upper panel). We aimed to measure bulk endocytosis following this principle.

In parallel, to selectively monitor CME, fluorescently-labelled transferrin was added to the culture medium during the 37°C internalization step. As transferrin uptake serves as a signature cargo for CME activity, it would show us exclusively this route (Fig. 4.6 A, lower panel).

In accordance with the existent literature and our expectations, quantitative analysis revealed that hyperosmotic and oxidative stress conditions led to a noticeable reduction in bulk endocytosis compared to the control, with a similar downward trend for their transferrin uptake rates (Fig. 4.6 B,C). Upon heat stress, both with and without recovery, we also saw a decrease in bulk and transferrin uptake (Fig. 4.6 B,C). On closer inspection, we found that the extent and pattern of the reduction varied per stressor. Osmotic stress effected a total protein internalization reduction by approximately 10–15%, while transferrin uptake declined even more sharply by 15–20%, suggesting a preferential impairment of CME over other endocytic routes. In contrast, oxidative stress showed the opposite pattern: transferrin uptake dropped by 20-25% while bulk protein internalization was more severely reduced by a more substantial 30-35%. This may indicate that non-CME pathways are more significantly affected under oxidative conditions, though further investigation is needed to clarify the mechanisms involved.

Heat stress, on the other hand, resulted in a comparable reduction in both total and transferrin internalization, although greater variability in transferrin uptake was observed across replicates.

This could point to a more integrated or coordinated modulation of endocytic processes, potentially involving shared regulatory components or signalling responses that synchronize CME with general endocytosis (Fig. 4.6 B–C).

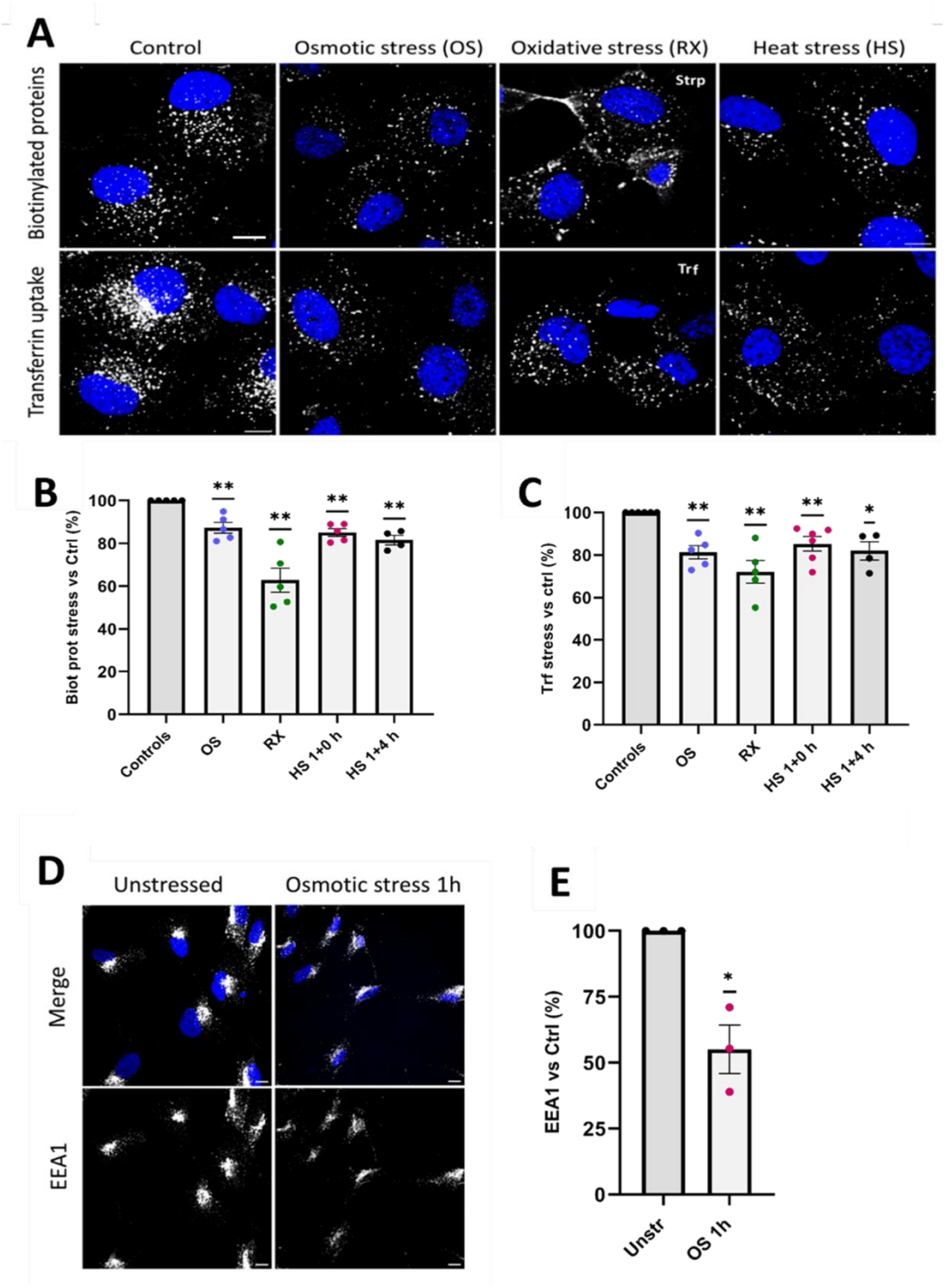

Figure 4.6: Both total bulk endocytic uptake and transferrin uptake are defective upon stress.
A) Representative confocal images of bulk endocytic uptake of biotinylated surface proteins (upper panel) and transferrin uptake (lower panel) under the different stressors. B, C) Quantification of fluorescent puncta (per cell) normalized to the control condition for the experiments described in A, respectively. Images were analyzed using the ComDet FIJI plugin. D) Representative confocal images of total levels of EEA1 in control and osmotically treated cells. A,D) Nuclei were visualized by DAPI (blue). E) Quantification of the

fluorescence intensity (per cell) normalized to controls from experiment D. Data represent mean ± SEM; n = 5 (A) and n=3 (D) independent experiments; One-sample T-test. *p < 0.05, **p < 0.01. All images were taken at 60X magnification. Scale bars = 10 μm.

To further investigate early endocytic machinery, we examined EEA1, a marker of early endosomes, via immunofluorescence. After 1 hour of osmotic stress, a reduction in total EEA1 signal intensity was observed (Fig. 4.6 D–E), supporting the notion that endocytic trafficking is suppressed under stress. This reduction may reflect impaired early endosome formation and maturation, consistent with decreased internalization observed in the biotin and transferrin assays.

4.5 Mass spectrometry: discovery phase

In the second stage of this project, we utilized label-free mass spectrometry to identify transmembrane proteins whose plasma membrane enrichment levels were altered in response to our selected stress conditions. This analysis was carried out in collaboration with Markus Räschle. Using our established unbiased biotinylation approach, we compared the surfaceomes of unstressed and stressed RPE-1 cells, aiming to identify changes in surface protein abundance that could be indicative of modulation by clathrin-mediated endocytosis.

We relied on a number of papers with similar methodologies that served as a model for our surfaceome protocol tests and optimizations (Ziegler et al., 2012; Matta et al., 2019; Ross et al., 2015; Rose et al., 2021). Their protocols provided valuable insights into sample preparation, emphasising the implementation of more stringent washing steps to reduce background noise and non-specific binding. We also established a no-biotin blank control as well as at least 3-4 replicates of each condition for comparison.

The surfaceome profiling was split across two mass spectrometry “sub-projects” (designated P0199 and P0207, according to the departmental queue system), covering all initial stress conditions, including the 4-hour recovery condition for heat stress, which, while not central to this thesis, was performed for completeness (Fig. 4.7 A). Mass spectrometry analysis yielded over 6,000 hits identified across all the datasets, after processing the raw files through MaxQuant and then Perseus (see methods for further information).

Principal component analysis (PCA) confirmed good clustering of biological replicates and clear separation between the different treatment conditions, supporting the consistency and reliability of the data (Fig. 4.7 B).

In order to process the long list of hits, multiple annotation database filters were applied to the primary Excel file. Established databases Gene Ontology (GO) resource (www.geneontology.org), which reflect annotations on molecular function, process, component or cellular location, were first used, in this case using location as a criterium. Similar to other studies (Özlü et al., 2015; Weekes et al., 2010), the plasma-membrane fraction was defined as the group of proteins annotated with GO terms “plasma membrane”, “cell surface”, “cell membrane”, or “extracellular”, and excluding the ones annotated with the term “Cytoplasm”. The filters greatly improved the rates of plasma membrane proteins from the first list.

This subpopulation should have represented only the surface exposed proteins that were targeted by our biotin enrichment method, though there were still many hits that were not bonafide plasma

membrane proteins or left many plasma membrane-associated proteins (a great number were intracellular). In order to improve selectivity towards our target proteins, a second layer of filtering was applied by cross-referencing our preliminary list with the *SURFY* database (Bausch-Fluck et al., 2018).

The "*in silico* human surfaceome" project was developed due to the intrinsic difficulty found in the correct and comprehensive identification of surfaceome proteins, developing the surface predictor *SURFY* based on a machine learning with experimentally verified high-confidence cell-surface proteins from the Cell Surface Protein Atlas (CSPA), after which they trained a classifier on 131 features specifically per protein topological domain. As a result, *SURFY* was validated to predict a human surfaceome of 2,886 proteins with an accuracy of 93.5%, and is reported to show excellent overlap with known cell-surface protein classes (e.g. receptors) (https://wlab.ethz.ch/surfaceome/).

SURFY's curation pipeline was particularly useful because it exclusively contains confirmed surface proteins. After applying SURFY as a last annotation and eliminating many proteins, our enrichment strategy was validated by comparing two control conditions: one with biotin labelling and one without. Plasma membrane proteins were found to be enriched more than fivefold in the biotin-labelled samples compared to the unlabelled controls, which provided validation for our approach.

With this refined dataset, we generated a preliminary list of candidate proteins potentially regulated by CME. These proteins showed statistically significant changes in membrane enrichment under stress conditions relative to the control, as visualized in the volcano plots for each treatment (Fig. 4.7 C). While the 4 h heat stress recovery condition was ultimately excluded from further analysis in this thesis, it provided a key insight: the condition led to a high upregulation of protein translation, consistent with our earlier findings using HSP70 as a readout and would introduce confounding variables that were outside the scope of this project.

Of the three primary stressors, oxidative stress yielded very few candidates meeting our CME-related criteria, making it a less promising avenue for follow-up studies. In contrast, heat stress (1 h, no recovery) and osmotic stress both presented a greater number of potential hits, positioning them as the most promising conditions for validation.

A

Mass-spectrometry project	Conditions tested	N° of replicates & experiments
P0199 Surface protein biotinylation	• Unstressed cells without Biotin • Unstressed cells with Biotin • Osmotically stressed cells with Biotin • Heat shocked cells (1h 42°C, no recovery) with Biotin	4 replicates per condition 2 independent experiments
P0207 Surface protein biotinylation	• Unstressed cells without Biotin • Unstressed cells with Biotin • Oxidatively stressed cells with Biotin • Heat shocked cells (1h 42°C, 4h at 37°C) with Biotin	3 replicates per condition 2 independent experiments
P0260 Lysates to obtain whole-cell proteome	• Unstressed cells • Oxidatively stressed cells • Osmotically stressed cells • Heat shocked cells (1h 42°C, no recovery) • Heat shocked cells (1h 42°C, 4h at 37°C)	4 replicates per condition 2 independent experiments

B

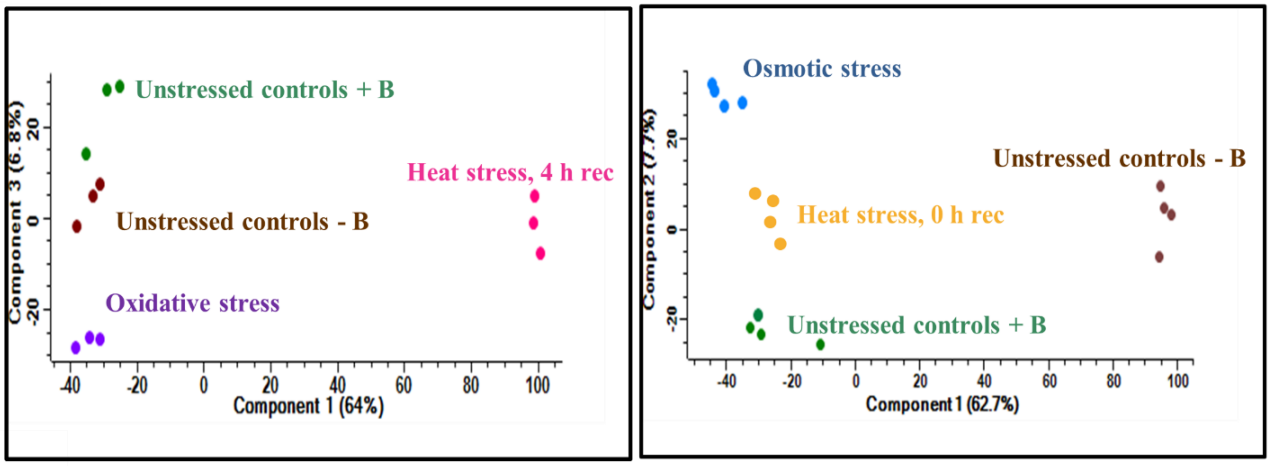

C

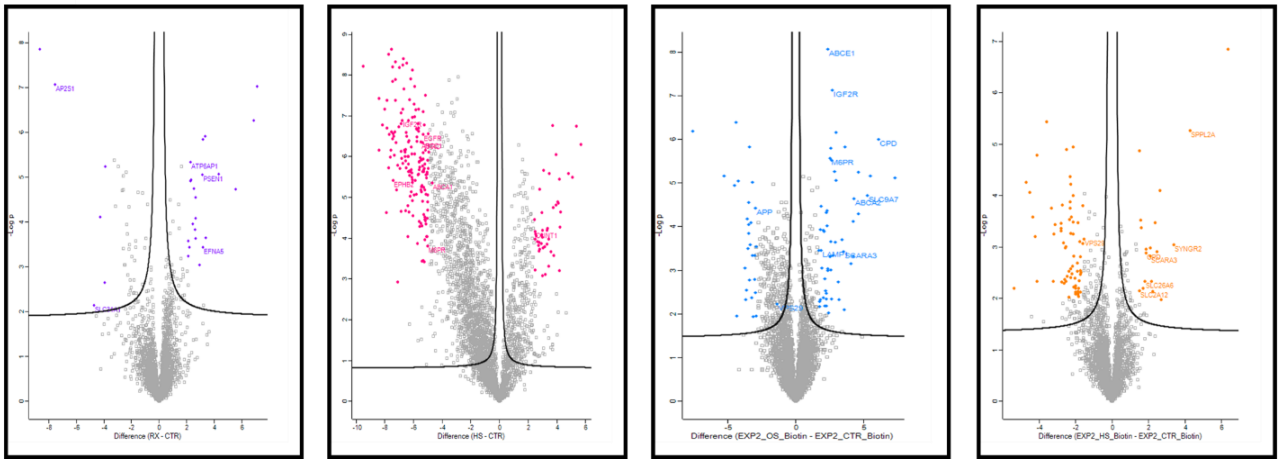

Figure 4.7: General mass spectrometry sub-project allocation and preliminary results

A) Table showing details about our mass spectrometry surfaceome profiling (P0199 and P0207) and our whole-proteome mass spectrometry (P0260). B) PCA analysis of the replicates from each surfaceome subproject, showing P0207 on the left and P0199 on the right. C) Preliminary volcano plots per stressor (colour coordinated to PCA) showing some interesting candidates possibly regulated by CME.

To account for changes in overall protein expression that could confound surface enrichment data, we performed a whole-proteome mass spectrometry experiment as a control (sub-project P0260) (Fig. 4.7 A and 4.8 A). This allowed us to cross-reference surfaceome data with total protein abundance.

It is important to mention that, in general, accurate and robust proteome-wide quantification using label-free approaches remains a challenge, since the sheer number of proteins to identify successfully hinges on a high mass resolution and accuracy, which are fundamental for reliable peptide identification (Cox et al., 2014). Unless a knowledge of baseline proteins that will not change in all the groups/replicates measured is previously known and can be used to normalize the readings, many of those identifications will be lost, especially in the case of high mass species (Compton et al., 2011). Since such normalization could not be applied to our readings, our final list of hits from this experiment was more limited than the one done with biotin enrichment. Despite the shortcomings, we still recovered 4838 hits in the final list (Fig. 4.8 A).

Interestingly, a comparison of these datasets revealed that only a small number of endocytic proteins displayed significant changes at the whole-cell lysate level (Fig. 4.8 B), suggesting that most of the observed surfaceome shifts are not driven by changes in expression but rather by redistribution within the cell.

Finally, we used the STRING database (www.string-db.org) to analyze shared hits across all three stress conditions. This pathway analysis revealed consistent downregulation of functional modules associated with energy metabolism, nucleotide biosynthesis, microtubule organization and transport, as well as aggrephagy and ubiquitin-proteasome activity. These pathways appeared to be deprioritized under stress, possibly reflecting a cellular shift toward survival and damage response programs. The top five underrepresented pathways are summarized in Fig. 4.8 C, with a complete list of associated proteins available in the supplementary tables.

A

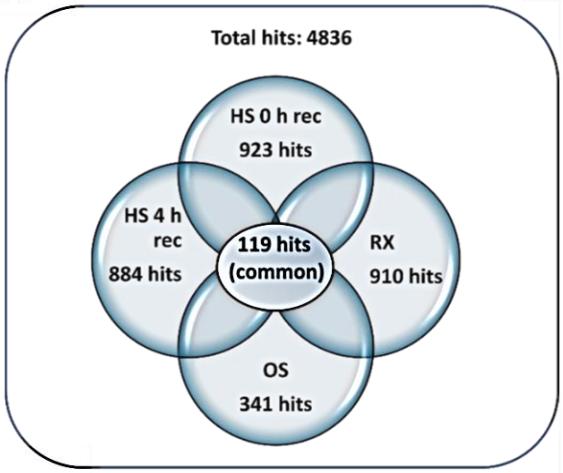

B

Endocytic protein	OS	RX	HS (4 h rec)	HS (0 h rec)
AP-2	=	=	=	=
Eps15	=	=	=	=
Eps15L1	=	=	=	=
Dynamin 2	=	<	=	=
Endophilin B1	=	=	<	=
Endophilin B2	=	=	=	=
Endophilin A2	=	<	<	=
SNX 9	=	<	=	=
PiCALM	=	=	=	=
CLC/ CHC	=	=	=	=
AAK1	=	=	=	=
GIT1	=	=	=	=
NECAP2	=	=	=	=
FCHO2	=	=	=	=
EPN1	=	=	=	=

C

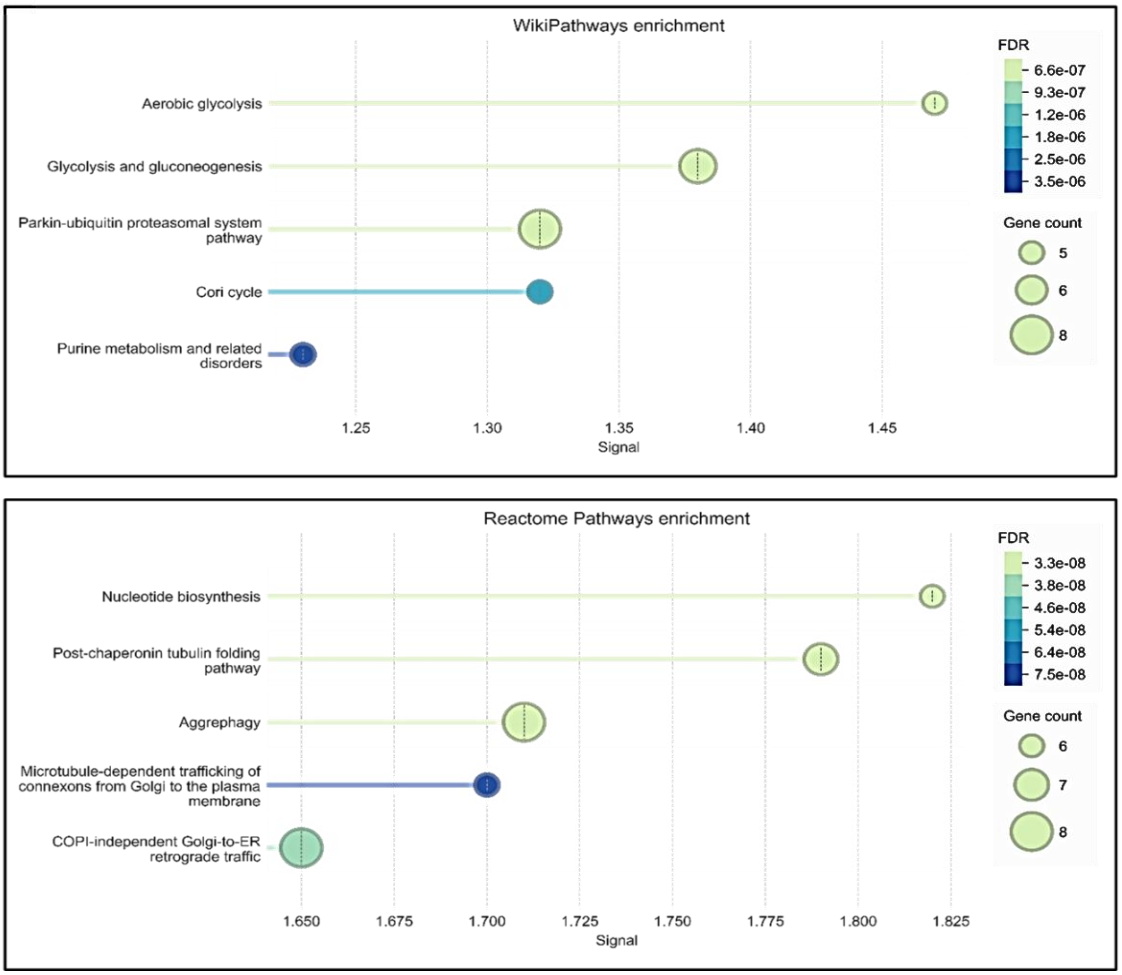

Figure 4.8: General statistics regarding our whole-proteome sub-project (P0260).
A) Scheme shows the number of whole-proteome mass spectrometry hits that were differentially expressed per condition, as well as the hits shared by all 4 stress conditions (P0260). B) Table detailing endocytic proteins and their levels in the list. C) String-db generated pathway analysis that were underrepresented when analysing the 119 common hits of all stressors.

4.6 Validation of mass spectrometry hits

4.6.1 Heat stress: SPPL2A

Normally present in late endosomes or lysosomes, Signal peptide peptidase-like 2A (SPPL2A) curiously appeared significantly enriched in plasma membrane according to our surfaceome mass spectrometry data of heat stressed cells and osmotically stressed ones. Along with SPPL2B they are part of a family of intramembrane aspartyl proteases that cleave type II transmemrane protein N-terminal fragments (NTFs) within their hydrophobc transmembrane segments (Friedmann et al., 2006; Mentrup et al., 2020; Mentrup & Schröder, 2022). Some of their substrates include CD74, TNF-α, Dectin-1, and LOX-1 NTFs. Interestingly, SPPL2B is the protein that functions generally at the plasma membrane (and early endosomes) and has functions primarily at a neutral pH (Mentrup et al., 2019) , whereas SPPL2A has been reported to function at acidic pH.

SPPL2A/B have some functional similarities and some mechanistical overlap, however, only SPPL2A has been found unequivocally established as essential for human immunity and linked to some human pathologies (Schneppenheim et al., 2013; Gradtke et al., 2021; Esmaeilzadeh et al., 2024). At this point of the investigation, we found its upregulated appearance in the membrane counterintuitive but undoubtedly interesting.

Following several attempts to validate this membrane enrichment, including challenges related to antibody sensitivity in surface eluates, we successfully confirmed the enrichment of the protein at the plasma membrane under heat stress conditions (Fig. 4.9 A, C). To rule out changes in total protein expression as a confounding factor, we quantified SPPL2A levels in the inputs (whole-cell lysate) under heat stress and controls and found no significant difference (Fig. 4.9 B), in line with the mass spectrometry whole proteome levels that were also unchanged. Additionally, quantification of the housekeeping protein used for normalization confirmed that the input samples were appropriately loaded and that membrane fractions showed negligible signal, supporting the specificity of the eluate signal (Fig. 4.9 D).

Validation of the protein's enrichment under osmotic stress was not pursued further, largely due to inconsistent results and considerable variability observed across Western blot attempts. While an example can be seen in Fig. 4.9 A, anecdotal observations and technical variability suggest that the osmotic stress condition did not reliably induce membrane enrichment for this protein.

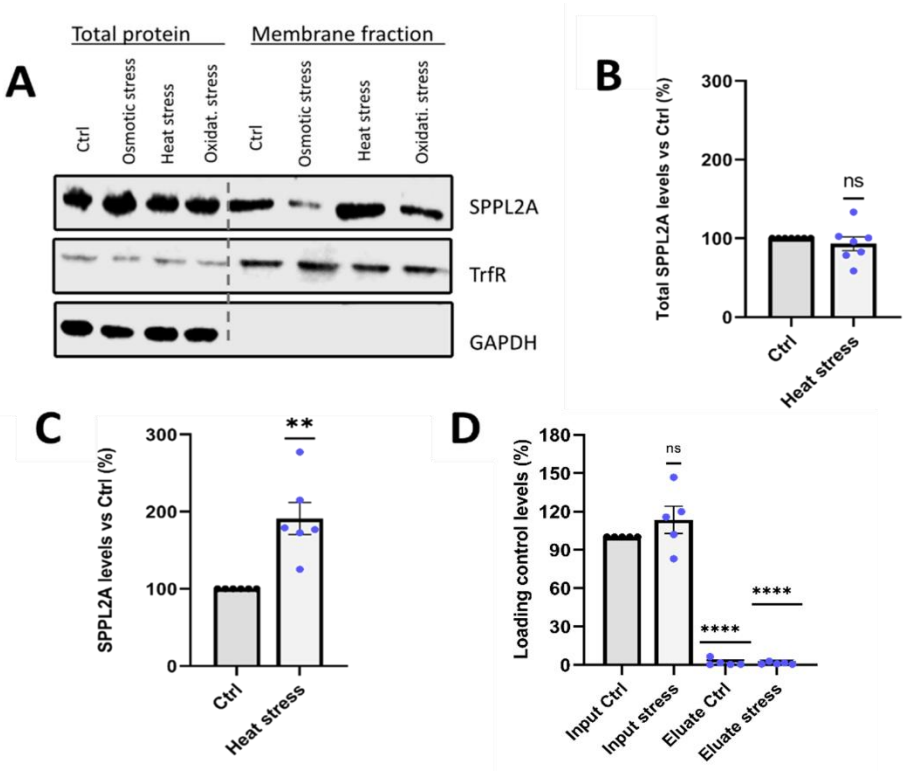

Figure 4.9: SPPL2A was found enriched in heat-stressed plasma membrane of cells.
A) Representative Western blot membranes of RPE cells biotinylation after treatment with our 3 stress conditions. Transferrin receptor was used as a membrane protein control, and GAPDH was used as a loading control. B) Quantification of inputs/ total SPPL2A levels on heat stress experiments (osmotic stress levels were not quantified due to not having enough experiments of this type). C) Quantification of SPPL2A enrichment on heat stress membrane versus control. D) Quantification of housekeeper protein expression levels in all heat stress experiments. Data represent mean ± SEM; n = 5-7 independent experiments; all expression levels were normalized to controls. One-sample T-test (ns, not significant; **p < 0.01, ****p < 0.0001).

4.6.2 Osmotic stress: NHE7, TrfR and CI-M6PR

Osmotic stress proved to be more fruitful in the validation of candidate surfaceome hits, with three proteins confirmed to be enriched at the plasma membrane of RPE-1 cells: NHE7, TrfR, and CI-M6PR. Each of these will be addressed separately in the sections below.

4.6.2.1 NHE7

NHE7 was introduced earlier in reference to the study by López-Hernández et al. (2020), which reported its enrichment at the plasma membrane in primary mouse astrocytes subjected to hyperosmotic stress (600 mOsm/kg). In their system, NHE7 contributed to multiple protective mechanisms, including the correction of cytoplasmic acidification and activation of autophagy to eliminate protein aggregates. In our own surfaceome mass spectrometry data, NHE7 was similarly found to be significantly enriched in the plasma membrane under both heat and osmotic stress. Unfortunately, this protein was not detected in our whole-cell lysate proteome dataset, and thus background expression levels remain unknown. Nonetheless, its appearance in the surfaceome

dataset provided a degree of confidence in the mass spectrometry findings, which warranted further validation through imaging.

To this end, we designed an experiment involving the overexpression of fluorescently tagged NHE7 in RPE-1 cells, followed by assessment of its localization under each stress condition. Given the qualitative nature of membrane localization, we established three discrete categories for plasma membrane enrichment: *no enrichment*, *some enrichment*, and *elevated enrichment* (Fig. 4.10 A). All images were randomized and blinded, and each cell was manually assigned to one of the three categories before results were quantified (Fig. 4.10 B–D). This assay was performed by Luwam Gebrezi, a bachelor student conducting her thesis under my supervision.

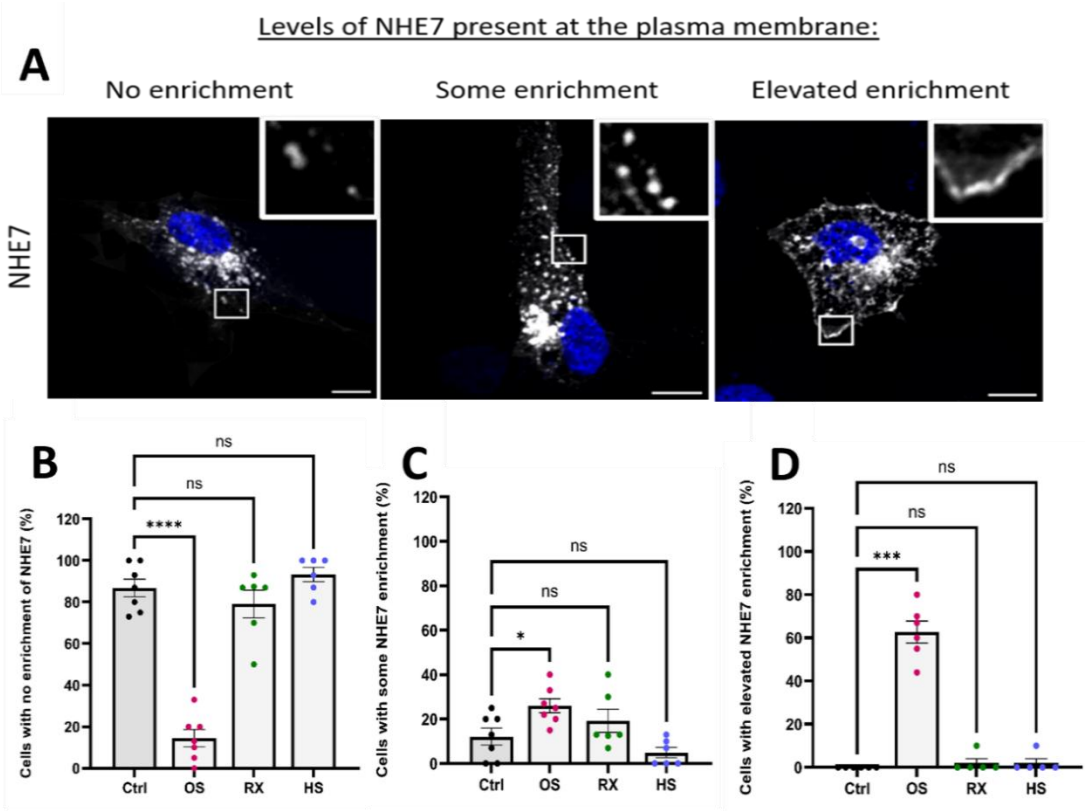

Figure 4.10: Validation of NHE7 membrane enrichment upon osmotic stress.
A) Representative confocal images showing RPE-1 cells overexpressing fluorescently-tagged NHE7, and an example of the three qualitative categories of membrane enrichment found in experiments. Nuclei were visualized by DAPI (blue). B-D) Quantification of the percentage of cells that were allocated to each category shown in A, per condition. Data represent mean ± SEM; n = 5-6 independent experiments; One-way ANOVA with Dunnett's post-test (ns, not significant; *p < 0.05, ***p < 0.001, ****p < 0.0001). Scale bars = 10 µm.

In line with our expectations, the osmotic stress condition yielded the lowest proportion of cells with no detectable membrane enrichment (Fig. 4.10 B), while also producing the highest proportion of cells categorized as showing elevated membrane enrichment (Fig. 4.10 D). The intermediate category, representing some enrichment, showed a variable distribution across conditions, with statistical significance reached only under osmotic stress (Fig. 4.10 C).

Contrary to what was suggested by the surfaceome mass spectrometry data, we did not observe significant membrane enrichment of NHE7 under heat stress in our imaging-based validation.

Similarly, oxidative stress did not result in detectable plasma membrane enrichment, further suggesting that the osmotic stress response is more robust and consistent in promoting NHE7 translocation to the membrane in RPE-1 cells.

4.6.2.2 TrfR and CI-M6PR

The mass spectrometry dataset revealed a significant enrichment of transferrin receptor (TrfR) at the plasma membrane, specifically under osmotic stress conditions. Interestingly, when examining the whole-cell lysate proteome data, we observed a somewhat counterintuitive trend: TrfR levels were significantly upregulated in all conditions *except* osmotic stress, where no change was detected. This discrepancy suggests that the membrane enrichment seen under osmotic stress likely stems from a redistribution of the receptor rather than an increase in total protein expression, supporting the idea of stress-induced repositioning of TrfR.

Another protein of interest that emerged from our preliminary candidate list was the cation-independent mannose-6-phosphate receptor (CI-M6PR).

In mammalian cells, the trafficking of lysosomal enzymes bearing mannose-6-phosphate (M6P) residues are mediated by two distinct type I transmembrane glycoproteins: the cation-dependent M6P receptor (CD-M6PR) and the cation-independent M6P receptor (CI-M6PR). These are the only known members of the P-type lectin receptor family. CD-M6PR functions exclusively within the intracellular environment, where it participates in the sorting of newly synthesized hydrolases from the trans-Golgi network (TGN) to endosomes. In contrast, CI-M6PR while predominantly intracellular, can localize to the plasma membrane where it has the additional capacity to mediate uptake of extracellular ligands carrying M6P residues (Gauthier et al., 2024).

Structurally, CI-M6PR is a type I membrane protein composed of a large N-terminal extracellular domain, a single transmembrane region, and a short cytoplasmic tail (Brown et al., 2009). The extracellular portion comprises 15 homologous domains, each resembling the structure of the single domain found in CD-M6PR. The principal function of CI-M6PR is to mediate the intracellular trafficking and recycling of lysosomal enzymes between the TGN, endosomes, and lysosomes. Notably, a portion of lysosomal enzymes that escape initial sorting can be recaptured from the extracellular milieu via CI-M6PR. In addition to its canonical cargo, CI-M6PR binds to a diverse array of ligands, including IGF-II, granzyme B, uPAR/plasminogen, glycosylated LIF, and retinoids, triggering rapid receptor internalization. This internalization is mediated by the conserved cytoplasmic sorting motif "YSKV," which interacts with adaptor proteins AP-1 and AP-2 (P. Ghosh et al., 2003) , ensuring efficient trafficking within the endocytic pathway.

In our mass spectrometry data, CI-M6PR showed membrane enrichment in both heat stress and osmotic stress conditions. This finding is particularly notable given that CI-M6PR also appeared on the list of osmotic stress-responsive genes in the study by López-Hernández et al. (2020). Yet, as with TrfR, background protein levels in whole-cell lysates showed no significant change under any of the stressors, again suggesting that the increase in membrane association is not due to elevated synthesis but to altered subcellular trafficking or retention.

Validation of these findings was carried out by immunoblot analysis of surface eluates, confirming membrane enrichment for TrfR under osmotic stress and CI-M6PR under both osmotic and heat stress (Fig. 4.11 A, B, and E). As with our previous validation experiments (e.g., SPPL2A), total

input protein levels and housekeeping protein controls were also quantified to ensure consistent loading and reliability of the surface enrichment data (Fig. 4.11 C-D).

CI-M6PR is known to undergo multiple post-translational modifications, including acetylation, glycosylation, and methylation. In our input samples, we observed that the antibody used for CI-M6PR detection frequently revealed one or two closely migrating bands. This band pattern likely reflects differences in glycosylation states, although this was not directly tested or confirmed by sequencing. We speculated whether these distinct protein forms might correspond to different functional states, such as preferential endocytosis of one form over the other. However, when we quantified the number of samples displaying single versus double bands, no clear correlation with any specific stress condition was found.

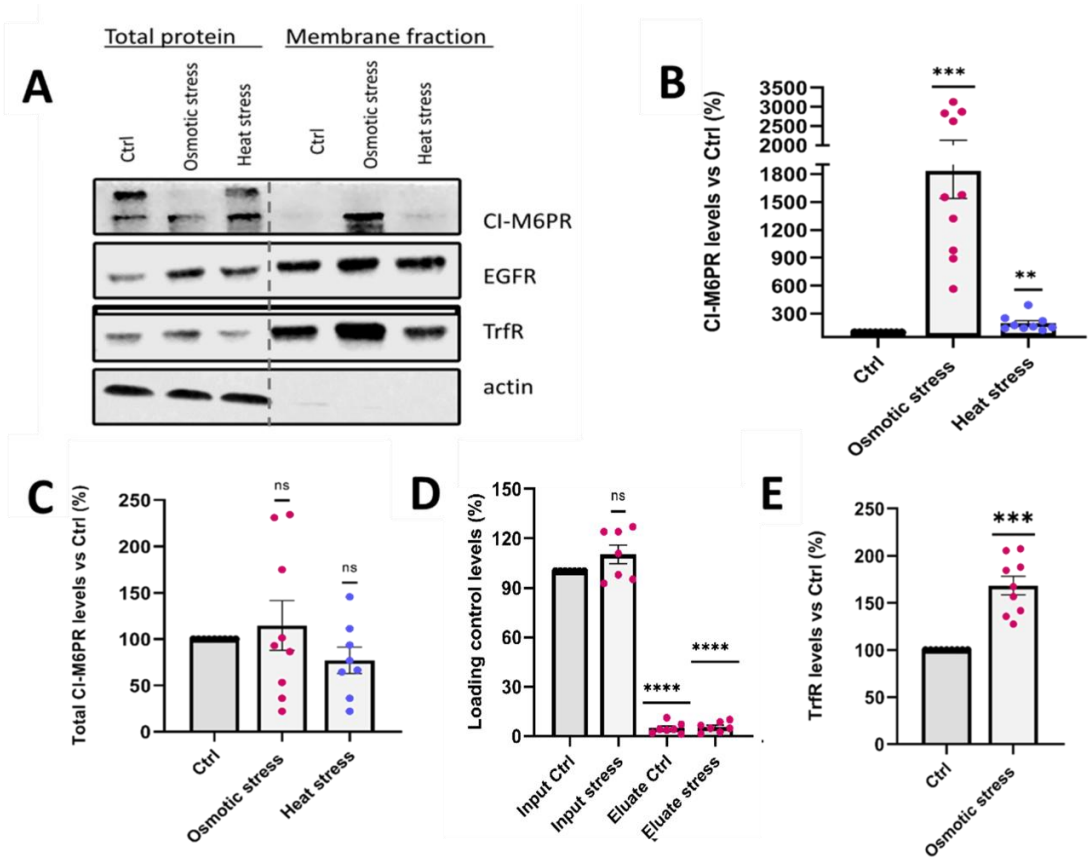

Figure 4.11: TrfR and CI-M6PR were found enriched in the membranes of stressed cells.

A) Representative western blot showing membrane-enriched levels of CI-M6PR and TrfR. EGFR is shown as a reference for another membrane protein. Actin was used as a loading control. B) Quantification of CI-M6PR levels normalized to control. C-D) Quantification of the inputs/ total protein level of CI-M6PR in C, and housekeeper protein levels in D. E) Quantification of transferrin receptor levels upon osmotic stress. Data represent mean ± SEM; n = 7-10 independent experiments (as shown by puncta); One-sample T test (ns, not significant, **p < 0.01, ***p < 0.001, ****p < 0.0001).

4.6.2.3 Other antigens targeted

In total, 18 antibodies were used while attempting to validate the mass spectrometry results, all of which can be seen in table 17.

Table 17: all the antibodies tested for validation and their results

Antigen tested	Result
CI-M6PR, CD-M6PR, TrfR, HSP70, SPPL2A, EGFR, Integrin-Beta-5	Worked well/ validated either in WB, IF or both
SCARA1, LAMP1, EEA1, APPL1, AP-2	The antibody was able to detect protein in inputs, but not sensitive enough for eluates
CTR1, Ephrin A5, Ephrin B2, AP-1	It did not work well either in WB or IF
ABCA1	No difference found in protein level (IF)
VPS29	Mixed results in WB

4.7 Osmotic Stress: Broader Analysis and CI-M6PR as a Principal Target

Our previous experiments identified two robustly validated candidates: TrfR and CI-M6PR, both of which were enriched in the plasma membrane under osmotic stress. This convergence on a single stress condition provided a strong rationale to further investigate the broader molecular landscape associated with osmotic stress and to uncover the underlying mechanisms behind these observations.

As a first step, we performed a global analysis using the STRING database to explore the biological processes linked to the 211 significant plasma membrane-associated proteins identified by mass spectrometry under osmotic stress (Fig. 4.12 A). This functional enrichment analysis yielded several highly represented pathways, most notably: regulation of lysosomal protein catabolism, amyloid-beta clearance/catabolism (which we broadly interpret as related to the clearance of protein aggregates), and endocytosis.

The prominence of endocytosis among the top enriched processes was reassuring, as it aligns with the primary focus of our project and the criteria used in our candidate selection. Interestingly, the enrichment of processes such as lysosomal catabolism and aggregate clearance stands in contrast to our earlier findings from the whole-proteome lysate mass spectrometry analysis, where stress conditions appeared to deprioritize these pathways (Fig. 4.5.2 C). This discrepancy suggests a potential stress-specific reorganization of protein trafficking and degradation machinery, particularly under osmotic stress.

Furthermore, the overlap between these enriched biological processes and the known functional roles of CI-M6PR is striking (Fig. 4.12 B). CI-M6PR is a key mediator of lysosomal enzyme trafficking, responsible for the delivery of acid hydrolases from the trans-Golgi network to the lysosome and also for their endocytic retrieval from the plasma membrane (Brown et al., 2009). Its internalization via clathrin-mediated endocytosis is a well-established mechanism essential to its function (P. Ghosh et al., 2003; Brown et al., 2009).

Shockingly, and after scouring the literature, we had the realization that, despite extensive research into M6PR trafficking and endosomal sorting, and several mechanistic studies using hyperosmotic

conditions as cell-biological tools, there is no primary research paper that goes into the details of this physiologically induced upregulation of the receptor at the cell surface after osmotic stress.

These considerations led us to hypothesize that CI-M6PR may play a pivotal and novel role in the cellular adaptation to osmotic stress in mammalian cells. To explore this possibility, we chose to further characterize the behaviour, regulation, and potential functional significance of CI-M6PR in the context of osmotic stress in the subsequent experiments.

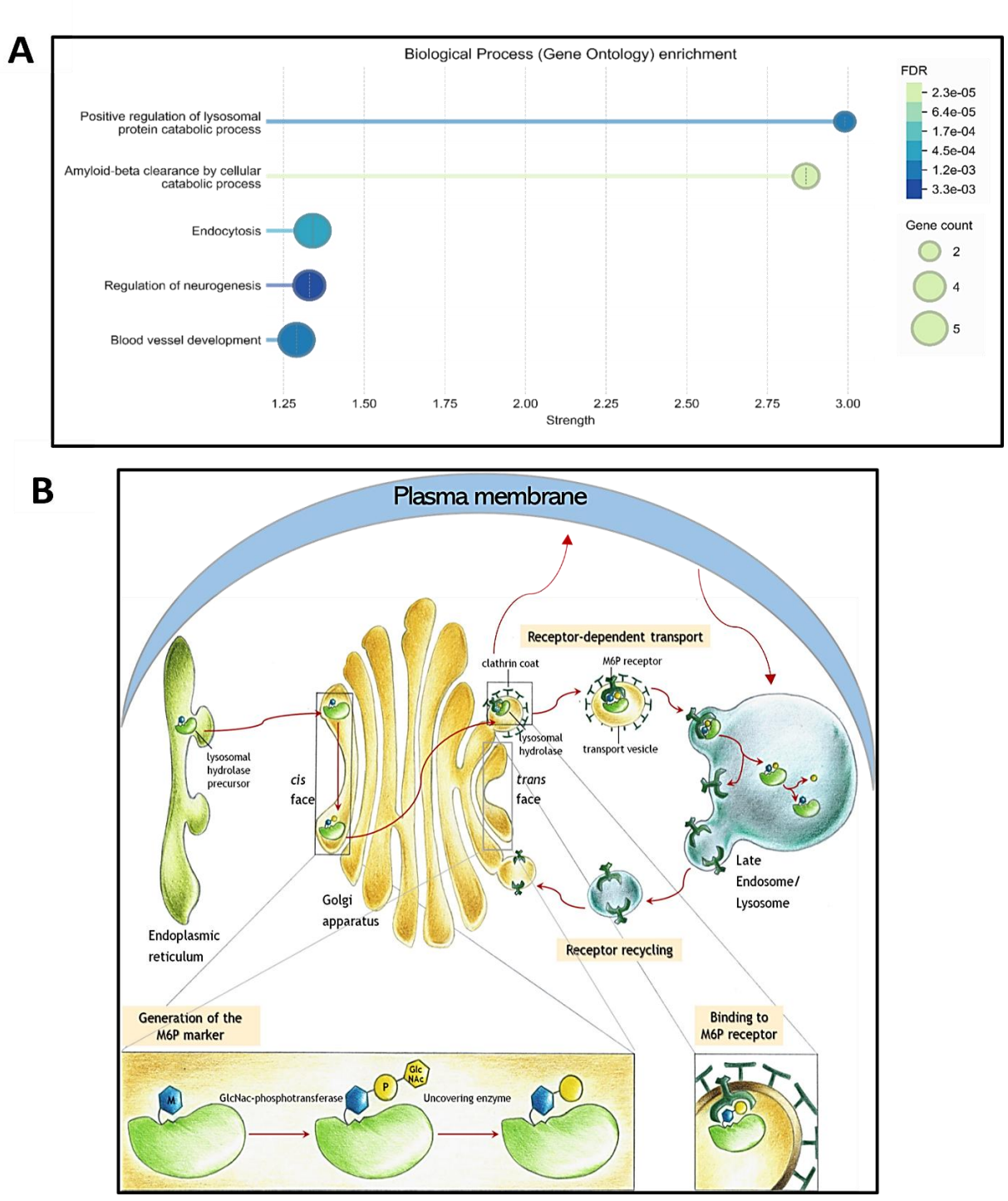

Figure 4.12: Zoom into osmotic stress biological changes and choice of CI-M6PR.
A) String database analysis of the top 5 biological processes represented by significantly enriched transmembrane proteins. B) Schematics of CI-M6PR main tasks as a transporter of lysosomal acid hydrolases

from the TGN to the lysosome or via the plasma membrane, internalizing to the lysosome, via the recognition of the M6P tag that proteins exhibit. Adapted from Coutinho et al., (2020).

4.8 Further characterization of CI-M6PR increase at the surface

4.8.1 Time series

To investigate how rapidly CI-M6PR accumulates at the plasma membrane following osmotic stress, we performed surface biotinylation at four early time points: 15 min, 30 min, 45 min, and 60 min post-stress induction (Fig. 4.13 A).

Unexpectedly, surface accumulation of CI-M6PR was already evident at the 15-minute mark, with the effect persisting across all subsequent time points (Fig. 4.13 A and B). This rapid response suggests that the redistribution of CI-M6PR to the plasma membrane is both early and dynamically regulated.

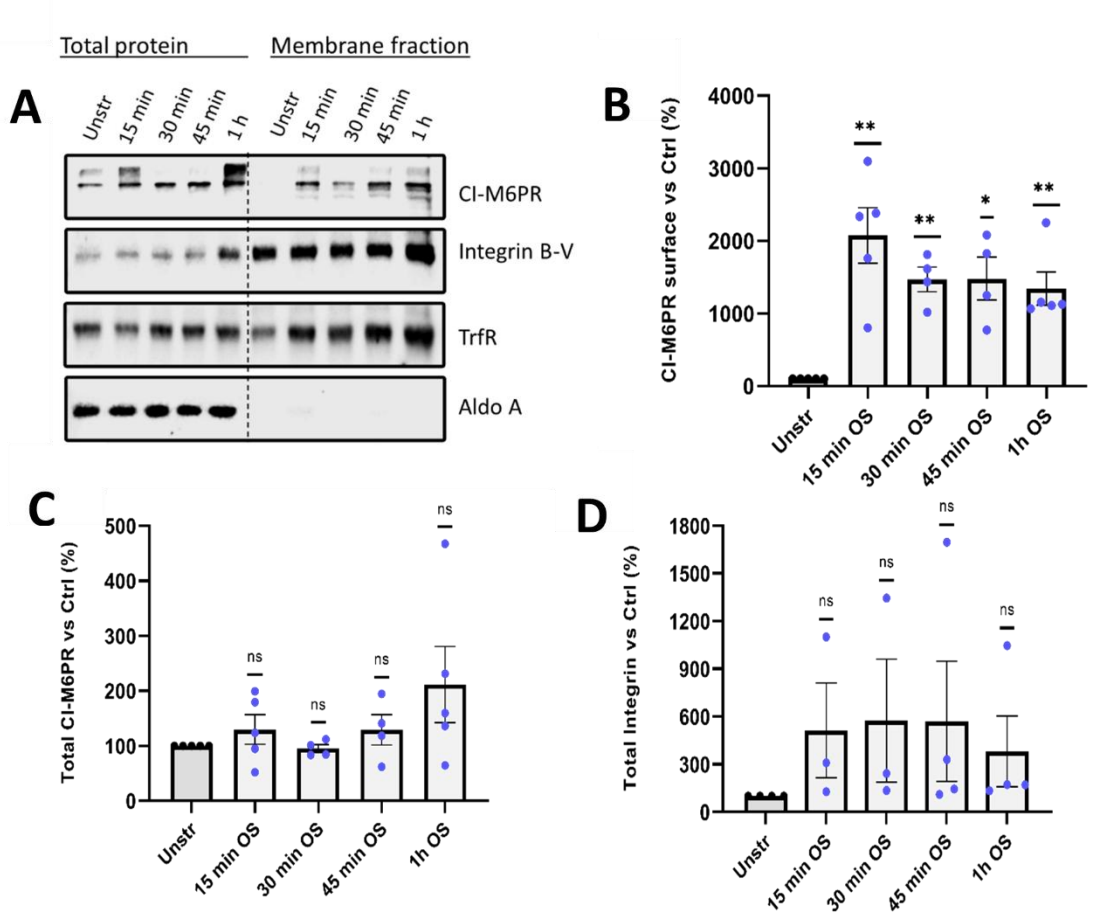

Figure 4.13: Time series biotinylation shows CI-M6PR accumulation already at 15 min.
A) Representative western blot membrane showing CI-M6PR levels in an osmotic stress time series biotinylation, after 15 min, 30 min, 45 min, and 1 h. Integrin-Beta-5 and TrfR were shown as alternative membrane proteins. Aldolase A was used as a loading control. B, C) Quantification of surface CI-M6PR and total CI-M6PR, respectively, normalized to controls. D) Quantification of integrin levels from the experiments in A. Data represent mean ± SEM; n = 3-5 independent experiments (as per puncta); One-sample T-test (ns, not significant *p < 0.05, **p < 0.01).

In parallel, total levels of CI-M6PR were assessed from whole-cell lysates. While considerable variability was observed between experiments, no significant differences were detected when compared to control samples (Fig. 4.13 C), further supporting the notion that the observed surface enrichment results from protein redistribution alone rather than increased expression.

To control for general membrane protein dynamics, we also examined the behaviour of another transmembrane protein, Integrin β5. Although its surface levels exhibited substantial variability under osmotic stress, the changes were not statistically significant relative to the control (Fig. 4.13 D), reinforcing the specificity of CI-M6PR's response.

The results here emphasise the impact of hyperosmotic stress exposure CI-M6PR-mediated adaptation program, since the enrichment readout can be seen this early in the event development.

4.8.2 Concentration series

As a follow up question, we sought to determine the threshold of hyperosmotic stress at which CI-M6PR surface accumulation begins to occur. To this end, we performed a biotinylation-based concentration series using increasing osmolarities: 400 mOsm/kg, 500 mOsm/kg, 600 mOsm/kg and our tested 750 mOsm/kg (Fig. 4.14 A). For reference, standard culture medium typically ranges between 285-310 mOsm/kg, which served as the control condition.

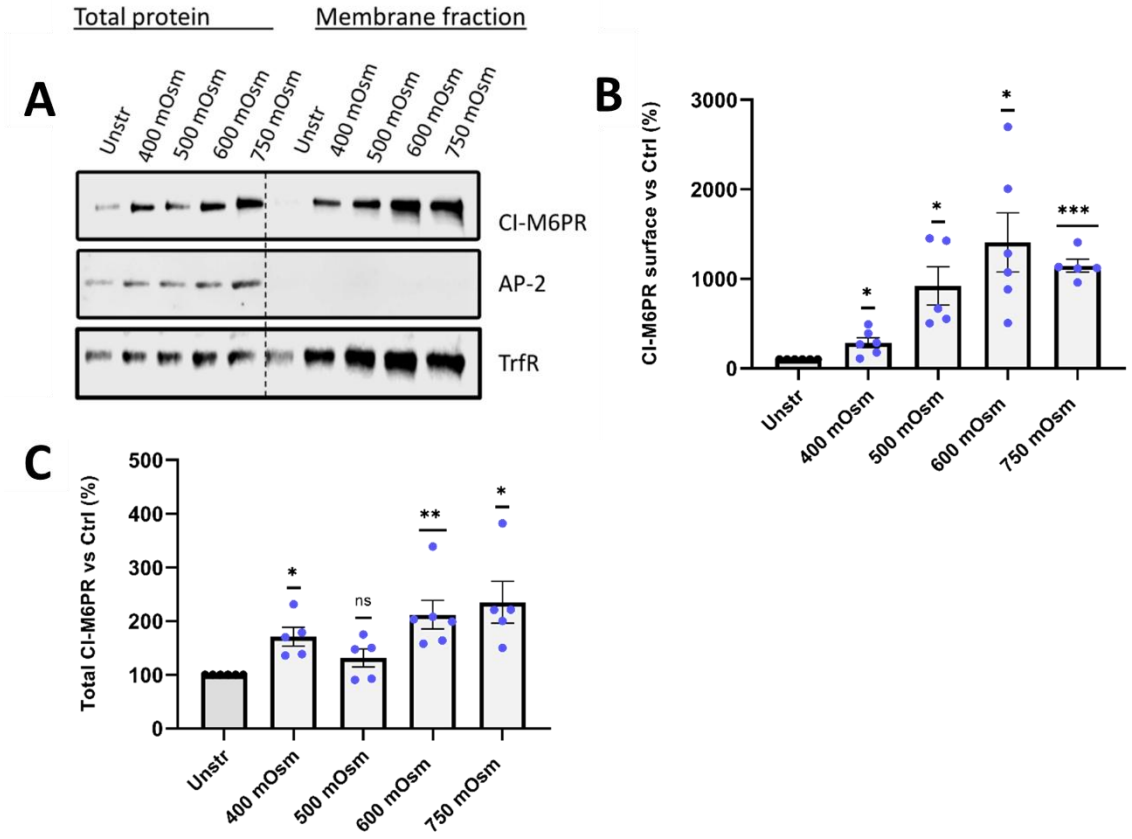

Figure 4.14: Concentration series biotinylation shows CI-M6PR accumulation already at 400 mOsm/kg.
A) Representative western blot membrane showing CI-M6PR levels in an osmotic stress concentration series biotinylation, using 400 mOsm/kg, 500 mOsm/kg, 600 mOsm/kg and our tested 750 mOsm/kg and 1 hour exposure. TrfR is shown as an alternative membrane protein. AP-2 was used as a loading control. B, C) Quantification of surface CI-M6PR and total CI-M6PR, respectively, normalized to controls. Data represent

mean ± SEM; n = 5-6 independent experiments (as per puncta); One-sample T-test (ns, not significant *p < 0.05, **p < 0.01, ***p < 0.001).

We confirmed that the increase in CI-M6PR membrane accumulation started already at the lowest osmolarity tested (400 mOsm/kg), although the effect was less pronounced compared to the higher osmolarities (Fig. 4.14 B). In parallel, total CI-M6PR levels were also assessed and quantified (Fig. 4.14 C), and, unexpectedly, a significant increase was observed at several osmolarities. This finding contrasts with the lysate mass spectrometry data, which showed no significant changes in total CI-M6PR levels. Together, these results highlight the inherent variability in cellular responses and underscore how experimental readouts can differ depending on the methodological approach.

The results from this set of experiments suggest that the mechanism being mediated by enrichment of CI-M6PR in the plasma membrane can be extrapolated to much lower osmotic medium concentrations, and likely to higher ones, possibly revealing a well establish osmotic stress adaptation program.

4.8.3 Osmotic stress induced by other osmolytes

Up to this point, mannitol had been the osmolyte of choice to increase the medium's osmolarity. To determine whether the plasma membrane enrichment of CI-M6PR observed under hyperosmotic stress was specific to mannitol or a more generalizable response to osmotic imbalance, we extended our analysis to include alternative osmolytes. Specifically, we adjusted the osmolarity to 750 mOsm/kg using either NaCl (Fig. 4.15 A) or sorbitol (Fig. 4.15 C), followed by surface biotinylation.

Our quantification revealed that CI-M6PR also accumulated at the plasma membrane under both of these conditions (Fig. 4.15 B and D), with these results indicating that the effect is not exclusive to mannitol and may represent a broader cellular response to hyperosmotic stress.

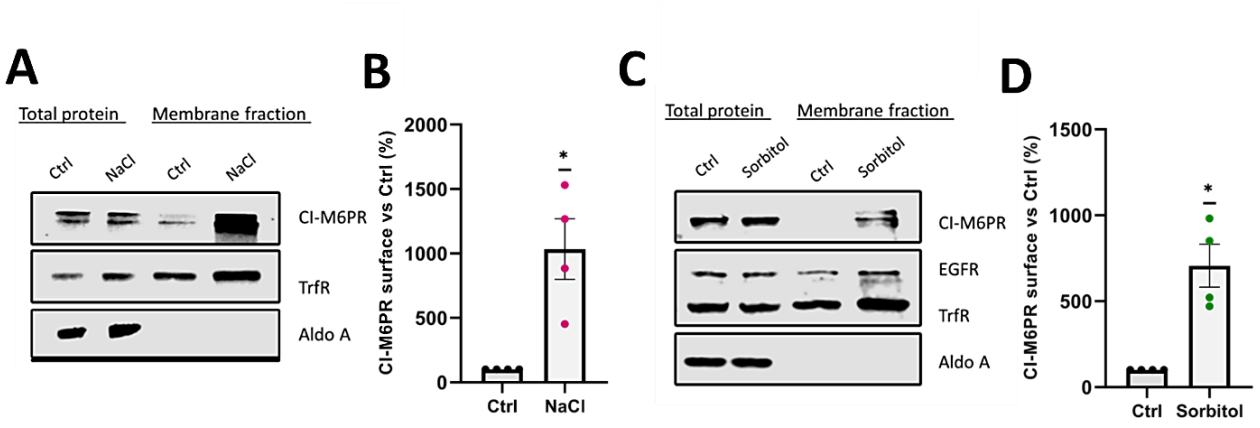

Figure 4.15: CI-M6PR is accumulated in the membrane upon other hyperosmotic solutions.
A, C) Representative western blot membrane showing CI-M6PR levels in a hyperosmotic solution adjusted with NaCl and Sorbitol, respectively. B, D) Quantification of the levels of CI-M6PR on cell surface, for experiments in A and C, respectively, normalized to controls. For both cases, Aldolase A was used as a loading control. EGFR and TrfR were shown as alternative membrane proteins. Data represent mean ± SEM; n = 4 independent experiments; One-sample T-test (*p < 0.05).

4.9 Mechanisms that promote CI-M6PR membrane enrichment

4.9.1 Increase upon CME inhibitor treatment

To determine whether the redistribution of CI-M6PR to the plasma membrane upon osmotic stress is dependent on CME, we employed the CME-specific inhibitor Pitstop. The aim was to assess whether inhibition of CME alone (through Pitstop dissolved in full cell culture medium), over a 1 h treatment period, could replicate the membrane accumulation observed under stress conditions.

Before our main experiment, we confirmed the efficacy of Pitstop in RPE-1 cells by demonstrating its ability to block transferrin uptake, a well-established readout for CME inhibition, for 15 min, checked by immunofluorescence (Fig. 4.16 A). Following this validation, surface biotinylation experiments were performed with two RPE cells subpopulations, one control treated only with vehicle DMSO, and one treated with pre-dissolved Pitstop in DMSO and mixed with full cell culture medium for 1 h (Fig. 4.16 B). The results revealed that CI-M6PR levels at the plasma membrane were indeed significantly elevated after Pitstop treatment (Fig. 4.16 C), supporting the notion that the stress-induced redistribution of CI-M6PR involves a CME-dependent mechanism.

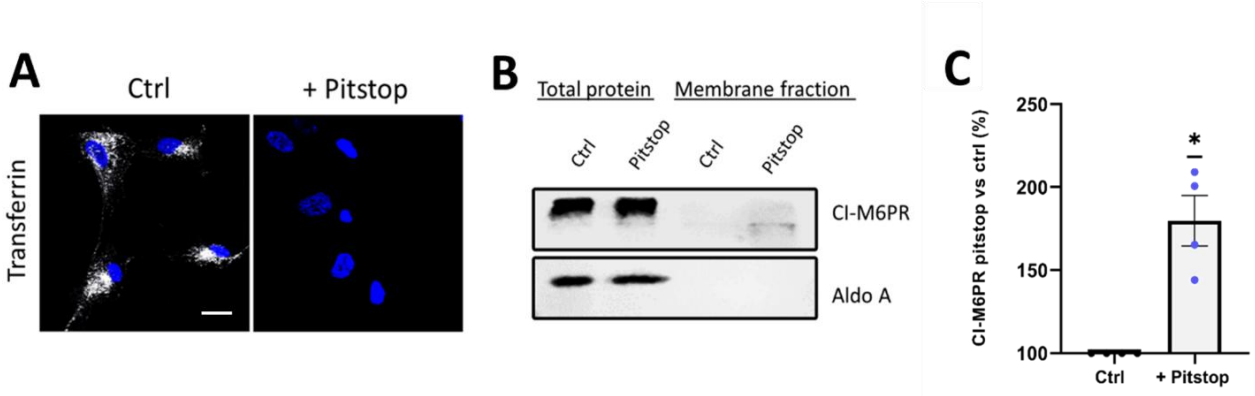

Figure 4.16: Inhibition of CME mimics CI-M6PR surface accumulation upon stress.
A) Representative confocal images that show that treatment with Pitstop is able to block transferrin uptake. Cells were incubated at 37°C with 30 µM Pitstop and 25 µg/ml fluorescently labelled transferrin for 15 min. After washing and fixation, nuclei were visualized by DAPI (blue). B) Representative western blot of a biotinylation experiment showing increased CI-M6PR levels upon 1 h Pitstop treatment. Aldolase A was used as housekeeping protein to demonstrate equal loading and the absence of intracellular proteins from the surface fraction. C) Quantification of CI-M6PR membrane enrichment, normalized to control, of experiments as depicted in (B). Data represent mean ± SEM; n = 4 independent experiments; One-sample t-test (*$p < 0.05$).

4.9.2 Reduced internalization of CI-M6PR upon osmotic and heat stress

Although the inhibition of CME via Pitstop mimics the stress-induced accumulation of CI-M6PR, it does not yet prove that an impairment of CI-M6PR internalization upon stress is causative for its surface accumulation. In order to get a definitive answer on the role of endocytosis in the surface enrichment of CI-M6PR, we devised an antibody feeding assay, in which the internalized amount of CI-M6PR was quantified at control and stress conditions after 15 min internalization at 37°C (Fig. 4.17 A). This assay was conducted for both osmotic and heat stress conditions, confirming that for both stressors CI-M6PR endocytosis is indeed decreased by 25-30%, respectively (Fig. 4.17 B).

After either control (untreated cells kept at 37°C in normal medium), osmotic stress or heat stress treatment for 1 h, RPE cells were immediately placed on ice where the cells were washed with cold PBS^{2+}. Surface CI-M6PR was labelled by incubating the cells for 30 min with CI-M6PR primary antibody previously dissolved on full cell culture medium. The cells were then washed twice to remove unbound primary antibody before being placed at 37°C for 15 min to allow endocytosis on full cell culture medium. After fixing with 4% PFA, blocking/permeabilizing and incubating the cells with secondary antibody and DAPI, the cells were mounted and imaged the following day.

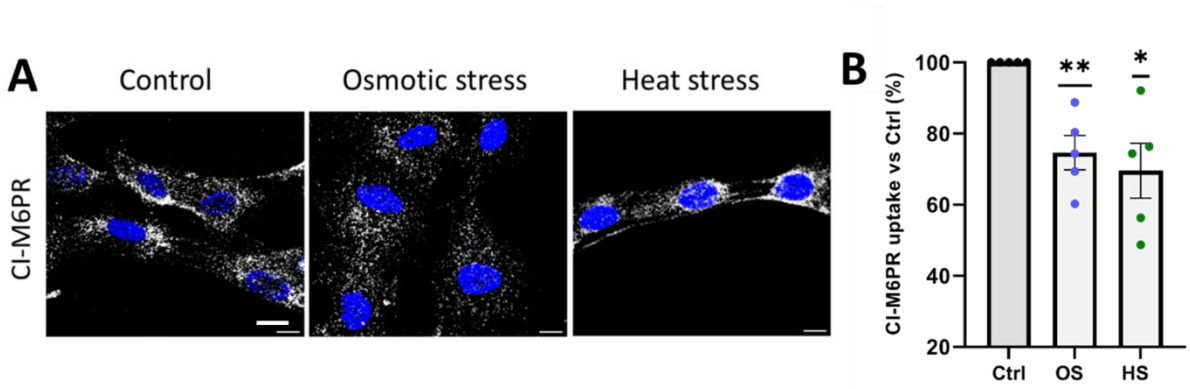

Figure 4.17: CI-M6PR endocytosis is impaired upon osmotic and heat stress.
A) Representative confocal images of an antibody feeding assay showing the internalization of CI-M6PR after 1 h osmotic or heat stress treatment followed by 15 min internalization at 37°C. Nuclei of fixed cells were visualized by DAPI (blue). B) Quantification of CI-M6PR uptake in both conditions, normalized to controls. Data represent mean ± SEM; n = 4-5 independent experiments (as per puncta); One-sample t-test (*p < 0.05, **p < 0.01). Scale bars = 10 μm.

We conclude, looking at the results of this assay, that for both stressors CI-M6PR endocytosis is indeed defective by a rate of, on average, 25-30%, respectively (Fig. 4.17 B).

4.9.3 Determinants in the CI-M6PR intracellular tail are sufficient for its stress-induced surface accumulation.

It is known that the endocytosis of CI-M6PR is mediated via endocytic recognition motifs (e.g. YSKV, LL motifs) contained in its intracellular tail (P. Ghosh et al., 2003; Simonetti et al., 2017). Therefore, we speculated that a CI-M6PR truncation mutant comprising only its transmembrane region and intracellular tail fused to EGFP should mimic the stress-induced surface accumulation of the full-length protein.

For the experiment, plasmid DNA encoding EGFP-tagged CI-M6PR tail chimera was amplified in *E. coli* cultures and extracted using a standard mini-prep kit. RPE cells were seeded on Matrigel-coated coverslips and transfected with the plasmid DNA the following day using a Lipofectamine 2000 with Opti-MEM mix. After 5–6 hours of incubation with the transfection mix, cells were returned to fresh growth medium and maintained under standard conditions. At least 24 hours post-transfection, cells were processed for immunofluorescence and subsequent confocal microscopy analysis.

By overexpressing this fusion protein in RPE cells and labelling the trans-Golgi network (TGN) via a TGN46-specific antibody we evaluated the distribution of the fusion protein under control and osmotic stress conditions. Pitstop treatment was used in parallel to assess the impact of an endocytosis inhibition on the CI-M6PR distribution in this assay (Fig.4.18 A and sup. Fig. 6.1).

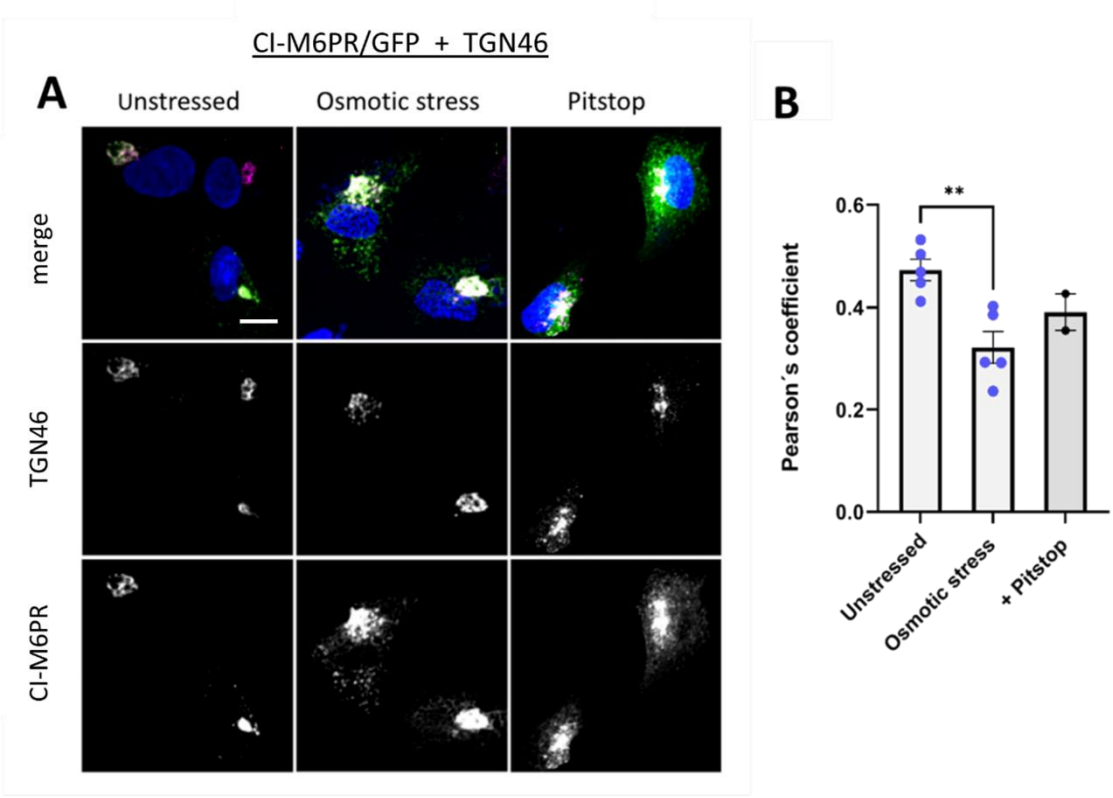

Figure 4.18: EGFP-CI-M6PR truncation mutant lacking extracellular domains still becomes redistributed upon osmotic stress.
A) Representative confocal microscope images showing the overexpression of the EGFP-tagged CI-M6PR variant lacking extracellular domains in unstressed conditions, after 1 h in 750 mM mannitol, and after 1 h 30 µM Pitstop treatment. A TGN46-specific antibody was used to label the TGN and CI-M6PR signal was measured in reference to the EGFP chimera fluorescence. Nuclei were visualized by DAPI (blue). Scale bar = 10 µm. B) Quantification of the Pearson's coefficient shows that co-localization between TGN46 and CI-M6PR decreases after both osmotic stress treatment and Pitstop. Data represent mean ± SEM; n = 2-5 independent experiments (indicated by puncta); Student's t-test (**$p < 0.01$).

In line with earlier studies overexpressing CI-M6PR (Waguri et al., 2003; Lin et al., 2004), we could see that CI-M6PR under unstressed conditions strongly co-localized with the TGN. Upon both, osmotic stress or endocytosis inhibition with Pitstop, we observed its partial redistribution away from the TGN towards vesicular structures and the plasma membrane. This displacement was reflected in a lower co-localization with TGN46 and thus a lower Pearson's coefficient (Fig. 4.18 B). This result allows us to infer that this redistribution is indeed dependent upon determinants within the short intracellular tail and can be mimicked by blocking CME. With this last experimental set, it all indicates towards a reduced uptake of CI-M6PR by CME upon stress.

4.9.4 Accumulation of other lysosomal proteins in the membrane points to a second mechanism for enrichment

Even though we had evidence of a decreased endocytic retrieval of CI-M6PR from the plasma membrane upon osmotic stress, impaired CME alone likely could not account for the large extent of CI-M6PR surface accumulation due to the following reasoning: 1) In all experiments, the stress-induced enrichment of CI-M6PR in the plasma membrane ranged on average from 6-15 times the levels of the unstressed condition. 2) However, the accumulation of CI-M6PR on the plasma membrane caused by 1 h of CME inhibition via Pitstop resulted only in 1,5-2 times the enrichment. 3) And most importantly, the antibody feeding assay showed that endocytosis was impaired by approximately 25%. These numbers pointed to the existence of at least one additional mechanism contributing to the plasma membrane accumulation of CI-M6PR.

Determined to try to find an explanation, I went back to the results for the surface proteome upon osmotic stress to look at the differentially enriched proteins. This revealed that there were many lysosomal transmembrane proteins (e.g. TMEM9, ACP2, LAMP1, LAMP2) and proteins connected to exocytosis (e.g. TGOLN2, ATP7A, SORT1) also enriched (Fig. 4.19 A). Surface biotinylations followed by Western blotting would have been ideal to validate these findings, however, antibodies were either not available to us or, in case of LAMP1, were only effective in detecting total protein levels lacking sufficient sensitivity to detect the protein in surface fractions.

Interestingly, for LAMP1, for example, its surface enrichment would be compatible with stress-induced changes in its endocytosis since LAMP1´s trafficking itinerary is known to encompass a delivery from the Golgi to the cell surface followed by endocytic retrieval (Ecard). However, since not all listed proteins are known to undergo endocytosis, e.g. ACP2 is only trafficked via the endosomal pathway (Bright et al., 2016; J. Lee et al., 2017); in contrast, all lysosomal proteins can be expected to be enriched at the plasma membrane upon lysosomal exocytosis. This was a hint towards the possibility of lysosomal exocytosis occurring alongside the decreased CME we found.

4.9.4.1 Lysosomal exocytosis contributes to stress-induced CI-M6PR surface accumulation.

Lysosomes are membrane-bound organelles characterized by a heterogeneous size (ranging from 100 to 1000 nm), a rounded morphology, and high abundance of copies, often up to several hundreds per cell (Tancini et al., 2020). Although they are typically concentrated in the perinuclear region, lysosomes are highly dynamic and move along microtubules in response to cellular needs, from the perinuclear area toward the plasma membrane and back toward the middle of the cell (Trojani et al., 2024).

Lysosomal exocytosis refers to the regulated release of lysosomal contents into the extracellular space. By tracking surface exposure of LAMP1 and employing inhibitors of SYT VII and LAMP1, Reddy et al., (2001) established lysosomal exocytosis as a bona fide plasma membrane repair mechanism activated in response to membrane damage. Beyond membrane repair, lysosomal exocytosis has since been linked to diverse biological processes, including bone resorption, antigen presentation, mitosis, and the clearance of heavy metals, toxic compounds, or misfolded proteins (Trojani et al., 2024).

This process, classified as an “unconventional secretion” pathway, involves the direct fusion of lysosomes with the plasma membrane. Prior to fusion, lysosomes migrate toward the cell periphery, where they dock and subsequently fuse with the plasma membrane, releasing their contents extracellularly. These events depend on a cytoplasmic Ca^{2+} increase and involve coordinated interactions between lysosomal and plasma membrane proteins (Medina et al., 2011; Kilpatrick et al., 2016). The rise in intracellular Ca^{2+}, either originating from lysosomes or the ER, is regulated by the nuclear translocation of TFEB, which upregulates the expression of TRPML1, a non-selective lysosomal Ca^{2+} channel that plays a key role in lysosomal exocytosis by facilitating Ca^{2+} release required for membrane fusion (W. Wang et al., 2015; Di Paola et al., 2018; Schmiege et al., 2021).

To test the hypothesis whether stress-induced lysosomal exocytosis contributes to the plasma membrane enrichment of CI-M6PR, surface biotinylation was conducted in combination with an inhibition of lysosomal exocytosis, For this, the TRPML1 Ca^{2+} channel inhibitor ML-SI3 was applied (Schmiege et al., 2021; Wünkhaus et al., 2024). This channel is present in the lysosomal membrane, and the Ca^{2+} efflux it mediates is necessary for the fusion, and therefore for lysosomal exocytosis to occur. To quantify the influence of the inhibitor on CI-M6PR levels, inhibitor-treated cells were compared to “mock” treated cells which had received only the solvent DMSO (Fig. 4.19 B). After scrutiny of the data, it was found that less CI-M6PR accumulated at the membrane upon osmotic stress when cells were treated with the TRPML1 inhibitor (Fig. 4.19 C and F), which suggests that increased lysosomal exocytosis is in fact part of the reason for the accumulation. However, the extent of the contribution is hard to judge since at this point a control experiment is still lacking which probes to which extent lysosomal exocytosis is actually inhibited in RPE-1 cells upon the chosen TRPML1 inhibitor concentration and treatment length.

As another layer of confirmation for the hypothesis, the opposite experiment was conducted. The TRPML1 Ca^{2+} channel agonist ML-SA1 (Feng et al., 2014; W. Wang et al., 2015; Wünkhaus et al., 2024) was applied, which promotes the fusion of lysosomes with the plasma membrane, therefore increasing their exocytosis. While we did not detect an effect of the agonist on the CI-M6PR surface levels in unstressed cells, there was a tendency to higher CI-M6PR surface levels upon agonist treatment in the context of osmotic stress (Fig. 4.19 D and E).

Indeed, when comparing the differences in stress-induced CI-M6PR surface levels in presence of the inhibitor or agonist normalized to the condition of only stress treatment, a significant decrease upon treatment with the lysosomal exocytosis inhibitor and a small, but significant increase upon application of the lysosomal exocytosis stimuli were observed (Fig. 4.19 F).

Again, a control experiment is needed to determine to which extent lysosomal exocytosis is actually triggered in RPE-1 cells upon the chosen TRPML1 agonist concentration and treatment length. The absence of an effect in the unstressed condition suggests that the agonist treatment was not very effective, leading only to observable effects in combination with the stress induction. When looking at other membrane proteins probed: 1) Integrin-beta 5 showed a slight increase observed in both unstressed and osmotically stressed membrane fractions that were treated with the inhibitor, whereas no visible difference was seen in the membrane fractions treated with the agonist, with the exception of the unstressed control treated with the agonist, that seemed to have a visible decrease, seen in the representative figure.4.19 D, 2) TrfR appeared with the expected increase in membrane fractions of osmotically treated cells, as previously described, but there was no visible differences

between the pairs of either treated with inhibitor/agonist and their mock duplicates (as seen in Fig. 4.19 B). Unfortunately, there were not enough sets of either of these available to offer a quantification.

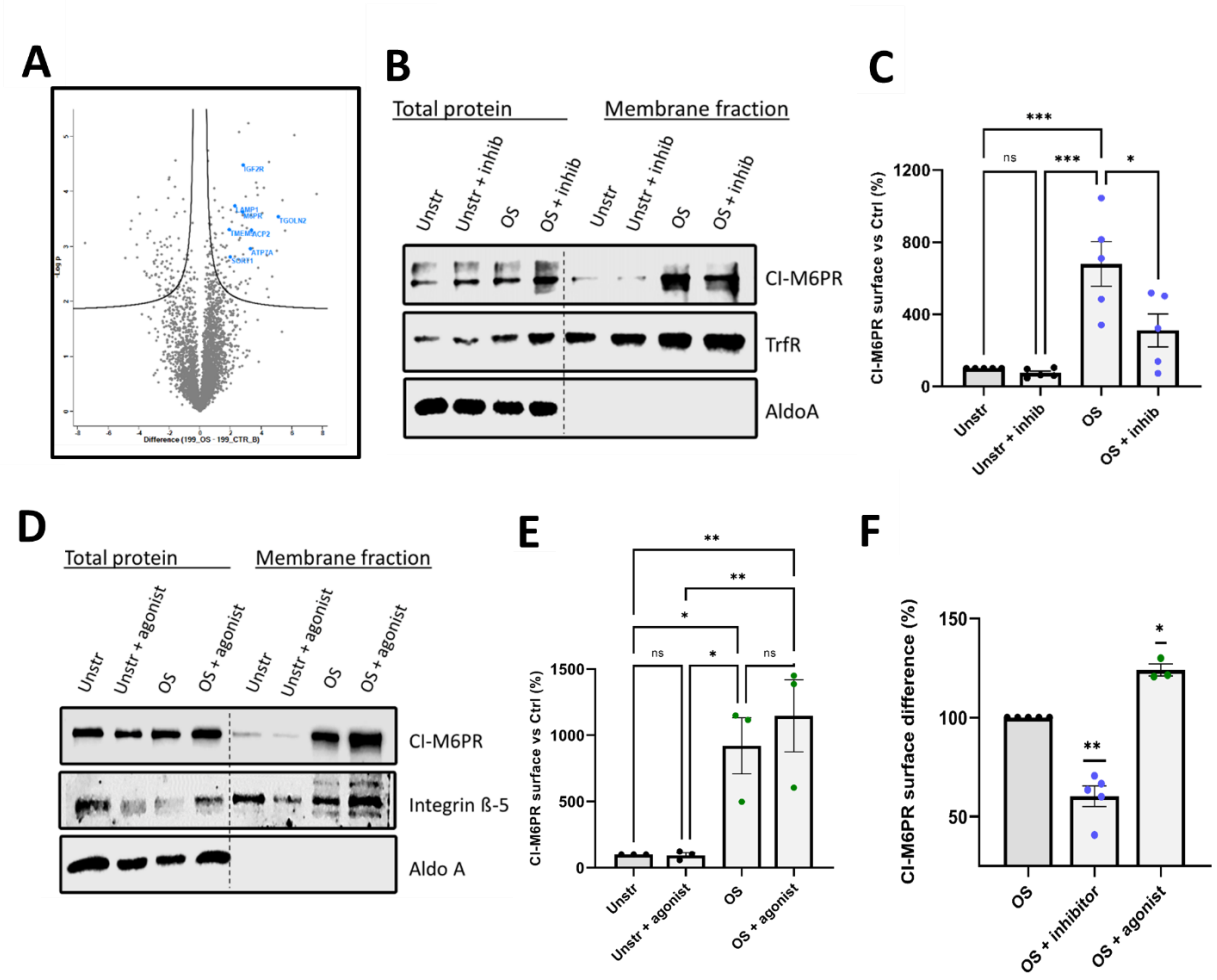

Figure 4.19: Lysosomal exocytosis contributes to CI-M6PR plasma membrane enrichment.
A) Volcano plot (depicting data from the experiment described in section 4.5) showing the surface enrichment of lysosomal proteins upon osmotic stress. B) Representative western blot showing a surface biotinylation of control and osmotically stressed cells, treated with either DMSO as vehicle control or 10 µM TRPML1 inhibitor. TrfR was probed to demonstrate the efficient enrichment of plasma membrane proteins in all surface samples. AldoA was used as a loading control and to show the absence of cytosolic proteins in the surface fractions. C) Quantification of CI-M6PR surface levels, normalized to the unstressed condition, based on experiments like in B. D) Representative western blot showing a surface biotinylation of control and osmotically stressed cells, treated with either DMSO as vehicle control or 50 µM TRPML1 agonist. E) Quantification of CI-M6PR surface levels, normalized to the unstressed condition, based on experiments like in D. F) Quantification of net difference between osmotic stress alone and osmotic stress + either inhibitor or agonist after normalization to the osmotic stress condition. Data represent mean ± SEM; n = 3-5 independent experiments (indicated by puncta). C, E) One-way ANOVA with Tukey's post-test. F) One-sample t-test (ns, not significant, *=$p < 0.05$, **=$p < 0.01$, ***=$p < 0.001$).

4.10 Functional investigation of CI-M6PR role in cell proliferation and survival

4.10.1 Successful downregulation of CI-M6PR by siRNA

Next, we wanted to probe the impact of CI-M6PR on the cell's ability to cope with osmotic stress, by studying the effects of the silencing CI-M6PR. For this, we tested the silencing efficiency of 3 siRNAs reported in other papers (see siRNAi table in methods for further information) (Fig. 4.20 A and C). We confirmed that after 2 rounds of silencing the siRNA-treated cells expressed less than 20% of the control level of CI-M6PR in cells treated with non-targeting siRNA, which was considered as successful depletion (Fig. 4.20 B and D).

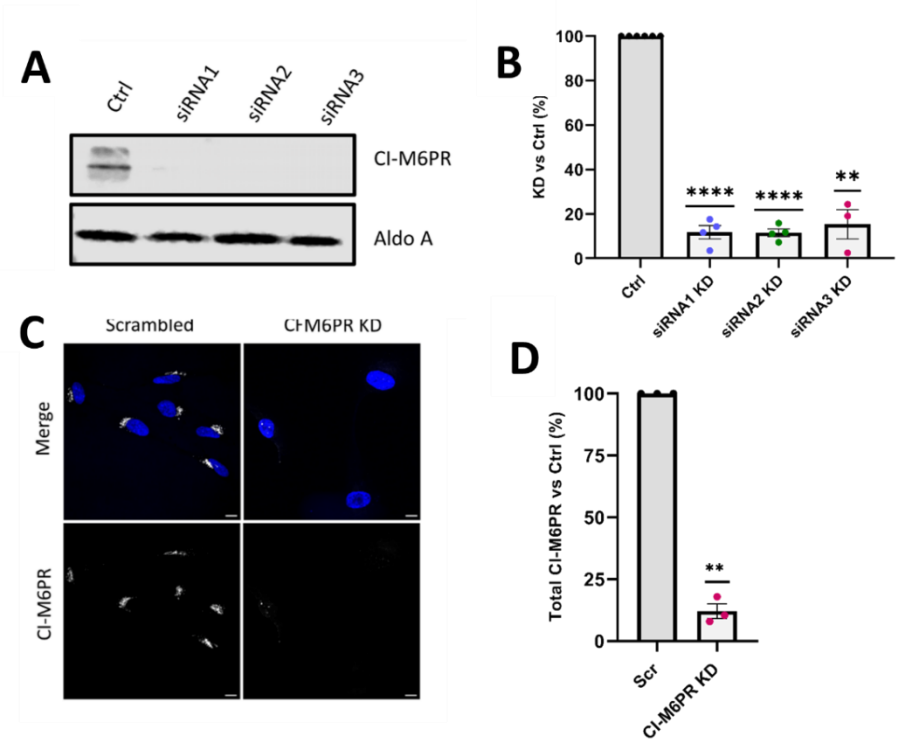

Figure 4.20: Efficient silencing of CI-M6PR.
A) Representative Western blot showing the levels of CI-M6PR after 2 rounds of silencing for 3 different siRNAs. Aldolase A was used as loading control. B) Quantification of the CI-M6PR levels from experiments as in A, normalized to control. C) Representative confocal images of an immunofluorescence staining of CI-M6PR after 2 rounds of siRNA knockdown. Nuclei were visualized by DAPI (blue). Scale bars = 10 µm. D) Quantification of the CI-M6PR levels from experiments as in C, normalized to its levels in cells treated with scrambled siRNA (Scr). Data represent mean ± SEM; n = 3-5 independent experiments (indicated by puncta), One-sample t-test (**p < 0.01, ****p < 0.0001).

4.10.2 Evaluating the impact of combined stress and CI-M6PR depletion on cell viability and proliferation

To investigate whether silencing of CI-M6PR has a beneficial or detrimental effect on cells, we assessed cell death, by measuring necrosis and apoptosis, as well as proliferation. For the evaluation of necrosis (via SYTOX labelling) and apoptosis (via the IncuCyte apoptosis assay), we selected a 6-hour time point (the intermediate time between the 4-hour and 8-hour time points used in our earlier experiments, Fig. 4.3) based on our prior observations of detectable differences. An

intermediate duration was expected to be sufficient to reveal any functional impact of CI-M6PR depletion.

Quantifications of SYTOX labelling indicated a significant increase in necrosis following CI-M6PR knockdown, which was further exacerbated by 6 hours of osmotic stress, nearly doubling the extent of necrosis compared to stressed cells which were not silenced (Fig. 4.21 A). A similar trend was observed in apoptosis measurements using the IncuCyte assay (Fig. 4.21 B), with the combined effect of knockdown and osmotic stress elevating apoptosis to approximately 2.5-fold above the levels of stressed cells which were not silenced. While both necrotic and apoptotic cell death were enhanced, the magnitude of change suggests that CI-M6PR may play a slightly more prominent role in regulating apoptotic pathways.

It is also worth noting that the overall cell death percentages measured in these assays were higher than those observed in earlier experiments using untreated RPE-1 cells or cells exposed to other stressors (Fig. 4.5). This likely reflects the added cellular burden introduced by the transfection procedure and siRNA reagents themselves, which may have contributed to elevated baseline stress and death rates.

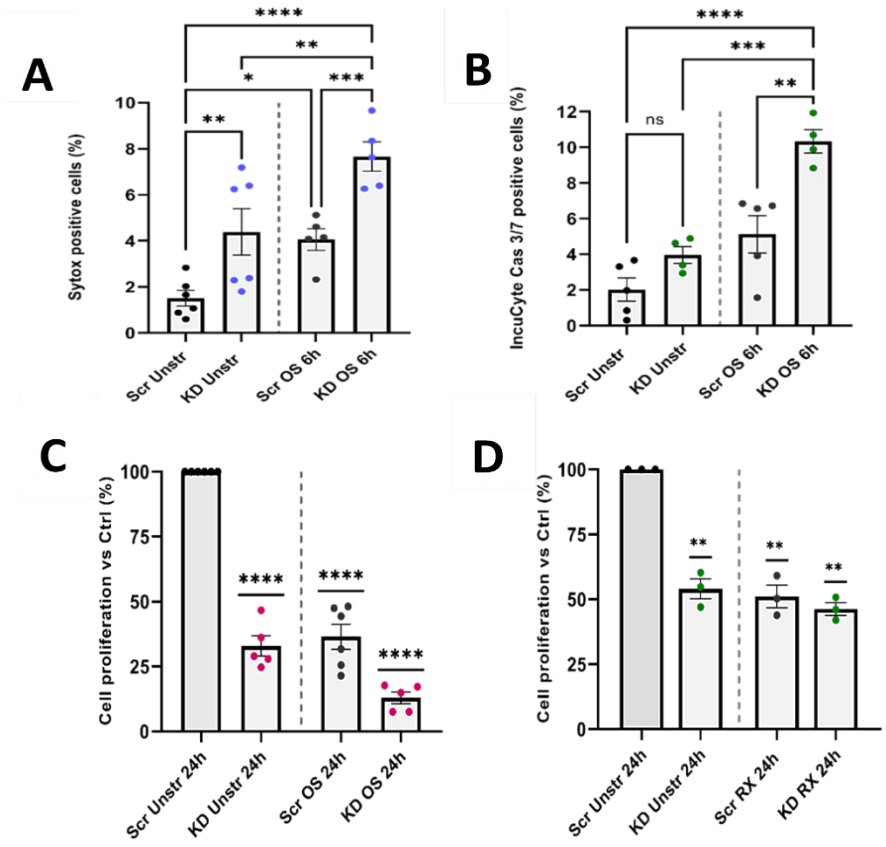

Figure 4.21: Cell death and proliferation decline induced by osmotic stress are further aggravated upon CI-M6PR silencing.
A) Quantification of SYTOX-positive necrotic cells control without stress (unstr) or treated for 6 h with osmotic stress (OS) in combination with either a treatment with scrambled (Scr) or CI-M6PR targeting siRNA #3 (KD). B) Quantification of apoptotic cells labelled by the IncuCyte apoptosis assay for the same conditions as in (A). C) Quantification of RPE cell proliferation (counted cell numbers shown normalized to control (Scr Unstr)) for cells treated with scrambled or CI-M6PR targeting siRNA #3 (KD) in absence of stress or upon 24 h osmotic stress. D) Quantification of RPE cell proliferation (counted cell numbers shown normalized to control (Scr Unstr) for cells treated with scrambled or CI-M6PR targeting siRNA #3 (KD) in absence of stress or upon 24 h oxidative stress (RX). Data represent mean ± SEM; n = 3-6 independent

experiments (as indicated by puncta). A,B) One-way ANOVA with Tukey's post-test. C, D) One-sample t-test (ns, not significant; *p < 0.05, **p < 0.01, ***p < 0.001, ****p < 0.0001).

The proliferation analysis revealed that osmotic stress alone already reduced the proliferation of control cells substantially, and this effect was further exacerbated by CI-M6PR silencing. Under combined stress and knockdown conditions, the cell cultures attained only 10-15% of the cell number observed in unstressed non-silenced control cells after 24 h of proliferation, indicating a pronounced downregulation of cell division (Fig. 4.21C). These findings strongly support the conclusion that CI-M6PR is essential for normal proliferation and that its loss is detrimental to cell viability under stress conditions.

To validate the specificity of these findings for osmotic stress, the proliferation assay was repeated using oxidative stress, a condition previously shown not to induce CI-M6PR redistribution to the plasma membrane. Similar to osmotic stress, oxidative stress reduced proliferation, however, there was no exacerbation upon CI-M6PR knockdown. This result supports our earlier conclusion that the detrimental impact of CI-M6PR depletion is particularly relevant upon osmotic stress when CI-M6PR is recruited to the plasma membrane.

4.11 Evaluating the impact of combined stress and M6PR depletion on lysosomes

4.11.1 Effect on lysosomal activity

Given the well-established role of CI-M6PR in mediating the transport of acid hydrolases from the TGN to lysosomes, we investigated whether its stress-induced redistribution impacts lysosomal abundance and function. To assess the first point, we examined the levels of the lysosome-associated membrane protein LAMP1 as a well-established lysosomal marker under osmotic stress in both control and CI-M6PR-silenced cells.

In contrast to the whole-proteome mass spectrometry results which indicated no significant change in total LAMP1 abundance in response to stress, our quantification of total LAMP1 signals per cell from confocal microscopy images (Fig. 4.22 A–B) revealed a small, but significant decrease in LAMP1 intensity following 1 h of osmotic stress which is likely indicative of a decreased lysosome number. In CI-M6PR knockdown cells under non-stress conditions, we observed a modest non significant increase in LAMP1 signal. The tendency to increased lysosome signal is in line with earlier reports showing an accumulation of LAMP1-positive organelles upon CI-M6PR knockdown (Takeda et al., 2019). Interestingly, lysosomes appeared also to have a broader spatial distribution within cells, suggesting enhanced lysosome dispersion. It would be interesting to further study the effects of this dispersion with more attention in a future experiment set.

The decrease in LAMP1 intensity upon osmotic stress was slightly but not significantly aggravated by combined loss of CI-M6PR. Therefore, CI-M6PR does not appear to be important for maintaining lysosomal numbers in osmotically stressed RPE-1 cells.

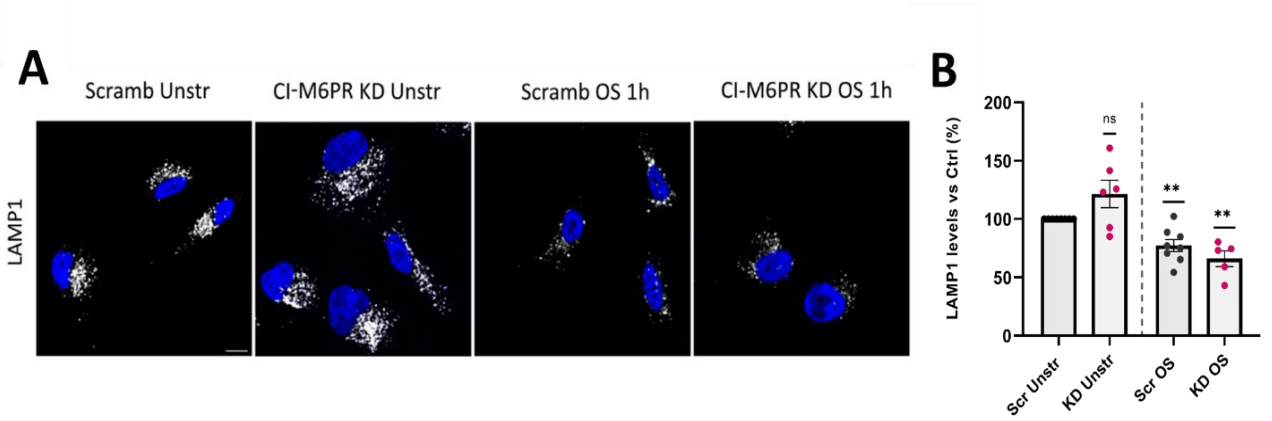

Figure 4.22: LAMP1 levels showed a decrease upon stress but a surprising increase upon KD.
A) Representative confocal images showing LAMP1 total cell levels on scrambled and CI-M6PR KD under normal and 1 h osmotic stress condition. Nuclei were visualized by DAPI (blue). B) Quantification of LAMP1 levels from experiment shown in A, normalized to control. Data represent mean ± SEM; n = 5-6 independent experiments (as per puncta); One-sample T-test (ns, not significant; **p < 0.01). Scale bars = 10 μm.

We continued on to measuring Cathepsin B activity as a functional readout for successful lysosomal hydrolase delivery by CI-M6PR. For this, we used live-cell imaging in combination with the commercially available “Magic Red” assay, which emits fluorescence upon cleavage of the artificial substrate by active Cathepsin B.

To validate the assay, we first tested control cells alongside cells subjected to 9 h nutrient starvation in serum-free medium, a condition known to induce lysosomal activity via activation of TFEB (Sardiello et al., 2009). Based on established literature (Kanamori et al., 2009; Ebner et al., 2023), we expected a significant increase in Cathepsin B activity following starvation, and indeed, a robust elevation in fluorescence signal was observed under these conditions (Fig. 4.23 A, B).

Unexpectedly, CI-M6PR knockdown alone also led to a marked increase in Cathepsin B activity, even in the absence of starvation, indicating a strong upregulation of Cathepsin B activity in the absence of CI-M6PR. When knockdown cells were subjected to nutrient deprivation, the signal nearly doubled compared to starved controls, suggesting additive effects of starvation and CI-M6PR depletion on Cathepsin B activity (Fig. 4.23 A, B).

Having established that the "Magic Red" assay reliably reports the known upregulation of Cathepsin B activity upon starvation, we went on to explore whether the surface accumulation of CI-M6PR might alter hydrolase trafficking and thereby have an impact on lysosomal hydrolase activity upon osmotic stress. For this, we repeated the experiment under osmotic stress conditions (Fig. 4.23 C). In contrast to the starvation condition, 1 h of osmotic stress in non-silenced cells caused a small, though significant downregulation of Cathepsin B activity which would be compatible with the idea of less CI-M6PR being available to deliver hydrolases from the TGN to lysosomes due to its stress-induced surface accumulation. However, the effect of CI-M6PR knockdown did not mimic this but remained consistent: CI-M6PR-depleted cells exhibited again higher Cathepsin B activity than controls. Combining osmotic stress and CI-M6PR knockdown produced a modest additional increase compared to the unstressed knockdown baseline (Fig. 4.23 D).

Even though the decreased lysosomal hydrolase activity upon 1 h of osmotic stress would have fit to the hypothesis of less CI-M6PR being able to transport hydrolases upon its osmotic stress-triggered surface accumulation, we wondered about the observed downregulation of Cathepsin B activity upon osmotic stress since López-Hernández, et al. (2020), had reported that Cathepsin activity increased by approximately 1.3-fold in astrocytes upon 5 h of osmotic stress (with mannitol),. This raised the possibility that Cathepsin activity may only rise over longer durations of stress exposure in line with a TFEB-triggered transcriptional response leading to its upregulation. To test this hypothesis, we conducted a time-course experiment of osmotic stress application, assessing Cathepsin activity after 1, 5, 7, and 9 h of mannitol incubation (Fig. 4.23 E). Contrary to the observations reported by López-Hernández et al. for astrocytes, we did not detect a significant increase in Cathepsin activity at any of the tested time points compared to controls. However, we did observe a marked increase in variability across biological replicates, particularly at later time points.

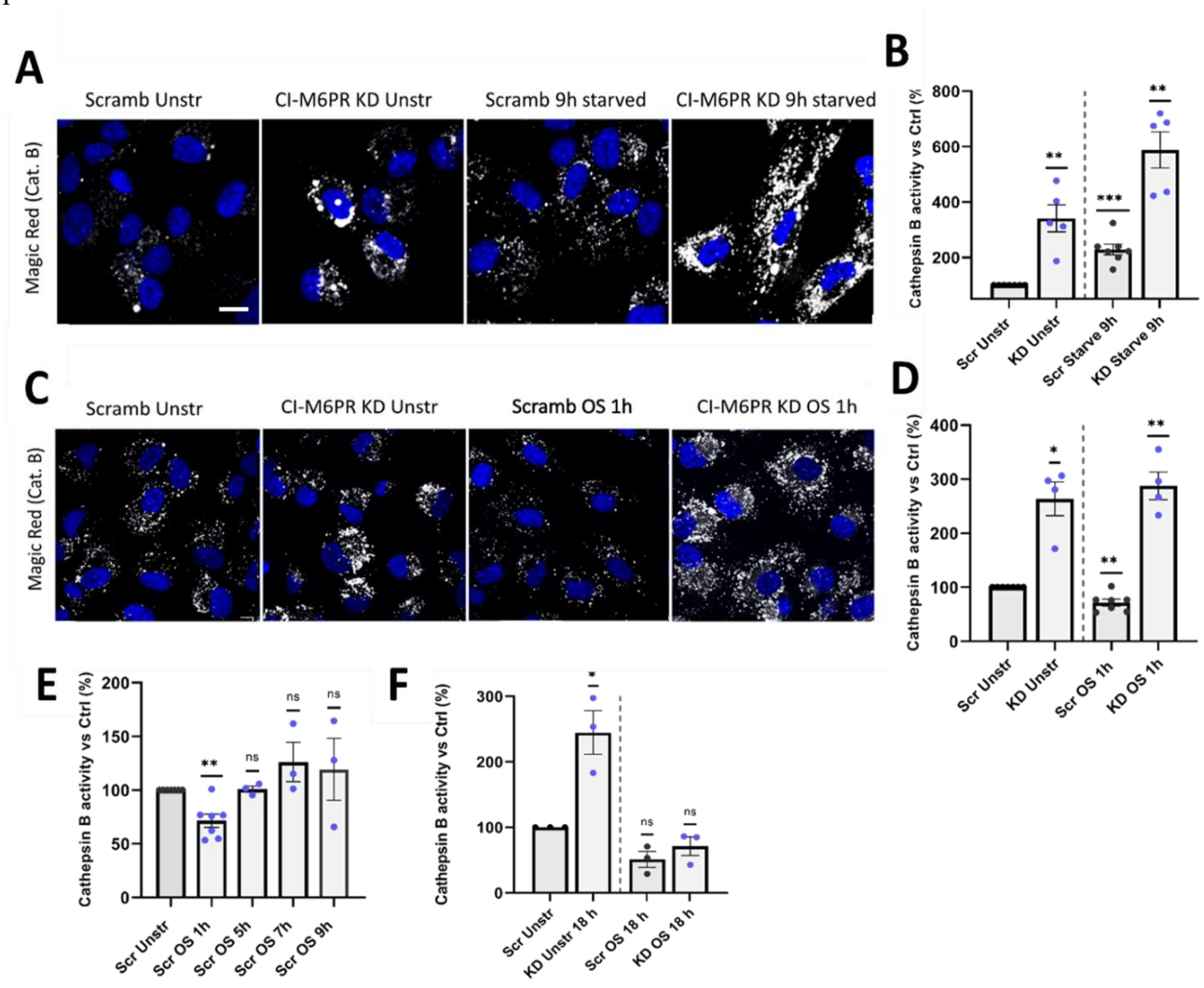

Figure 4.23: Osmotic stress does not increase Cathepsin B activity while CI-M6PR depletion does.
A, C) Representative confocal images of Magic Red fluorescence (indicator of Cathepsin B activity) in non-silenced (Scr) and CI-M6PR depleted cells (KD) under normal conditions and 9 h starvation (A) or 1 h of osmotic stress (C). Nuclei were visualized by DAPI (blue). Scale bars = 10 µm. B,D) Quantification of Cathepsin B activities for experiments as depicted in A and C, respectively. E) Quantification of Cathepsin B activity for non-silenced cells (Scr) that were unstressed or exposed to 1, 5, 7 or 9 h of osmotic stress. F) Quantification of Cathepsin B activity in non-silenced and CI-M6PR depleted (KD) cells that were unstressed or exposed to 18 h of osmotic stress. Data represent mean ± SEM; n = 3-6 independent

experiments (as indicated by puncta); One-sample t-test (ns, not significant; *=p < 0.05, **=p < 0.01, ***=p < 0.001).

As we continued investigating the temporal dynamics of lysosomal function, we also considered whether in RPE-1 cells an even more prolonged stress exposure might be needed to further impact Cathepsin B activity. Given the observed increases in cell death and decreases in proliferation upon extended stress durations, we hypothesized that these effects could be linked to lysosomal hydrolase missorting. To explore this possibility, we measured Cathepsin B activity in non-silenced and CI-M6PR knockdown cells following 18 h of osmotic stress (Fig. 4.23 F).

The results showed a modest, but non-significant, reduction in Cathepsin B activity in stressed cells compared to their respective controls suggesting that the increased cell death and reduced proliferation observed under osmotic stress are not directly attributable to hydrolase missorting or compromised lysosomal enzyme activity. Consistent with previous observations, non-stressed CI-M6PR knockdown cells continued to display elevated Cathepsin B activity relative to scrambled controls. Interestingly, in contrast to the Cathepsin B activity levels in knockdown cells remaining high after 1 h of osmotic stress, after 18 h of osmotic stress the hydrolase activity levels in knockdown cells came down to the levels of non-silenced controls, suggesting a complex interplay between osmotic stress effects and CI-M6PR depletion on Cathepsin B activity.

4.11.2 Testing compensation effect by CD-M6PR

How is lysosomal hydrolase delivery maintained at functionally sufficient levels following significant silencing of CI-M6PR, a major transporter in this pathway?

In an effort to understand the unexpected increase in Cathepsin B activity following CI-M6PR knockdown, we revisited the dataset of lysosomal proteins enriched at the plasma membrane under osmotic stress conditions. As shown in the volcano plot (in Fig. 4.24 A), both mannose-6-phosphate receptors, CI-M6PR and CD-M6PR (referred to in the plot as “IGF2R” and “M6PR”, respectively), were identified among the enriched proteins, appearing in close proximity on the plot. These two receptors belong to the family of p-type lectins known to bind mannose-6-phosphate on acid hydrolases and mediate their transport from the TGN to lysosomes (Coutinho et al., 2012b).

Given that both receptors were found enriched at the plasma membrane under stress, we hypothesized that CD-M6PR might partially compensate for the loss of CI-M6PR by taking over hydrolase trafficking in line with earlier reports (Sohar et al., 1998; Bannoud et al., 2018), thereby explaining the elevated Cathepsin B activity observed upon CI-M6PR silencing.

To be able to test this hypothesis, we obtained a CD-M6PR-specific antibody. Since this antibody unfortunately did not work in western blotting, we performed immunofluorescence stainings to probe its expression in RPE-1 cells under basal and osmotic stress conditions, check for co-localization with CI-M6PR and visualize the potential redistribution of both receptors upon osmotic stress in non-silenced RPE-1 cells (Fig. 4.24 B). When quantifying the total fluorescence of both M6PRs, we observed approximately the same levels of CD-M6PR on stressed vs controls, and a small but significant reduction for CI-M6PR (Fig. 4.24 C), which is within the range of variability seen for total CI-M6PR measured on our earlier Western blot-based results for CI-M6PR (Fig. 4.11 and 4.13). Albeit part of this reduction could be due to the fact that the fluorophore detected in that

channel (Alexa 488 secondary antibody signal) had been in occasions weaker for detection, and some of the more scattered signal (e.g. any less visible peripheral distribution) could escape thresholding during image analysis. Since we sometimes had this issue when performing immunofluorescence with multi-channel images that includes 488, we tend to assign more trust to measurements through Western blot, and immunofluorescence results should be interpreted a bit more cautiously and validated further for quantitative comparison.

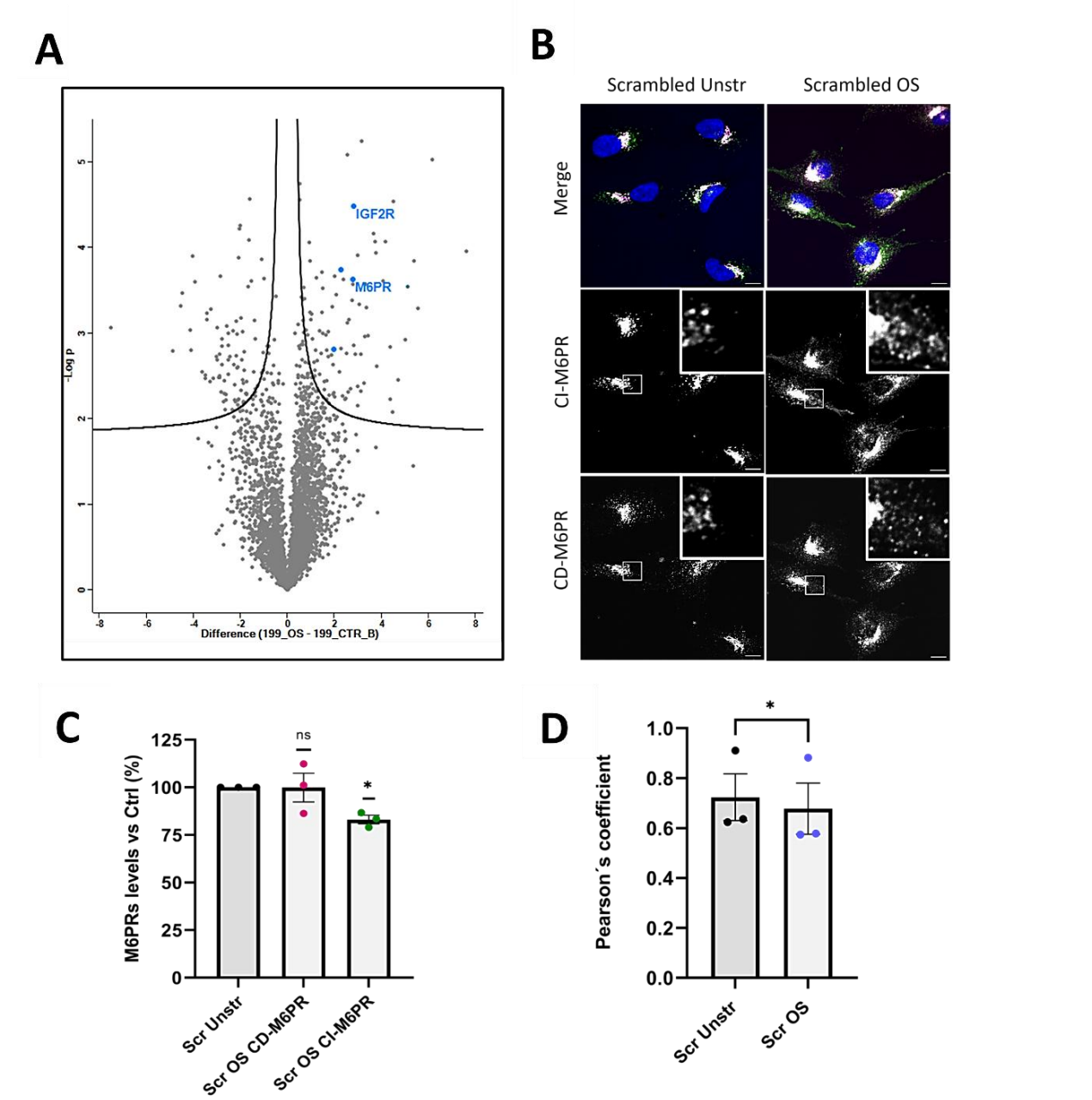

Figure 4.24: CD-M6PR localizes like CI-M6PR to the perinuclear area and redistributes, albeit to a lower degree, upon stress.
A) Volcano plot showing both M6PRs enriched at the surface after 1 h osmotic stress (IGF2R = CI-M6PR and M6PR = CD-M6PR). B) Representative confocal images showing both M6PRs in non-silenced (scrambled) unstressed and 1 h osmotically stressed (OS) cells. Cells were fixed and stained with antibodies against the respective M6PR. Nuclei were visualized by DAPI (blue). Scale bars = 10 µm. C) Quantification of the total level of both M6PRs based on experiments as depicted in B, normalized to control. D) Pearson's coefficient showing the degree of co-localization between the two M6PRs based on experiments as depicted in B. C,D) Data represent mean ± SEM; n = 3 independent experiments (as indicated by dots). C) One-sample t-test. D) Student's t-test (ns, not significant; *=$p < 0.05$).

Under unstressed conditions, as expected, both receptors predominantly localized to the perinuclear region, where the TGN is located, reflected in a solid co-localization (Fig. 4.24 B,C). Upon osmotic stress, both showed a partial shift toward the cell periphery (Fig 4.24 B). This redistribution was more pronounced for CI-M6PR, in agreement with our surface biotinylation-based mass spectrometry data (Fig. 4.24 A). This difference in the degree of redistribution is reflected in the significantly lower co-localization of both receptors upon stress (Fig. 4.24 C). Overall, our results support the possibility that CD-M6PR may play a compensatory role in unstressed and stressed cells. Therefore, we went on to test whether the two M6PRs indeed compensate for each other in RPE-1 cells.

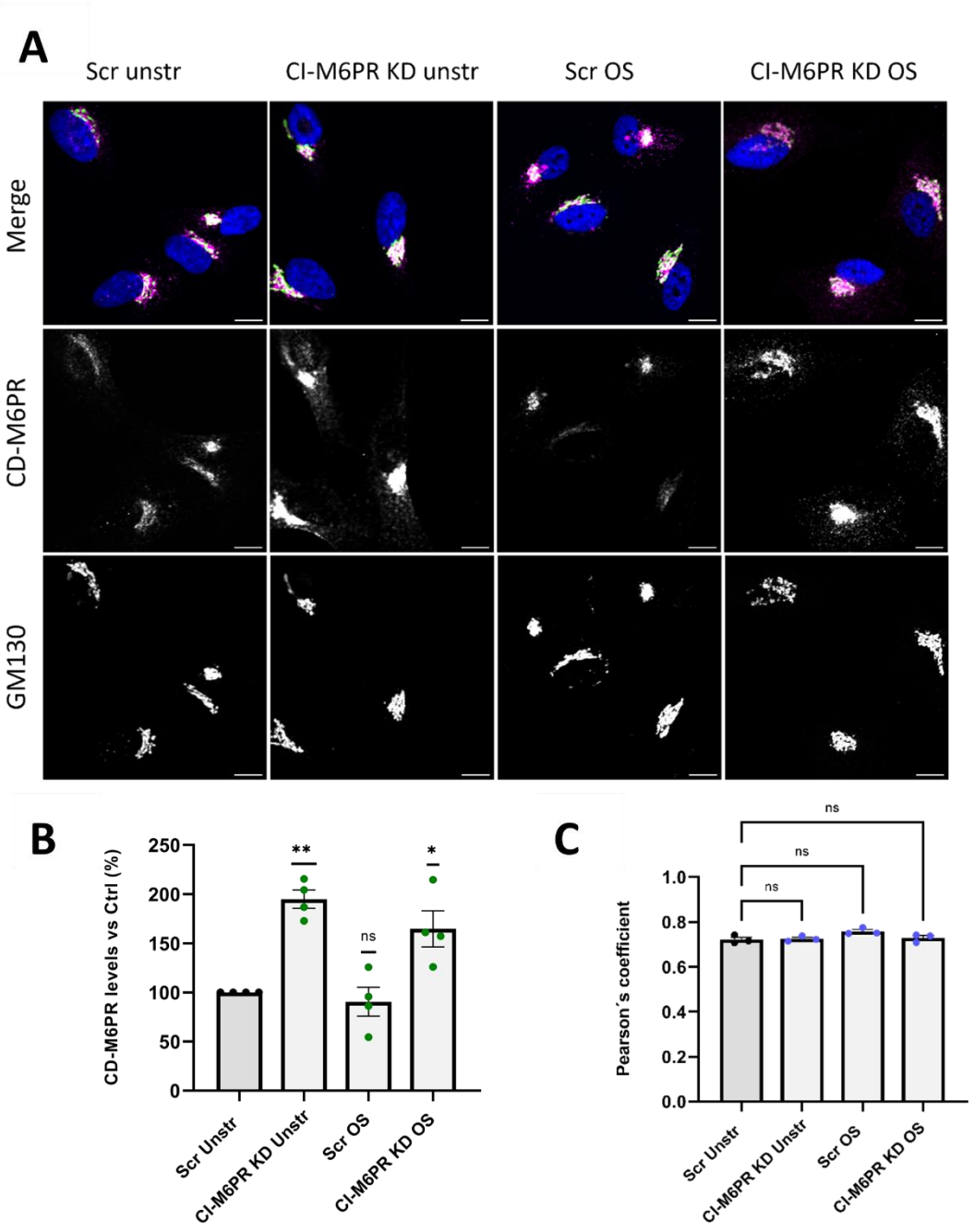

Figure 4.25: CD-M6PR is upregulated upon the silencing of CI-M6PR.
A) Representative confocal images showing CD-M6PR levels in non-silenced (scr) and CI-M6PR KD (siRNA #3) cells, both in unstressed (unstr) and 1 h osmotically stressed (OS) cells. Cells were fixed and

stained with antibodies against CD-M6PR and GM130. GM130 is shown as a Golgi marker. Nuclei were visualized by DAPI (blue). Scale bars = 10 μm. B) Quantification of CD-M6PR levels, normalized to controls, based on experiments like depicted in A. C) Quantification of Pearson's coefficient to show the colocalization degree between CD-M6PR and GM130 based on experiments like depicted in B. B,C) Data represent mean ± SEM; n = 3-4 independent experiments (as indicated by puncta). B) One sample T-test C) One-way ANOVA with Tukey's post-test (ns, not significant; *=$p < 0.05$, **=$p < 0.01$).

We started by probing whether the depletion of CI-M6PR would have an influence on CD-M6PR levels. For this, we performed an immunofluorescence analysis on non-silenced and CI-M6PR KD cells under both unstressed and osmotic stress conditions (Fig. 4.25 A). Cells were co-stained for GM130, a marker for the Golgi apparatus, to aid in subcellular localization analysis. In non-silenced cells exposed to osmotic stress, CD-M6PR levels were largely unchanged compared to unstressed controls. However, in CI-M6PR KD cells, CD-M6PR expression increased significantly, to similar extents in unstressed and stressed cells (Fig. 4.25 B).

These findings provide a plausible explanation for the previously observed maintenance of lysosomal hydrolase activity following CI-M6PR depletion. The upregulation of CD-M6PR upon CI-M6PR depletion suggests a compensatory mechanism, wherein CD-M6PR assumes part of the trafficking role typically carried out by CI-M6PR. This compensatory upregulation may underscore the physiological importance of proper hydrolase delivery for cell function and survival.

Interestingly, in scrambled cells subjected to 1 h of osmotic stress, much of the CD-M6PR signal was found to still colocalize with the Golgi/perinuclear region (Fig. 4.25 C), indicating that even under stress conditions, CD-M6PR may continue to fulfill its canonical trafficking function despite partial accumulation at the plasma membrane.

4.11.3 CI-M6PR is upregulated upon CD-M6PR depletion

To be able to co-deplete CI-M6PR and the compensating CD-M6PR, we purchased 3 siRNAs that were reported in the literature to efficiently target CD-M6PR (see siRNA table for further information) and tested them for their silencing efficiency (Fig. 4.26 A-B). Again, since the anti-CD-M6PR antibody we had purchased did not work for Western blots, we turned to immunofluorescence experiments to validate the knockdown. Anti CD-M6PR siRNA#3 proved to work very efficiently, downregulating the CD-M6PR levels to below 25% (Fig. 4.26 A,B).

Having established the CD-M6PR knockdown and knowing that CD-M6PR is upregulated in response to CI-M6PR silencing, we next asked whether the reciprocal effect occurs, namely, whether CI-M6PR is upregulated upon silencing of CD-M6PR.

To address this question, we performed two rounds of silencing with the anti-CD-M6PR siRNAs testing the effect of all three siRNAs individually to exclude an off-target effect on CI-M6PR expression (Fig. 4.26 C). While siRNA#2 did not appear to affect CI-M6PR expression, both siRNA#1 and siRNA#3 induced a noticeable upregulation of CI-M6PR, with siRNA3 producing the strongest effect in line with its efficient downregulation of CD-M6PR (Fig. 4.26 D). This result further supports the existence of a bidirectional compensatory mechanism between the two M6PRs.

Curiously, we had initially intended to use the detection of TrfR as loading control since there was no prior data that it should be affected by CD-M6PR knockdown. But then we noticed that its expression level was similarly affected as the one of CI-M6PR with siRNA1 and siRNA3 upregulating TrfR expression. Certainly, more research is needed to unravel the influence of CD-M6PR expression on TrfR levels.

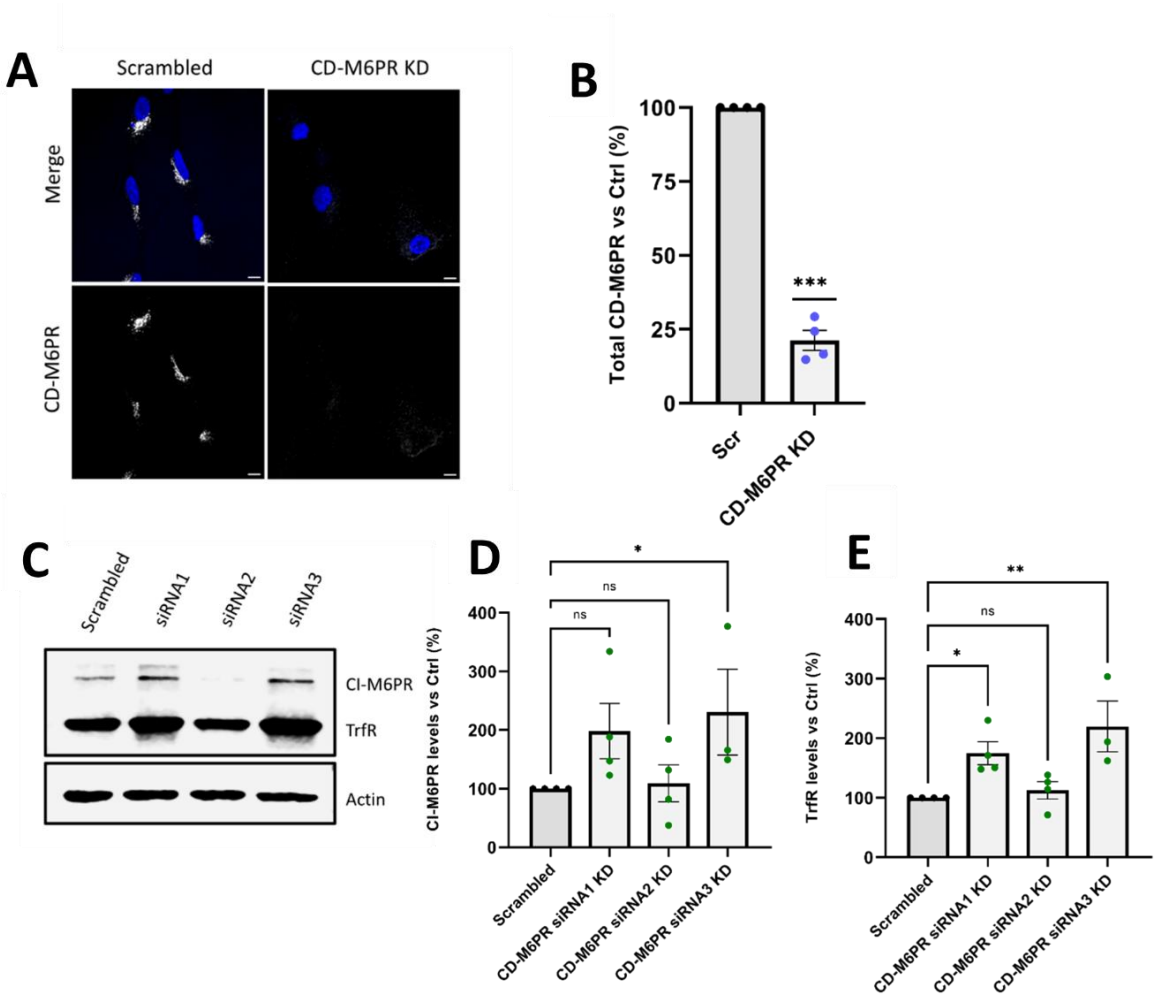

Figure 4.26: CI-M6PR compensates for the silencing of CD-M6PR.
A) Representative confocal images showing CD-M6PR signals after 2 rounds of silencing with siRNA3. Nuclei were visualized by DAPI (blue). B) Quantification of the knockdown efficiency of experiment in A. C) Representative Western blot membrane showing the signal of CI-M6PR after 2 rounds of silencing with 3 CD-M6PR siRNAs. TrfR is shown as another membrane protein. Actin was used as a loading control. D) Quantification of CI-M6PR levels shown in C, normalized to controls. E) Quantification of TrfR levels shown in C, normalized to controls. Data represent mean ± SEM; n = 3-4 independent experiments (as per puncta). One-sample T-test and One-way ANOVA with Dunnet's post-test (ns, not significant; *p < 0.05, **p < 0.01, ***p < 0.001).

4.11.4 The combined silencing of both M6PRs still leads to increased Cathepsin B activity

Given that each M6PR appears to compensate for the other upon individual silencing, the next logical step was to investigate the effects of a double knockdown targeting both receptors simultaneously. Specifically, we asked whether dual depletion would impair hydrolase trafficking and consequently reduce Cathepsin B activity.

To address this, we performed the Magic Red assay on RPE-1 cells subjected to double knockdown of CI-M6PR and CD-M6PR, and quantified Cathepsin B activity under both basal and hyperosmotic conditions (Fig. 4.27 A). Contrary to our expectations, Cathepsin B activity remained markedly elevated in double knockdown cells regardless of stress treatment (Fig. 4.27 B) arguing for yet another compensatory mechanism taking over in absence of the two M6PRs. Since there are other proteins reported to be involved to acid hydrolase trafficking (Reczek et al., 2007; Canuel et al., 2008; Braulke & Bonifacino, 2009; Coutinho et al., 2012a; Aguilera et al., 2023), this is certainly possible, but we decided not to pursue the knockdown approach further since it did not help to answer the question in how far the surface accumulation of CI-M6PR (and CD-M6PR) upon stress has beneficial effects on the stressed cells due to the confounding compensatory mechanisms.

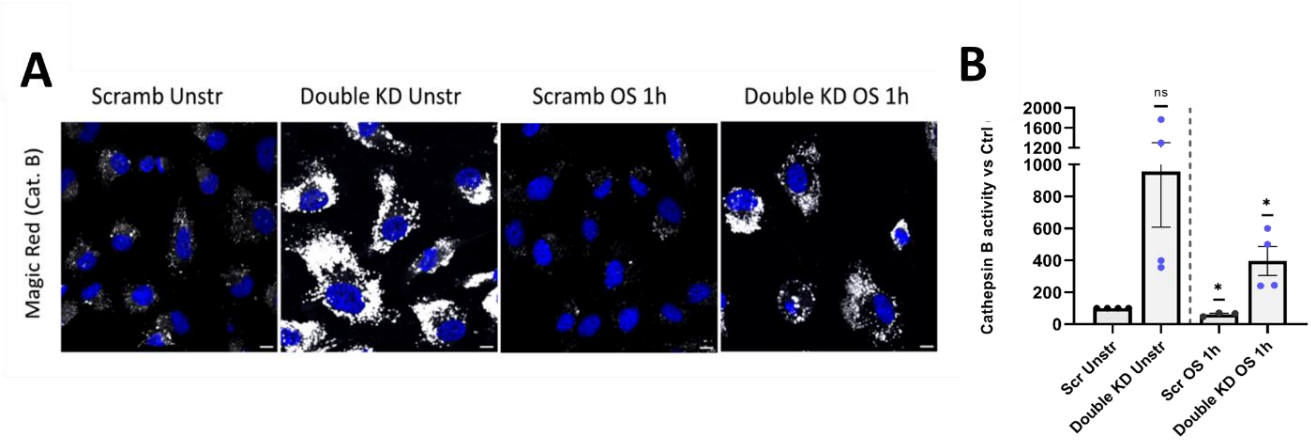

Figure 4.27: Double M6PR KD still results in higher Cathepsin B activity.
A) Representative confocal images of Cathepsin B activity in scrambled and double M6PRs KD under normal and 1 h osmotic stress. Nuclei were visualized by DAPI (blue). B) Quantification of Cathepsin B levels for experiments seen in A, normalized to controls. Data represent mean ± SEM; n = 4 independent experiments; One-sample T-test (ns, not significant; *p < 0.05). Scale bars = 10 µm

4.11.5 Effect on lysosomal morphology

During our repeated Magic Red experiments, noticeable differences in lysosomal morphology emerged across the various experimental conditions. This observation led us to hypothesize that osmotic stress and M6PR knockdown might affect not only lysosome number but also their size, swelling, or degree of aggregation. Such morphological changes could represent part of the cellular coping mechanism in response to stress.

To further investigate this, we performed live-cell imaging using Acridine Orange, a dye that permeates live cells and selectively accumulates in acidic organelles such as lysosomes and melanosomes. This assay was applied to all previously tested conditions: non-silenced controls, single KDs, and double KDs, both with and without osmotic stress (Fig. 4.28 A).

Our analysis was comprehensive and multi-parametric. First, Acridine Orange fluorescence intensity was quantified across conditions, revealing trends consistent with those observed in the Magic Red assay (Fig. 4.28 B,C), i.e. a tendency to a lower number of lysosomal structures upon 1 h of osmotic stress and a tendency to increased lysosomes upon CI-M6PR KD and double M6PR KD. Second, the number of lysosomes per cell was quantified using the ComDet plugin in FIJI. For

this, lysosome counts per image were normalized to cell number and averaged for each experimental group (Fig. 4.28 D).

While results varied across conditions, a significant increase in lysosome number was observed specifically in the double KD group. Lastly and most importantly, lysosomal size was measured using the same FIJI plugin. This analysis revealed a significant increase in average lysosome size in all experimental conditions compared to unstressed controls, suggesting lysosomal swelling or aggregation as a common stress response (Fig. 4.28 E).

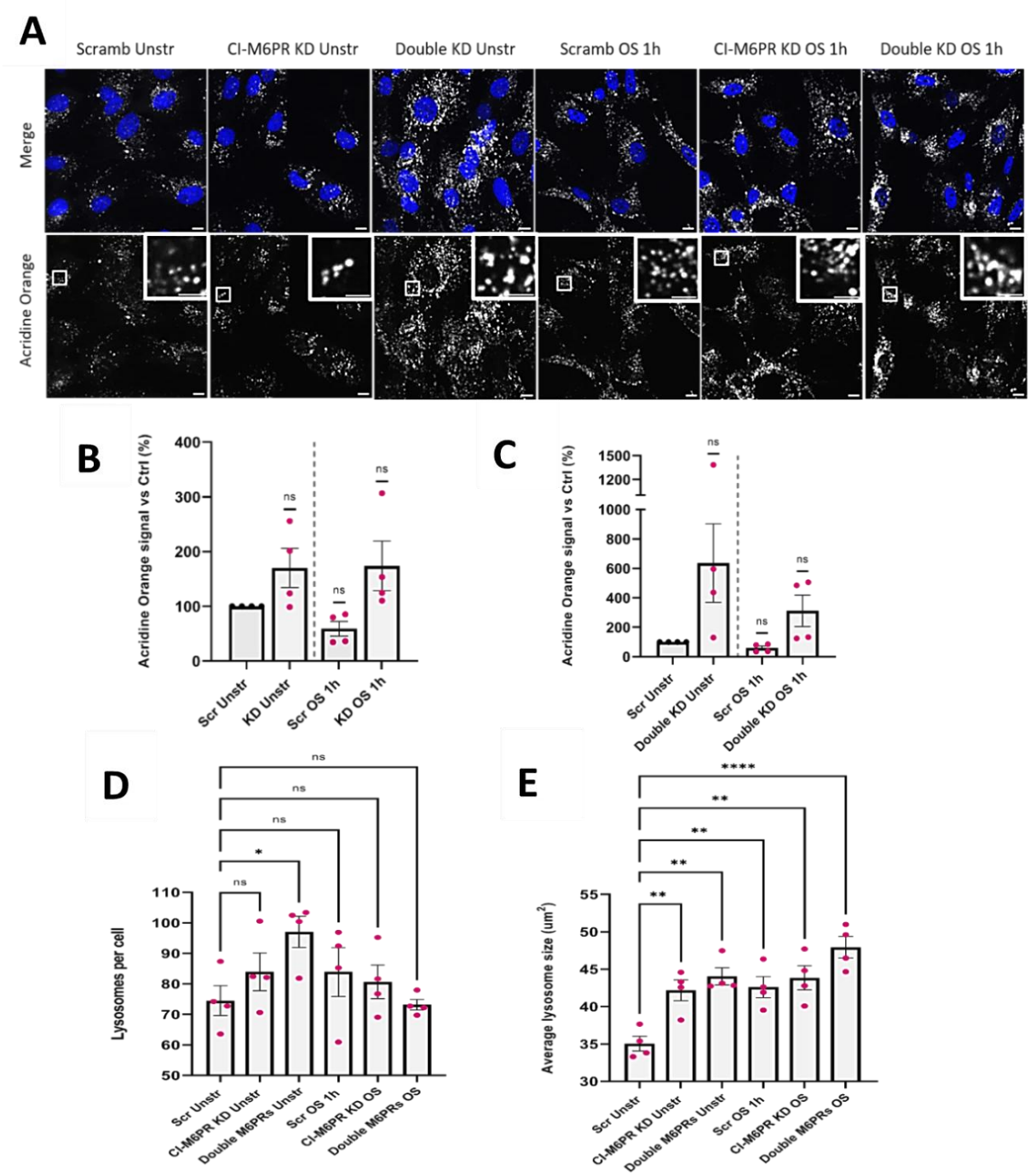

Figure 4.28: M6PRs silencing mostly reveals no effect in lysosomal number, but it promotes significant increase in lysosomal average size suggesting potential downstream coping response.
A) Representative confocal images showing acridine orange signals in non-silenced (scramb), after 2 rounds of CI-M6PR silencing with siRNA3 (CI-M6PR KD) and double silencing of CI-M6PR and CD-M6PR (both silenced with siRNA3 of their siRNA set), with and without osmotic stress treatment. Nuclei were visualized

by DAPI (blue). B) Quantification of the intensity of acridine orange signal per cell for CI-M6PR KD, normalized to Scr unstressed control, from experiment in A. C) Quantification of the intensity of acridine orange signal per cell for double M6PR KD, normalized to Scr unstressed control, from experiment in A. D) Quantification of lysosome number per cell, as per puncta segmented by ComDet plugin, from experiment in A. E) Quantification of the average lysosome size in each condition tested in experiment in A, detected using the same ComDet plugin. Data represent mean ± SEM; n = 4 independent experiments (as per puncta). One-sample T-test and One-way ANOVA with Tukey's post-test (ns, not significant; *p < 0.05, **p < 0.01, ****p < 0.0001).

4.12 Functional investigation of the IGF2 receptor role of CI-M6PR during osmotic stress

In our first hypothesis, we examined whether the surface accumulation of CI-M6PR upon osmotic stress might be beneficial for stressed cells by improving the delivery of hydrolases to the lysosome. However, our experiments showed rather a transient decrease in hydrolase activity upon osmotic stress which might be a detrimental site effect of the surface accumulation of CI-M6PR by leaving too little CI-M6PR for the TGN-to-lysosome hydrolase delivery. However, we were not able to mimic this potential partial loss of CI-M6PR functionality upon stress by CI-M6PR KD due to unforeseen compensatory mechanisms. Nevertheless, the surface-stranded CI-M6PR does not appear to improve the degradative capacity of osmotically stressed cells. Therefore, we considered alternative scenarios for how surface accumulation of CI-M6PR could help cells to cope with osmotic stress.

In this second hypothesis, we explored an alternative role for CI-M6PR, based on its known function as a receptor for IGF-II.

Insulin-like growth factors (IGFs), specifically IGF-I and IGF-II, are small mitogenic polypeptides that play critical roles in regulating cell proliferation, survival, differentiation, and transformation across a variety of tissues, including muscle, bone, and cartilage (Brown et al., 2009). Both ligands primarily exert their biological effects through the IGF-I receptor (IGF1R), a tyrosine kinase receptor, although IGF-II can also bind to the IGF-II/CI-M6PR. Unlike IGF1R, IGF2R lacks intrinsic kinase activity and is considered a non-signalling receptor. While IGF2R itself does not directly initiate signalling cascades, its ability to sequester ligands like IGF-II can indirectly influence cellular signalling by modulating ligand availability at the cell surface (P. Ghosh et al., 2003). Beyond its binding to IGF-II, CI-M6PR is also capable of binding to a variety of ligands, including granzyme B, uPAR/plasminogen, glycosylated LIF, and retinoids, all of which are internalized through rapid receptor endocytosis.

According to the literature, IGF2R/CI-M6PR normally modulates mitogenic signalling by binding and sequestering IGF2, thereby attenuating IGF1R-mediated proliferation and acting as a tumour suppressor (Brown et al., 2009; Kerr & Baxter, 2022) . However, some studies such as those by Takeda et al., (2019), reported reduced proliferation upon CI-M6PR knockdown in certain cell types. Since osmotic stress led to a decreased proliferative capacity of RPE-1 cells which was further aggravated by the KD of IGF2R/CI-M6PR, we hypothesized that the surface accumulation of IGF2R/CI-M6PR upon cell stress might exert a proliferation-promoting function.

To assess whether IGF2R/CI-M6PR indeed exerts a pro-proliferative regulatory function in RPE-1 cells, under normal conditions and particularly upon osmotic stress, we employed two complementary approaches: 1) blockade of IGF-II binding to IGF2R/CI-M6PR using a neutralizing

antibody in absence and presence of IGF2R/CI-M6PR KD followed by a quantification of cell proliferation, and 2) exogenous administration of recombinant IGF-II in in absence and presence of IGF2R/CI-M6PR KD, again followed by a quantification of cell proliferation (Fig. 4.29 A,B).

For the first experiment, we included a control to all the conditions where cells were treated with the same concentration of a non-targeting mouse IgG instead of the neutralizing antibody, to account for potential side effects of the antibody incubation (Fig. 4.29 A). Strangely, this control set did not always show the same behaviour, expressed as percentage of proliferation, as the previous proliferation experiments we conducted. Possibly, the treatment with non-targeting antibodies had indeed unforeseen side effects. Unfortunately, we did not include a control without any antibody treatment so that this point remains unclear. Alternatively, we imagine this could be attributed to cell variability across different cell batches.

Looking at the impact of the neutralizing antibody on scrambled cells (Fig. 4.29 A), there was no anti-proliferative effect of disrupting IGF-II binding to f IGF2R/CI-M6PR, instead we rather noticed a tendency to slightly more proliferation than controls. The lack of an anti-proliferative effect makes sense given that under normal conditions there would not be much IGF2R/CI-M6PR in the plasma membrane for the antibody to act on (approx. 5-10% of the total protein pool) according to the literature (Brown et al., 2009) consistent with the low signals for IGF2R/CI-M6PR we observed by surface biotinylation in the surface fraction of unstressed cells). We saw the same slightly higher proliferation tendency in the unstressed IGF2R/CI-M6PR KD cells. Unfortunately, in contrast to our hypothesis, when we looked at the effect of the neutralizing antibody upon hyperosmotic stress, where we assume IGF2R/CI-M6PR to be accumulated at the plasma membrane and therefore able to bind to IGF-2 with putative pro-proliferative effects, we still did not see any decline in proliferation. The same was true for the stressed IGF2R/CI-M6PR KD cells where no effect was expected. All of this suggests that there is not much effect of blocking CI-M6PR/IGF2R-binding domain on proliferation arguing against a pro-proliferative function of surface-resident IGF2R/CI-M6PR in RPE-1 cells.

One caveat we noticed regarding our neutralizing antibody experiment was that we did not know how much IGF-II was present in our cell culture system in absence of exogenous administration. Since RPE-1 cell cultures might not produce IGF-II themselves, we decided to test for a putative pro-proliferative effect of the exogenous application of recombinant IGF-II and assess its ability to improve proliferation in osmotically stressed cells in presence of IGF2R/CI-M6PR. In fact, the quality of the recombinant human IGF-II is controlled by the manufacturer by its ability to induce proliferation. For this experimental set, we included a control to all the conditions where cells were treated with the same concentration of BSA, as a mock treatment (Fig. 4.29 B). The mock controls in this case were closer again to what we had expected given our previous proliferation experiments, recapitulating the aggravating effect of IGF2R/CI-M6PR depletion on the proliferation decline seen in osmotically stressed cells.

Unfortunately, our results showed hardly any effect of IGF-II on RPE-1 cell proliferation at the concentration used (100 ng/ml) (Fig. 4.29 B) which had been shown to efficiently promote cell proliferation in other cell types (Y. Han et al., 2009; Chen et al., 2011; Bella et al., 2020). We saw a slight insignificant improvement of proliferation in the non-silenced cells, which would, if at all given the large error bars, support the idea of IGF2R/CI-M6PR sequestering IGF-II since there should not be much CI-M6PR present at the surface in this condition to bind to IGF-II and thereby

interfere with its IGF1R binding. However, since there was no comparable IGF-II effect on the proliferation of cells depleted for IGF2R/CI-M6PR, the slight increase in the proliferation of the non-silenced cells is more likely random variation within a small sample size. Also, in case of the stressed cells, there was no beneficial effect of IGF-II treatment, emphasising that IGF-II, at least at the used concentration, does not promote proliferation in RPE-1 cells.

In conclusion, we observed no significant differences in proliferation of RPE-1 cells upon addition of IGF2 or blocking of its binding to IGF2R/CI-M6PR. These findings do not support a role for CI-M6PR in modulating IGF2-dependent proliferation in RPE-1 cells, either at steady state or under osmotic stress. However, these experiments lack a number of important controls as I will discuss later which could not be performed anymore due to lack of time.

Still, and although the aggravated effect of osmotic stress combined with IGF2R/CI-M6PR loss suggests that stress-induced surface accumulation of the receptor may be beneficial and aid in cell survival, the molecular mechanism underlying this effect remains unclear.

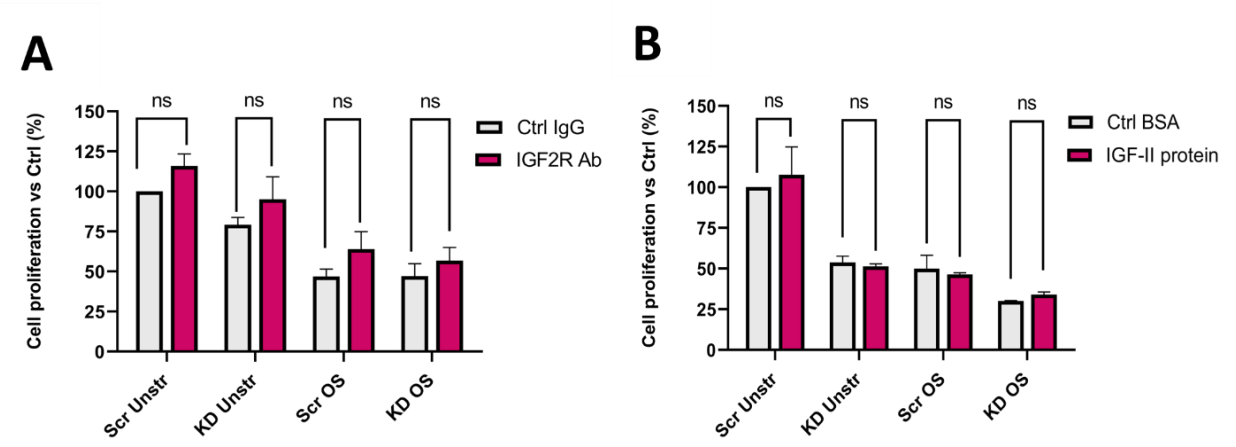

Figure 4.29: No evidence for a role of CI-M6PR as positive regulator of cell proliferation via IGF-II binding.
A,B) Quantification of RPE cell proliferation (counted cell numbers shown normalized to control (Scr Unstr) for cells treated with scrambled (scr) or CI-M6PR targeting siRNA #3 (KD) in absence of stress or upon 24 h osmotic stress and upon treatment with 10 µg /ml anti-IGF2R antibodies neutralizing its binding to IGF-II or with the same concentration of non-targeting IgG as control treatment (A) or upon treatment with 100 ng/ml IGF-II or the same concentration of BSA as control treatment. Data represent mean ± SEM; n = 3-4 independent experiments; One-sample T-test and Student's T-test (ns, not significant).

5. Discussion

5.1. General summary of findings

Understanding how human cells adapt to acute stress and which specific molecular programs they activate remains an underexplored area in cell biology. In particular, the dynamic remodelling of the surface proteome (surfaceome), alterations in bulk endocytosis, and cargo-specific adaptations of endocytosis in response to stress are insufficiently characterized. To address this knowledge gap, we employed an unbiased surface biotinylation approach combined with discovery-based mass spectrometry to monitor stress-induced changes in protein surface levels under conditions of heat shock, oxidative stress, and hyperosmotic stress. Our findings revealed a general reduction in both bulk endocytic flux and transferrin uptake across all stress conditions, though the magnitude and nature of these changes varied, likely reflecting distinct stressor-specific modulations of endocytic pathways.

Through quantitative label-free proteomics following enrichment of biotinylated proteins, we identified several stress-responsive membrane-associated proteins of which we successfully validated the following ones: SPPL2A was selectively altered in response to heat stress; NHE7 and TrfR were modulated under hyperosmotic conditions; and CI-M6PR was consistently enriched at the plasma membrane following either heat or osmotic stress. These stress-induced redistributions were found to depend at least in part on clathrin-mediated endocytosis for CI-M6PR, whose internalization we demonstrated to be functionally impaired under heat and osmotic stress using antibody-feeding assays.

Subsequent mechanistic studies focused on CI-M6PR revealed that its membrane enrichment under osmotic stress follows a swift and defined timeline and is also dose-dependent. Using an overexpression model of the intracellular CI-M6PR tail fused to a fluorescent tag, we visualized its intracellular redistribution upon stress and confirmed that its surface accumulation is dependent upon endocytic CME motifs in its tail.

Functionally, CI-M6PR appears to play a protective role in the cellular stress response. Knockdown of CI-M6PR in RPE-1 cells led to increased cell death and reduced proliferation, indicating its importance in maintaining cellular viability under stress. Moreover, we further characterized CI-M6PR's canonical role as a lysosomal transporter under these conditions and revealed a compensatory mechanism involving CD-M6PR: when either receptor was silenced, the other partially compensated, as observed through immunofluorescence analysis and Cathepsin B activity assays. Finally, acridine orange staining demonstrated lysosomal swelling and fusion events (both hallmarks of a robust lysosomal response) upon silencing of one or both M6PRs, suggesting that stress-induced lysosomal remodelling is both functionally significant and warrants further investigation.

Even though there are pieces of the puzzle that are still missing, these findings might have some very interesting implications for health and disease that should not be missed.

5.2 Choice of cell model: rationale and considerations

The selection of an appropriate cell model is a critical aspect of experimental design, particularly when investigating cellular adaptation mechanisms under stress. Despite the fact that we started our experimental tuning with the very established HeLa cell model, we decided against using them for our stress investigation since due to being an advanced cancer cell line they are already well detached from the reality of a more physiologically relevant model. Therefore, for this study we employed hTERT-immortalized RPE-1 cells, a widely used, non-transformed human epithelial cell line. This choice was guided by several strategic and biological considerations.

RPE-1 cells are derived from the human retinal pigment epithelium and were immortalized through the ectopic expression of the catalytic subunit of human telomerase (hTERT), allowing sustained proliferative capacity without undergoing malignant transformation (Rambhatla et al., 2002; Shitova et al., 2024). Unlike many cancer-derived cell lines, RPE-1 cells retain a stable, near-diploid karyotype, intact DNA damage response pathways, and a non-transformed phenotype, making them particularly suitable for studies aimed at understanding basal cellular processes, including vesicular trafficking, membrane homeostasis, and stress responses (Kuznetsova et al., 2014). Their well-preserved epithelial features, such as polarity, tight junction formation, and a functional endo-lysosomal system, provide a physiologically relevant framework for dissecting membrane trafficking pathways and stress adaptation in epithelial-like settings.

Importantly, RPE cells display robust and reproducible responses to various environmental perturbations, including oxidative and osmotic stress. These features render them a tractable model for probing signalling and trafficking pathways in a genetically and phenotypically consistent background. Furthermore, their responsiveness to stimuli is well documented in the literature across multiple domains, including cell cycle control, DNA repair, and organelle dynamics, which aligns with the objectives of this project (Storm et al., 2020; Tong & Wang, 2020).

However, as with all immortalized in vitro models, RPE-1 cells also come with certain limitations. The hTERT-driven immortalization process, while avoiding the extensive genomic instability typical of tumour-derived lines, may still influence the regulation of key cellular checkpoints and signalling pathways related to stress sensing and apoptosis (Shitova et al., 2024). Additionally, while RPE-1 cells provide a homogeneous and reproducible model system, they do not fully recapitulate the complexity of tissue architecture, cell-cell interactions, or stromal signalling that occur in vivo or in primary cultures (Soodabeh et al., 2015). Thus, while our findings in RPE-1 cells offer important mechanistic insights into how mammalian cells respond to acute environmental stressors, particularly at the level of endocytic sorting and trafficking, they should be considered foundational observations requiring further validation in additional cellular systems.

To strengthen the generalizability of our conclusions, future studies should incorporate comparative analyses in other cell types, including primary epithelial cells and ex vivo organotypic cultures. Such efforts would be essential to establish the physiological relevance of the identified mechanisms in more complex biological contexts. Nonetheless, the use of RPE-1 cells in this study served as a reliable and biologically meaningful platform for dissecting acute stress-induced changes in the surface proteome and membrane trafficking, under controlled and reproducible experimental conditions.

5.3 Strategic selection of cellular stress treatments

To ensure biological relevance, the stressors and their dosages in this study were selected to mimic physiologically or as close to pathologically plausible conditions as possible. They were meant to be strong enough to elicit a measurable cellular response, yet not so severe as to cause irreversible damage (section 4.2).

Heat stress was applied at 42°C for 1 h, a condition comparable to high-grade fever, and previously shown to activate the heat shock response without triggering extensive translational arrest (Vega et al., 2010; Zhou et al., 2015). This exposure window was chosen to preserve the study's focus on dynamic membrane remodelling via clathrin-mediated endocytosis (CME), avoiding confounding stress-related pathways that operate by slower transcriptional mechanisms.

For **osmotic stress**, hyperosmolar conditions were selected based on evidence that RPE cells, especially under disease states like diabetic retinopathy (Willermain et al., 2018), are subject to substantial osmotic fluctuations. After assessing a range between 600-900 mOsm/kg, we chose an intermediate 750 mOsm/kg to stimulate the cells. An interesting fact is that hyperosmolarity is known to drive processes such as membrane transporter relocalization and intracellular protein aggregation, providing a robust and quantifiable cellular readout (López-Hernández, Haucke, et al., 2020).

Among commonly used **oxidative stress** inducers, BHP was selected for its favourable properties. Unlike H_2O_2 or paraquat, BHP is moderately lipophilic, enabling direct membrane integration and localized ROS generation without strong dependence on metal ions or cellular enzymes (Rabin et al., 2012). Its chemical stability ensures reproducible dosing, even in serum-containing media, and its stress kinetics can be finely tuned by adjusting concentration and exposure time (Spector et al., 2002; Glotin et al., 2006). Moreover, BHP is optically silent, making it compatible with fluorescence-based assays (Sun et al., 2014). Due to variability in the literature regarding TBH treatment parameters, with concentrations ranging from 10 to 250 µM and exposure times spanning 15 min to 72 h, we aimed to identify a condition that would elicit a measurable oxidative response within our chosen 1 h time frame. While chronic, sublethal exposures (10-50 µM for ≥12 h) are common, shorter exposures generally required higher concentrations to induce detectable stress responses (Rabin et al., 2012; X. Xu et al., 2016). Based on this, we evaluated intermediate doses (50-150 µM), monitoring oxidative stress using CellROX Green, a nuclear-localizing ROS indicator. Among the tested doses, 75 µM TBH produced a reproducible increase in fluorescence without signs of overt toxicity and was therefore selected as a condition that balances robust ROS generation with minimal cytotoxicity, in line with the literature (Zhao et al., 2017; Jung et al., 2022).

5.3.1 Validation and effectiveness of the selected stress conditions

Each of the selected stressors was validated based on their ability to elicit canonical cellular responses consistent with known literature, while remaining within a tolerable range that caused, at most, a slight increase in cell death upon longer application and allowed for the study of downstream processes such as CME.

5.3.1.1 Hyperosmotic stress

Osmotic stress was confirmed to be effective through multiple lines of evidence. Notably, our proteomic analyses revealed alterations in plasma membrane-associated proteins, including NHE7 and CI-M6PR, consistent with findings reported by López-Hernández et al. (2020), who described NHE7 membrane recruitment in response to hyperosmolarity. Morphologically, cells displayed the expected volume shrinkage phenotype, evident in both immunofluorescence imaging and proliferation assays, and a moderate presence of protein aggregates, measured by the Proteostat assay. Finally, these effects were accompanied by a measurable, though limited, degree of cell death, further supporting the notion that hyperosmotic stress was sufficient to perturb cell physiology without inducing widespread cytotoxicity.

Most studies investigating the cellular effects of hyperosmotic stress in mammalian systems typically employ osmolarities ranging between 500-610 mOsm/kg, which already seem to trigger inflammatory, angiogenic, and cell-cycle responses (Luh et al., 1996; Santos et al., 2003; Y. K. Han et al., 2010; Arsenijevic et al., 2013). The stress-exposure durations of the studies span from 2 to 96 h. While these parameters are generally sufficient to induce stress-related transcriptional responses, a few notable exceptions illustrate the tolerance of certain cell types to higher osmolar loads. For instance, Costa et al. (2013) exposed RPE cells for 10 min to 658 mOsm/kg mannitol without notable cytotoxicity, and (Schwartz et al., 2009) evaluated inflammatory responses in human epithelial cell lines (HT29, T24, and A549) exposed to inert osmolytes like Mannitol at 300, 600, and 900 mOsm/kg for up to 48 h, showing a higher secretion of proinflammatory cytokines (IL-8, IL-6, IL-1β and TNF-α).

These findings support a broader dynamic range of resilience to osmotic exposure than typically probed. In general, short-term exposures (minutes to several hours) are employed to probe acute stress responses such as inflammation or apoptosis (Luh et al., 1996; Arsenijevic et al., 2013), whereas longer exposures (≥2 days) are used to study osmoadaptation mechanisms, involving transcriptional regulators like NFAT5 (Santos et al., 2003; Y. K. Han et al., 2010; Arsenijevic et al., 2013; Miyano et al., 2025). Given that most prior studies limit osmolarity to ~600 mOsm/kg but often extend the exposure duration well beyond our 1 h time point, we chose to increase the osmolar load in our RPE-1 cell model to elicit a robust yet controlled stress response within a shorter time frame. This approach was further justified by our own observations that such conditions were well tolerated by the cells, as demonstrated by the minimal impact on cell viability (see Sections 4.2.2 and 4.3). We also provided an answer to the question of what would happen at lower osmolarities, since we later also evaluated lower medium osmolarities and our results were reproduced throughout the whole spectrum applied, including 400, 500, 600 and finally 750 mOsm/kg.

When it comes to studies that focus on stress effects on CME in human cells, we found that numerous studies across diverse human cell lines have reported that increasing extracellular osmolarity, whether through hypertonic sucrose or other osmolytes, leads to a marked inhibition of CME, which appears to be a consistent cellular response to hyperosmotic conditions (Hansen, 1993; Wu et al., 2001; Wang et al., 2011; Hong et al., 2012). However, it is noteworthy that the majority of these studies employed high, non-physiological osmolarities (around 500-600 mOsm/kg), often aimed at completely disrupting endocytic function. In contrast, only a few investigations, such as Wang et al. (2011), explored more moderate osmotic elevations, intended to approximate physiologically relevant stress. This distinction is important, as it suggests that while extreme

osmotic shifts can serve as useful tools to dissect endocytic mechanisms, they may not accurately reflect how CME operates or adapts under more subtle, physiologically encountered osmotic stress.

5.3.1.2 Therapeutic use of high osmolarity in clinical practice

To contextualize that the use of a concentration of 750 mOsm/kg as employed by our study is not outside of the range encountered by human cells, we bring forward the use of high osmolarity in the realm of medicine.

It has been the case for more than 30 years that osmotically active solutions like mannitol and hypertonic saline have been used to treat intracranial hypertension and neurosurgical emergencies (Scheller et al., 1991; Castillo et al., 2009). This means exposing the patients to a very high osmolarity of either mannitol or NaCl solutions.

Mannitol has been traditionally the agent of choice and is administered rapidly in 15-20% solutions (osmolarity: 1200-1400 mOsm/kg), exerting peak effects within 30-45 min, returning to baseline within 2-12 h, and excreted unchanged by the kidneys (Scheller et al., 1991). An acute infusion of mannitol solution produces a marked but transient rise in arterial and cerebral perfusion pressures, accompanied by increased cardiac output and filling pressures (Bratton et al., 2007). Cardiac output can increase by up to approximately 30%, enhancing cerebral blood flow. Research indicates that mannitol significantly influences systemic vascular resistance through its rheological properties, thereby improving oxygen delivery at both systemic and cerebral levels (Rudehill et al., 1993).

The ability of hyperosmotic solutions to lower intracranial pressure has been recognized for decades, though the underlying mechanisms remain debated. One explanation suggests that increased circulating volume elevates systemic arterial pressure, which, if cerebral autoregulation is intact, triggers vasoconstriction, reducing cerebral blood volume and intracranial pressure (Meier-Hellmann et al., 1995; Nau et al., 1997). Another view attributes the effect to improved blood rheology, promoting vasoconstriction under preserved autoregulatory conditions (Winkler & Munoz-Ruiz, 1995). A further hypothesis proposes that the osmotic action of hypertonic solutions reduces cerebrospinal fluid volume in both supra- and infratentorial compartments, thereby lowering intracranial pressure (Battison et al., 2005).

In recent years, hypertonic saline has emerged as an alternative, particularly in trauma and hemorrhagic shock, with concentrations ranging from 3% to 23.5%, (osmolarity: 1000-7500 mOsm/kg) leading to progressively higher plasma osmolarity and more prolonged reduction in cerebral edema due to sustained sodium-driven water shifts (Castillo et al., 2009).

5.3.1.3 Heat and oxidative stress

In the case of **oxidative stress**, treatment with 75 µM TBH led to elevated nuclear oxidation signal at this concentration, measured by CellROX Green nuclear fluorescence. The effect was further corroborated by presence of redox-related enzymes (e.g. GPX1, GPX4, SOD2), as identified by mass spectrometry, suggesting an early-stage oxidative response. While individual protein changes did not consistently reach statistical significance, the overall trend indicated an activation of cellular antioxidant mechanisms.

Heat stress presented a more nuanced profile. Our observation that a 1 h exposure to 42°C did not result in a detectable increase in HSP70 levels, in fact aligns with reports suggesting that some markers of the heat shock response require a short recovery period post-stress to accumulate (ref), likely due to the comparatively slow process of transcriptional upregulation. Indeed, our MS-based analysis of the cellular proteome after a 1 h heat shock followed by 4 h recovery revealed upregulation of several HSR-associated proteins, including components of the translational and chaperone machinery (e.g. HSP90, HSP105,GSK3) consistent with classical HSR activation (Vega et al., 2010; Zhou et al., 2015). These findings confirm that the stress duration and intensity were sufficient to trigger a proteostatic response while minimizing confounding effects.

Overall, each stressor was effective in eliciting biologically relevant responses within the selected 1 h treatment window, and importantly, the chosen conditions allowed us to assess endocytic responses under stress without overwhelming the system. The correct choice of stressors was reaffirmed by experimental results showing indeed a CME modulation, including altered transferrin uptake and surface proteome variations in our 1 h timeframe (see Fig. 4.6 and 4.7, respectively), supporting our hypothesis that CME plays a role in stress adaptation.

Furthermore, long-term assessments demonstrated that the chosen stress conditions were well-tolerated by RPE-1 cells, meeting a key criterion of our experimental design. Cell death rates remained low (0.5-3%) even several hours post-treatment, while the most pronounced long-term impact was observed on cell proliferation, suggesting that cells enter a temporary growth arrest rather than undergoing apoptosis. This is consistent with literature reporting stress-induced proliferative slowing as an adaptive mechanism (Dmitrieva et al., 2001; Arsenijevic et al., 2013). As we aimed to explore whether CME might contribute to stress adaptation and survival, the relatively low cytotoxicity, combined with evidence of altered trafficking, pointed to a functional remodelling of the membrane proteome that may support cellular resilience.

5.4 Both CME and bulk endocytosis in general were impaired in all 3 stress conditions.

Our quantitative analysis revealed that all three stress conditions led to a noticeable reduction in bulk endocytosis compared to the control, based on both the internalization of biotinylated proteins and transferrin uptake assays, although the extent and pattern of the reduction varied per stressor.

5.4.1 Effect of hyperosmotic conditions on endocytosis

The plasma membrane tension developed from either being exposed to hypotonic or hypertonic conditions exert plays an important role in endocytosis. Hypotonic extracellular conditions lead to cellular swelling accompanied by increased plasma membrane tension, whereas hypertonic environments cause cell shrinkage and a reduction in membrane tension (López-Hernández, Haucke, et al., 2020). Because endocytosis fundamentally involves the remodelling and invagination of the plasma membrane, alterations in membrane tension are anticipated to influence the efficiency of internalization. Elevated membrane tension impedes membrane deformation, thereby suppressing endocytic activity under hypotonic conditions. Conversely, the reduction in membrane tension during hypertonic stress would, in principle, be expected to facilitate membrane

curvature and promote endocytosis (Boulant et al., 2011). Interestingly, experimental observations dating back more than four decades challenged this assumption (Daukas & Zigmond, 1985), showing that hypertonic conditions can, in fact, inhibit rather than enhance endocytic uptake.

Several studies across diverse human cell lines have, since then, consistently reported a marked inhibition of CME following exposure to hyperosmotic conditions, particularly with hypertonic sucrose. This inhibition is typically measured by a significant reduction in transferrin uptake and by structural disruptions to clathrin-coated pits, as observed via microscopy or FRAP analyses (Hansen, 1993; Wu et al., 2001; Wang et al., 2011; Hong et al., 2012). Since it was first described by (J. E. Heuser & Anderson, 1989), it is now a commonly accepted mechanism that hypertonic environments disassemble or disrupt clathrin lattices at the plasma membrane, thereby impairing receptor internalization (Hansen, 1993; X. Wu et al., 2001; S. Wang et al., 2011; Hong et al., 2012; López-Hernández, Haucke, et al., 2020). Importantly, this inhibition appears reversible: CME function rapidly resumes upon return to isotonic conditions (J. Heuser, 1989; Hansen, 1993; S. Wang et al., 2011).

Notably, Wang et al. (2011) provided a more nuanced perspective using human type I alveolar epithelial cells. Under moderate hyperosmotic stress (400-600 mOsm), they observed a transient reduction in both clathrin-mediated and fluid-phase endocytosis, while caveolar uptake increased. This was quantified using pathway-specific cargoes (transferrin for CME, lactosyl-ceramide for caveolae, and dextran for fluid-phase endocytosis) and linked to changes in caveolin-1 localization and dynamics. These findings suggest that cells may compensate for CME inhibition under osmotic stress by upregulating alternative pathways such as caveolae-mediated endocytosis, highlighting a potential adaptive crosstalk between endocytic routes in response to environmental stress.

Moreover, broader signalling cascades are known to be activated by osmotic stress. Environmental stressors such as high osmolarity activate a suite of mitogen-activated protein kinase (MAPK) pathways, most notably the p38 MAPK and JNK pathways (Gatsios et al., 1998; Bode et al., 1999; Volonté et al., 2001; Arsenijevic et al., 2013). These cascades mediate diverse cellular responses including proliferation arrest, apoptosis, and cytoskeletal remodelling (Ono & Han, 2000; Volonté et al., 2001). In their study, (Volonté et al., 2001) found that the activation of p38 and c-Src are linked to phosphorylation of caveolin-1, a scaffolding protein associated with lipid raft-mediated signalling and membrane trafficking. They reported that phosphorylated caveolin-1 redistributes to focal adhesions following osmotic shock, potentially involving integrin-mediated adhesion signalling with stress responses. Intriguingly, this phenomenon appears specific to osmotic stress, as heat shock fails to trigger similar phosphorylation events or p38 activation in their study.

Our results revealed that total protein internalization was reduced by approximately 10-15%, while transferrin uptake declined even more sharply by 15-20%, suggesting a preferential impairment of CME over other endocytic routes. Our findings are consistent with these earlier and current observations, as we observed a more marked suppression of clathrin-mediated endocytosis under hyperosmotic stress, accompanied by the surface accumulation of specific cargo proteins. This suggests that additional biophysical or molecular constraints, beyond membrane tension alone, are responsible for modulating endocytic efficiency during osmotic stress.

Lastly, it is important to consider the osmolarity range used across studies. While most reports document a 60-90% suppression of CME, these effects were typically achieved using severe osmotic stress aimed at functionally ablating CME. Only a few studies, such as Wang et al. (2011),

attempted to model more physiologically relevant stress levels for the cells being studied. This implies that under moderate, non-lethal osmotic shifts, CME impairment is likely partial rather than complete and underscores the importance of dose-dependent and context-specific interpretations of endocytic modulation by osmotic stress.

5.4.2 Effect of oxidative stress on endocytosis

In contrast, our data on oxidative stress showed the opposite pattern: transferrin uptake dropped by 20-25% while bulk protein internalization was more severely reduced by a more substantial 30-35%. This may indicate that non-CME pathways are more significantly affected under oxidative conditions, though further investigation is needed to clarify the mechanisms involved.

Despite the widespread recognition of oxidative stress as a modulator of endocytic trafficking (Thibaut-Vercruyssen et al., 1992; Cavalli et al., 2001; Aguilar-Gaytan & Mas-Oliva, 2003; Cheng & Vieira, 2006; Bi et al., 2017), relatively few studies have specifically focused on the acute effects of *mild* oxidative stress induced by TBH in the range of 50-100 µM over short durations (1-6 h) (Rabin et al., 2012; X. Xu et al., 2016). The majority of available literature instead explores chronic, low-dose TBH exposure, typically 10-50 µM applied over 12-72 h. Furthermore, most of the studies reviewed that had chronic TBH exposure in human RPE cells had the primary aim of mimicking persistent sublethal oxidative insults, such as those observed in degenerative diseases like AMD (Hanus et al., 2013; Zhao et al., 2017; Terluk et al., 2019; Y. Li et al., 2023).

Nonetheless, even brief exposure to oxidative stress appears to have a tangible impact on endocytic function across several human cell types, including astrocytes, endothelial cells, and epithelial-derived lines. Evidence suggests that acute oxidative conditions can transiently impair clathrin-mediated endocytosis (CME), largely by affecting key molecular components such as dynamin and HSC70, both of which are essential for vesicle scission and uncoating, respectively. Moreover, several papers have reported a decrease in the uptake of LDL and TrfR upon oxidative stress treatment (Thibaut-Vercruyssen et al., 1992; Malorni et al., 1993; Aguilar-Gaytan & Mas-Oliva, 2003; Cheng & Vieira, 2006; Parry et al., 2008; Volpert et al., 2017). Specifically, (Volpert et al., 2017) showed that oxidative stress diminished CME efficiency in astrocytes, correlating with impaired recruitment of adaptor proteins and vesicle budding machinery.

Interestingly, the effects of oxidative stress on endocytosis are not restricted to inhibition. In some contexts, oxidative signalling appears to reprogram internalization pathways altogether. A notable example comes from a study by (Khan et al., 2006), in which TBH treatment of human carcinoma cells led to the aberrant phosphorylation EGFR. This post-translational cargo modification altered the internalization route of EGFR from its canonical CME pathway to a clathrin-independent, caveolin-1–mediated mechanism. Using colocalization analyses and plasma membrane-to-perinuclear tracking, the study illustrated how oxidative cues could shift not just the rate, but the *mode* of endocytosis. This may reflect an adaptive strategy wherein cells under oxidative stress reroute specific cargos away from lysosomal degradation, potentially favouring recycling or alternate signalling fates.

It has also been found that broader signalling cascades, like the p38 stress response pathway, is activated by oxidative stress stimuli (Huot et al., 1997; Ushio-Fukai et al., 1998; Volonté et al., 2001).

Such findings underscore the nuanced and cargo-specific regulation of endocytic pathways under oxidative stress. Rather than a uniform downregulation, oxidative stimuli may lead to selective suppression, redirection, or even enhancement of alternative pathways, depending on the stress intensity, duration, and cellular context. Further research using controlled mild acute stress paradigms (especially in physiologically relevant cell types) will be essential to dissect the full landscape of stress-adaptive endocytic plasticity.

5.4.3 Effect of heat stress on endocytosis: an ongoing question

Our results on heat stress demonstrated a comparable reduction in both total and transferrin internalization, although greater variability in transferrin uptake was observed across replicates. This could point to a more integrated or coordinated modulation of endocytic processes, potentially involving shared regulatory components or signalling responses that synchronize CME with general endocytosis. Unfortunately, it remains unclear what exactly could be happening due to the gap in literature regarding mechanisms operating upon acute heat stress exposure. No primary studies were found which directly apply acute (< 2 h) heat shock (42-45 °C) to human cells and quantify CME via transferrin uptake, clathrin dynamics, or pit lifetime. López-Hernández et al., (2020) acknowledge effects of heat shock on endocytosis in general in their review, but also do not report on relevant mechanistic studies.

5.4.4 Compensatory clathrin-independent endocytosis under stress conditions and limitations of our study

CME can be functionally compensated by alternative pathways under certain stress conditions (Sandvig et al., 2018) (Fig.5.1). For instance, cytosolic acidification like the one we find after hyperosmotic stress, has been shown to inhibit CME but to enhance clathrin-independent endocytosis (CIE), suggesting adaptive flexibility in endocytic routing (Damke et al., 1995). Another study reported that inhibition of CME by hyperosmotic treatment led to only around a 50% reduction in ricin uptake, underscoring the significant contribution of Cdc42-dependent, clathrin-independent pathways (Howes et al., 2010).

However, endocytic activity is also highly sensitive to cellular context (Sandvig et al., 2018). Cell density, for example, has long been recognized as a modulator of endocytic efficiency, likely due to associated changes in lipid composition and intracellular trafficking dynamics (Snijder et al., 2009; Kavaliauskiene et al., 2014; Frechin et al., 2015). In polarized cells such as epithelial cells, endocytosis becomes spatially regulated (Fig.5.1). For example, in MDCK cells, clathrin-independent uptake of ricin is differentially controlled at the apical and basolateral membranes via specific kinases and signalling pathways, such as PKA, PKC, and calmodulin, with caveolae localized exclusively to the basolateral domain (Scheiffele et al., 1998; Sandvig & van Deurs, 2005).

Given that our study utilizes the non-transformed, immortalized epithelial cell line RPE-1 as an in vitro model, it is important to acknowledge inherent limitations in replicating the full physiological complexity of polarized tissues. While RPE-1 cells retain many features of native epithelial polarity, including contact inhibition and cilia formation, the absence of three-dimensional architecture and interactions with extracellular matrix or vasculature in standard culture conditions likely constrains the degree of polarization achievable in vitro. As such, the functional implications of polarity-

specific endocytic pathways observed in vivo will likely not be fully recapitulated. Future studies employing 3D organoid models or ex vivo systems will be crucial to validate and extend our findings within a more physiologically relevant context.

Altogether, these considerations underscore that endocytic pathway engagement is not only adaptable to stress or perturbation but is also finely regulated by intrinsic cellular factors such as polarity, signalling architecture, and membrane organization. A complete understanding of endocytic dynamics, therefore, must account for both the biochemical state of the cell and its structural and spatial context.

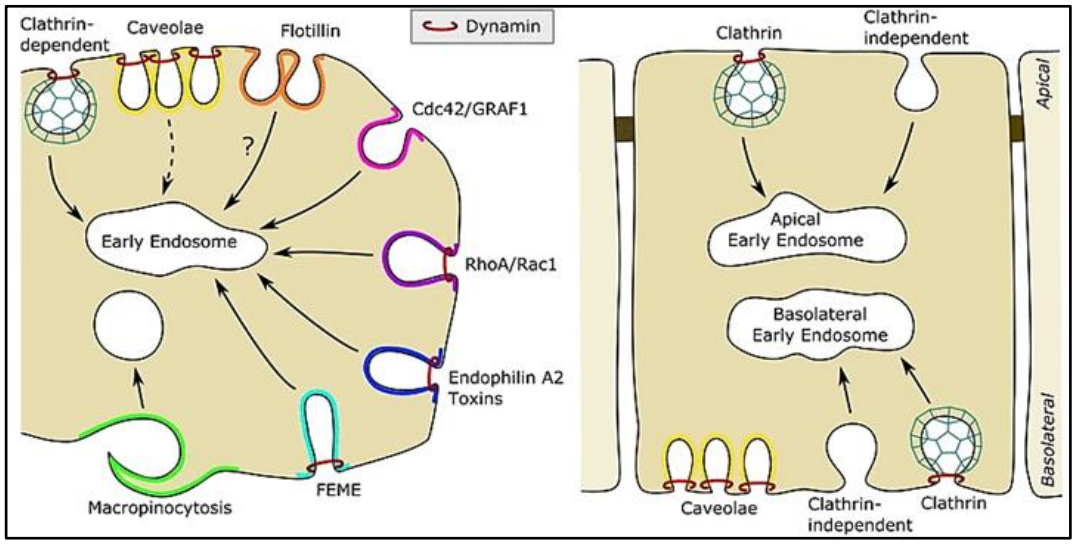

Fig. 5.1: Overview of Endocytic Pathways in Epithelial Cells
There is a diversity of endocytic mechanisms in non-polarized (left) and polarized (right) epithelial cells. In addition to clathrin-mediated endocytosis, several clathrin-independent pathways are depicted, including caveolae-dependent endocytosis, flotillin-associated uptake, Cdc42-dependent but dynamin-independent uptake, Rho/Rac-mediated mechanisms, endophilin-driven tubulation, fast endophilin-mediated endocytosis (FEME), and macropinocytosis. In polarized epithelial cells, clathrin-independent endocytosis at the apical membrane is selectively regulated by signalling pathways, such as those involving protein kinase A, with no corresponding effect on the basolateral side. Notably, caveolae are restricted to the basolateral membrane in MDCK cells. Adapted from (Sandvig et al., 2018).

5.5 Mass spectrometry and candidate search challenges

Since the sensitivity of MS is low for detecting molecules with concentrations below 50 pg/mL, MS analysis of membrane proteins is frequently preceded by an enrichment step (de Jong & Kocer, 2023). Specifically, plasma membrane proteins, regardless of the cell or tissue of origin, have been under-represented in proteomics analysis mainly because of their low abundance, requiring enrichment through subfractionation or isolation not only to reduce the complexity of the sample but also to help overcome the low abundance as they only represent a small fraction of the cell. (Griffin & Schnitzer, 2011).

Although it is established in the literature that the use of plasma membrane isolation systems such as our choice of Sulfo-NHS-SS-biotin, based on live cell labelling plus label-free mass spectrometry provides reproducible, high-specificity plasma membrane proteomics, with the potential of a high protein yield and identification, there are factors to consider when dealing with this method in order to maximize its possibilities of success in the scientific quest.

One important area to consider is **sample preparation**, which represents a critical determinant of data quality in mass spectrometry, particularly in label-free proteomics where both protein identification and inter-sample reproducibility are essential. This challenge becomes especially pronounced when studying plasma membrane proteins, which present several unique biochemical and analytical obstacles.

First, these proteins are embedded in lipid bilayers, making them highly hydrophobic and prone to aggregation upon extraction. Effective solubilization often necessitates the use of strong detergents or chaotropic agents such as SDS or urea, which are typically incompatible with downstream MS analysis and must be removed prior to digestion, which risks protein loss and selective depletion of more hydrophobic species (de Jong & Kocer, 2023).

Second, transmembrane domains frequently lack sufficient lysine and arginine residues, resulting in poor tryptic digestion and limited peptide coverage, further hampering identification (M. Wang et al., 2012).

Another important factor, especially highlighted in a study such as ours, where we could be searching for very small protein differences in populations, is that many membrane proteins are present at already low abundance relative to cytosolic proteins and are particularly susceptible to ion suppression by co-eluting high-abundance peptides (Griffin & Schnitzer, 2011).

Finally, when using whole-cell lysates, these issues are exacerbated by the presence of interfering lipids, residual detergents, and abundant soluble proteins, all of which increase sample complexity and require extensive cleanup or fractionation. These preparatory steps, while necessary, introduce variability and potential sample loss, thereby complicating robust identification and quantification of condition-dependent changes in membrane protein composition (M. Wang et al., 2012).

In addition to the challenges presented when preparing the samples for detection, there is another dimension when it comes to the **correct identification of plasma membrane proteins** from a label-free mass spectrometry hit matrix.

To begin with, plasma membrane proteins are often co-purified with abundant intracellular contaminants (e.g., cytosolic or mitochondrial proteins), even when using subcellular fractionation or surface biotinylation, leading to false positives, i.e. high contamination levels despite enrichment efforts (Garapati et al., 2023).

Furthermore, without clear quantitative thresholds for surface enrichment (especially in label-free studies vulnerable to run-to-run variability and ion suppression) confidence in genuine membrane protein hits remains low (B. Sun & Hood, 2014).

Lastly, but most relevant to mention is the issue of many proteins having multiple localizations (e.g., plasma membrane, endosomes, Golgi, lysosomes), and available databases often listing broad or outdated annotations. This makes it difficult to confidently classify a protein as resident of the "plasma membrane" based on bioinformatic filters alone. For example, a receptor may shuttle between the plasma membrane and intracellular compartments depending on cell state. As a result, annotation databases and predictive algorithms (e.g., UniProt, GO, TMHMM) frequently provide incomplete or conflicting localization data, making it challenging to confirm true plasma membrane localization without orthogonal validation. There are many bioinformatics initiatives and projects undertaking systematic efforts towards correcting the existing annotation and providing a better

algorithm or system for classification (da Cunha et al., 2009; Schiess et al., 2009; Bausch-Fluck et al., 2018; Z. Hu et al., 2021), but this is still underway.

5.5.1 How efficient was our experiment?

Evaluating the efficiency of our surface protein enrichment and the mass spectrometry-based quantification of the surfaceomes is very difficult to do, due to all the challenges listed in the previous section. If we first focus on a possible definition of the "efficiency" of the surfaceome isolation and mass spectrometry-based identification, we come across 3 partly overlapping metrics which try to describe how well a surface-biotin enrichment might have worked:

1) **Purity**: what percentage of the proteins that end up in the enriched fraction are bona fide plasma membrane or plasma membrane-associated proteins?
2) **Coverage (depth)**: how many distinct plasma membrane proteins were actually recovered?
3) **Yield:** how much of the surface-protein mass present on the starting cells was captured? In fact, this is rarely reported because the true denominator is hard to measure.

From the 3, only "purity" and "coverage" are frequently found documented. Some exemplary papers, that employed Sulfo-NHS-SS-biotin in combination with streptavidin/neutravidin beads in the context of a protocol similar to ours, supply the following information regarding their datasets (Hörmann et al., 2016; Niehage et al., 2016; Ito et al., 2020; Langó et al., 2023; Garapati et al., 2023):

- Among the researched papers, Hörmann et al., (2016) was the only study that provided a clear measurement of **purity**, indicating that 54% of the proteins listed had an explicit plasma membrane annotation (347 out of 642). After extensive further computational curation by added interactors and prediction tools analysis, they concluded that around 90% of the proteins in the eluate were plasma membrane-associated. The other studies did not provide a purity percentage, but rather use abstract terms, such as "highly enriched in plasma-membrane proteins".
- Regarding **coverage**, it seems that the protein-level pull-downs analyzed by mass spectrometry typically yield a few hundred confidently assigned plasma membrane proteins (Hörmann et al., 2016; Niehage et al., 2016; Ito et al., 2020). For peptide-level capture workflows (Garapati et al., 2023; Langó et al., 2023) reported a coverage into the 600-1400 protein range on standard Orbitrap systems (representing state-of-the-art for depth).

Given this context, I can now evaluate the efficiency of the isolation and identification of plasma membrane proteins in terms of purity, which is the most intuitive notion for me. For example, taking the full list of hits obtained for osmotically stressed vs control cells (project P0199) I come to the following assessment:

- Total identified hits were 2513.
- After filtering for the GO annotations "plasma membrane" and "cell membrane," as described in section 4.5, 1039 hits remained amounting to 41%.
- After removing any hits that contained also "cytoplasm" as annotation, 827 proteins were left amounting to 32,9%. However, since it has been established that proteins can sometimes have multiple cellular localizations or pivot between places, this exclusion could remove some proteins which are effectively plasma membrane-associated.

In conclusion, 33 to 41% of the total mass spectrometry-based hit list are likely to represent surface proteins. The in silico human surfaceome is predicted to comprise 2886 proteins (Bausch-Fluck) which corresponds to 14.3% of the entire human proteome according to the authors. Therefore, we achieved an enrichment of at least two-fold and covered with 827-1039 presumed plasma membrane proteins 29-36% of the predicted pool of 2886 human surface proteins. The actual coverage might be even higher since not the entire in silico surfaceome will be expressed in an individual cell line. Nevertheless, this coverage still leaves room for improvement, but it was sufficient to identify interesting hits like the CI-M6PR which we were able to validate with our follow-up experiments.

5.6 Challenges in the validation of mass spectrometry-derived candidates

A critical step in proteomic studies is the validation of differentially enriched protein candidates identified through mass spectrometry. However, the success of this step depends heavily on both the sensitivity and specificity of the proteomic approach and the availability of high-quality validation tools, especially antibodies with high specificity and affinity for immunoblotting or immunofluorescence.

In this regard, SILAC, i.e. stable isotope labeling of amino acids in culture, represents a powerful alternative quantitative proteomic strategy. SILAC incorporates isotopically labelled amino acids into proteins during cell growth, enabling direct comparison of “light” and “heavy” peptide pairs within the same MS run. Because the samples are mixed at the protein level before processing, both conditions undergo identical handling, digestion, and chromatographic separation, thereby minimizing technical variability. This approach yields highly precise peptide intensity ratios and it enables the detection of smaller changes in protein abundance with high accuracy and reproducibility. For instance, López-Hernández et al. (2020) employed SILAC to examine the effects of AP-2 deletion and thus endocytosis inhibition on the surfaceome and were able to detect modest fold changes in plasma membrane proteins and thus potentially identify more significant candidate proteins. The higher level of sensitivity allows researchers to capture nuanced alterations that may be masked in less quantitative approaches.

In contrast, LFQ requires separate preparation and analysis of each sample, introducing greater run-to-run variability and lowering sensitivity for subtle changes. As a result, the list of confidently identified candidate proteins in our dataset likely represents those undergoing more robust trafficking or abundance changes at the cell surface under stress conditions, which can be seen as an advantage. In addition, going label-free is more cost-effective and required less time in cell culture for cell-type specific adaptation and incorporation of isotopes.

Another important point to make is that validation efforts are complicated by the limited availability and performance of commercial antibodies, particularly when examining low-abundance proteins in plasma membrane fractions. Even for proteins with clear fold differences in the mass spectrometry data, successful detection via western blotting or immunostaining is highly dependent on antibody affinity, epitope accessibility, and the efficiency of membrane protein recovery. For example, membrane proteins with multiple transmembrane domains or extensive glycosylation may yield weak or inconsistent signals, complicating interpretation.

With all that in mind, from the 18 candidates that were probed for validation (see section 4.6.2.3), only 4 were robustly confirmed and in concordance with the mass spectrometry results in regards to their up- or downregulation in the stressed samples (NHE7, SPPL2A, TrfR and CI-M6PR).

In the following sections, we will take a closer look at the candidates that were successfully validated in our study.

5.6.1 SPPL2A is enriched in the plasma membrane under heat shock: observations and limitations in validation.

The results of the surface biotinylation-labelled mass spectrometry screening pointed out that this protein was highly enriched in the plasma membrane of RPE cells treated with both hyperosmotic and heat stress. It also showed a very high fold enrichment of the stressed cell population vs the controls, of around 14-fold increase for osmotic stress and an even higher 22-fold increase for heat stress.

When we tried to validate through Western blot however, surprisingly we found an enrichment of this protein that amounted to about only twice the enrichment in the plasma membrane of heat stressed RPE-1 cells compared to unstressed controls (see Fig. 4.9 C). Unfortunately, we could only validate it under heat shock conditions, despite also appearing so highly upregulated in our osmotic stress dataset. This discrepancy raises the question of whether the lack of validation under osmotic stress was due to genuine biological differences or technical limitations, particularly considering the sensitivity and performance of the available antibody across different western blot conditions. Notably, reliable detection of SPPL2A via immunoblotting was only achieved toward the later stages of our validation workflow. By that time, our focus had shifted toward characterizing CI-M6PR in more detail, and we opted not to pursue further investigation of SPPL2A due to time constraints.

SPPL2A along with SPPL2B, is a member of a family of intramembrane aspartyl proteases that cleave type II transmembrane protein NTFs (Friedmann et al., 2006). Surprisingly, even though SPPL2B is the protein that generally acts at the plasma membrane and that functions primarily at neutral pH (as opposed to SPPL2A) (Mentrup et al., 2019), this protein variant was not present in our mass spectrometry list.

Regarding the osmotic stress condition, additional experiments are warranted to determine whether SPPL2A´s supposed upregulated during osmotic stress (based on mass spectrometry) can indeed not be confirmed by alternative approaches, since its osmotic stress-induced upregulation would be biologically plausible. SPPL2A is primarily localized to late endosomes and lysosomes (Behnke et al., 2011), and in our study, we observed robust evidence of lysosomal exocytosis under osmotic stress, as discussed later. It would therefore be consistent with this phenomenon for SPPL2A to become transiently enriched at the plasma membrane as part of a broader cellular response involving plasma membrane and/or organelle remodelling.

Recent studies have broadened our understanding of signal peptide peptidase (SPP) and SPP-like (SPPL) intramembrane proteases, revealing that their substrate repertoire includes both tail-anchored (TA) and type II membrane proteins (Mentrup et al., 2024). While SPP was originally identified as the main protease for TA protein cleavage (Boname et al., 2014), subsequent findings more recently demonstrated that SPPL2A and SPPL2B, also mediate similar functions. SPPL3

appears unique in its ability to directly cleave type II proteins with large ectodomains, facilitating their shedding; however, evidence now suggests that SPPL2A can also process larger substrates without prior ectodomain trimming (Spitz et al., 2020), challenging previous assumptions about substrate requirements.

Despite these advances, the full range of physiological substrates for SPP/SPPL proteases remains incompletely characterized, and the biochemical or structural features dictating substrate recognition and cleavage specificity are still poorly understood. Notably, functional overlap exists between SPPL2A and SPPL2B, as exemplified by their cooperative degradation of LOX-1 NTFs, which accumulate in SPPL2A/B double knockout mice (Mentrup et al., 2019). This suggests a broader physiological role for these proteases in modulating receptor-mediated processes such as oxidized LDL uptake in vascular tissues.

Additionally, (Ballin et al., 2023) screened 18 SNARE proteins in cellular protease-substrate co-expression assays and confirmed that vesicle-associated membrane proteins (VAMP1-4), which are responsible for membrane fusion events, have been identified as SPPL2A/B substrates. Given that the majority of SNAREs are TA proteins, this underscores a potential regulatory role for SPPL proteases in intracellular trafficking beyond classical secretion. Other well-characterized substrates include TNFα, Bri2, and Fas ligand, indicating a broader immunomodulatory role (Mentrup et al., 2020; Spitz et al., 2020).

Especially interesting for us is a study by (Zahn et al., 2013). They demonstrated that a differential substrate specificity is also seen for TrfR: SPPL2B primarily cleaves TrfR-NTFs, with some involvement from SPPL2A, as supported by colocalization analyses. It would be a relevant question for us if this limited involvement in the cleavage of TrfR is mostly due to SPPL2A not usually being colocalized with TrfR in the plasma membrane and that in the context we found in our results, where SPPL2A is indeed in a position to cleave TrfR it increases this contribution. It would be worth designing western blot and immunofluorescence experiments with proper controls that could follow-up and answer if this is the case. If so, would this cleavage impact CME in a significant way?

Finally, our validation of SPPL2A upregulation during heat shock adds a layer of complexity. To our knowledge, lysosomal exocytosis has not been reported as a major feature of the heat shock response. Thus, the appearance of SPPL2A at the plasma membrane under heat shock might suggest that this form of stress could also trigger lysosomal fusion events, or that SPPL2A might be regulated by alternative trafficking or membrane remodelling mechanisms unrelated to classical lysosomal exocytosis. These hypotheses remain speculative but highlight the need for further experimental work, such as colocalization studies or functional assays, to determine the stress-specific regulation and trafficking routes of SPPL2A.

5.6.2 NHE7 accumulates at the plasma membrane under osmotic stress

NHE7 was initially introduced in this study in the context of prior findings by López-Hernández et al. (2020), who demonstrated its redistribution to the plasma membrane in primary mouse astrocytes exposed to hyperosmotic stress (600 mOsm/kg). In that system, NHE7 played a protective role by counteracting cytosolic acidification and promoting autophagy, aiding in the clearance of stress-induced protein aggregates. These observations highlighted the potential of NHE7 as a crucial

element of the cellular adaptive response to osmotic imbalance. Consistent with this, our surfaceome mass spectrometry analysis identified NHE7 as significantly enriched at the plasma membrane in RPE-1 cells subjected to both hyperosmotic and heat stress. Although NHE7 was not detected in our whole-cell lysate proteome, limiting conclusions about baseline expression levels, its robust appearance in the surface-specific dataset supported the biological relevance of its surface redistribution.

Importantly, the presence of NHE7 in both the surfaceome proteomics and follow-up Western blot experiments provided strong orthogonal validation of our findings. This was further substantiated by complementary immunofluorescence microscopy, which visually confirmed the stress-induced membrane redistribution of NHE7. Collectively, our data not only reinforce the role of NHE7 under osmotic stress but also extend the previous observations in astrocytes to a different mammalian cell type: RPE-1 cells. Moreover, by systematically testing multiple stressors, we show that NHE7 redistribution is highly specific to osmotic stress, rather than a general feature of all cellular stress conditions (Fig. 4.10 A-D). These findings underscore the specificity and reproducibility of our proteomic approach and point to NHE7 as a potential conserved component of the osmotic stress response across cell types.

5.6.3 TrfR also accumulates in RPE-1 cells at the surface under osmotic stress

Transferrin receptor is a well-characterized cargo of CME and mediates iron uptake. Its surface levels are tightly regulated through rapid cycles of endocytosis and recycling (Mayle et al., 2012).

In our study, we observed a marked upregulation of plasma membrane-localized TrfR in response to an acute exposure to osmotic stress. Specifically, exposure to hyperosmotic conditions (750 mOsm) for 1 h resulted in a 125-200% increase in TfR levels at the plasma membrane compared to unstressed controls (Fig. 4.11 E).

Although no statistical evaluation was possible due to the low number of biological replicates, our preliminary data also suggested that this upregulation begins as early as 15 min post-treatment, albeit at lower magnitude than observed at 1 h, and was visible across different osmolytes, including mannitol, sorbitol, and NaCl (Fig. 4.13 and 4.15). These findings are consistent with prior studies reporting that hyperosmotic stress impairs CME efficiency, leading to a temporary accumulation of endocytic cargo at the plasma membrane (Hansen, 1993; X. Wu et al., 2001; S. Wang et al., 2011).

The observed accumulation of TrfR likely reflects a stress-induced disruption of endocytic flux, whereby clathrin-coated pit formation and/or vesicle scission is impaired, leading to delayed internalization of surface proteins. This interpretation is further supported by our complementary findings that confirm a reduction in transferrin uptake under the same osmotic stress conditions, indicative of defective CME. These data align with earlier work showing that osmotic stress can immobilize clathrin lattices and inhibit transferrin internalization, an effect that is rapidly reversible upon return to isotonic conditions (Heuser & Anderson, 1989; Wang et al., 2011).

In summary, TrfR surface accumulation serves as both a readout and functional consequence of impaired CME during osmotic stress, and our results underscore the utility of this receptor as a sensitive marker for tracking changes in endocytic flux under perturbed physiological conditions. It is not out of the realm of possibility that this accumulation could be the result of an early molecular regulation mechanism that concludes in abortive CCPs, This could be at the level of modulation of

EAPs; major coat proteins like clathrin heavy or light chain, AP2 or Dynamin 2 could be targeted by post-translational modifications such as phosphorylation (e.g. mediated by c-Src kinase hierarchy hub) or there could be interference at the level of scaffolding proteins such as FCHo ½ (see table 1.1 and Fig.1.6) but at these level these are purely speculations.

5.6.4 CI-M6PR surface enrichment under osmotic stress

Following its identification as a top hit in our mass spectrometry screen, we validated the stress-induced enrichment of CI-M6PR at the plasma membrane through surface biotinylation followed by immunoblotting assays.

Remarkably, while both osmotic and heat stress triggered increased surface levels of CI-M6PR, the magnitude of this enrichment varied substantially between the two conditions. Under unstressed physiological conditions, it has been reported that around 10% of this receptor is found at the plasma membrane (Klumperman et al., 1993), which seems to coincide with how little signal we are able to pick up by Western blot on unstressed membrane fractions (Figs 4.11, 4.13, 4.14 and 4.15). Treatment with hyperosmotic stress led to a dramatic 6- to 15-fold increase in CI-M6PR surface abundance compared to unstressed controls (Figs 4.11, 4.13, 4.14 and 4.15), whereas heat shock resulted in a more modest 1.5- to 3-fold increase (Fig. 4.11).

We continued to explore the characterization of this phenomenon, as described below.

5.7 CI-M6PR redistribution to the plasma membrane under hyperosmotic stress is time and dose-dependent.

To assess how generalizable and dynamic the CI-M6PR enrichment at the plasma membrane under hyperosmotic conditions is, we systematically examined how different osmolytes, exposure durations, and osmolarity thresholds influence its localization.

Initially, mannitol was employed as the primary osmolyte to elevate extracellular osmolarity in our assays. However, to determine whether the observed dramatic CI-M6PR surface accumulation was a specific effect of this compound or reflected a broader cellular adaptation to osmotic imbalance, we expanded our experimental design to include other commonly used osmolytes. When the medium osmolarity was adjusted to 750 mOsm/kg with either NaCl or sorbitol, we again detected a clear enrichment of CI-M6PR at the plasma membrane via surface biotinylation (Fig. 4.15 A-D). These findings demonstrate that the effect is not limited to a specific osmolyte and instead appears to represent a conserved response mechanism to hyperosmotic stress, independent of the chemical nature of the osmolyte used.

We next addressed the temporal dynamics of this enrichment. Using mannitol-induced stress, CI-M6PR surface levels were measured at four early time points: 15, 30, 45, and 60 min post-stress induction (Fig. 4.13). Notably, an increase in surface-localized CI-M6PR was already evident as early as 15 minutes, with the enrichment persisting across all subsequent time points. This suggests a rapid and sustained redistribution of CI-M6PR to the plasma membrane following osmotic challenge.

Kinetics experiments on CI-M6PR conducted on HEp-2 cells (Hirst et al., 1998) demonstrated that CI-M6PR undergoes rapid early trafficking following biosynthesis. Upon release from the Golgi, a

substantial fraction of newly synthesized CI-M6PR destined to the plasma membrane is detectable within MVBs as early as 5 min at 37°C, reaching peak accumulation by 10 min and remaining as a narrow temporal pulse. In a previous study by the same lab, they observed a similar route and kinetics for pulses of newly synthesized TrfR before appearing at the plasma membrane (Futter et al., 1995). Hirst et al., (1998) also reported that the residence time of CI-M6PR within MVBs appears to be under 15 min, indicating swift progression through this compartment. Furthermore, other studies found that the complete recycling circuit, including return to the TGN, exceeds 1 h (Duncan & Kornfeld, 1988; Goda & Pfeffer, 1988). At steady state, most CI-M6PR resides in the TGN or in transit between the MVB and TGN, suggesting that observed peripheral CI-M6PR-positive structures likely represent recycling intermediates and that this receptor could traffic through the plasma membrane. Notably, variations in steady-state distribution across cell types may reflect cell-specific differences in trafficking kinetics through compartments such as the TGN (Griffiths et al., 1988; Kornfeld & Mellman, 1989; Griffiths et al., 1990), but this is a good starting point.

Based on this timeframe, our data seems to fit with the idea that newly synthetized CI-M6PR could have been transported to the plasma membrane maybe even earlier than the 15 min that was our earliest timepoint. It also seems plausible that the defect in CME that contributed to their surface enrichment started early too, at least as early if not earlier than those 15 min, and therefore CI-M6PR recycling circuit was interrupted. Unfortunately, there are no studies at present that looked at the influence of hyperosmotic stress at either the kinetics or the influence that this stressor could have on the molecular machinery behind a possible CME dysregulation.

Since we have chosen a rather high mannitol concentration for our screen that might not be encountered often under physiological conditions, we were also very interested on whether or not the effect was also visible under lower osmolarities. For this we tested the threshold osmolarity required to trigger CI-M6PR translocation. A concentration series was performed using increasing osmolarities (400, 500, 600, and 750 mOsm/kg), with isotonic medium (295-300 mOsm/kg) serving as a control (Fig. 4.14). Even the lowest level of hyperosmotic stress (400 mOsm/kg) was sufficient to induce detectable CI-M6PR accumulation at the membrane, though the extent of enrichment scaled up with increasing osmolarity. These results indicate a graded cellular response, where the degree of osmotic stress modulates the extent of membrane remodelling, and are also in line with the studies that show that effects of endocytosis impairment increase with higher osmotic stress (J. E. Heuser & Anderson, 1989; López-Hernández, Haucke, et al., 2020; Abouelezz & Almeida-Souza, 2022).

Together, these findings emphasize that CI-M6PR surface enrichment under osmotic stress is a robust and rapid phenomenon, not restricted to mannitol, and can be triggered even by moderate osmolarity shifts. The data point to an early and scalable response mechanism, possibly linked to adaptive membrane remodelling processes, which warrants further investigation into its physiological relevance and underlying trafficking pathways.

5.8 CI-M6PR redistribution: differential contributions of endocytosis and exocytosis

One of the main objectives of this study was to identify surface proteins whose abundance is dynamically modulated by endocytosis during cellular stress. To assess whether CME directly contributes to the plasma membrane enrichment of CI-M6PR, we performed an antibody-feeding assay under control, heat, and hyperosmotic conditions. After 15 min of internalization at 37 °C, CI-M6PR endocytosis was reduced by ~25–30% for both stressors (Fig. 4.17)., providing clear evidence that impaired CME is involved in the observed fold changes in surface levels.

Since CI-M6PR internalization is known to rely on cytoplasmic endocytic motifs such as YSKV and dileucine (LL) sequences (P. Ghosh et al., 2003; Simonetti et al., 2017), we tested whether these motifs alone were sufficient to reproduce the stress-induced redistribution. For this, we overexpressed an EGFP-tagged CI-M6PR chimeric protein containing only the transmembrane region and cytoplasmic tail in RPE-1 cells and monitored its localization relative to TGN46 (Fig. 4.18). Under unstressed conditions, the chimera co-localized strongly with the TGN, consistent with previous reports (Waguri et al., 2003; Lin et al., 2004). Hyperosmotic stress caused partial redistribution to vesicular structures and the plasma membrane, reflected in reduced TGN co-localization (lower Pearson's coefficient). These results indicate that determinants within the short cytoplasmic tail are sufficient for the observed redistribution and that blocking CME can mimic this effect.

We have previously discussed how hyperosmotic stress lowers plasma membrane tension, increases molecular crowding, and acidifies the cytosol and that this condition is known to suppress CME. Such changes could disrupt the recruitment of EAPs, alter post-translational modifications of CME determinants within the CI-M6PR tail or provoke unknown mechanisms unrelated with endocytosis. To determine the extent to which CME blockade alone accounts for surface accumulation of CI-M6PR, we inhibited CME entirely with Pitstop, to simulate the maximum contribution CME could have under the strongest CME impairment (no CME). After 1 h of Pitstop, CI-M6PR surface levels rose only ~1.5-2-fold, similar to the effect of heat shock (Fig. 4.16). This suggests that defective CME alone, assuming effective inhibition, is sufficient to explain the modest accumulation observed under heat stress but cannot account for the much stronger enrichment induced by hyperosmotic stress. The latter likely involves additional trafficking mechanisms.

Indeed, our experiments confirmed that hyperosmotic stress impairs CME, albeit rather mildly with the chosen stress conditions in RPE-1 cells, consistent with literature describing transferrin uptake inhibition under similar conditions, and we further demonstrated that it also induces lysosomal exocytosis. Given the physiological localization of CI-M6PR in late endosomes and the trans-Golgi network, its delivery to the plasma membrane through lysosome-plasma membrane fusion events provides an explanation for the enhanced accumulation under osmotic stress.

Interestingly, this mechanistic balance contrasts with findings for NHE7 in primary astrocytes (López-Hernández et al., 2020), where CME contributed more substantially to surface enrichment than osmotic stress-specific effects. In our system, the contribution appears inverted, with osmotic stress-driven mechanisms, particularly lysosomal exocytosis, accounting for the majority of CI-M6PR accumulation.

Collectively, these results support a model in which CI-M6PR surface enrichment arises from stressor-specific pathways: a combination of impaired internalization and lysosomal exocytosis under hyperosmotic conditions, versus primarily reduced endocytosis under heat shock. This divergence highlights the mechanistic complexity of plasma membrane remodelling during environmental stress and positions CI-M6PR as a sensitive marker for trafficking shifts in RPE cells.

5.8.1 Lysosomal exocytosis: TRPML1 and TFEB as coordinators of the stress response

Lysosomal exocytosis, traditionally viewed as a degradative process, has emerged as a critical cytoprotective mechanism enabling the rapid expulsion of damaged organelles, toxic metabolites, and cytoplasmic components (Buratta et al., 2020; Tancini et al., 2020). This process relies heavily on precise calcium signalling, with the lysosomal Ca^{2+} channel TRPML1 playing a central role. TRPML1 releases luminal Ca^{2+} to trigger SNARE-dependent fusion of lysosomes with the plasma membrane and contributes to lysosomal trafficking and positioning (W. Wang et al., 2015; X. Li et al., 2016; Trojani et al., 2024). Importantly, TRPML1 can be activated directly by oxidative stress (X. Zhang et al., 2016) or through pharmacological agonists such as ML-SA1, both of which enhance lysosomal exocytosis (Feng et al., 2014; Somogyi et al., 2023).

The functional output of TRPML1 activation, however, appears to depend on the intensity of the oxidative challenge. Ravi et al. (2016) reported that 1 h of low-to-moderate levels of oxidative stress (10-100 µM TBH) stimulate lysosomal exocytosis, whereas higher oxidative loads (>200 µM TBH) inhibit it. Mechanistically, TRPML1-driven Ca^{2+} efflux facilitates VAMP7-mediated lysosome-plasma membrane fusion events, while extracellular Ca^{2+} influx further supports the process: removal of extracellular Ca^{2+} markedly reduces basal exocytosis, whereas its elevation enhances basal rates by ~40% (Peña et al., 2015; Ravi et al., 2016). Thus, lysosomal exocytosis activation by mild oxidative stress depends primarily on TRPML1, whereas inhibition under severe oxidative stress likely reflects impaired plasma membrane Ca^{2+} entry.

The mechanistic scope of TRPML1 may extend beyond lysosomal Ca^{2+} release. Kilpatrick et al. (2016) demonstrated that TRPML1, despite its predominant lysosomal localization, supports both Ca^{2+} release and entry, possibly through cross-talk with ER Ca^{2+} channels. This raises the intriguing possibility that TRPML1 acts as a hub coordinating calcium flux between multiple organelles to regulate lysosomal exocytosis and related trafficking events, which is a connection that remains underexplored.

Calcium signalling is also tightly linked to the transcriptional regulation of lysosomal function via TFEB, a master regulator of lysosomal biogenesis and autophagy. Under stress conditions such as hypertonicity, intracellular Ca^{2+} changes can activate the Ca^{2+}/calmodulin-dependent phosphatase calcineurin, which in turn dephosphorylates TFEB, promoting its nuclear translocation (Cheung & Cousin, 2013). Once in the nucleus, TFEB binds to Coordinated Lysosomal Expression And Regulation (CLEAR) elements, driving the transcription of lysosomal and autophagy-related genes (Sardiello et al., 2009). TFEB activation has been shown not only to induce autophagy, but also to enhance lysosomal proteolysis likely via increased phosphatidylinositol-3,5-bisphosphate synthesis under hyperosmotic stress, and to directly regulate lysosomal exocytosis (Medina et al., 2011; Nunes et al., 2013; Xiao et al., 2014; Hasegawa et al., 2017; López-Hernández, Puchkov, et al., 2020; Tan et al., 2022).

Notably, TFEB promotes lysosomal exocytosis not only by increasing lysosome biogenesis but also by enhancing their positioning and proximity to the plasma membrane. It does so partly through transcriptional upregulation of TRPML1, which triggers Ca^{2+} release required for VAMP7-mediated fusion events. In addition, TFEB regulates lysosomal positioning via the TMEM55B/JIP4 pathway, which coordinates lysosome movement in response to stress conditions (Willett et al., 2017). This dynamic repositioning of lysosomes may be essential for efficient exocytosis and for tuning the degradative versus secretory roles of lysosomes under different stress contexts.

Given the results of our experiments and as we preciously discussed, we know that exocytosis is the biggest contributor towards the plasma membrane accumulation of CI-M6PR and other lysosomal proteins we found on our surfaceome screening. Independent of how it came to be accumulated in the membrane, we also found a predominant presence of NHE7 in plasma membrane of osmotically stressed cells that we validated. Summarizing (López-Hernández, Puchkov, et al., 2020), the elevated presence of NHE7 in the membrane carried out a series of changes, some of which is the increase of intracellular Ca^{2+} through the action of the NCX1 $Na^{+/}$ Ca^{2+} exchanger, the activation of Calcineurin, which in turn activated TFEB, promoting autophagy gene expression, all of this in response to hyperosmotic conditions. This fits with our model that proposes that an increase in the influx of Ca^{2+} (promoted by elevated NHE7 and other contributors) spikes the activation of Calcineurin and TFEB, affecting the localization of lysosomes, expression of lysosomal biogenesis genes and finally lysosomal exocytosis that we see as a result. Due to many touching points in the circuit, there could be a positive amplification, that would give wave to more than one lysosomal exocytosis event.

Now, since we do not have more timepoints beyond 1 h that confers what happens with the levels of the proteins at the membrane, or confirmation experiments that directly test the role of TFEB in this specific RPE-1 context, all of this remain suppositions. Also, give the huge central hub that TFEB represents, taking part in so many molecular cascades, we also know that not one universal mechanism is enough to activated it and effect through it in all mammalian cells (Tan et al., 2022). More experiments are needed to elucidate and confirm these suspicions and further complete the picture.

One final point worth mentioning is the current impossibility to quantify the extent of the contribution of lysosomal exocytosis to the fold-change in the accumulation of the proteins we see in the membrane, e.g. CI-M6PR. Although our experiment with TRPML1 inhibitor seemed to show a large variation comparing to the osmotic stress-provoked enrichment, the counter experiment with this channel agonist was less clear. Unfortunately, due to time constraints towards the end of the thesis, there was an impossibility to test and determine the correct dosage for the agonist to function in our RPE-1 model. It could be that the concentration we chose was not appropriate, or that another agonist could have been more potent in stimulating TRPML1 for example in a study where the experimenters found that ML-SA1 was weaker in their stimulus than ML-SA3 and so opted for the later when studying the effect of starvation (W. Wang et al., 2015). Furthermore, unfortunately, we lacked positive controls that would tell us what the effective inhibition and stimulation effect would be in our cells, so we were blind to this comparison.

Taken together, our findings would fit into a complex, multilayered regulatory network in which TRPML1 and TFEB act as key nodes linking calcium dynamics, lysosomal positioning, and stress adaptation. While much is known about their individual roles, significant gaps remain in

understanding how TRPML1-TFEB cross-talk is coordinated in our cell model, to what extent the effect of lysosomal exocytosis contribute to our mechanism and results, and how relevant it is overall for the survival of our cells in this context. Addressing these questions could clarify how cells fine-tune lysosomal exocytosis to balance degradation, repair, and signalling under environmental and physiological challenges.

5.8.2 Stress-induced perturbations in membrane trafficking: CME-dependent mechanisms that could be driving CI-M6PR surface enrichment.

Our findings add to a growing body of evidence that stress-induced alterations in membrane trafficking can lead to selective enrichment of certain proteins at the cell surface. A relevant precedent comes from NHE7, which was reported to accumulate at the plasma membrane under hyperosmotic stress in astrocytes due to defective endocytosis (López-Hernández et al., 2020), although the exact molecular basis of this defect remains unknown.

In summary, in our system, CI-M6PR displayed a similar pattern of surface accumulation. This accumulation began rapidly, already increasing within 15 min of osmotic stress and persisting for at least 1 h. Under heat stress, the magnitude of accumulation after 1 h could be explained entirely by the degree of clathrin-mediated endocytosis (CME) impairment measured in our antibody feeding assay (~25–30% reduction), further cemented by blocking of CME through Pitstop, which after 1 h provoked a CI-M6PR surface levels rise of ~1.5-2-fold. In contrast, osmotic stress–induced accumulation was only partially accounted for by CME inhibition, but what exactly could be happening here?

While it is widely recognized that M6PRs cycle between the TGN, endosomes, and the plasma membrane, the exact pathways, especially those mediating their return to the TGN, remain unresolved. Some evidence indicates that MPRs may travel from early endosomes to the TGN, potentially via recycling endosomes, whereas other studies propose a route through late endosomes before reaching the TGN (Díaz & Pfeffer, 1998; Hirst et al., 1998; Anitei & Hoflack, 2012). This localization pattern implies that the receptor could naturally cycle through the plasma membrane during its trafficking itinerary. The sustained presence of CI-M6PR at the cell surface during osmotic stress, suggests that despite ongoing delivery, there is a defect early in the CME pathway, potentially at the stage of clathrin-coated pit formation or prior to vesicle fission. Mechanistically, this could result from post-translational modifications of early endocytic machinery components such as AP-2, which directly binds CI-M6PR via YSKV and dileucine motifs (P. Ghosh et al., 2003), or dynamin-2 (Liberali et al., 2008), or alternatively from modifications to the receptor itself that impair its recognition by the endocytic coat.

Support for this last hypothesis comes from large-scale RNAi screens. Anitei et al. (2014) identified 127 kinases and phosphatases influencing M6PR trafficking or the organization of its associated compartments. Of these, 47 were previously shown to affect CME (Collinet et al., 2010), and knockdown of 11 caused CI-M6PR surface accumulation (Sup. Table 20). Notably, silencing of ERBB2 (part of several cell surface receptor complexes) altered the AP-2-positive compartment, making it a potential candidate for mediating stress-dependent changes in CI-M6PR internalization. ERBB2 is known to regulate the outgrowth and stabilization of peripheral microtubules (Zaoui et al., 2010), raising the possibility that osmotic stress may influence CI-M6PR trafficking indirectly through cytoskeletal remodelling.

The precise molecular mechanisms by which hyperosmotic stress perturbs CI-M6PR endocytosis remain unresolved. Given the parallels with NHE7 accumulation, it is conceivable that osmotic stress triggers a coordinated modulation of multiple membrane proteins through combined effects on endocytic retrieval and exocytic delivery.

5.8.3 Interplay between lysosomal exocytosis and endocytosis: a paradigm shift?

Until now, we have emphasized the role that Ca^{2+} signalling has for lysosomal exocytosis, but it is not limited to this context. In parallel, both CME and CIE pathways can be stimulated by elevated cytosolic Ca^{2+} levels, as demonstrated in pancreatic β-cells, likely reflecting the intimate coupling between exocytosis and endocytosis (Doherty & McMahon, 2008, 2009). Interestingly, the CIE route described in this context is actin- and dynamin-dependent and requires higher Ca^{2+} concentrations than CME, reminiscent of fast, CIE observed at synapses (Jockusch et al., 2005). In these systems, CME appears to mediate slower vesicle retrieval, contributing to the maintenance of synaptic surface area, whereas faster CIE serves more immediate needs.

Lysosomal exocytosis represents just one of several membrane trafficking events initiated during cell injury and repair. In some systems, rapid endocytosis has been observed within seconds of plasma membrane damage, such as that induced by streptolysin-O pore formation, and this repair-associated uptake occurs only in the presence of extracellular Ca^{2+} (Idone, Tam, Goss, et al., 2008). Such rapid endocytic events contribute to membrane resealing by removing lesions, thereby protecting cells from mechanical stress, microbial toxins, and pore-forming proteins produced by the immune system (B. P. Morgan, 1989; Togo et al., 1999; Idone, Tam, & Andrews, 2008). Accumulating evidence supports a coordinated sequence in which lysosomal exocytosis is rapidly followed by endocytosis as part of a damage-control and recovery program (Krause et al., 1994; Togo et al., 1999; Miyake et al., 2001; Cocucci et al., 2004; Idone, Tam, Goss, et al., 2008). However, the temporal order, molecular cross-talk, and regulatory triggers of this sequence are still not well defined. It is known that injury-induced Ca^{2+} influx can trigger exocytosis by activating Ca^{2+} membrane sensors, with Syt VII being a prime candidate in mammals (Reddy et al., 2001). Ubiquitously expressed, Syt VII regulates lysosomal and other calcium-dependent vesicle exocytosis (Chakrabarti et al., 2003) while also coordinating their subsequent endocytosis through recruitment of protein complexes (Dasgupta & Kelly, 2003; Jarousse et al., 2003), thereby coupling membrane repair and vesicle recycling. However, live-cell imaging approaches, particularly simultaneous visualization of exocytic and endocytic events using TIRF microscopy, could provide more insights into their spatial and temporal relationship.

Interestingly, no studies to date have examined how this dual mechanism operates under hyperosmotic stress. It remains possible that such a stressor might disrupt or delay the endocytic phase, postponing membrane retrieval until the cell has engaged other osmoadaptive programs to mitigate the immediate consequences of the osmotic challenge.

Our findings on CI-M6PR surface accumulation under osmotic stress raise the intriguing possibility that this receptor could serve as a readout, or maybe even a participant, of an altered exo-endocytic balance in stressed cells. In a canonical repair context, lysosomal exocytosis delivers membrane to the cell surface and is quickly followed by compensatory endocytosis to restore surface area and internalize damaged components. Under hyperosmotic conditions, however, the endocytic arm of this cycle may be selectively impaired or postponed, allowing surface-resident proteins such as CI-

M6PR to persist for extended periods. Mechanistically, this could arise from osmotic stress-induced modulation of early CME components (e.g., AP-2, dynamin-2) or altered actin dynamics, both of which are sensitive to ionic and osmotic changes. Simultaneously, lysosomal exocytosis might be actively promoted as part of the osmoadaptive response, potentially facilitated by Ca^{2+} influx via channels like TRPML1 or indirectly through pH-sensitive transporters such as NHE7, thereby increasing CI-M6PR delivery to the surface. The combination of elevated exocytic input and reduced endocytic retrieval would be expected to yield the sustained surface enrichment we observed. If this model is correct, osmotic stress is not merely stalling endocytosis but actively shifting the balance of membrane trafficking in favour of surface accumulation, possibly to meet uncharacterized adaptive needs, such as altered signalling, cargo sorting, or transient remodelling of the cell-environment interface.

The specific functional contributions of these parallel pathways remain an active area of investigation, particularly in light of the central role that the exo-endocytic cycle plays in health and disease (Aridor & Hannan, 2000, 2002).

5.9 IGF2R function of CI-M6PR: still unresolved

Most of the current literature state that CI-M6PR is currently regarded as a tumour suppressor gene (Hébert, 2006), since it regulates uptake of IGF-II, lysosomal enzymes, glycosylated LIF, and granzyme B (which regulates cytotoxic T cell-induced apoptosis) as well as control of TGF- β activation, all processes that require careful control to prevent carcinogenesis. Furthermore, many studies that utilize siRNA or antisense knockdown of IGF2, IGF1R, or IR-A in cancer cells consistently seem to inhibit proliferation whilst many studies with overexpression of IGF2 or IR-A seem to enhance it (Cullen et al., 1992; Ellis et al., 1996; Vella et al., 2002; Brierley et al., 2010; Ji et al., 2024), coupled with some mutational analyses that confirm that CI-M6PR binding is the key function mediating this effect (Ellis et al., 1996; Schaffer et al., 2003). A point mutation in domain 11 at residue 1572 (Thr to Ile) was reported to completely abolish IGF-II binding (Linnell et al., 2001).

Still, occasional studies seem to find an opposite effect (Takeda et al., 2019), so perhaps there are some exceptions given specific cell type or conditions. There seems to be very few studies that focus on RPE-1 cells and that also involve the effects of IGF-II in the same proliferation context. (Kaven et al., 2000) was the only study found that compares proliferative effects on multiple individual growth factors on human RPE cells, however, they did not include IGF-II or use neutralizing antibodies/inhibitors.

Given the well-documented role of CI-M6PR as an IGF-II binding receptor, we tested whether its stress-induced accumulation at the plasma membrane might have a role in proliferation through IGF-II–dependent mechanisms. Studies suggests that IGF2R/CI-M6PR, although lacking intrinsic kinase activity, can modulate mitogenic signalling indirectly by sequestering IGF-II and thereby regulating IGF1R activation (Brown et al., 2009; Kerr & Baxter, 2022). Based on our observation that CI-M6PR depletion aggravated the proliferation defect under osmotic stress, we hypothesized a proliferative role for surface-resident CI-M6PR in RPE-1 cells.

To evaluate this, we first blocked IGF-II binding with a neutralizing antibody, and in a separate approach, supplemented cells with recombinant IGF-II, both in the presence and absence of CI-

M6PR knockdown. Contrary to expectations, neutralizing IGF-II binding had no inhibitory effect on proliferation, even under hyperosmotic stress where we assumed CI-M6PR surface levels were elevated.

Similarly, exogenous IGF-II (100 ng/ml) failed to enhance proliferation in either control or CI-M6PR-depleted cells, whether stressed or unstressed. These findings indicate that in RPE-1 cells, CI-M6PR does not exert a measurable pro-proliferative effect via IGF-II binding, and that IGF-II itself is not a major driver of proliferation under our experimental conditions. While experimental caveats—such as unknown endogenous IGF-II levels and potential antibody side effects—cannot be excluded, the lack of any consistent proliferative response strongly argues against an IGF-II–dependent function for CI-M6PR in this context.

The results of the IGF2R neutralizing antibody and the IGF-II treatment were inconclusive at best. The **reliability of our experiments** was lacking in many ways, in part because of the following **caveats**:

- We did not have any positive controls: we could not know if our neutralizing antibodies or our IGFII protein was causing the blocking effect or stimulation that we were expecting, e.g. we needed to add a control that we knew would definitely show enhanced proliferation.
- Although we had the assumption that CI-M6PR was enriched in the plasma membrane of osmotically stressed cells, we only had information about the enrichment of this molecule short-term (1 h); we did not really know the levels of CI-M6PR on the plasma membrane after 24 hours of stress, since we never measured it. This information is important to determine how much saturation our treatments would cause.
- Since IGF-II primarily promotes proliferation via IGF1R (Denley et al., 2003), and our experiments did not inhibit or control for potential compensatory or opposing effects mediated by this receptor, we cannot exclude the possibility that IGF1R activity masked any contribution from CI-M6PR.
- Under the physiological pH of the cell surface (pH 7.4), CI-M6PR is capable of binding a wide range of ligands, including TGF-β, granzyme B, retinoic acid, glycosylated leukemia inhibitory factor (LIF), and IGF-II, among others (Brown et al., 2009). We did not assess the basal levels of these potential ligands, including endogenous IGF-II, in our culture medium prior to experimentation. The presence of one or more of these ligands could have influenced proliferation outcomes, either by engaging CI-M6PR directly or by competing for receptor occupancy, thereby modulating the availability of IGF-II for IGF1R binding. Such interactions could potentially mask or confound the detection of any proliferation-specific effects attributable to CI-M6PR under our experimental conditions.

As an important point to remark, the analysis of such type of experiments seem to be further complicated by reports of autocrine and paracrine growth loops involving CI-M6PR, validated in multiple tumour types (Pacher et al., 2007; Steller et al., 1995; Vella et al., 2002, 2019).

Some **improvements** to our experiment that would help clarify the potential role of CI-M6PR in modulating proliferation through its interaction with IGF-II would be:

- To add positive controls to know the extent of the effect we want to see,
- To apply additional strategies to help disentangle the contribution of IGF1R-mediated signalling from that of CI-M6PR. Since our initial approach using neutralizing antibodies

and IGF-II supplementation provided little insight, a more targeted and mechanistically informative setup would involve first to determine if IGF1R is expressed in our cells and to what extent. However, if it is not expressed, that could be a reasonable explanation for the lack of effect of IGF-II. If we confirm the expression of this receptor, we would need to include an IGF1R-specific inhibitor as a control. This would allow us to determine whether observed effects on proliferation are indeed mediated through IGF1R or are independent and potentially attributable to CI-M6PR.

- To titrate recombinant IGF-II in combination with increasing concentrations of neutralizing antibodies against IGF2R. If a dose-dependent increase in proliferation is observed upon antibody treatment, it would support the notion that CI-M6PR normally acts to sequester IGF-II and suppress mitogenic signalling. Conversely, if proliferation remains unchanged or decreases, it will argue against a significant inhibitory role of CI-M6PR in this context.
- To measure the basal levels of other ligands, such as retinoic acid, which could have a confounding effect on the rates of proliferation of the cells.

As a complementary experiment, it could be interesting to generate specific CI-M6PR mutants to dissect its IGF-II-binding function. For instance, constructs encoding a) full-length wild-type CI-M6PR, b) a mutant with a point mutation or deletion in repeat 11 (the domain responsible for IGF-II binding), and c) a soluble form containing only the IGF-II-binding domain could be employed. These constructs could be introduced into cells where endogenous CI-M6PR has been silenced using siRNA or CRISPR-Cas9, thereby allowing for controlled "rescue" experiments. By comparing proliferation rates across these conditions, the specific contribution of the IGF-II-binding function of CI-M6PR could be assessed with minimal confounding from endogenous protein, providing a clearer interpretation of its role in regulating proliferation.

5.10 Potential functional implications of CI-M6PR surface enrichment in hyperosmotic stress adaptation: far from a complete answer

The marked accumulation of CI-M6PR at the plasma membrane during osmotic stress raises important questions about its physiological consequences. At first glance, such enrichment might be interpreted as a passive readout of disrupted CME or increased lysosomal exocytosis, with no direct functional impact on the cell. In this scenario, the receptor would simply serve as a passive marker of stalled endocytosis or enhanced lysosomal exocytosis, without directly influencing cellular function. However, this explanation appears incomplete in light of our data, which show stressor-specific contributions from both CME inhibition and lysosomal exocytosis, and a persistence of surface enrichment long after the initial stress pulse. These observations suggest that CI-M6PR surface accumulation may be more than an inert by-product of altered trafficking and could have physiological implications.

One plausible mechanism is that an increased proportion of CI-M6PR at the plasma membrane could alter the receptor's interaction with extracellular ligands, including secreted lysosomal enzymes such as cathepsins, or with mannose-6-phosphate-bearing cargo in the extracellular milieu. Such interactions might influence pericellular proteolysis, extracellular matrix remodelling, or the uptake of specific ligands by neighbouring cells. Alternatively, prolonged surface residency could expose the receptor to regulatory events, such as proteolytic shedding or phosphorylation, that do

not occur during its normal rapid cycling, thereby modifying its signalling potential or trafficking itinerary. Given the receptor's canonical role in retrieving lysosomal hydrolases from the endocytic pathway back to the TGN, one would expect that surface accumulation might also indirectly deplete the intracellular receptor pool, slowing the replenishment of lysosomal hydrolases and impacting degradative capacity. Finally, in the context of stress-induced lysosomal exocytosis, CI-M6PR enrichment at the plasma membrane could be part of a coordinated remodelling of the cell surface to modulate membrane composition, adhesion, or repair processes, thereby linking stress sensing to adaptive changes in trafficking.

Nevertheless, our preliminary functional assays provide compelling indications that this event may be an adaptation to increase cellular resilience to osmotic stress. Upon silencing of CI-M6PR (Fig. 4.23), we proved that lysosomal hydrolases transport was not impacted by the depletion of this receptor, and that part of the reason for this was the overcompensation of CD-M6PR in the absence of CI-M6PR (Fig. 4.25). Furthermore, though it was not tested directly in this study, there is the possibility that Sortilin could be acting synergistically alongside CD-M6PR or when both M6PRs are depleted (Fig. 4.27). Sortilin, along with LIMP2, have been linked to the transport of lysosomal hydrolases and have been reported to overcompensate in their transport in contexts where M6PRs are impaired or non-existent (Canuel et al., 2008, 2009; Coutinho et al., 2012a; Bannoud et al., 2018; Aguilera et al., 2023), and has been found significantly upregulated on our surfaceome screening, alongside both M6PRs, as the volcano plot in Fig. 5.2 depicts.

Clearly, there are mechanisms in place that render hydrolase trafficking in RPE-1 cells very robust in the face of stress since this overcompensation is shown to happen and also because Cathepsin B activity only declines in a short time window (1 h of osmotic stress) but normalizes under ongoing stress (Fig. 4.23).

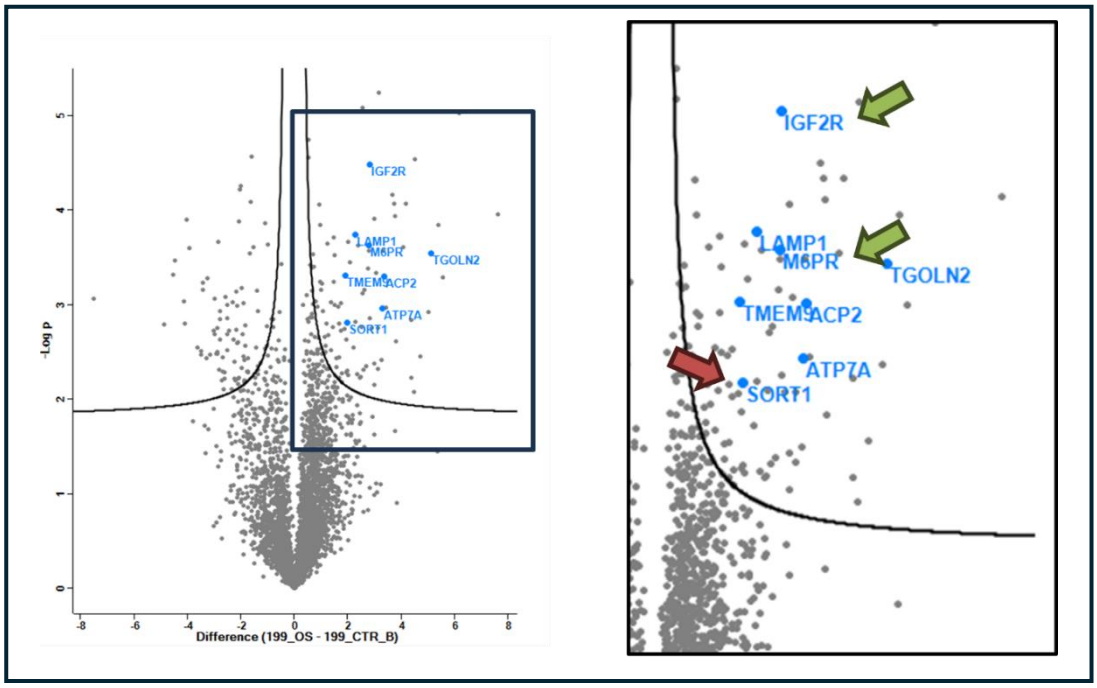

Fig. 5.2: Volcano plot shows Sortilin1 as significantly upregulated in the plasma membrane of osmotically stressed compared to unstressed cells. The green arrows show both M6PRs (higher arrow: CI-M6PR, lower arrow: CD-M6PR) and red arrow shows the presence of Sortilin1.

Silencing CI-M6PR not only impaired basal proliferation but also markedly exacerbated cell death and proliferative defects under osmotic stress, an effect not observed during oxidative stress, suggesting a specific link between CI-M6PR function and osmotic stress adaptation. This observation points toward a protective or compensatory role for CI-M6PR in maintaining proliferative capacity under hypertonic conditions, potentially by modulating membrane trafficking events critical for stress resilience, although the precise mechanisms remain to be elucidated.

The importance of such a mechanism could be of interest when placed in the broader context of hyperosmotic stress-induced changes in cell cycle regulation. As reported by Arsenijevic et al. (2013), exposure to hyperosmotic stress for just 4 h alters the expression of over 150 genes, notably in categories related to response to abiotic stimuli, transcriptional regulation, and the most relevant here, control of cell proliferation. These transcriptional shifts are consistent with an early osmoadaptive program that coordinates changes in gene expression, protein synthesis, and cell cycle checkpoints to facilitate survival. Indeed, they showed that hyperosmotic stress causes cells to accumulate at both G1/S and G2/M transitions, driven by downregulation of cyclins D1 and B1, upregulation of p27, and modest reductions in cdk4 activity, while cdk2 and cdk1 remain stable (Arsenijevic et al., 2013). Given the dependency of cdk activity on cyclin availability, these alterations likely inactivate cdk4 and cdk1, enforcing cell cycle arrest.

In our assays evaluating the functional contribution of the CI-M6PR/IGF2 receptor to cell proliferation (Fig. 4.29), neither supplementation with IGF2 nor inhibition of its binding to IGF2R/CI-M6PR produced significant changes in RPE-1 cell proliferation. These results argue against a role for CI-M6PR in regulating IGF2-driven proliferative responses in RPE-1 cells, both under basal conditions and during osmotic stress, but a sounder experimental design is still needed to produce more conclusive answers.

Lastly, one line of thought for CI-M6PR involvement in proliferation is that its altered distribution under osmotic stress might impair the trafficking or recycling of signalling receptors or lysosomal enzymes necessary for checkpoint recovery, tipping the balance toward prolonged arrest or cell death. Moreover, because CI-M6PR interacts with components of the clathrin machinery (e.g., AP-2) and shares regulatory kinases/phosphatases with other surface receptors, stress-induced modifications to its endocytic determinants could serve as an upstream trigger linking membrane trafficking perturbations to cell cycle control. All of these ideas are, at this point, completely speculative, and experimental pipelines would be needed to corroborate the merit in any of them.

Taken together, these findings reinforce the idea that different stressors activate distinct signalling and trafficking outcomes, and that CI-M6PR may participate in an osmotic stress-specific adaptive module. The consistent and early appearance of CI-M6PR at the plasma membrane, coupled with its impact on survival during stress when depleted, supports its potential relevance. However, more detailed mechanistic studies, particularly focusing on its extracellular versus intracellular ligands, its interactions with integrins or MAPK cascade components, and its trafficking itinerary under stress, are needed to clarify its precise role in cell survival and adaptation.

Outlook and future perspectives

The cellular plasma membrane is not only a selective barrier but also a dynamic interface that enables rapid adaptation to environmental challenges. This thesis has explored how stress conditions, particularly osmotic stress, can reshape the endocytic and exocytic balance, leading to selective enrichment of proteins such as CI-M6PR at the cell surface. While our findings provide new insight into the interplay between CME, lysosomal exocytosis, and stress responses, they also underscore how little is still known about the fine-scale mechanisms governing these processes during cellular adaptation.

One key area ripe for future investigation is the mechanistic coupling between endocytosis and exocytosis under stress. Current models tend to view these as separate trafficking routes; however, our work suggests that stress may simultaneously modulate both, perhaps through shared upstream regulators such as Ca^{2+} signalling hubs, cytoskeletal rearrangements, or membrane tension sensors. Unravelling these points of convergence could reveal new paradigms as a coordinated stress adaptation strategy.

Another emerging theme is the central role of TFEB in integrating stress signals into lysosomal biogenesis, trafficking, and exocytosis. TFEB sits at the crossroads of multiple signalling pathways (mTORC1, Wnt, AKT, Ca^{2+}/Calcineurin), linking nutrient sensing, osmotic adaptation, and oxidative stress responses. Yet, the specific triggers and thresholds for TFEB activation under different stress modalities remain poorly defined. Further, TFEB's transcriptional program influences not only lysosome abundance and positioning but also the availability of membrane trafficking components, positioning it as a potential "master regulator" of stress-adaptive trafficking. Targeting TFEB or its regulatory network could have an even broader therapeutic potential in contexts as diverse as neurodegeneration, metabolic disease, and cancer.

From a broader perspective, stress adaptation research is still disproportionately skewed toward transcriptional and metabolic responses, with endocytic trafficking remaining relatively underexplored. Given that membrane protein composition dictates how a cell perceives and responds to its surroundings, understanding how stress reshapes the plasma membrane proteome via altered trafficking will be crucial. High-resolution temporal studies, combining live-cell imaging, proximity labelling, and quantitative plus phosphoproteomics, could reveal the sequence of trafficking events and molecular regulation that define the early versus late phases of stress adaptation.

Finally, the disease relevance of stress-adaptive trafficking represents a fertile ground for translation. Many pathological conditions, ranging from lysosomal storage disorders to tumour progression, are characterized by both chronic stress and altered endosomal-lysosomal dynamics. Our findings point to the possibility that manipulating specific trafficking nodes (e.g., AP-2 recruitment, TRPML1 activity, or CI-M6PR cycling) could selectively modulate cell surface composition and, by extension, influence cell survival, proliferation, and signalling in disease contexts.

In sum, this work provides a starting point for rethinking stress adaptation not only as a gene expression program but also as a dynamic reconfiguration of the cellular membrane trafficking network. By bridging the mechanistic gap between endocytosis, exocytosis, and transcriptional control, future research can uncover novel adaptive strategies that cells employ and potentially exploit these pathways for therapeutic benefit.

6. Supplementary

Wiki-pathways associated mass spectrometry hits

All the proteins were found downregulated in all stress conditions unless otherwise stated

Aerobic glycolysis	
LDHA	L-lactate dehydrogenase A chain
ALDOA	Fructose-bisphosphate aldolase A
PKM	Pyruvate kinase PKM; Pyruvate kinase
TPI1	Triosephosphate isomerase
GPI	Glucose-6-phosphate isomerase
Glycolysis and gluconeogenesis	
LDHA	L-lactate dehydrogenase A chain
ALDOA	Fructose-bisphosphate aldolase A
PKM	Pyruvate kinase PKM; Pyruvate kinase
TPI1	Triosephosphate isomerase
GPI	Glucose-6-phosphate isomerase
PFKP	ATP-dependent 6-phosphofructokinase, platelet type
GOT1	Aspartate aminotransferase, cytoplasmic
Parkin-ubiquitin proteasomal system pathway	
TUBB4B	Tubulin beta-4B chain
TUBB6	Tubulin beta-6 chain
TUBA1C	Tubulin alpha-1C chain;Tubulin alpha chain
TUBA1B	Tubulin alpha-1B chain
TUBA4A	Tubulin alpha-4A chain
TUBB8	Tubulin beta-8 chain;Tubulin beta chain
HSPA5	Endoplasmic reticulum chaperone BiP
PSMD13	26S proteasome non-ATPase regulatory subunit 13
HERC4	Probable E3 ubiquitin-protein ligase HERC4

UBA6	Ubiquitin-like modifier-activating enzyme 6
UBXN1	UBX domain-containing protein 1
HUWE1	E3 ubiquitin-protein ligase HUWE1
Cori cycle	
LDHA	L-lactate dehydrogenase A chain
ALDOA	Fructose-bisphosphate aldolase A
PFKP	ATP-dependent 6-phosphofructokinase, platelet type
TPI1	Triosephosphate isomerase
Purine metabolism and related disorders	
ATIC	Bifunctional purine biosynthesis protein ATIC
ADSL	Adenylosuccinate lyase
ADSS2	Adenylosuccinate synthetase isozyme 2
PFAS	Phosphoribosylformylglycinamidine synthase
PNP	Purine nucleoside phosphorylase

Reactome pathways hits

Nucleotide biosynthesis	
ATIC	Bifunctional purine biosynthesis protein ATIC
PFAS	Phosphoribosylformylglycinamidine synthase
ADSL	Adenylosuccinate lyase
ADSS2	Adenylosuccinate synthetase isozyme 2
CAD	Multifunctional protein CAD;Glutamine amidotransferase; Aspartate carbamoyltransferase
IMPDH2	Inosine-5-monophosphate dehydrogenase 2
Post-chaperonin tubulin folding pathway	
TUBB4B	Tubulin beta-4B chain
TUBB6	Tubulin beta-6 chain
TUBA1C	Tubulin alpha-1C chain;Tubulin alpha chain

TUBA1B	Tubulin alpha-1B chain
TUBA4A	Tubulin alpha-4A chain
TBCD	Tubulin-specific chaperone D
TBCB	Tubulin-folding cofactor B
HSPA5*	Endoplasmic reticulum chaperone BiP

* Only protein that is upregulated in all sets

Microtubule-dependent trafficking of connexons from Golgi to the ER	
TUBB4B	Tubulin beta-4B chain
TUBB6	Tubulin beta-6 chain
TUBA1C	Tubulin alpha-1C chain;Tubulin alpha chain
TUBA1B	Tubulin alpha-1B chain
TUBA4A	Tubulin alpha-4A chain
TUBB8	Tubulin beta-8 chain;Tubulin beta chain
COPI-independent Golgi-to-ER retrograde traffic	
TUBB4B	Tubulin beta-4B chain
TUBB6	Tubulin beta-6 chain
TUBA1C	Tubulin alpha-1C chain; Tubulin alpha chain
TUBA1B	Tubulin alpha-1B chain
TUBA4A	Tubulin alpha-4A chain
TUBB8	Tubulin beta-8 chain; Tubulin beta chain
DYNC1H1	Cytoplasmic dynein 1 heavy chain 1
PAFAH1B2	Platelet-activating factor acetylhydrolase IB subunit alpha2

RACGAP1 Rac GTPase-activating protein 1 upreg in all sets except for OS, where it is visibly downreg

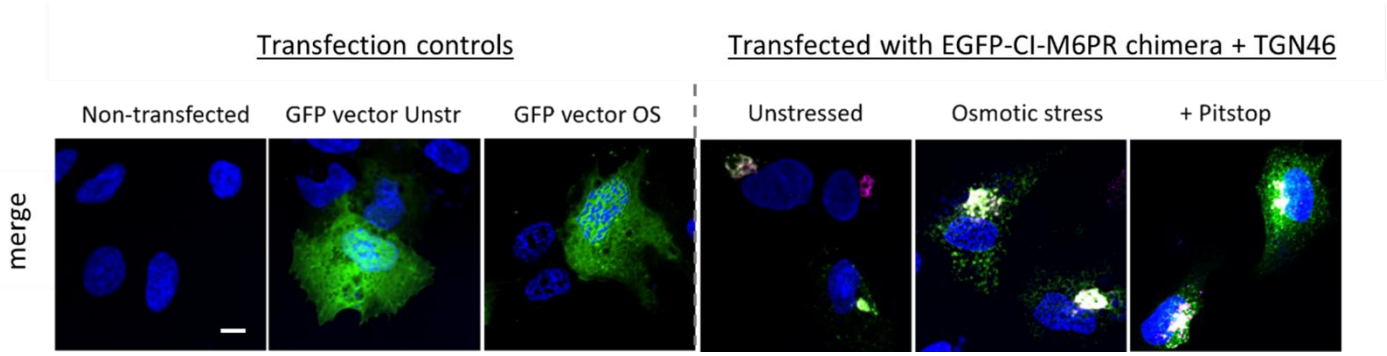

Fig. 6.1: EGFP-CI-M6PR truncation mutant lacking extracellular domains still becomes redistributed upon osmotic stress. (supplementary images Section 4.9.3)
Representative confocal microscope images showing all the conditions tested for this experiments testing the overexpression of the EGFP-tagged CI-M6PR (shown in green), including the transfection controls seen as the 3 first images: non-transfected or negative control (left most image), cells treated with an empty GFP vector in unstressed cells (second left) and under 1 h of osmotic stress treatment (third image from the left) as proof of transfection efficiency baselines on each condition. The right 3 images correspond to the unstressed (middle right image), osmotically stressed with 750 mM mannitol (second to last from the right image) and after 1 h 30 µM Pitstop treatment (utmost right image), the 3 images from the right side also display the TGN46 marker (shown in magenta) for colocalization analysis (seen in section 4.9.3) All pictures are merged with nuclei, showed with DAPI (shown in blue). Scale bar = 10 µm.

Table 20: Genes that upon knockdown cause peripheral distribution or plasma membrane accumulation of CI-M6PR. Adapted from Anitei et al., (2014)

Gene	Protein
ADRA2A	adrenergic, alpha-2A-, receptor
EPHA1	EPH receptor A1
GPR4	G protein-coupled receptor 4
INPP5J	inositol polyphosphate-5-phosphatase J
LATS2	LATS, large tumor suppressor, homolog 2 (Drosophila)
MADD	MAP-kinase activating death domain
NMUR1	neuromedin U receptor 1
PIK3AP1	phosphoinositide-3-kinase adaptor protein 1
PIK3CB	phosphoinositide-3-kinase, catalytic, beta polypeptide
PIK3R4	phosphoinositide-3-kinase, regulatory subunit 4, p150
PTPN4	protein tyrosine phosphatase, non-receptor type 4 (megakaryocyte)

List of figures

List of tables

Abbreviations

AMPK Adenosine Monophosphate-activated Protein Kinase

ANOVA Analysis of Variance

ARE Antioxidant Response Elements

AP Adaptor Protein complex (e.g.AP-1, AP-2)

AQP1 Aquaporin-1

ASK3 Apoptosis Signal-regulating Kinase 3

ASM Acid Sphingomyelinase

Bsep Bile salt export pump

C/EBP (homologous protein)

CD36 cluster of differentiation 36- platelet glycoprotein 4,

CAMs Cell Adhesion Molecules

°C grade, Celsius

CI-M6PR Cation-independent mannose-6 phosphate

CD-M6PR Cation-dependent mannose-6-phosphate

CNM Centronuclear Myopathy

CMT Charcot-Marie-Tooth disease

CTxB Cholera Toxin B subunit

CHCs Clathrin heavy chains

CLCs Clathrin light chains

CCPs Clathrin-coated pits

CCVs Clathrin-coated vesicles

CME Clathrin-Mediated Endocytosis

CIE Clathrin-Independent Endocytosis

DMSO Dimethyl sulfoxide

EEA1 Early Endosome Antigen 1

EAPs Endocytic Accessory Proteins

ER Endoplasmic Reticulum

EGFR Epidermal Growth Factor Receptor

FBS Fetal Bovine Serum

GPCR G Protein-coupled receptors

GO Gene Ontology

GLUT1 Glucose transporter 1

GSH Glutathione

GPx Glutathione Peroxidase

GM130 Golgi Matrix protein 130

GPI Glycosylphosphatidylinositol

HSEs Heat Shock Elements

HSPs Heat Shock Proteins e.g. Hsp70

HSR Heat Shock Response

HSF Heat Shock transcription factor

HS Heat stress

HSC70 Heat Shock Cognate Protein 70

HFF-1 Human Foreskin Fibroblast cell line

H_2O_2 Hydrogen peroxide

•OH Hydroxyl radicals

H hour

HIFs Hypoxia-inducible factors

IGF Insulin-like Growth Factor.(e.g. IGF-II)

IL Interleukin- (e.g. IL-2, IL-4)

JNK c-Jun N-terminal kinase

KD Knockdown

kDa kiloDalton

Keap1 Kelch-like ECH-associated protein 1

LAMP1 Lysosome-Associated Membrane Protein 1

LDL Low-density lipoprotein

LDLR Low-density lipoprotein receptor

LOX-1 Lectin-like oxidized low-density lipoprotein receptor-1

M6P Mannose-6-phosphate

MAPK Mitogen-Activated Protein Kinase

MTOC Microtubule organizing centre

ML-SA1 Mucolipin Synthetic Agonist 1

ML-SI3 Mucolipin-specific synthetic inhibitor 3

mOsm/kg Miliosmol per kg

LFQ Label-free quantification

LLPS Liquid-liquid phase separation

min minute

Mrp2 Multidrug resistance-associated protein 2

mTOR mechanistic Target of Rapamycin

MVBs multivesicular bodies

NaCl Sodium chloride

NFAT5 Nuclear Factor of Activated T-cells 5

NF-κB Nuclear Factor kappa-light-chain-enhancer of activated B cells

NHE7 Sodium/Hydrogen Exchanger 7

Nrf2 Nuclear factor erythroid 2-related factor 2

NTFs N-terminal fragments

OS Osmotic stress

redox Oxidation-reduction

PAR Poly(ADP-ribose)

PCA Principal Component Analysis

PK Protein kinase e.g. PKA, PKC

PN Proteostasis Network

RCS Reactive Carbonyl species

RNS Reactive Nitrogen species

ROS Reactive Oxygen species

RTKs Receptor Tyrosine kinases

GSH/GSSG reduced to oxidized Glutathione

TrxR Thioredoxin Reductase

RPE-1 Retinal pigment epithelium cell line

RX Oxidative stress

Scr/ Scramb Scrambled

siRNA small interfering RNA

SNAP23 Synaptosomal-associated protein 23

SNARE Soluble NSF Attachment Protein Receptor

SEM Standard error of the mean

(O_2^-) Superoxide anion

SOD Superoxide dismutase

SPPL2A/B Signal peptide peptidase-like 2A or B

SURFY- in silico human surfaceome curation pipeline

SYT-VII Synaptotagmin VII

SYNT4 Syntaxin-4

TBH Tert-Butyl Hydroperoxide

TFEB Transcription Factor EB

TGN46 Trans-Golgi Network protein 46

UPR Unfolded Protein Response

Trx Thioredoxin

TonEBP Tonicity Enhancer Binding protein

TonE Tonicity-responsive Enhancer elements

TrfR Transferrin Receptor

TRPML1 Transient Receptor Potential Mucolipin 1

Unstr Unstressed condition/ control

VAMP Vesicle-associated membrane protein (e.g. VAMP4, VAMP7)

Eidestattliche Erklärung

Ich erkläre hiermit, dass die eigereichte Dissertation von mir, Fiorella Mazzone, selbständig angefertigt wurde. Alle Hilfsmittel und Hilfestellungen in der Arbeit habe ich angegeben.

Die Dissertation oder Teile daraus wurden nicht als Prüfungsarbeit für eine Staatliche oder andere wissenschaftliche Prüfung eingereicht.

Die gleiche oder eine andere Abhandlung der Dissertation wurde nicht bein einem anderen Fachbereich oder einer anderen Universität eingereicht.

_____

Datum, Unterschrift Doktorandin

Darlegung aller Benutzen Hilfsmittel und Hilfestellungen

Name der Doktorandin: Fiorella Mazzone

Thema der Dissertation: "Dynamic modulation of endocytic protein sorting for counteracting stress conditions"

Zur Erstellung der Arbeit wurde das Micorsoft Office 365 Softwarpaket genutzt. Das Literaturverzeichnis und die Literaturverweise wurden mit Zotero erstellt. Die statistischen Analysen und Auswertungen wurden mit Graph Pad Prism durchgeführt. Die Abbildungen wurden mit der Affinity Designer erstellt. Die Analyse des Massenspektrometrischen Datensets wurde mit Perseus erstellt. Interaktionsnetzwerke wurden mit Hilfe von STRING dargestellt. Mikroskopische Aufnahmen wurden mit NIS Elements aufgenommen und mit Fiji analysiert. Western Blots wurden mit der Licor Acquisition Software aufgenommen und mit Image Studio ausgewertet. Eine detailiertere Auflistung der verwendeten Programme findet sich im Kapitel zu den Materialien.

DeepL und ChatGPT wurden für Übersetzungen und zum Optimieren von Formulierungen benutzt.

_____

Datum, Unterschift Doktorand/in

Darlegung des Eigenanteils

Name der Doktorandin: Fiorella Mazzone

Thema der Dissertation: "Dynamic modulation of endocytic protein sorting for counteracting stress conditions"

Anteil Dritter an der Dissertation:

Konzeption und Versuchsdesign: Prof. Dr. Tanja Maritzen (in Teilen)

Interpretation und Diskussion der Ergebnisse: Prof. Dr. Tanja Maritzen (in Teilen)

Datenerhebung und Datenanalyse:

Die in Abb. 4.5 F gezeigten Experimente zur Messung der Zellproliferation unter verschiedenen Stressbedingungen sowie die Klonierung des m-cherry-getaggten NHE7 und die in Abb. 4.10 gezeigten Experimente damit und die darauf basierende qualitative Kategorisierung der NHE7-Membrananreicherung wurden von Luwam Gebrezi im Rahmen ihrer Bachelorarbeit unter meiner Betreuung durchgeführt.

Die in Abb. 4.5 A-B gezeigten SYTOX-Assays zur Quantifizierung des durch die verschiedenen Stressoren verursachten Zelltodes wurden von Sophie Meinhold im Rahmen ihrer Bachelorarbeit unter meiner Betreuung durchgeführt.

Die massenspektrometrischen Messungen der Oberflächen-Biotinylierungen von gestressten und ungestressten Zellen (P0199 und P0207) und die anschließende Auswertung der Daten sowie die massenspektrometrischen Messungen des vollständigen Proteoms gestresster und ungestresster Zellen (P0260) inklusive der anschließenden Datenanalyse wurden von Dr. Markus Räschle (Zentrum für MS-Analytik, RPTU Kaierslautern-Landau) durchgeführt.

_____ _____

Datum, Unterschrift Doktorandin Datum, Unterschrift Betreuerin

Fiorella R. Mazzone

Education

PHD CANDIDATE, RHEINLAND-PFÄLZICHE TECHNISCHE UNIVERSITÄT KAISERSLAUTERN-LANDAU (RPTU)

FEBRUARY 2022 – AUGUST 2025

- Department of Nanophysiology
- Research assistant position
- Member of Research Training Group RTG 2737 "Stressistance" -Deutsche Forschungsgemeinschaft- (DFG)

MASTER'S IN MOLECULAR AND DEVELOPMENTAL STEM CELL BIOLOGY, RUHR-UNIVERSITÄT (RUB) BOCHUM, GERMANY

OCTOBER 2019 – NOVEMBER 2021

- Master thesis: department of Neuroanatomy
- Title: "Effect of Hyperthermia on Stem Cell Proliferation and Maturation modelled in Organotypic Hippocampal Slice Culture"

BASED APPRENTICESHIP, INSTITUTO NACIONAL DE CANCER (INCA), RIO DE JANEIRO- BRAZIL

MARCH 2011 – AUGUST 2012

- Full scholarship: selected and awarded by the Brazilian Ministry of Health
- Department of Genetics
- Project: "Mutation analysis on the short arm of chromosome 27 (p27) as potential markers for neuroblastoma in susceptible children."

BACHELOR'S IN MOLECULAR BIOLOGY, UNIVERSIDAD NACIONAL DE SAN LUIS, ARGENTINA

FEBRUARY 2006 – MARCH 2010

- Bachelor thesis performed at Middlesex University, London, UK.
- Thesis project: "Search for biomarkers in epithelial-origin cancers sub-types."

Relevant courses and workshops

- **Good Manufacturing Practices (GMP) 2 day-workshop -**ALFATRAINING (2024)
- **Advanced Proteomics course**, CRG Barcelona (June 12-16, 2023)
- **Scientific writing course** TU-Nachwuchsring (2023)
- **Peer-reviewed publishing-** TU-Nachwuchsring (2023)
- **Mastering Presentation skills & techniques**, HPS Campus (2023)
- **Image J basic workshop**, BioVoxxel (2023)
- **Statistics workshop**, Sum of Squares (2023)

Skills & Abilities

Languages: Spanish (native- C2)
English (proficient C1-C2)
Portuguese: fluent (B2)
Italian: intermediate (B1)
German: intermediate (B1)
French: pre-intermediate (A2-B1)

Computational skills: Microsoft office, GraphPad Prism, Fiji/ImageJ; Perseus

Methods: cell culture, cell transfection, western blotting, mass spectrometry, image analysis, advanced fluorescence microscopy, PCR, immunohistochemistry, genetic marker analysis, cytogenetics and karyotyping

Publications

Ebding, Johannes; **Mazzone, Fiorella**; Kins, Stefan; Pielage, Jan; Maritzen, Tanja. How neurons cope with oxidative stress. Biol Chem. 2025 Feb 25. doi: 10.1515/hsz-2024-0146. Online ahead of print.

References

Abouelezz, A., & Almeida-Souza, L. (2022). The mammalian endocytic cytoskeleton. *European Journal of Cell Biology*, *101*(2), 151222. https://doi.org/10.1016/j.ejcb.2022.151222

Aguilar-Gaytan, R., & Mas-Oliva, J. (2003). Oxidative stress impairs endocytosis of the scavenger receptor class A. *Biochemical and Biophysical Research Communications*, *305*(3), 510–517. https://doi.org/10.1016/S0006-291X(03)00796-4

Aguilera, A. C., Leiva, N., Alvarez, P. A., Pulcini, G., Pereyra, L. L., Morales, C. R., Sosa, M. Á., & Carvelli, L. (2023). Sortilin knock-down alters the expression and distribution of cathepsin D and prosaposin and up-regulates the cation-dependent mannose-6-phosphate receptor in rat epididymal cells. *Scientific Reports*, *13*(1), 3461. https://doi.org/10.1038/s41598-023-29157-z

Aisen, P. (2004). Transferrin receptor 1. *The International Journal of Biochemistry & Cell Biology*, *36*(11), 2137–2143. https://doi.org/10.1016/j.biocel.2004.02.007

Åkerfelt, M., Morimoto, R. I., & Sistonen, L. (2010). Heat shock factors: Integrators of cell stress, development and lifespan. *Nature Reviews Molecular Cell Biology*, *11*(8), 545–555. https://doi.org/10.1038/nrm2938

Anding, A. L., & Baehrecke, E. H. (2017). Cleaning House: Selective Autophagy of Organelles. *Developmental Cell*, *41*(1), 10–22. https://doi.org/10.1016/j.devcel.2017.02.016

Andrews, N. W. (2017). Detection of Lysosomal Exocytosis by Surface Exposure of Lamp1 Luminal Epitopes. In K. Öllinger & H. Appelqvist (Eds.), *Lysosomes: Methods and Protocols* (pp. 205–211). Springer. https://doi.org/10.1007/978-1-4939-6934-0_13

Anitei, M., & Hoflack, B. (2012). Bridging membrane and cytoskeleton dynamics in the secretory and endocytic pathways. *Nature Cell Biology*, *14*(1), 11–19. https://doi.org/10.1038/ncb2409

Aperia, A., Akkuratov, E. E., Fontana, J. M., & Brismar, H. (2016). Na+-K+-ATPase, a new class of plasma membrane receptors. *American Journal of Physiology-Cell Physiology*, *310*(7), C491–C495. https://doi.org/10.1152/ajpcell.00359.2015

Appelqvist, H., Wäster, P., Eriksson, I., Rosdahl, I., & Öllinger, K. (2013). Lysosomal exocytosis and caspase-8-mediated apoptosis in UVA-irradiated keratinocytes. *Journal of Cell Science*, *126*(24), 5578–5584. https://doi.org/10.1242/jcs.130633

Aridor, M., & Hannan, L. A. (2000). Traffic jam: A compendium of human diseases that affect intracellular transport processes. *Traffic (Copenhagen, Denmark)*, *1*(11), 836–851. https://doi.org/10.1034/j.1600-0854.2000.011104.x

Aridor, M., & Hannan, L. A. (2002). Traffic jams II: An update of diseases of intracellular transport. *Traffic (Copenhagen, Denmark)*, *3*(11), 781–790. https://doi.org/10.1034/j.1600-0854.2002.31103.x

Arsenijevic, T., Vujovic, A., Libert, F., Op de Beeck, A., Hébrant, A., Janssens, S., Grégoire, F., Lefort, A., Bolaky, N., Perret, J., Caspers, L., Willermain, F., & Delporte, C. (2013). Hyperosmotic stress induces cell cycle arrest in retinal pigmented epithelial cells. *Cell Death & Disease*, *4*(6), e662–e662. https://doi.org/10.1038/cddis.2013.189

Ballabio, A., & Bonifacino, J. S. (2020). Lysosomes as dynamic regulators of cell and organismal homeostasis. *Nature Reviews Molecular Cell Biology*, *21*(2), 101–118. https://doi.org/10.1038/s41580-019-0185-4

Ballin, M., Griep, W., Patel, M., Karl, M., Mentrup, T., Rivera-Monroy, J., Foo, B., Schwappach, B., & Schröder, B. (2023). The intramembrane proteases SPPL2A and SPPL2B regulate the homeostasis

of selected SNARE proteins. *The FEBS Journal*, *290*(9), 2320–2337. https://doi.org/10.1111/febs.16610

Banani, S. F., Lee, H. O., Hyman, A. A., & Rosen, M. K. (2017). Biomolecular condensates: Organizers of cellular biochemistry. *Nature Reviews Molecular Cell Biology*, *18*(5), 285–298. https://doi.org/10.1038/nrm.2017.7

Bannoud, N., Carvelli, F. L., Troncoso, M., Sartor, T., Vargas-Roig, L. M., & Sosa, M. (2018). Cation-dependent mannose-6-phosphate receptor expression and distribution are influenced by estradiol in MCF-7 breast cancer cells. *PLOS ONE*, *13*(8), e0201844. https://doi.org/10.1371/journal.pone.0201844

Basiglio, C. L., Toledo, F. D., Boaglio, A. C., Arriaga, S. M., Ochoa, J. E., Sánchez Pozzi, E. J., Mottino, A. D., & Roma, M. G. (2014). Physiological concentrations of unconjugated bilirubin prevent oxidative stress-induced hepatocanalicular dysfunction and cholestasis. *Archives of Toxicology*, *88*(2), 501–514. https://doi.org/10.1007/s00204-013-1143-0

Battison, C., Andrews, P. J. D., Graham, C., & Petty, T. (2005). Randomized, controlled trial on the effect of a 20% mannitol solution and a 7.5% saline/6% dextran solution on increased intracranial pressure after brain injury. *Critical Care Medicine*, *33*(1), 196–202; discussion 257-258. https://doi.org/10.1097/01.ccm.0000150269.65485.a6

Bausch-Fluck, D., Goldmann, U., Müller, S., van Oostrum, M., Müller, M., Schubert, O. T., & Wollscheid, B. (2018). The in silico human surfaceome. *Proceedings of the National Academy of Sciences of the United States of America*, *115*(46), E10988–E10997. https://doi.org/10.1073/pnas.1808790115

Bella, P., Farini, A., Banfi, S., Parolini, D., Tonna, N., Meregalli, M., Belicchi, M., Erratico, S., D'Ursi, P., Bianco, F., Legato, M., Ruocco, C., Sitzia, C., Sangiorgi, S., Villa, C., D'Antona, G., Milanesi, L., Nisoli, E., Mauri, P., & Torrente, Y. (2020). Blockade of IGF2R improves muscle regeneration and ameliorates Duchenne muscular dystrophy. *EMBO Molecular Medicine*, *12*(1), e11019. https://doi.org/10.15252/emmm.201911019

Bezanilla, F. (2008). How membrane proteins sense voltage. *Nature Reviews Molecular Cell Biology*, *9*(4), 323–332. https://doi.org/10.1038/nrm2376

Bi, C., Tham, D. K. L., Perronnet, C., Joshi, B., Nabi, I. R., & Moukhles, H. (2017). The Oxidative Stress-Induced Increase in the Membrane Expression of the Water-Permeable Channel Aquaporin-4 in Astrocytes Is Regulated by Caveolin-1 Phosphorylation. *Frontiers in Cellular Neuroscience*, *11*, 412. https://doi.org/10.3389/fncel.2017.00412

Bitsikas, V., Corrêa, I. R., & Nichols, B. J. (2014). Clathrin-independent pathways do not contribute significantly to endocytic flux. *eLife*, *3*, e03970. https://doi.org/10.7554/eLife.03970

Bode, J., Gatsios, P., & Ludwig, S. (1999). The mitogen-activated protein (MAP) kinase p38 and its upstream activator MAP kinase kinase 6 are involved in the activation of signal transducer and activator of transcription by hyperosmolarity. *Journal of Biological Chemistry. Volume 274, Issue 42, 30222 - 30227*

Boname, J. M., Bloor, S., Wandel, M. P., Nathan, J. A., Antrobus, R., Dingwell, K. S., Thurston, T. L., Smith, D. L., Smith, J. C., Randow, F., & Lehner, P. J. (2014). Cleavage by signal peptide peptidase is required for the degradation of selected tail-anchored proteins. *The Journal of Cell Biology*, *205*(6), 847–862. https://doi.org/10.1083/jcb.201312009

Boucrot, E., Ferreira, A. P. A., Almeida-Souza, L., Debard, S., Vallis, Y., Howard, G., Bertot, L., Sauvonnet, N., & McMahon, H. T. (2015). Endophilin marks and controls a clathrin-independent endocytic pathway. *Nature*, *517*(7535), 460–465. https://doi.org/10.1038/nature14067

Boucrot, E., & Kirchhausen, T. (2007). Endosomal recycling controls plasma membrane area during mitosis. *Proceedings of the National Academy of Sciences*, *104*(19), 7939–7944. https://doi.org/10.1073/pnas.0702511104

Boulant, S., Kural, C., Zeeh, J.-C., Ubelmann, F., & Kirchhausen, T. (2011). Actin dynamics counteract membrane tension during clathrin-mediated endocytosis. *Nature Cell Biology*, *13*(9), 1124–1131. https://doi.org/10.1038/ncb2307

Bratton, S. L., Chestnut, R. M., Ghajar, J., McConnell Hammond, F. F., Harris, O. A., Hartl, R., Manley, G. T., Nemecek, A., Newell, D. W., Rosenthal, G., Schouten, J., Shutter, L., Timmons, S. D., Ullman, J. S., Videtta, W., Wilberger, J. E., & Wright, D. W. (2007). II. Hyperosmolar Therapy. *Journal of Neurotrauma*, *24*(supplement 1), S-14. https://doi.org/10.1089/neu.2007.9994

Braulke, T., & Bonifacino, J. S. (2009). Sorting of lysosomal proteins. *Biochimica et Biophysica Acta (BBA) - Molecular Cell Research*, *1793*(4), 605–614. https://doi.org/10.1016/j.bbamcr.2008.10.016

Brierley, G. V., Macaulay, S. L., Forbes, B. E., Wallace, J. C., Cosgrove, L. J., & Macaulay, V. M. (2010). Silencing of the Insulin Receptor Isoform A Favors Formation of Type 1 Insulin-Like Growth Factor Receptor (IGF-IR) Homodimers and Enhances Ligand-Induced IGF-IR Activation and Viability of Human Colon Carcinoma Cells. *Endocrinology*, *151*(4), 1418–1427. https://doi.org/10.1210/en.2009-1006

Bright, N. A., Davis, L. J., & Luzio, J. P. (2016). Endolysosomes Are the Principal Intracellular Sites of Acid Hydrolase Activity. *Current Biology*, *26*(17), 2233–2245. https://doi.org/10.1016/j.cub.2016.06.046

Brown, J., Jones, E. Y., & Forbes, B. E. (2009). Interactions of IGF-II with the IGF2R/Cation-Independent Mannose-6-Phosphate Receptor. In *Vitamins & Hormones* (Vol. 80, pp. 699–719). Elsevier. https://doi.org/10.1016/S0083-6729(08)00625-0

Brozzi, A., Urbanelli, L., Luc Germain, P., Magini, A., & Emiliani, C. (2013). hLGDB: A database of human lysosomal genes and their regulation. *Database*, *2013*, bat024. https://doi.org/10.1093/database/bat024

Buratta, S., Tancini, B., Sagini, K., Delo, F., Chiaradia, E., Urbanelli, L., & Emiliani, C. (2020). Lysosomal Exocytosis, Exosome Release and Secretory Autophagy: The Autophagic- and Endo-Lysosomal Systems Go Extracellular. *International Journal of Molecular Sciences*, *21*(7), Article 7. https://doi.org/10.3390/ijms21072576

Burgdorf, S., & Kurts, C. (2008). Endocytosis mechanisms and the cell biology of antigen presentation. *Current Opinion in Immunology*, *20*(1), 89–95. https://doi.org/10.1016/j.coi.2007.12.002

Burton, G. J., & Jauniaux, E. (2011). Oxidative stress. *Best Practice & Research Clinical Obstetrics & Gynaecology*, *25*(3), 287–299. https://doi.org/10.1016/j.bpobgyn.2010.10.016

Cadenas, E., & Davies, K. J. A. (2000). Mitochondrial free radical generation, oxidative stress, and aging1. *Free Radical Biology and Medicine*, *29*(3), 222–230. https://doi.org/10.1016/S0891-5849(00)00317-8

Campos-Toimil, M., Edwardson, J. M., & Thomas, P. (2002). Acetylcholine-induced zymogen granule exocytosis: Comparison between acini and single pancreatic acinar cells. *Pancreas*, *24*(2), 179–183. https://doi.org/10.1097/00006676-200203000-00009

Canuel, M., Korkidakis, A., Konnyu, K., & Morales, C. R. (2008). Sortilin mediates the lysosomal targeting of cathepsins D and H. *Biochemical and Biophysical Research Communications*, *373*(2), 292–297. https://doi.org/10.1016/j.bbrc.2008.06.021

Canuel, M., Libin, Y., & Morales, C. (2009). The interactomics of sortilin: An ancient lysosomal receptor evolving new functions. *Histology and Histopathology*, *24*, 481–492. https://doi.org/10.14670/HH-24.481

Castillo, L. B., Bugedo, G. A., & Paranhos, J. L. (2009). Mannitol or hypertonic saline for intracranial hypertension? A point of view. *Critical Care and Resuscitation*, *11*(2), 151–154. https://doi.org/10.1016/s1441-2772(23)01540-5

Cavalli, V., Vilbois, F., Corti, M., Marcote, M. J., Tamura, K., Karin, M., Arkinstall, S., & Gruenberg, J. (2001). The Stress-Induced MAP Kinase p38 Regulates Endocytic Trafficking via the GDI:Rab5 Complex. *Molecular Cell*, *7*(2), 421–432. https://doi.org/10.1016/S1097-2765(01)00189-7

Chakrabarti, S., Kobayashi, K. S., Flavell, R. A., Marks, C. B., Miyake, K., Liston, D. R., Fowler, K. T., Gorelick, F. S., & Andrews, N. W. (2003). Impaired membrane resealing and autoimmune myositis in synaptotagmin VII-deficient mice. *The Journal of Cell Biology*, *162*(4), 543–549. https://doi.org/10.1083/jcb.200305131

Chang, T.-Y., Chang, C. C. Y., Ohgami, N., & Yamauchi, Y. (2006). Cholesterol Sensing, Trafficking, and Esterification. *Annual Review of Cell and Developmental Biology*, *22*(Volume 22, 2006), 129–157. https://doi.org/10.1146/annurev.cellbio.22.010305.104656

Chen, D. Y., Stern, S. A., Garcia-Osta, A., Saunier-Rebori, B., Pollonini, G., Bambah-Mukku, D., Blitzer, R. D., & Alberini, C. M. (2011). A critical role for IGF-II in memory consolidation and enhancement. *Nature*, *469*(7331), 491–497. https://doi.org/10.1038/nature09667

Cheng, J., & Vieira, A. (2006). Oxidative stress disrupts internalization and endocytic trafficking of transferrin in a human malignant keratinocyte line. *Cell Biochemistry and Biophysics*, *45*(2), 177–184. https://doi.org/10.1385/CBB:45:2:177

Cocucci, E., Racchetti, G., Podini, P., Rupnik, M., & Meldolesi, J. (2004). Enlargeosome, an exocytic vesicle resistant to nonionic detergents, undergoes endocytosis via a nonacidic route. *Molecular Biology of the Cell*, *15*(12), 5356–5368. https://doi.org/10.1091/mbc.e04-07-0577

Compton, P. D., Zamdborg, L., Thomas, P. M., & Kelleher, N. L. (2011). On the Scalability and Requirements of Whole Protein Mass Spectrometry. *Analytical Chemistry*, *83*(17), 6868–6874. https://doi.org/10.1021/ac2010795

Conner, S. D., & Schmid, S. L. (2002). Identification of an adaptor-associated kinase, AAK1, as a regulator of clathrin-mediated endocytosis. *The Journal of Cell Biology*, *156*(5), 921–929. https://doi.org/10.1083/jcb.200108123

Cota, D., Proulx, K., Smith, K. A. B., Kozma, S. C., Thomas, G., Woods, S. C., & Seeley, R. J. (2006). Hypothalamic mTOR Signaling Regulates Food Intake. *Science*, *312*(5775), 927–930. https://doi.org/10.1126/science.1124147

Coutinho, M. F., Prata, M. J., & Alves, S. (2012a). A shortcut to the lysosome: The mannose-6-phosphate-independent pathway. *Molecular Genetics and Metabolism*, *107*(3), 257–266. https://doi.org/10.1016/j.ymgme.2012.07.012

Coutinho, M. F., Prata, M. J., & Alves, S. (2012b). Mannose-6-phosphate pathway: A review on its role in lysosomal function and dysfunction. *Molecular Genetics and Metabolism*, *105*(4), 542–550. https://doi.org/10.1016/j.ymgme.2011.12.012

Cox, J., Hein, M. Y., Luber, C. A., Paron, I., Nagaraj, N., & Mann, M. (2014). Accurate Proteome-wide Label-free Quantification by Delayed Normalization and Maximal Peptide Ratio Extraction, Termed

MaxLFQ. *Molecular & Cellular Proteomics : MCP*, *13*(9), 2513–2526. https://doi.org/10.1074/mcp.M113.031591

Cullen, K. J., Lippman, M. E., Chow, D., Hill, S., Rosen, N., & Zwiebel, J. A. (1992). Insulin-like growth factor-II overexpression in MCF-7 cells induces phenotypic changes associated with malignant progression. *Molecular Endocrinology*, *6*(1), 91–100. https://doi.org/10.1210/mend.6.1.1310798

da Cunha, J. P. C., Galante, P. a. F., de Souza, J. E., de Souza, R. F., Carvalho, P. M., Ohara, D. T., Moura, R. P., Oba-Shinja, S. M., Marie, S. K. N., Silva, W. A., Perez, R. O., Stransky, B., Pieprzyk, M., Moore, J., Caballero, O., Gama-Rodrigues, J., Habr-Gama, A., Kuo, W. P., Simpson, A. J., … de Souza, S. J. (2009). Bioinformatics construction of the human cell surfaceome. *Proceedings of the National Academy of Sciences of the United States of America*, *106*(39), 16752–16757. https://doi.org/10.1073/pnas.0907939106

Damke, H., Baba, T., van der Bliek, A. M., & Schmid, S. L. (1995). Clathrin-independent pinocytosis is induced in cells overexpressing a temperature-sensitive mutant of dynamin. *The Journal of Cell Biology*, *131*(1), 69–80. https://doi.org/10.1083/jcb.131.1.69

Damm, E.-M., Pelkmans, L., Kartenbeck, J., Mezzacasa, A., Kurzchalia, T., & Helenius, A. (2005). Clathrin- and caveolin-1-independent endocytosis: Entry of simian virus 40 into cells devoid of caveolae. *The Journal of Cell Biology*, *168*(3), 477–488. https://doi.org/10.1083/jcb.200407113

Dasgupta, S., & Kelly, R. B. (2003). Internalization signals in synaptotagmin VII utilizing two independent pathways are masked by intramolecular inhibitions. *Journal of Cell Science*, *116*(Pt 7), 1327–1337. https://doi.org/10.1242/jcs.00290

Daukas, G., & Zigmond, S. H. (1985). Inhibition of receptor-mediated but not fluid-phase endocytosis in polymorphonuclear leukocytes. *The Journal of Cell Biology*, *101*(5 Pt 1), 1673–1679. https://doi.org/10.1083/jcb.101.5.1673

de Araujo, M. E. G., Liebscher, G., Hess, M. W., & Huber, L. A. (2020). Lysosomal size matters. *Traffic*, *21*(1), 60–75. https://doi.org/10.1111/tra.12714

de Jong, E., & Kocer, A. (2023). Current Methods for Identifying Plasma Membrane Proteins as Cancer Biomarkers. *Membranes*, *13*(4), 409. https://doi.org/10.3390/membranes13040409

De Wit, R., Makkinje, M., Boonstra, J., Verkleij, A. J., & Post, J. A. (2001). Hydrogen peroxide reversibly inhibits epidermal growth factor (EGF) receptor internalization and coincident ubiquitination of the EGF receptor and Eps15. *The FASEB Journal*, *15*(2), 306–308. https://doi.org/10.1096/fj.00-0454fje

Di Paola, S., Scotto-Rosato, A., & Medina, D. L. (2018). TRPML1: The Ca(2+)retaker of the lysosome. *Cell Calcium*, *69*, 112–121. https://doi.org/10.1016/j.ceca.2017.06.006

Díaz, E., & Pfeffer, S. R. (1998). TIP47: A Cargo Selection Device for Mannose 6-Phosphate Receptor Trafficking. *Cell*, *93*(3), 433–443. https://doi.org/10.1016/S0092-8674(00)81171-X

Dmitrieva, N. I., Michea, L. F., Rocha, G. M., & Burg, M. B. (2001). Cell cycle delay and apoptosis in response to osmotic stress. *Comparative Biochemistry and Physiology. Part A, Molecular & Integrative Physiology*, *130*(3), 411–420. https://doi.org/10.1016/s1095-6433(01)00439-1

Doherty, G. J., & McMahon, H. T. (2008). Mediation, modulation, and consequences of membrane-cytoskeleton interactions. *Annual Review of Biophysics*, *37*, 65–95. https://doi.org/10.1146/annurev.biophys.37.032807.125912

Doherty, G. J., & McMahon, H. T. (2009). Mechanisms of Endocytosis. *Annual Review of Biochemistry*, *78*(1), 857–902. https://doi.org/10.1146/annurev.biochem.78.081307.110540

Duncan, J. R., & Kornfeld, S. (1988). Intracellular movement of two mannose 6-phosphate receptors: Return to the Golgi apparatus. *The Journal of Cell Biology*, *106*(3), 617–628. https://doi.org/10.1083/jcb.106.3.617

Dunn, K. W., Kamocka, M. M., & McDonald, J. H. (2011). A practical guide to evaluating colocalization in biological microscopy. *American Journal of Physiology-Cell Physiology*, *300*(4), C723–C742. https://doi.org/10.1152/ajpcell.00462.2010

Ebner, M., Fröhlich, F., & Haucke, V. (2025). Mechanisms and functions of lysosomal lipid homeostasis. *Cell Chemical Biology*, *32*(3), 392–407. https://doi.org/10.1016/j.chembiol.2025.02.003

Ebner, M., Puchkov, D., López-Ortega, O., Muthukottiappan, P., Su, Y., Schmied, C., Zillmann, S., Nikonenko, I., Koddebusch, J., Dornan, G. L., Lucht, M. T., Koka, V., Jang, W., Koch, P. A., Wallroth, A., Lehmann, M., Brügger, B., Pende, M., Winter, D., & Haucke, V. (2023). Nutrient-regulated control of lysosome function by signaling lipid conversion. *Cell*, *186*(24), 5328-5346.e26. https://doi.org/10.1016/j.cell.2023.09.027

Ellis, J. C., Leav, A., Yang, Z., Zweibel, A., Lippman, E., Cullen, K. J., & Lombardi, V. T. (1996). Affinity for the Insulin-Like Growth Factor-II (IGF-II) Receptor Inhibits Autocrine IGF-II Activity in MCF-7 Breast Cancer Cells. *Molecular Endocrinology 0888-8809/96*

Ellis, R. J. (2001). Macromolecular crowding: Obvious but underappreciated. *Trends in Biochemical Sciences*, *26*(10), 597–604. https://doi.org/10.1016/S0968-0004(01)01938-7

Esmaeilzadeh, H., Pouladfar, G., Gholami, M. A., & Mohtadi, H. (2024). Mendelian Susceptibility to Mycobacterial Disease with Signal Peptide Peptidase-like 2A (SPPL2A) Deficiency: A Case Report. *Iranian Journal of Allergy, Asthma and Immunology*. https://doi.org/10.18502/ijaai.v23i5.16753

Feng, X., Xiong, J., Lu, Y., Xia, X., & Zhu, M. X. (2014). Differential mechanisms of action of the mucolipin synthetic agonist, ML-SA1, on insect TRPML and mammalian TRPML1. *Cell Calcium*, *56*(6), 446–456. https://doi.org/10.1016/j.ceca.2014.09.004

Ferraris, J. D., Williams, C. K., Persaud, P., Zhang, Z., Chen, Y., & Burg, M. B. (2002). Activity of the TonEBP/OREBP transactivation domain varies directly with extracellular NaCl concentration. *Proceedings of the National Academy of Sciences of the United States of America*, *99*(2), 739–744. https://doi.org/10.1073/pnas.241637298

Frechin, M., Stoeger, T., Daetwyler, S., Gehin, C., Battich, N., Damm, E.-M., Stergiou, L., Riezman, H., & Pelkmans, L. (2015). Cell-intrinsic adaptation of lipid composition to local crowding drives social behaviour. *Nature*, *523*(7558), 88–91. https://doi.org/10.1038/nature14429

Friedmann, E., Hauben, E., Maylandt, K., Schleeger, S., Vreugde, S., Lichtenthaler, S. F., Kuhn, P.-H., Stauffer, D., Rovelli, G., & Martoglio, B. (2006). SPPL2a and SPPL2b promote intramembrane proteolysis of TNFα in activated dendritic cells to trigger IL-12 production. *Nature Cell Biology*, *8*(8), 843–848. https://doi.org/10.1038/ncb1440

Fujimoto, T., & Parmryd, I. (2017). Interleaflet Coupling, Pinning, and Leaflet Asymmetry—Major Players in Plasma Membrane Nanodomain Formation. *Frontiers in Cell and Developmental Biology*, *4*. https://doi.org/10.3389/fcell.2016.00155

Futter, C. E., Connolly, C. N., Cutler, D. F., & Hopkins, C. R. (1995). Newly Synthesized Transferrin Receptors Can Be Detected in the Endosome before They Appear on the Cell Surface *. *Journal of Biological Chemistry*, *270*(18), 10999–11003. https://doi.org/10.1074/jbc.270.18.10999

Galluzzi, L., Yamazaki, T., & Kroemer, G. (2018). Linking cellular stress responses to systemic homeostasis. *Nature Reviews Molecular Cell Biology*, *19*(11), 731–745. https://doi.org/10.1038/s41580-018-0068-0

Garapati, K., Ding, H., Charlesworth, M. C., Kim, Y., Zenka, R., Saraswat, M., Mun, D.-G., Chavan, S., Shingade, A., Lucien, F., Zhong, J., Kandasamy, R. K., & Pandey, A. (2023). sBioSITe enables sensitive identification of the cell surface proteome through direct enrichment of biotinylated peptides. *Clinical Proteomics*, *20*(1), 56. https://doi.org/10.1186/s12014-023-09445-6

Gatsios, P., Terstegen, L., Schliess, F., Häussinger, D., Kerr, I. M., Heinrich, P. C., & Graeve, L. (1998). Activation of the Janus kinase/signal transducer and activator of transcription pathway by osmotic shock. *Journal of Biological Chemistry*, *273*(36), 22962–22968. https://doi.org/10.1074/jbc.273.36.22962

Gauthier, C., El Cheikh, K., Basile, I., Daurat, M., Morère, E., Garcia, M., Maynadier, M., Morère, A., & Gary-Bobo, M. (2024). Cation-independent mannose 6-phosphate receptor: From roles and functions to targeted therapies. *Journal of Controlled Release*, *365*, 759–772. https://doi.org/10.1016/j.jconrel.2023.12.014

Ghosh, P., Dahms, N. M., & Kornfeld, S. (2003). Mannose 6-phosphate receptors: New twists in the tale. *Nature Reviews Molecular Cell Biology*, *4*(3), 202–213. https://doi.org/10.1038/nrm1050

Ghosh, R. N., & Maxfield, F. R. (1995). Evidence for nonvectorial, retrograde transferrin trafficking in the early endosomes of HEp2 cells. *Journal of Cell Biology*, *128*(4), 549–561. https://doi.org/10.1083/jcb.128.4.549

Glotin, A.-L., Calipel, A., Brossas, J.-Y., Faussat, A.-M., Tréton, J., & Mascarelli, F. (2006). Sustained versus Transient ERK1/2 Signaling Underlies the Anti- and Proapoptotic Effects of Oxidative Stress in Human RPE Cells. *Investigative Ophthalmology & Visual Science*, *47*(10), 4614–4623. https://doi.org/10.1167/iovs.06-0297

Go, W. Y., Liu, X., Roti, M. A., Liu, F., & Ho, S. N. (2004). NFAT5/TonEBP mutant mice define osmotic stress as a critical feature of the lymphoid microenvironment. *Proceedings of the National Academy of Sciences of the United States of America*, *101*(29), 10673–10678. https://doi.org/10.1073/pnas.0403139101

Goda, Y., & Pfeffer, S. R. (1988). Selective recycling of the mannose 6-phosphate/IGF-II receptor to the trans Golgi network in vitro. *Cell*, *55*(2), 309–320. https://doi.org/10.1016/0092-8674(88)90054-2

Goldstein, J. L., & Brown, M. S. (2009). The LDL Receptor. *Arteriosclerosis, Thrombosis, and Vascular Biology*, *29*(4), 431–438. https://doi.org/10.1161/ATVBAHA.108.179564

Gradtke, A.-C., Mentrup, T., Lehmann, C. H. K., Cabrera-Cabrera, F., Desel, C., Okakpu, D., Assmann, M., Dalpke, A., Schaible, U. E., Dudziak, D., & Schröder, B. (2021). Deficiency of the Intramembrane Protease SPPL2a Alters Antimycobacterial Cytokine Responses of Dendritic Cells. *The Journal of Immunology*, *206*(1), 164–180. https://doi.org/10.4049/jimmunol.2000151

Griffin, N. M., & Schnitzer, J. E. (2011). Overcoming Key Technological Challenges in Using Mass Spectrometry for Mapping Cell Surfaces in Tissues. *Molecular & Cellular Proteomics : MCP*, *10*(2), R110.000935. https://doi.org/10.1074/mcp.R110.000935

Griffiths, G., Hoflack, B., Simons, K., Mellman, I., & Kornfeld, S. (1988). The mannose 6-phosphate receptor and the biogenesis of lysosomes. *Cell*, *52*(3), 329–341. https://doi.org/10.1016/S0092-8674(88)80026-6

Griffiths, G., Matteoni, R., Back, R., & Hoflack, B. (1990). Characterization of the cation-independent mannose 6-phosphate receptor-enriched prelysosomal compartment in NRK cells. *Journal of Cell Science*, *95 (Pt 3)*, 441–461. https://doi.org/10.1242/jcs.95.3.441

Guo, Y., Yu, S., Zhang, C., & Kong, A.-N. T. (2015). Epigenetic regulation of Keap1-Nrf2 signaling. *Free Radical Biology and Medicine*, *88*, 337–349. https://doi.org/10.1016/j.freeradbiomed.2015.06.013

Halvey, P. J., Hansen, J. M., Johnson, J. M., Go, Y.-M., Samali, A., & Jones, D. P. (2007). Selective Oxidative Stress in Cell Nuclei by Nuclear-Targeted D-Amino Acid Oxidase. *Antioxidants & Redox Signaling*, *9*(7), 807–816. https://doi.org/10.1089/ars.2007.1526

Han, Y., Cui, J., Tao, J., Guo, L., Guo, P., Sun, M., Kang, J., Zhang, X., Yan, C., & Li, S. (2009). CREG inhibits migration of human vascular smooth muscle cells by mediating IGF-II endocytosis. *Experimental Cell Research*, *315*(19), 3301–3311. https://doi.org/10.1016/j.yexcr.2009.09.013

Han, Y. K., Kim, Y.-G., Kim, J. Y., & Lee, G. M. (2010). Hyperosmotic stress induces autophagy and apoptosis in recombinant Chinese hamster ovary cell culture. *Biotechnology and Bioengineering*, *105*(6), 1187–1192. https://doi.org/10.1002/bit.22643

Hansen. (1993). Clathrin and HA2 adaptors: Effects of potassium depletion, hypertonic medium, and cytosol acidification. *The Journal of Cell Biology*, *121*(1), 61–72. https://doi.org/10.1083/jcb.121.1.61

Hanus, J., Zhang, H., Wang, Z., Liu, Q., Zhou, Q., & Wang, S. (2013). Induction of necrotic cell death by oxidative stress in retinal pigment epithelial cells. *Cell Death & Disease*, *4*(12), e965–e965. https://doi.org/10.1038/cddis.2013.478

Harayama, T., & Riezman, H. (2018). Understanding the diversity of membrane lipid composition. *Nature Reviews Molecular Cell Biology*, *19*(5), 281–296. https://doi.org/10.1038/nrm.2017.138

Hasegawa, J., Strunk, B. S., & Weisman, L. S. (2017). PI5P and PI(3,5)P2: Minor, but Essential Phosphoinositides. *Cell Structure and Function*, *42*(1), 49–60. https://doi.org/10.1247/csf.17003

Hasler, U., Nunes, P., Bouley, R., Lu, H. A. J., Matsuzaki, T., & Brown, D. (2008). Acute hypertonicity alters aquaporin-2 trafficking and induces a MAPK-dependent accumulation at the plasma membrane of renal epithelial cells. *The Journal of Biological Chemistry*, *283*(39), 26643–26661. https://doi.org/10.1074/jbc.M801071200

Hébert, E. (2006). Mannose-6-phosphate/insulin-like growth factor II receptor expression and tumor development. *Bioscience Reports*, *26*(1), 7–17. https://doi.org/10.1007/s10540-006-9002-3

Hentze, N., Le Breton, L., Wiesner, J., Kempf, G., & Mayer, M. P. (2016). Molecular mechanism of thermosensory function of human heat shock transcription factor Hsf1. *eLife*, *5*, e11576. https://doi.org/10.7554/eLife.11576

Heuser, J. (1980). Three-dimensional visualization of coated vesicle formation in fibroblasts. *The Journal of Cell Biology*, *84*(3), 560–583. https://doi.org/10.1083/jcb.84.3.560

Heuser, J. (1989). Effects of cytoplasmic acidification on clathrin lattice morphology. *The Journal of Cell Biology*, *108*(2), 401–411. https://doi.org/10.1083/jcb.108.2.401

Heuser, J. E., & Anderson, R. G. (1989). Hypertonic media inhibit receptor-mediated endocytosis by blocking clathrin-coated pit formation. *The Journal of Cell Biology*, *108*(2), 389–400. https://doi.org/10.1083/jcb.108.2.389

Hinze, C., & Boucrot, E. (2018). Endocytosis in proliferating, quiescent and terminally differentiated cells. *Journal of Cell Science*, *131*(23), jcs216804. https://doi.org/10.1242/jcs.216804

Hirota, K., Murata, M., Sachi, Y., Nakamura, H., Takeuchi, J., Mori, K., & Yodoi, J. (1999). Distinct Roles of Thioredoxin in the Cytoplasm and in the Nucleus: A two-step mechanism of redox regulation of transcription factor NF-κB *. *Journal of Biological Chemistry*, *274*(39), 27891–27897. https://doi.org/10.1074/jbc.274.39.27891

Hirst, J., Futter, C. E., & Hopkins, C. R. (1998). The Kinetics of Mannose 6-Phosphate Receptor Trafficking in the Endocytic Pathway in HEp-2 Cells: The Receptor Enters and Rapidly Leaves Multivesicular Endosomes without Accumulating in a Prelysosomal Compartment. *Molecular Biology of the Cell*, *9*(4), 809–816. https://doi.org/10.1091/mbc.9.4.809

Ho, S. N. (2006). Intracellular water homeostasis and the mammalian cellular osmotic stress response. *Journal of Cellular Physiology*, *206*(1), 9–15. https://doi.org/10.1002/jcp.20445

Hoeller, D., Volarevic, S., & Dikic, I. (2005). Compartmentalization of growth factor receptor signalling. *Current Opinion in Cell Biology*, *17*(2), 107–111. https://doi.org/10.1016/j.ceb.2005.01.001

Holst, M. R., Vidal-Quadras, M., Larsson, E., Song, J., Hubert, M., Blomberg, J., Lundborg, M., Landström, M., & Lundmark, R. (2017). Clathrin-Independent Endocytosis Suppresses Cancer Cell Blebbing and Invasion. *Cell Reports*, *20*(8), 1893–1905. https://doi.org/10.1016/j.celrep.2017.08.006

Honegger, A. M., Schmidt, A., Ullrich, A., & Schlessinger, J. (1990). Separate endocytic pathways of kinase-defective and -active EGF receptor mutants expressed in same cells. *Journal of Cell Biology*, *110*(5), 1541–1548. https://doi.org/10.1083/jcb.110.5.1541

Hong, G., Wu, J. Z., Robinson, J. T., Wang, H., Zhang, B., & Dai, H. (2012). Three-dimensional imaging of single nanotube molecule endocytosis on plasmonic substrates. *Nature Communications*, *3*(1), 700. https://doi.org/10.1038/ncomms1698

Hörmann, K., Stukalov, A., Müller, A. C., Heinz, L. X., Superti-Furga, G., Colinge, J., & Bennett, K. L. (2016). A Surface Biotinylation Strategy for Reproducible Plasma Membrane Protein Purification and Tracking of Genetic and Drug-Induced Alterations. *Journal of Proteome Research*, *15*(2), 647–658. https://doi.org/10.1021/acs.jproteome.5b01066

Howes, M. T., Mayor, S., & Parton, R. G. (2010). Molecules, mechanisms, and cellular roles of clathrin-independent endocytosis. *Current Opinion in Cell Biology*, *22*(4), 519–527. https://doi.org/10.1016/j.ceb.2010.04.001

Hu, Y., Jiang, L., Wang, G., Song, Y., Shan, Z., Wang, X., Deng, G., Shi, J., Tian, G., Zeng, X., Liu, L., Chen, H., & Li, C. (2024). M6PR interacts with the HA2 subunit of influenza A virus to facilitate the fusion of viral and endosomal membranes. *Science China Life Sciences*, *67*(3), 579–595. https://doi.org/10.1007/s11427-023-2471-4

Hu, Z., Yuan, J., Long, M., Jiang, J., Zhang, Y., Zhang, T., Xu, M., Fan, Y., Tanyi, J. L., Montone, K. T., Tavana, O., Chan, H. M., Hu, X., Vonderheide, R. H., & Zhang, L. (2021). The Cancer Surfaceome Atlas integrates genomic, functional and drug response data to identify actionable targets. *Nature Cancer*, *2*(12), 1406–1422. https://doi.org/10.1038/s43018-021-00282-w

Huot, J., Houle, F., Marceau, F., & Landry, J. (1997). Oxidative stress-induced actin reorganization mediated by the p38 mitogen-activated protein kinase/heat shock protein 27 pathway in vascular endothelial cells. *Circulation Research*, *80*(3), 383–392. https://doi.org/10.1161/01.res.80.3.383

Idone, V., Tam, C., & Andrews, N. W. (2008). Two-way traffic on the road to plasma membrane repair. *Trends in Cell Biology*, *18*(11), 552–559. https://doi.org/10.1016/j.tcb.2008.09.001

Idone, V., Tam, C., Goss, J. W., Toomre, D., Pypaert, M., & Andrews, N. W. (2008). Repair of injured plasma membrane by rapid Ca2+-dependent endocytosis. *Journal of Cell Biology*, *180*(5), 905–914. https://doi.org/10.1083/jcb.200708010

Ingólfsson, H. I., Melo, M. N., van Eerden, F. J., Arnarez, C., Lopez, C. A., Wassenaar, T. A., Periole, X., de Vries, A. H., Tieleman, D. P., & Marrink, S. J. (2014). Lipid Organization of the Plasma Membrane. *Journal of the American Chemical Society*, *136*(41), 14554–14559. https://doi.org/10.1021/ja507832e

Ishizawar, R., & Parsons, S. J. (2004). C-Src and cooperating partners in human cancer. *Cancer Cell*, *6*(3), 209–214. https://doi.org/10.1016/j.ccr.2004.09.001

Ito, S., Oishi, M., Ogata, S., Uemura, T., Couraud, P.-O., Masuda, T., & Ohtsuki, S. (2020). Identification of Cell-Surface Proteins Endocytosed by Human Brain Microvascular Endothelial Cells In Vitro. *Pharmaceutics*, *12*(6), Article 6. https://doi.org/10.3390/pharmaceutics12060579

Izquierdo, L. A., Barros, D. M., Vianna, M. R. M., Coitinho, A., de Silva, T. D., Choi, H., Moletta, B., Medina, J. H., & Izquierdo, I. (2002). Molecular Pharmacological Dissection of Short- and Long-Term Memory. *Cellular and Molecular Neurobiology*, *22*(3), 269–287. https://doi.org/10.1023/A:1020715800956

Jahn, R., & Südhof, T. C. (1999). Membrane Fusion and Exocytosis. *Annual Review of Biochemistry*, *68*(Volume 68, 1999), 863–911. https://doi.org/10.1146/annurev.biochem.68.1.863

Jarousse, N., Wilson, J. D., Arac, D., Rizo, J., & Kelly, R. B. (2003). Endocytosis of synaptotagmin 1 is mediated by a novel, tryptophan-containing motif. *Traffic (Copenhagen, Denmark)*, *4*(7), 468–478. https://doi.org/10.1034/j.1600-0854.2003.00101.x

Jaye, S., Sandau, U. S., & Saugstad, J. A. (2024). Clathrin mediated endocytosis in Alzheimer's disease: Cell type specific involvement in amyloid beta pathology. *Frontiers in Aging Neuroscience*, *16*. https://doi.org/10.3389/fnagi.2024.1378576

Ji, B., Ito, K., Sekine, S., Tajima, A., & Horie, T. (2004). Ethacrynic-acid-induced glutathione depletion and oxidative stress in normal and Mrp2-deficient rat liver. *Free Radical Biology and Medicine*, *37*(11), 1718–1729. https://doi.org/10.1016/j.freeradbiomed.2004.08.020

Ji, J., Bi, F., Zhang, X., Zhang, Z., Xie, Y., & Yang, Q. (2024). Single-cell transcriptome analysis revealed heterogeneity in glycolysis and identified IGF2 as a therapeutic target for ovarian cancer subtypes. *BMC Cancer*, *24*(1), 926. https://doi.org/10.1186/s12885-024-12688-7

Jockusch, W. J., Praefcke, G. J. K., McMahon, H. T., & Lagnado, L. (2005). Clathrin-dependent and clathrin-independent retrieval of synaptic vesicles in retinal bipolar cells. *Neuron*, *46*(6), 869–878. https://doi.org/10.1016/j.neuron.2005.05.004

Jones, D. P. (2008). Radical-free biology of oxidative stress. *American Journal of Physiology-Cell Physiology*, *295*(4), C849–C868. https://doi.org/10.1152/ajpcell.00283.2008

Jung, W. K., Park, S.-B., Yu, H. Y., Kim, Y. H., & Kim, J. (2022). Effect of Esculetin on Tert-Butyl Hydroperoxide-Induced Oxidative Injury in Retinal Pigment Epithelial Cells In Vitro. *Molecules*, *27*(24), Article 24. https://doi.org/10.3390/molecules27248970

Kanamori, H., Takemura, G., Maruyama, R., Goto, K., Tsujimoto, A., Ogino, A., Li, L., Kawamura, I., Takeyama, T., Kawaguchi, T., Nagashima, K., Fujiwara, T., Fujiwara, H., Seishima, M., & Minatoguchi, S. (2009). Functional Significance and Morphological Characterization of Starvation-Induced Autophagy in the Adult Heart. *The American Journal of Pathology*, *174*(5), 1705–1714. https://doi.org/10.2353/ajpath.2009.080875

Kaur, S., Fielding, A. B., Gassner, G., Carter, N. J., & Royle, S. J. (2014). An unmet actin requirement explains the mitotic inhibition of clathrin-mediated endocytosis. *eLife*, *3*, e00829. https://doi.org/10.7554/eLife.00829

Kavaliauskiene, S., Nymark, C.-M., Bergan, J., Simm, R., Sylvänne, T., Simolin, H., Ekroos, K., Skotland, T., & Sandvig, K. (2014). Cell density-induced changes in lipid composition and intracellular trafficking. *Cellular and Molecular Life Sciences*, *71*(6), 1097–1116. https://doi.org/10.1007/s00018-013-1441-y

Kaven, C., Spraul ,Christoph W., Zavazava ,Nicholas, Lang ,Gerhard K., & and Lang, G. E. (2000). Growth factor combinations modulate human retinal pigment epithelial cell proliferation. *Current Eye Research*, *20*(6), 480–487. https://doi.org/10.1076/0271-3683(200006)2061-YFT480

Kerr, A., & Baxter, R. C. (2022). Noncoding RNA actions through IGFs and IGF binding proteins in cancer. *Oncogene*, *41*(25), 3385–3393. https://doi.org/10.1038/s41388-022-02353-3

Khan, E. M., Heidinger, J. M., Levy, M., Lisanti, M. P., Ravid, T., & Goldkorn, T. (2006). Epidermal Growth Factor Receptor Exposed to Oxidative Stress Undergoes Src- and Caveolin-1-dependent Perinuclear Trafficking *. *Journal of Biological Chemistry*, *281*(20), 14486–14493. https://doi.org/10.1074/jbc.M509332200

Kholodenko, B. N. (2006). Cell-signalling dynamics in time and space. *Nature Reviews Molecular Cell Biology*, *7*(3), 165–176. https://doi.org/10.1038/nrm1838

Kilpatrick, B. S., Yates, E., Grimm, C., Schapira, A. H., & Patel, S. (2016). Endo-lysosomal TRP mucolipin-1 channels trigger global ER Ca2+ release and Ca2+ influx. *Journal of Cell Science*, *129*(20), 3859–3867. https://doi.org/10.1242/jcs.190322

Kim, H.-J., Joo, H. J., Kim, Y. H., Ahn, S., Chang, J., Hwang, K.-B., Lee, D.-H., & Lee, K.-J. (2011). Systemic Analysis of Heat Shock Response Induced by Heat Shock and a Proteasome Inhibitor MG132. *PLOS ONE*, *6*(6), e20252. https://doi.org/10.1371/journal.pone.0020252

King, L. S., Kozono, D., & Agre, P. (2004). From structure to disease: The evolving tale of aquaporin biology. *Nature Reviews. Molecular Cell Biology*, *5*(9), 687–698. https://doi.org/10.1038/nrm1469

Kirkham, M., & Parton, R. G. (2005). Clathrin-independent endocytosis: New insights into caveolae and non-caveolar lipid raft carriers. *Biochimica Et Biophysica Acta*, *1745*(3), 273–286. https://doi.org/10.1016/j.bbamcr.2005.06.002

Klumperman, J., Hille, A., Veenendaal, T., Oorschot, V., Stoorvogel, W., von Figura, K., & Geuze, H. J. (1993). Differences in the endosomal distributions of the two mannose 6-phosphate receptors. *The Journal of Cell Biology*, *121*(5), 997–1010. https://doi.org/10.1083/jcb.121.5.997

Kornfeld, S., & Mellman, I. (1989). The biogenesis of lysosomes. *Annual Review of Cell Biology*, *5*, 483–525. https://doi.org/10.1146/annurev.cb.05.110189.002411

Koyama, H., Kamogashira, T., & Yamasoba, T. (2024). Heavy Metal Exposure: Molecular Pathways, Clinical Implications, and Protective Strategies. *Antioxidants*, *13*(1), 76. https://doi.org/10.3390/antiox13010076

Krause, T. L., Fishman, H. M., Ballinger, M. L., & Bittner, G. D. (1994). Extent and mechanism of sealing in transected giant axons of squid and earthworms. *The Journal of Neuroscience: The Official Journal of the Society for Neuroscience*, *14*(11 Pt 1), 6638–6651. https://doi.org/10.1523/JNEUROSCI.14-11-06638.1994

Kültz, D. (2003). Evolution of the cellular stress proteome: From monophyletic origin to ubiquitous function. *The Journal of Experimental Biology*, *206*(Pt 18), 3119–3124. https://doi.org/10.1242/jeb.00549

Kuznetsova, A. V., Kurinov, A. M., & Aleksandrova, M. A. (2014). Cell Models to Study Regulation of Cell Transformation in Pathologies of Retinal Pigment Epithelium. *Journal of Ophthalmology*, *2014*(1), 801787. https://doi.org/10.1155/2014/801787

Langó, T., Kuffa, K., Tóth, G., Turiák, L., Drahos, L., & Tusnády, G. E. (2023). Comprehensive Discovery of the Accessible Primary Amino Group-Containing Segments from Cell Surface Proteins by Fine-Tuning a High-Throughput Biotinylation Method. *International Journal of Molecular Sciences*, *24*(1), Article 1. https://doi.org/10.3390/ijms24010273

Lara-Guzmán, O. J., Gil-Izquierdo, Á., Medina, S., Osorio, E., Álvarez-Quintero, R., Zuluaga, N., Oger, C., Galano, J.-M., Durand, T., & Muñoz-Durango, K. (2018). Oxidized LDL triggers changes in oxidative stress and inflammatory biomarkers in human macrophages. *Redox Biology*, *15*, 1–11. https://doi.org/10.1016/j.redox.2017.11.017

Laulagnier, K., Schieber, N. L., Maritzen, T., Haucke, V., Parton, R. G., & Gruenberg, J. (2011). Role of AP1 and Gadkin in the traffic of secretory endo-lysosomes. *Molecular Biology of the Cell*, *22*(12), 2068–2082. https://doi.org/10.1091/mbc.e11-03-0193

Lee, J., Kim, J., Son, K., d'Alexandry d'Orengiani, A.-L. P. H., & Min, J.-Y. (2017). Acid phosphatase 2 (ACP2) is required for membrane fusion during influenza virus entry. *Scientific Reports*, *7*(1), 43893. https://doi.org/10.1038/srep43893

Lee, V. H. L. (2000). Membrane transporters. *European Journal of Pharmaceutical Sciences*, *11*, S41–S50. https://doi.org/10.1016/S0928-0987(00)00163-9

Li, D., Randhawa, V. K., Patel, N., Hayashi, M., & Klip, A. (2001). Hyperosmolarity reduces GLUT4 endocytosis and increases its exocytosis from a VAMP2-independent pool in l6 muscle cells. *The Journal of Biological Chemistry*, *276*(25), 22883–22891. https://doi.org/10.1074/jbc.M010143200

Li, H., You, L., Xie, J., Pan, H., & Han, W. (2017). The roles of subcellularly located EGFR in autophagy. *Cellular Signalling*, *35*, 223–230. https://doi.org/10.1016/j.cellsig.2017.04.012

Li, Y., Zhu, X., Wang, K., Zhu, L., Murray, M., & Zhou, F. (2023). Ginkgo biloba extracts (GBE) protect human RPE cells from t-BHP-induced oxidative stress and necrosis by activating the Nrf2-mediated antioxidant defence. *Journal of Pharmacy and Pharmacology*, *75*(1), 105–116. https://doi.org/10.1093/jpp/rgac069

Liang, X., Arullampalam, P., Yang, Z., & Ming, X.-F. (2019). Hypoxia Enhances Endothelial Intercellular Adhesion Molecule 1 Protein Level Through Upregulation of Arginase Type II and Mitochondrial Oxidative Stress. *Frontiers in Physiology*, *10*, 1003. https://doi.org/10.3389/fphys.2019.01003

Liberali, P., Rämö, P., & Pelkmans, L. (2008). Protein Kinases: Starting a Molecular Systems View of Endocytosis. *Annual Review of Cell and Developmental Biology*, *24*(1), 501–523. https://doi.org/10.1146/annurev.cellbio.041008.145637

Lifton, R. P., Gharavi, A. G., & Geller, D. S. (2001). Molecular Mechanisms of Human Hypertension. *Cell*, *104*(4), 545–556. https://doi.org/10.1016/S0092-8674(01)00241-0

Lin, S. X., Mallet, W. G., Huang, A. Y., & Maxfield, F. R. (2004). Endocytosed Cation-Independent Mannose 6-Phosphate Receptor Traffics via the Endocytic Recycling Compartment en Route to the trans-Golgi Network and a Subpopulation of Late Endosomes. *Molecular Biology of the Cell*, *15*(2), 721–733. https://doi.org/10.1091/mbc.e03-07-0497

Linnell, J., Groeger, G., & Hassan, A. B. (2001). Real Time Kinetics of Insulin-like Growth Factor II (IGF-II) Interaction with the IGF-II/Mannose 6-Phosphate Receptor: THE EFFECTS OF DOMAIN 13

AND pH *. *Journal of Biological Chemistry*, *276*(26), 23986–23991. https://doi.org/10.1074/jbc.M100700200

Liu, X. F., Dd, Z., T, X., Th, M., Cb, L., Hj, L., F, W., C, S., C, L., Cw, L., & Jl, H. (2017). Nrf2, a Potential Therapeutic Target against Oxidative Stress in Corneal Diseases. *Oxidative Medicine and Cellular Longevity*, *2017*. https://doi.org/10.1155/2017/2326178

Loboda, A., M, D., E, P., A, J., & J, D. (2016). Role of Nrf2/HO-1 system in development, oxidative stress response and diseases: An evolutionarily conserved mechanism. *Cellular and Molecular Life Sciences : CMLS*, *73*(17). https://doi.org/10.1007/s00018-016-2223-0

López-Hernández, T., Haucke, V., & Maritzen, T. (2020). Endocytosis in the adaptation to cellular stress. *Cell Stress*, *4*(10), 230–247. https://doi.org/10.15698/cst2020.10.232

López-Hernández, T., Puchkov, D., Krause, E., Maritzen, T., & Haucke, V. (2020). Endocytic regulation of cellular ion homeostasis controls lysosome biogenesis. *Nature Cell Biology*, *22*(7), 815–827. https://doi.org/10.1038/s41556-020-0535-7

Lorent, J. H., Levental, K. R., Ganesan, L., Rivera-Longsworth, G., Sezgin, E., Doktorova, M., Lyman, E., & Levental, I. (2020). Plasma membranes are asymmetric in lipid unsaturation, packing and protein shape. *Nature Chemical Biology*, *16*(6), 644–652. https://doi.org/10.1038/s41589-020-0529-6

Luh, E. H., Shackford, S. R., Shatos, M. A., & Pietropaoli, J. A. (1996). The effects of hyperosmolarity on the viability and function of endothelial cells. *The Journal of Surgical Research*, *60*(1), 122–128. https://doi.org/10.1006/jsre.1996.0020

Lundmark, R., Doherty, G. J., Howes, M. T., Cortese, K., Vallis, Y., Parton, R. G., & McMahon, H. T. (2008). The GTPase-activating protein GRAF1 regulates the CLIC/GEEC endocytic pathway. *Current Biology: CB*, *18*(22), 1802–1808. https://doi.org/10.1016/j.cub.2008.10.044

Ma, X., Xu, L., Alberobello, A. T., Gavrilova, O., Bagattin, A., Skarulis, M., Liu, J., Finkel, T., & Mueller, E. (2015). Celastrol Protects against Obesity and Metabolic Dysfunction through Activation of a HSF1-PGC1α Transcriptional Axis. *Cell Metabolism*, *22*(4), 695–708. https://doi.org/10.1016/j.cmet.2015.08.005

Macheda, M. L., Rogers, S., & Best, J. D. (2005). Molecular and cellular regulation of glucose transporter (GLUT) proteins in cancer. *Journal of Cellular Physiology*, *202*(3), 654–662. https://doi.org/10.1002/jcp.20166

Mahat, D. B., Salamanca, H. H., Duarte, F. M., Danko, C. G., & Lis, J. T. (2016). Mammalian Heat Shock Response and Mechanisms Underlying Its Genome-wide Transcriptional Regulation. *Molecular Cell*, *62*(1), 63–78. https://doi.org/10.1016/j.molcel.2016.02.025

Malorni, W., Iosi, F., Santini, M. T., & Testa, U. (1993). Menadione-induced oxidative stress leads to a rapid down-modulation of transferrin receptor recycling. *Journal of Cell Science*, *106*(1), 309–318. https://doi.org/10.1242/jcs.106.1.309

Matta, C., Boocock, D. J., Fellows, C. R., Miosge, N., Dixon, J. E., Liddell, S., Smith, J., & Mobasheri, A. (2019). Molecular phenotyping of the surfaceome of migratory chondroprogenitors and mesenchymal stem cells using biotinylation, glycocapture and quantitative LC-MS/MS proteomic analysis. *Scientific Reports*, *9*(1), 9018. https://doi.org/10.1038/s41598-019-44957-y

Maxfield, F. R., & McGraw, T. E. (2004). Endocytic recycling. *Nature Reviews Molecular Cell Biology*, *5*(2), 121–132. https://doi.org/10.1038/nrm1315

Mayle, K. M., Le, A. M., & Kamei, D. T. (2012). The intracellular trafficking pathway of transferrin. *Biochimica et Biophysica Acta (BBA) - General Subjects*, *1820*(3), 264–281. https://doi.org/10.1016/j.bbagen.2011.09.009

McMahon, H. T., & Boucrot, E. (2011). Molecular mechanism and physiological functions of clathrin-mediated endocytosis. *Nature Reviews Molecular Cell Biology*, *12*(8), 517–533. https://doi.org/10.1038/nrm3151

Medina, D. L., Fraldi, A., Bouche, V., Annunziata, F., Mansueto, G., Spampanato, C., Puri, C., Pignata, A., Martina, J. A., Sardiello, M., Palmieri, M., Polishchuk, R., Puertollano, R., & Ballabio, A. (2011). Transcriptional Activation of Lysosomal Exocytosis Promotes Cellular Clearance. *Developmental Cell*, *21*(3), 421–430. https://doi.org/10.1016/j.devcel.2011.07.016

Meier-Hellmann, A., Reinhart, K., & Bloos, F. (1995). Hypertonic Solutions in Emergency Medicine. In J.-L. Vincent (Ed.), *Yearbook of Intensive Care and Emergency Medicine* (pp. 935–944). Springer. https://doi.org/10.1007/978-3-642-79154-3_79

Mentrup, T., Cabrera-Cabrera, F., Fluhrer, R., & Schröder, B. (2020). Physiological functions of SPP/SPPL intramembrane proteases. *Cellular and Molecular Life Sciences*, *77*(15), 2959–2979. https://doi.org/10.1007/s00018-020-03470-6

Mentrup, T., Leinung, N., Patel, M., Fluhrer, R., & Schröder, B. (2024). The role of SPP/SPPL intramembrane proteases in membrane protein homeostasis. *The FEBS Journal*, *291*(1), 25–44. https://doi.org/10.1111/febs.16941

Mentrup, T., & Schröder, B. (2022). Signal peptide peptidase-like 2 proteases: Regulatory switches or proteasome of the membrane? *Biochimica et Biophysica Acta (BBA) - Molecular Cell Research*, *1869*(1), 119163. https://doi.org/10.1016/j.bbamcr.2021.119163

Mentrup, T., Theodorou, K., Cabrera-Cabrera, F., Helbig, A. O., Happ, K., Gijbels, M., Gradtke, A.-C., Rabe, B., Fukumori, A., Steiner, H., Tholey, A., Fluhrer, R., Donners, M., & Schröder, B. (2019). Atherogenic LOX-1 signaling is controlled by SPPL2-mediated intramembrane proteolysis. *Journal of Experimental Medicine*, *216*(4), 807–830. https://doi.org/10.1084/jem.20171438

Mettlen, M., Chen, P.-H., Srinivasan, S., Danuser, G., & Schmid, S. L. (2018). Regulation of Clathrin-Mediated Endocytosis. *Annual Review of Biochemistry*, *87*(Volume 87, 2018), 871–896. https://doi.org/10.1146/annurev-biochem-062917-012644

Meyer-Helms, B., Stahnke, T., Goldbaum, O., & Richter-Landsberg, C. (2007). Effect of proteasomal inhibition by MG-132 on inclusion body formation in astrocytes. *BMC Neuroscience*, *8*(1), P12. https://doi.org/10.1186/1471-2202-8-S1-P12

Miyakawa, H., Woo, S. K., Dahl, S. C., Handler, J. S., & Kwon, H. M. (1999). Tonicity-responsive enhancer binding protein, a rel-like protein that stimulates transcription in response to hypertonicity. *Proceedings of the National Academy of Sciences of the United States of America*, *96*(5), 2538–2542. https://doi.org/10.1073/pnas.96.5.2538

Miyake, K., McNeil, P. L., Suzuki, K., Tsunoda, R., & Sugai, N. (2001). An actin barrier to resealing. *Journal of Cell Science*, *114*(Pt 19), 3487–3494. https://doi.org/10.1242/jcs.114.19.3487

Miyano, T., Suzuki, A., Konta, H., & Sakamoto, N. (2025). Hyperosmotic Stress Promotes the Nuclear Translocation of TFEB in Tubular Epithelial Cells Depending on Intracellular Ca2+ Signals via TRPML Channels. *Cellular and Molecular Bioengineering*, *18*(1), 39–52. https://doi.org/10.1007/s12195-024-00839-6

Morgan, B. P. (1989). Complement membrane attack on nucleated cells: Resistance, recovery and non-lethal effects. *Biochemical Journal*, *264*(1), 1–14. https://doi.org/10.1042/bj2640001

Morgan, M. R., Humphries, M. J., & Bass, M. D. (2007). Synergistic control of cell adhesion by integrins and syndecans. *Nature Reviews Molecular Cell Biology*, *8*(12), 957–969. https://doi.org/10.1038/nrm2289

Morimoto, R. I. (2011). The Heat Shock Response: Systems Biology of Proteotoxic Stress in Aging and Disease. *Cold Spring Harbor Symposia on Quantitative Biology*, *76*, 91–99. https://doi.org/10.1101/sqb.2012.76.010637

Nau, R., Desel, H., Lassek, C., Thiel, A., Schinschke, S., Rössing, R., Kolenda, H., & Prange, H. W. (1997). Slow elimination of mannitol from human cerebrospinal fluid. *European Journal of Clinical Pharmacology*, *53*(3–4), 271–274. https://doi.org/10.1007/s002280050375

Neuhofer, W. (2010). Role of NFAT5 in Inflammatory Disorders Associated with Osmotic Stress. *Current Genomics*, *11*(8), 584–590. https://doi.org/10.2174/138920210793360961

Neuhofer, W., Woo, S. K., Na, K. Y., Grunbein, R., Park, W. K., Nahm, O., Beck, F.-X., & Kwon, H. M. (2002). Regulation of TonEBP transcriptional activator in MDCK cells following changes in ambient tonicity. *American Journal of Physiology. Cell Physiology*, *283*(6), C1604-1611. https://doi.org/10.1152/ajpcell.00216.2002

Niehage, C., Karbanová, J., Steenblock, C., Corbeil, D., & Hoflack, B. (2016). Cell Surface Proteome of Dental Pulp Stem Cells Identified by Label-Free Mass Spectrometry. *PLOS ONE*, *11*(8), e0159824. https://doi.org/10.1371/journal.pone.0159824

Nunes, P., Ernandez, T., Roth, I., Qiao, X., Strebel, D., Bouley, R., Charollais, A., Ramadori, P., Foti, M., Meda, P., Féraille, E., Brown, D., & Hasler, U. (2013). Hypertonic stress promotes autophagy and microtubule-dependent autophagosomal clusters. *Autophagy*, *9*(4), 550–567. https://doi.org/10.4161/auto.23662

Ono, K., & Han, J. (2000). The p38 signal transduction pathway Activation and function. *Cellular Signalling*, *12*(1), 1–13. https://doi.org/10.1016/S0898-6568(99)00071-6

Orlowski, J., & Grinstein, S. (2004). Diversity of the mammalian sodium/proton exchanger SLC9 gene family. *Pflügers Archiv*, *447*(5), 549–565. https://doi.org/10.1007/s00424-003-1110-3

Oyarzún, J. E., Lagos, J., Vázquez, M. C., Valls, C., De la Fuente, C., Yuseff, M. I., Alvarez, A. R., & Zanlungo, S. (2019). Lysosome motility and distribution: Relevance in health and disease. *Biochimica et Biophysica Acta (BBA) - Molecular Basis of Disease*, *1865*(6), 1076–1087. https://doi.org/10.1016/j.bbadis.2019.03.009

Özlü, N., Qureshi, M. H., Toyoda, Y., Renard, B. Y., Mollaoglu, G., Özkan, N. E., Bulbul, S., Poser, I., Timm, W., Hyman, A. A., Mitchison, T. J., & Steen, J. A. (2015). Quantitative comparison of a human cancer cell surface proteome between interphase and mitosis. *The EMBO Journal*, *34*(2), 251–265. https://doi.org/10.15252/embj.201385162

Pacher, M., Seewald, M. J., Mikula, M., Oehler, S., Mogg, M., Vinatzer, U., Eger, A., Schweifer, N., Varecka, R., Sommergruber, W., Mikulits, W., & Schreiber, M. (2007). Impact of constitutive IGF1/IGF2 stimulation on the transcriptional program of human breast cancer cells. *Carcinogenesis*, *28*(1), 49–59. https://doi.org/10.1093/carcin/bgl091

Pang, X., He, X., Qiu, Z., Zhang, H., Xie, R., Liu, Z., Gu, Y., Zhao, N., Xiang, Q., & Cui, Y. (2023). Targeting integrin pathways: Mechanisms and advances in therapy. *Signal Transduction and Targeted Therapy*, *8*(1), 1. https://doi.org/10.1038/s41392-022-01259-6

Parry, S. N., Ellis, N., Li, Z., Maitz, P., & Witting, P. K. (2008). Myoglobin induces oxidative stress and decreases endocytosis and monolayer permissiveness in cultured kidney epithelial cells without affecting viability. *Kidney & Blood Pressure Research*, *31*(1), 16–28. https://doi.org/10.1159/000112921

Parton, R. G., & del Pozo, M. A. (2013). Caveolae as plasma membrane sensors, protectors and organizers. *Nature Reviews Molecular Cell Biology*, *14*(2), 98–112. https://doi.org/10.1038/nrm3512

Parton, R. G., & Simons, K. (2007). The multiple faces of caveolae. *Nature Reviews Molecular Cell Biology*, *8*(3), 185–194. https://doi.org/10.1038/nrm2122

Pickett, J. A., & Edwardson, J. M. (2006). Compound Exocytosis: Mechanisms and Functional Significance. *Traffic*, *7*(2), 109–116. https://doi.org/10.1111/j.1600-0854.2005.00372.x

Rabin, D. M., Rabin, R. L., Blenkinsop, T. A., Temple, S., & Stern, J. H. (2012). Chronic oxidative stress upregulates Drusen-related protein expression in adult human RPE stem cell-derived RPE cells: A novel culture model for dry AMD. *Aging*, *5*(1), 51–66. https://doi.org/10.18632/aging.100516

Rambhatla, L., Chiu, C.-P., Glickman, R. D., & Rowe-Rendleman, C. (2002). In Vitro Differentiation Capacity of Telomerase Immortalized Human RPE Cells. *Investigative Ophthalmology & Visual Science*, *43*(5), 1622–1630.

Rand, R. P. (2004). Probing the role of water in protein conformation and function. *Philosophical Transactions of the Royal Society of London. Series B, Biological Sciences*, *359*(1448), 1277–1284; discussion 1284-1285. https://doi.org/10.1098/rstb.2004.1504

Rao, S. K., Huynh, C., Proux-Gillardeaux, V., Galli, T., & Andrews, N. W. (2004). Identification of SNAREs Involved in Synaptotagmin VII-regulated Lysosomal Exocytosis*. *Journal of Biological Chemistry*, *279*(19), 20471–20479. https://doi.org/10.1074/jbc.M400798200

Ratcliffe, P. J. (2013). Oxygen sensing and hypoxia signalling pathways in animals: The implications of physiology for cancer. *The Journal of Physiology*, *591*(8), 2027–2042. https://doi.org/10.1113/jphysiol.2013.251470

Ravi, S., Peña, K. A., Chu, C. T., & Kiselyov, K. (2016). Biphasic regulation of lysosomal exocytosis by oxidative stress. *Cell Calcium*, *60*(5), 356–362. https://doi.org/10.1016/j.ceca.2016.08.002

Reczek, D., Schwake, M., Schröder, J., Hughes, H., Blanz, J., Jin, X., Brondyk, W., Patten, S. V., Edmunds, T., & Saftig, P. (2007). LIMP-2 Is a Receptor for Lysosomal Mannose-6-Phosphate-Independent Targeting of β-Glucocerebrosidase. *Cell*, *131*(4), 770–783. https://doi.org/10.1016/j.cell.2007.10.018

Reddy, A., Caler, E. V., & Andrews, N. W. (2001). Plasma Membrane Repair Is Mediated by Ca2+-Regulated Exocytosis of Lysosomes. *Cell*, *106*(2), 157–169. https://doi.org/10.1016/S0092-8674(01)00421-4

Reinecke, J., & Caplan, S. (2014). Endocytosis and the Src family of non-receptor tyrosine kinases. *Biomolecular Concepts*, *5*(2), 143–155. https://doi.org/10.1515/bmc-2014-0003

Ren, L., Mellander, L. J., Keighron, J., Cans, A.-S., Kurczy, M. E., Svir, I., Oleinick, A., Amatore, C., & Ewing, A. G. (2016). The evidence for open and closed exocytosis as the primary release mechanism. *Quarterly Reviews of Biophysics*, *49*, e12. https://doi.org/10.1017/S0033583516000081

Robinson, M. S. (2015). Forty Years of Clathrin-coated Vesicles. *Traffic*, *16*(12), 1210–1238. https://doi.org/10.1111/tra.12335

Ron, D., & Walter, P. (2007). Signal integration in the endoplasmic reticulum unfolded protein response. *Nature Reviews Molecular Cell Biology*, *8*(7), 519–529. https://doi.org/10.1038/nrm2199

Rose, M., Cardon, T., Aboulouard, S., Hajjaji, N., Kobeissy, F., Duhamel, M., Fournier, I., & Salzet, M. (2021). Surfaceome Proteomic of Glioblastoma Revealed Potential Targets for Immunotherapy. *Frontiers in Immunology*, *12*, 746168. https://doi.org/10.3389/fimmu.2021.746168

Rosenbaum, D. M., Rasmussen, S. G. F., & Kobilka, B. K. (2009). The structure and function of G-protein-coupled receptors. *Nature*, *459*(7245), 356–363. https://doi.org/10.1038/nature08144

Ross, E., Ata, R., Thavarajah, T., Medvedev, S., Bowden, P., Marshall, J. G., & Antonescu, C. N. (2015). AMP-Activated Protein Kinase Regulates the Cell Surface Proteome and Integrin Membrane Traffic. *PLOS ONE*, *10*(5), e0128013. https://doi.org/10.1371/journal.pone.0128013

Rothberg, K. G., Heuser, J. E., Donzell, W. C., Ying, Y. S., Glenney, J. R., & Anderson, R. G. (1992). Caveolin, a protein component of caveolae membrane coats. *Cell*, *68*(4), 673–682. https://doi.org/10.1016/0092-8674(92)90143-z

Rudehill, A., Gordon, E., Ohman, G., Lindqvist, C., & Andersson, P. (1993). Pharmacokinetics and effects of mannitol on hemodynamics, blood and cerebrospinal fluid electrolytes, and osmolality during intracranial surgery. *Journal of Neurosurgical Anesthesiology*, *5*(1), 4–12. https://doi.org/10.1097/00008506-199301000-00002

S, R., S, M., P, N., Ws, R., & Cg, V. (2021). Health benefits of cyanidin-3-glucoside as a potent modulator of Nrf2-mediated oxidative stress. *Inflammopharmacology*, *29*(4). https://doi.org/10.1007/s10787-021-00799-7

Sáez, J. C., Berthoud, V. M., Brañes, M. C., Martínez, A. D., & Beyer, E. C. (2003). Plasma Membrane Channels Formed by Connexins: Their Regulation and Functions. *Physiological Reviews*, *83*(4), 1359–1400. https://doi.org/10.1152/physrev.00007.2003

Saftig, P., & Haas, A. (2016). Turn up the lysosome. *Nature Cell Biology*, *18*(10), 1025–1027. https://doi.org/10.1038/ncb3409

Sandilands, E., & Frame, M. C. (2008). Endosomal trafficking of Src tyrosine kinase. *Trends in Cell Biology*, *18*(7), 322–329. https://doi.org/10.1016/j.tcb.2008.05.004

Sandvig, K., Kavaliauskiene, S., & Skotland, T. (2018). Clathrin-independent endocytosis: An increasing degree of complexity. *Histochemistry and Cell Biology*, *150*(2), 107–118. https://doi.org/10.1007/s00418-018-1678-5

Sandvig, K., & van Deurs, B. (2005). Delivery into cells: Lessons learned from plant and bacterial toxins. *Gene Therapy*, *12*(11), 865–872. https://doi.org/10.1038/sj.gt.3302525

Santos, B. C., Pullman, J. M., Chevaile, A., Welch, W. J., & Gullans, S. R. (2003). Chronic hyperosmolarity mediates constitutive expression of molecular chaperones and resistance to injury. *American Journal of Physiology. Renal Physiology*, *284*(3), F564-574. https://doi.org/10.1152/ajprenal.00058.2002

Sardiello, M., Palmieri, M., di Ronza, A., Medina, D. L., Valenza, M., Gennarino, V. A., Di Malta, C., Donaudy, F., Embrione, V., Polishchuk, R. S., Banfi, S., Parenti, G., Cattaneo, E., & Ballabio, A. (2009). A Gene Network Regulating Lysosomal Biogenesis and Function. *Science*, *325*(5939), 473–477. https://doi.org/10.1126/science.1174447

Schaffer, B. S., Lin, M.-F., Byrd, J. C., Park, J. H. Y., & MacDonald, R. G. (2003). Opposing Roles for the Insulin-Like Growth Factor (IGF)-II and Mannose 6-Phosphate (Man-6-P) Binding Activities of the IGF-II/Man-6-P Receptor in the Growth of Prostate Cancer Cells. *Endocrinology*, *144*(3), 955–966. https://doi.org/10.1210/en.2002-220751

Scheiffele, P., Verkade, P., Fra, A. M., Virta, H., Simons, K., & Ikonen, E. (1998). Caveolin-1 and -2 in the exocytic pathway of MDCK cells. *The Journal of Cell Biology*, *140*(4), 795–806. https://doi.org/10.1083/jcb.140.4.795

Scheller, M. S., Zornow, M. H., & Seok, Y. (1991). A comparison of the cerebral and hemodynamic effects of mannitol and hypertonic saline in a rabbit model of acute cryogenic brain injury. *Journal of Neurosurgical Anesthesiology*, *3*(4), 291–296. https://doi.org/10.1097/00008506-199112000-00009

Schiess, R., Mueller, L. N., Schmidt, A., Mueller, M., Wollscheid, B., & Aebersold, R. (2009). Analysis of Cell Surface Proteome Changes via Label-free, Quantitative Mass Spectrometry. *Molecular & Cellular Proteomics*, *8*(4), 624–638. https://doi.org/10.1074/mcp.M800172-MCP200

Schmid, E. M., & McMahon, H. T. (2007). Integrating molecular and network biology to decode endocytosis. *Nature*, *448*(7156), 883–888. https://doi.org/10.1038/nature06031

Schmid, S. L. (2017). Reciprocal regulation of signaling and endocytosis: Implications for the evolving cancer cell. *The Journal of Cell Biology*, *216*(9), 2623–2632. https://doi.org/10.1083/jcb.201705017

Schmiege, P., Fine, M., & Li, X. (2021). Atomic insights into ML-SI3 mediated human TRPML1 inhibition. *Structure*, *29*(11), 1295-1302.e3. https://doi.org/10.1016/j.str.2021.06.003

Schneppenheim, J., Dressel, R., Hüttl, S., Lüllmann-Rauch, R., Engelke, M., Dittmann, K., Wienands, J., Eskelinen, E.-L., Hermans-Borgmeyer, I., Fluhrer, R., Saftig, P., & Schröder, B. (2013). The intramembrane protease SPPL2a promotes B cell development and controls endosomal traffic by cleavage of the invariant chain. *Journal of Experimental Medicine*, *210*(1), 41–58. https://doi.org/10.1084/jem.20121069

Schwartz, L., Guais, A., Pooya, M., & Abolhassani, M. (2009). Is inflammation a consequence of extracellular hyperosmolarity? *Journal of Inflammation (London, England)*, *6*, 21. https://doi.org/10.1186/1476-9255-6-21

Sekhon, B. S. (2010). Matrix metalloproteinases – an overview. *Research and Reports in Biology*, *1*, 1–20. https://doi.org/10.2147/RRB.S12043

Sekine, S., Ito, K., & Horie, T. (2008). Canalicular Mrp2 localization is reversibly regulated by the intracellular redox status. *American Journal of Physiology-Gastrointestinal and Liver Physiology*, *295*(5), G1035–G1041. https://doi.org/10.1152/ajpgi.90404.2008

Shao, S., & Hegde, R. S. (2011). Membrane Protein Insertion at the Endoplasmic Reticulum. *Annual Review of Cell and Developmental Biology*, *27*, 25–56. https://doi.org/10.1146/annurev-cellbio-092910-154125

Sheff, D. R., Daro, E. A., Hull, M., & Mellman, I. (1999). The Receptor Recycling Pathway Contains Two Distinct Populations of Early Endosomes with Different Sorting Functions. *Journal of Cell Biology*, *145*(1), 123–139. https://doi.org/10.1083/jcb.145.1.123

Shitova, M., Alpeeva, E., & Vorotelyak, E. (2024). Review of hTERT-Immortalized Cells: How to Assess Immortality and Confirm Identity. *International Journal of Molecular Sciences*, *25*(23), Article 23. https://doi.org/10.3390/ijms252313054

Sies, H., Berndt, C., & Jones, D. P. (2017). Oxidative Stress. *Annual Review of Biochemistry*, *86*(Volume 86, 2017), 715–748. https://doi.org/10.1146/annurev-biochem-061516-045037

Simonetti, B., Danson, C. M., Heesom, K. J., & Cullen, P. J. (2017). Sequence-dependent cargo recognition by SNX-BARs mediates retromer-independent transport of CI-MPR. *Journal of Cell Biology*, *216*(11), 3695–3712. https://doi.org/10.1083/jcb.201703015

Snijder, B., Sacher, R., Rämö, P., Damm, E.-M., Liberali, P., & Pelkmans, L. (2009). Population context determines cell-to-cell variability in endocytosis and virus infection. *Nature*, *461*(7263), 520–523. https://doi.org/10.1038/nature08282

Sohar, I., Sleat, D., Gong Liu, C., Ludwig, T., & Lobel, P. (1998). Mouse mutants lacking the cation-independent mannose 6-phosphate/insulin-like growth factor II receptor are impaired in lysosomal enzyme transport: Comparison of cation-independent and cation-dependent mannose 6-phosphate receptor-deficient mice. *The Biochemical Journal*, *330 (Pt 2)*(Pt 2), 903–908. https://doi.org/10.1042/bj3300903

Soodabeh, S., A, M., & M, A. (2015). From in vitro Experiments to in vivo and Clinical Studies; Pros and Cons. *Current Drug Discovery Technologies*, *12*(4). https://doi.org/10.2174/1570163813666160114093140

Spector, A., Ma, W., Sun, F., Li, D., & Kleiman, N. J. (2002). *The Effect of H2O2 and Tertiary Butyl Hydroperoxide Upon a Murine Immortal Lens Epithelial Cell Line, aaaaaTN4-*.

Spitz, C., Schlosser, C., Guschtschin-Schmidt, N., Stelzer, W., Menig, S., Götz, A., Haug-Kröper, M., Scharnagl, C., Langosch, D., Muhle-Goll, C., & Fluhrer, R. (2020). Non-canonical Shedding of TNFα by SPPL2a Is Determined by the Conformational Flexibility of Its Transmembrane Helix. *iScience*, *23*(12), 101775. https://doi.org/10.1016/j.isci.2020.101775

Steller, M. A., Delgado, C. H., & Zou, Z. (1995). Insulin-like growth factor II mediates epidermal growth factor-induced mitogenesis in cervical cancer cells. *Proceedings of the National Academy of Sciences of the United States of America*, *92*(26), 11970–11974. https://doi.org/10.1073/pnas.92.26.11970

Storm, T., Burgoyne, T., & Futter, C. E. (2020). Membrane trafficking in the retinal pigment epithelium at a glance. *Journal of Cell Science*, *133*(16), jcs238279. https://doi.org/10.1242/jcs.238279

Sun, B., & Hood, L. (2014). Protein-Centric N-Glycoproteomics Analysis of Membrane and Plasma Membrane Proteins. *Journal of Proteome Research*, *13*(6), 2705–2714. https://doi.org/10.1021/pr500187g

Sun, S., Li, F., Liu, F., Wang, J., & Peng, X. (2014). Fluorescence detecting of paraquat using host-guest chemistry with cucurbit[8]uril. *Scientific Reports*, *4*(1), 3570. https://doi.org/10.1038/srep03570

Symons, J., Cho, K.-J., Chang, J., Du, G., Waxham, M. N., Hancock, J. F., Levental, I., & Levental, K. R. (2021). Lipidomic atlas of mammalian cell membranes reveals hierarchical variation induced by culture conditions, subcellular membranes, and cell lineages. *Soft Matter*, *17*(2), 288–297. https://doi.org/10.1039/d0sm00404a

Takata, K., Matsuzaki, T., & Tajika, Y. (2004). Aquaporins: Water channel proteins of the cell membrane. *Progress in Histochemistry and Cytochemistry*, *39*(1), 1–83. https://doi.org/10.1016/j.proghi.2004.03.001

Takeda, T., Komatsu, M., Chiwaki, F., Komatsuzaki, R., Nakamura, K., Tsuji, K., Kobayashi, Y., Tominaga, E., Ono, M., Banno, K., Aoki, D., & Sasaki, H. (2019). Upregulation of IGF2R evades lysosomal dysfunction-induced apoptosis of cervical cancer cells via transport of cathepsins. *Cell Death & Disease*, *10*(12), 876. https://doi.org/10.1038/s41419-019-2117-9

Tan, A., Prasad, R., Lee, C., & Jho, E. (2022). Past, present, and future perspectives of transcription factor EB (TFEB): Mechanisms of regulation and association with disease. *Cell Death & Differentiation*, *29*(8), 1433–1449. https://doi.org/10.1038/s41418-022-01028-6

Tancini, B., Buratta, S., Delo, F., Sagini, K., Chiaradia, E., Pellegrino, R. M., Emiliani, C., & Urbanelli, L. (2020). Lysosomal Exocytosis: The Extracellular Role of an Intracellular Organelle. *Membranes*, *10*(12), 406. https://doi.org/10.3390/membranes10120406

Terluk, M. R., Ebeling, M. C., Fisher, C. R., Kapphahn, R. J., Yuan, C., Kartha, R. V., Montezuma, S. R., & Ferrington, D. A. (2019). N-Acetyl-L-cysteine Protects Human Retinal Pigment Epithelial Cells from Oxidative Damage: Implications for Age-Related Macular Degeneration. *Oxidative Medicine and Cellular Longevity*, *2019*(1), 5174957. https://doi.org/10.1155/2019/5174957

Thibaut-Vercruyssen, R., Poumay, Y., & Ronveaux-Dupal, M. F. (1992). Influence of a short oxidative stress on the LDL endocytosis by human endothelial cells: An ultrastructural study. *Journal of Submicroscopic Cytology and Pathology*, *24*(1), 61–73.

Thiruvengadam, M., Subramanian, U., & Venkidasamy, B. (2021). *Bioactive Compounds in Oxidative Stress-Mediated Diseases: Targeting the NRF2/ARE Signaling Pathway and Epigenetic Regulation*. https://www.mdpi.com/2076-3921/10/12/1859

Togo, T., Alderton, J. M., Bi, G. Q., & Steinhardt, R. A. (1999). The mechanism of facilitated cell membrane resealing. *Journal of Cell Science*, *112 (Pt 5)*, 719–731. https://doi.org/10.1242/jcs.112.5.719

Tong, Y., & Wang, S. (2020). Not All Stressors Are Equal: Mechanism of Stressors on RPE Cell Degeneration. *Frontiers in Cell and Developmental Biology*, *8*. https://doi.org/10.3389/fcell.2020.591067

Trojani, M.-C., Santucci-Darmanin, S., Breuil, V., Carle, G. F., & Pierrefite-Carle, V. (2024). Lysosomal exocytosis: From cell protection to protumoral functions. *Cancer Letters*, *597*, 217024. https://doi.org/10.1016/j.canlet.2024.217024

Trouillon, R., & Ewing, A. G. (2013). Amperometric measurements at cells support a role for dynamin in the dilation of the fusion pore during exocytosis. *Chemphyschem: A European Journal of Chemical Physics and Physical Chemistry*, *14*(10), 2295–2301. https://doi.org/10.1002/cphc.201300319

Trouillon, R., & Ewing, A. G. (2014). Actin controls the vesicular fraction of dopamine released during extended kiss and run exocytosis. *ACS Chemical Biology*, *9*(3), 812–820. https://doi.org/10.1021/cb400665f

Tu, B. P., & Weissman, J. S. (2004). Oxidative protein folding in eukaryotes: Mechanisms and consequences. *Journal of Cell Biology*, *164*(3), 341–346. https://doi.org/10.1083/jcb.200311055

Tu, W., Wang, H., Li, S., Liu, Q., & Sha, H. (2019). The Anti-Inflammatory and Anti-Oxidant Mechanisms of the Keap1/Nrf2/ARE Signaling Pathway in Chronic Diseases. *Aging and Disease*, *10*(3), Article 3. https://doi.org/10.14336/AD.2018.0513

Ushio-Fukai, M., Alexander, R. W., Akers, M., & Griendling, K. K. (1998). P38 Mitogen-activated protein kinase is a critical component of the redox-sensitive signaling pathways activated by angiotensin II. Role in vascular smooth muscle cell hypertrophy. *The Journal of Biological Chemistry*, *273*(24), 15022–15029. https://doi.org/10.1074/jbc.273.24.15022

van Meer, G., & de Kroon, A. I. P. M. (2011). Lipid map of the mammalian cell. *Journal of Cell Science*, *124*(1), 5–8. https://doi.org/10.1242/jcs.071233

van Roy, F., & Berx, G. (2008). The cell-cell adhesion molecule E-cadherin. *Cellular and Molecular Life Sciences*, *65*(23), 3756–3788. https://doi.org/10.1007/s00018-008-8281-1

Vega, V. L., Charles, W., & De Maio, A. (2010). A new feature of the stress response: Increase in endocytosis mediated by Hsp70. *Cell Stress and Chaperones*, *15*(5), 517–527. https://doi.org/10.1007/s12192-009-0165-2

Vella, V., Nicolosi, M. L., Giuliano, M., Morrione, A., Malaguarnera, R., & Belfiore, A. (2019). Insulin Receptor Isoform A Modulates Metabolic Reprogramming of Breast Cancer Cells in Response to IGF2 and Insulin Stimulation. *Cells*, *8*(9), Article 9. https://doi.org/10.3390/cells8091017

Vella, V., Pandini, G., Sciacca, L., Mineo, R., Vigneri, R., Pezzino, V., & Belfiore, A. (2002). A Novel Autocrine Loop Involving IGF-II and the Insulin Receptor Isoform-A Stimulates Growth of Thyroid Cancer. *The Journal of Clinical Endocrinology & Metabolism*, *87*(1), 245–254. https://doi.org/10.1210/jcem.87.1.8142

Volonté, D., Galbiati, F., Pestell, R. G., & Lisanti, M. P. (2001). Cellular Stress Induces the Tyrosine Phosphorylation of Caveolin-1 (Tyr14) via Activation of p38 Mitogen-activated Protein Kinase and c-Src kinase: Evidence for caveolae, the actin cytoskeleton, and focal adhesions as mechanical sensors of osmotic stress *. *Journal of Biological Chemistry*, *276*(11), 8094–8103. https://doi.org/10.1074/jbc.M009245200

Volpert, G., Ben-Dor, S., Tarcic, O., Duan, J., Saada, A., Merrill, A. H., Jr, Pewzner-Jung, Y., & Futerman, A. H. (2017). Oxidative stress elicited by modifying the ceramide acyl chain length reduces the rate of clathrin-mediated endocytosis. *Journal of Cell Science*, *130*(8), 1486–1493. https://doi.org/10.1242/jcs.199968

Waguri, S., Dewitte, F., Le Borgne, R., Rouillé, Y., Uchiyama, Y., Dubremetz, J.-F., & Hoflack, B. (2003). Visualization of TGN to Endosome Trafficking through Fluorescently Labeled MPR and AP-1 in Living Cells. *Molecular Biology of the Cell*, *14*(1), 142–155. https://doi.org/10.1091/mbc.e02-06-0338

Wang, M., Heo, G.-Y., Omarova, S., Pikuleva, I. A., & Turko, I. V. (2012). Sample Pre-Fractionation for Mass Spectrometry Quantification of Low-Abundance Membrane Proteins. *Analytical Chemistry*, *84*(12), 5186–5191. https://doi.org/10.1021/ac300587v

Wang, S., Singh, R. D., Godin, L., Pagano, R. E., & Hubmayr, R. D. (2011). Endocytic response of type I alveolar epithelial cells to hypertonic stress. *American Journal of Physiology-Lung Cellular and Molecular Physiology*, *300*(4), L560–L568. https://doi.org/10.1152/ajplung.00309.2010

Wang, W., Gao, Q., Yang, M., Zhang, X., Yu, L., Lawas, M., Li, X., Bryant-Genevier, M., Southall, N. T., Marugan, J., Ferrer, M., & Xu, H. (2015). Up-regulation of lysosomal TRPML1 channels is essential for lysosomal adaptation to nutrient starvation. *Proceedings of the National Academy of Sciences of the United States of America*, *112*(11), E1373–E1381. https://doi.org/10.1073/pnas.1419669112

Watanabe, K., Morishita, K., Zhou, X., Shiizaki, S., Uchiyama, Y., Koike, M., Naguro, I., & Ichijo, H. (2021). Cells recognize osmotic stress through liquid–liquid phase separation lubricated with poly(ADP-ribose). *Nature Communications*, *12*(1), 1353. https://doi.org/10.1038/s41467-021-21614-5

Waters, J. C. (2009). Accuracy and precision in quantitative fluorescence microscopy. *Journal of Cell Biology*, *185*(7), 1135–1148. https://doi.org/10.1083/jcb.200903097

Weekes, M. P., Antrobus, R., Lill, J. R., Duncan, L. M., Hör, S., & Lehner, P. J. (2010). Comparative Analysis of Techniques to Purify Plasma Membrane Proteins. *Journal of Biomolecular Techniques : JBT*, *21*(3), 108–115.

Wightman, R. M., & Haynes, C. L. (2004). Synaptic vesicles really do kiss and run. *Nature Neuroscience*, *7*(4), 321–322. https://doi.org/10.1038/nn0404-321

Wiley, H. S., Herbst, J. J., Walsh, B. J., Lauffenburger, D. A., Rosenfeld, M. G., & Gill, G. N. (1991). The role of tyrosine kinase activity in endocytosis, compartmentation, and down-regulation of the

epidermal growth factor receptor. *Journal of Biological Chemistry*, *266*(17), 11083–11094. https://doi.org/10.1016/S0021-9258(18)99131-3

Willermain, F., Libert, S., Motulsky, E., Salik, D., Caspers, L., Perret, J., & Delporte, C. (2014). Origins and consequences of hyperosmolar stress in retinal pigmented epithelial cells. *Frontiers in Physiology*, *5*. https://doi.org/10.3389/fphys.2014.00199

Willermain, F., Scifo, L., Weber, C., Caspers, L., Perret, J., & Delporte, C. (2018). Potential Interplay between Hyperosmolarity and Inflammation on Retinal Pigmented Epithelium in Pathogenesis of Diabetic Retinopathy. *International Journal of Molecular Sciences*, *19*(4), Article 4. https://doi.org/10.3390/ijms19041056

Willett, R., Martina, J. A., Zewe, J. P., Wills, R., Hammond, G. R. V., & Puertollano, R. (2017). TFEB regulates lysosomal positioning by modulating TMEM55B expression and JIP4 recruitment to lysosomes. *Nature Communications*, *8*(1), 1580. https://doi.org/10.1038/s41467-017-01871-z

Winkler, S. R., & Munoz-Ruiz, L. (1995). Mechanism of action of mannitol. *Surgical Neurology*, *43*(1), 59. https://doi.org/10.1016/0090-3019(95)80039-j

Wu, L.-G., Hamid, E., Shin, W., & Chiang, H.-C. (2014). Exocytosis and Endocytosis: Modes, Functions, and Coupling Mechanisms. *Annual Review of Physiology*, *76*, 301–331. https://doi.org/10.1146/annurev-physiol-021113-170305

Wu, X., Zhao, X., Baylor, L., Kaushal, S., Eisenberg, E., & Greene, L. E. (2001). Clathrin exchange during clathrin-mediated endocytosis. *Journal of Cell Biology*, *155*(2), 291–300. https://doi.org/10.1083/jcb.200104085

Wünkhaus, D., Tang, R., Nyame, K., Laqtom, N. N., Schweizer, M., Scotto Rosato, A., Krogsæter, E. K., Wollnik, C., Abu-Remaileh, M., Grimm, C., Hermey, G., Kuhn, R., Gruber-Schoffnegger, D., & Markmann, S. (2024). TRPML1 activation ameliorates lysosomal phenotypes in CLN3 deficient retinal pigment epithelial cells. *Scientific Reports*, *14*(1), 17469. https://doi.org/10.1038/s41598-024-67479-8

Xiao, Q., Yan, P., Ma, X., Liu, H., Perez, R., Zhu, A., Gonzales, E., Burchett, J. M., Schuler, D. R., Cirrito, J. R., Diwan, A., & Lee, J.-M. (2014). Enhancing Astrocytic Lysosome Biogenesis Facilitates Aβ Clearance and Attenuates Amyloid Plaque Pathogenesis. *Journal of Neuroscience*, *34*(29), 9607–9620. https://doi.org/10.1523/JNEUROSCI.3788-13.2014

Xu, H., & Ren, D. (2015). Lysosomal Physiology. *Annual Review of Physiology*, *77*(Volume 77, 2015), 57–80. https://doi.org/10.1146/annurev-physiol-021014-071649

Xu, X., Li, M., Chen, W., Yu, H., Yang, Y., & Hang, L. (2016). Apigenin Attenuates Oxidative Injury in ARPE-19 Cells thorough Activation of Nrf2 Pathway. *Oxidative Medicine and Cellular Longevity*, *2016*(1), 4378461. https://doi.org/10.1155/2016/4378461

Zahn, C., Kaup, M., Fluhrer, R., & Fuchs, H. (2013). The transferrin receptor-1 membrane stub undergoes intramembrane proteolysis by signal peptide peptidase-like 2b. *The FEBS Journal*, *280*(7), 1653–1663. https://doi.org/10.1111/febs.12176

Zaoui, K., Benseddik, K., Daou, P., Salaün, D., & Badache, A. (2010). ErbB2 receptor controls microtubule capture by recruiting ACF7 to the plasma membrane of migrating cells. *Proceedings of the National Academy of Sciences of the United States of America*, *107*(43), 18517–18522. https://doi.org/10.1073/pnas.1000975107

Zhang, Q., Cao, Y.-Q., & Tsien, R. W. (2007). Quantum dots provide an optical signal specific to full collapse fusion of synaptic vesicles. *Proceedings of the National Academy of Sciences*, *104*(45), 17843–17848. https://doi.org/10.1073/pnas.0706906104

Zhang, T., Zhang, J., Wang, H., Zou, T., Cheng, S., Yu, Y., Wu, J., Pan, Y., Duan, X., & Wang, H. (2025). Lateral Organization and Dynamics of the Realistic Plasma Membrane. *The Journal of Physical Chemistry B*, *129*(22), 5501–5510. https://doi.org/10.1021/acs.jpcb.5c00909

Zhao, W., Feng, H., Sun, W., Liu, K., Lu, J.-J., & Chen, X. (2017). Tert-butyl hydroperoxide (t-BHP) induced apoptosis and necroptosis in endothelial cells: Roles of NOX4 and mitochondrion. *Redox Biology*, *11*, 524–534. https://doi.org/10.1016/j.redox.2016.12.036

Zhou, J., Wan, J., Gao, X., Zhang, X., Jaffrey, S. R., & Qian, S.-B. (2015). Dynamic m6A mRNA methylation directs translational control of heat shock response. *Nature*, *526*(7574), 591–594. https://doi.org/10.1038/nature15377

Ziegler, A., Cerciello, F., Bigosch, C., Bausch-Fluck, D., Felley-Bosco, E., Ossola, R., Soltermann, A., Stahel, R. A., & Wollscheid, B. (2012). Proteomic surfaceome analysis of mesothelioma. *Lung Cancer*, *75*(2), 189–196. https://doi.org/10.1016/j.lungcan.2011.07.009